Biogeochemistry of dissolved organic matter in the Gulf of Cádiz:

optical and chemical characterization

Valentina Amaral Acosta

Doctoral Thesis
2021

Biogeochemistry of dissolved organic matter in the Gulf of Cádiz

optical and chemical characterization

Valentina Amaral Acosta

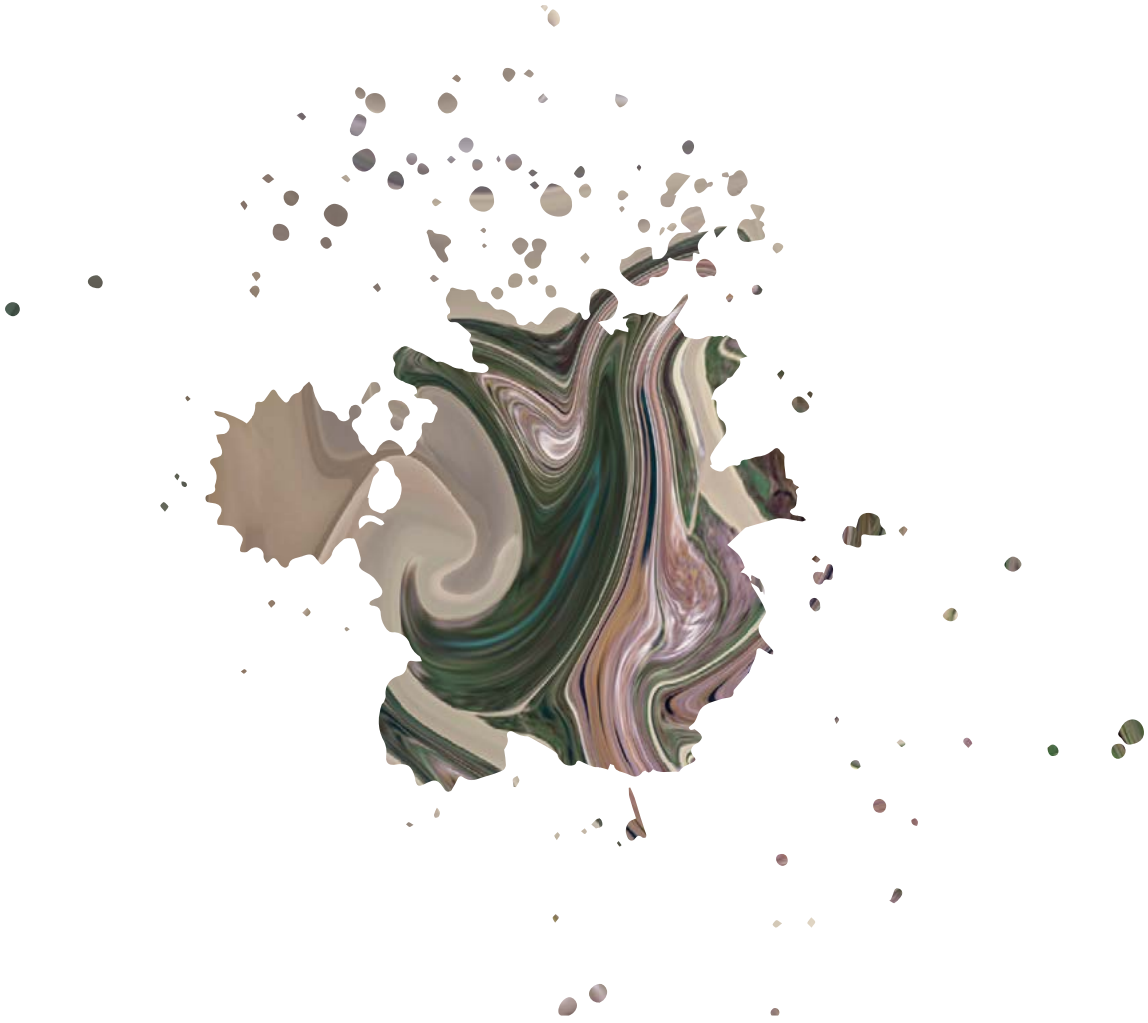

Doctoral Thesis
2021

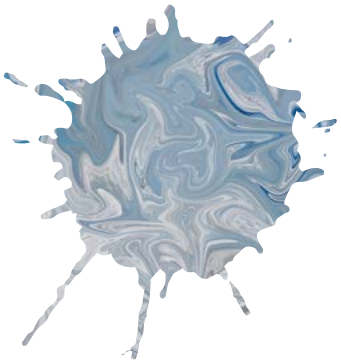

Tesis Doctoral

Biogeoquímica de la materia orgánica disuelta en el golfo de Cádiz: caracterización óptica y química

FACULTAD DE CIENCIAS DEL MAR Y AMBIENTALES
DEPARTAMENTO DE QUÍMICA-FÍSICA

Valentina Amaral Acosta
Cádiz, 2021

Esta Tesis Doctoral ha sido realizada dentro del Grupo de Investigación del Plan Andaluz de Oceanografía y Contaminación del litoral (RNM0144), de la Facultad de Ciencias del Mar y Ambientales de la Universidad de Cádiz. El trabajo de investigación se ha llevado a cabo gracias a la concesión de una Beca de Posgrados en el Exterior de la Agencia Nacional de Investigación e Innovación de Uruguay y se ha desarrollado en el marco de los siguientes proyectos del Programa Español de Ciencia y Tecnología (CICYT): *Ciclo del carbono y flujos de gases invernadero en el golfo de Cádiz* (CTM2014-59244-C3-1-R) y *Modelización de los aportes continentales al golfo de Cádiz: Dinámica de los estuarios en un escenario de cambio climático* (RTI2018-100865-B-C21).

Memoria presentada por Valentina Amaral Acosta para optar al grado de Doctor por la Universidad de Cádiz

Valentina Amaral Acosta

D. JESÚS M. FORJA PAJARES, Catedrático del Departamento de Química Física de la Universidad de Cádiz y D. CRISTINA ROMERA CASTILLO, Investigadora Posdoctoral del Instituto de Ciencias del Mar, Consejo Superior de Investigaciones Científicas, como sus Directores

HACEN CONSTAR:

Que el trabajo recogido en la presente Memoria de Tesis Doctoral, titulada "**Biogeoquímica de la materia orgánica disuelta en el golfo de Cádiz: caracterización óptica y química**", presentada por la Magister en Geociencias Valentina Amaral Acosta reúne todos los requisitos legales y autorizan su presentación y defensa para optar al grado de Doctor por la Universidad de Cádiz.

Cádiz, 2021

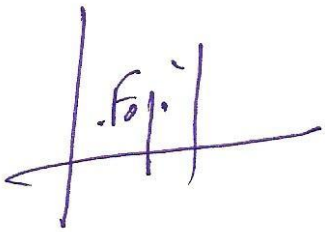

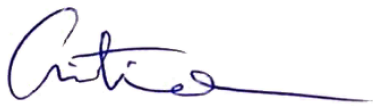

Dr. Jesús Forja Pajares Dra. Cristina Romera-Castillo

Agradecimientos

Tras casi 5 años después-licencias extraordinarias, becas, visas, mudanzas, una hija y una pandemia mundial mediante- llegó el momento de escribir los agradecimientos. Quisiera dar las gracias a todas las personas que se cruzaron en mi camino durante este tiempo y contribuyeron en este proceso de una u otra forma.

A mi grupo de trabajo del CURE, Ecología Funcional de Sistemas Acuáticos, Universidad de la República en Uruguay, por su apoyo para que pudiera realizar el doctorado en el exterior. En especial a Gige, Lorena, Laura, Danilo y a mi gran compañera y amiga Irene. Además quisiera agradecer a mis colegas Cristina y Florencia por su amistad.

A mis directores de tesis, Jesús y Cristina, por su tiempo y dedicación. Jesús, gracias por introducirme y enseñarme el mundillo de la Oceanografía Química. Te agradezco por tu paciencia, casi infinita, humildad, tu calma y tranquilidad, buena predisposición para con mis ocurrencias, consejos y esa actitud de que todo tiene solución. A Cristina por sus palabras de aliento y ánimo, enseñarme a trabajar de forma ordenada y centrada, manteniendo el foco, siempre con espíritu colaborador, crítico, curioso y creativo. Espero poder seguir trabajando y colaborando con ambos. Tanto en lo académico como en lo personal, mi más sincero agradecimiento para los dos. Además quisiera agradecer al resto de los integrantes del Departamento de Química Física de la UCA y del INMAR, en especial a Dori, siempre dispuesta ayudar y con esa buena energía que te caracteriza. A Ana, Jose, Juncal, Maru y Bea por su ayuda con el cromatógrafo de gases, los muestreos y embarques, ¡los TEPs! que quedaron en el backstage! entre otras tantas ocurrencias. A Bibi. A Maider y Anabel que tuve el gusto de codirigir sus tesis con Jesús. A Pablo Lara y su gente por los análisis de PAH, Laura Martin y Ana Bartual por prestarme material para experimentos que al final no resultaron pero formaron parte de este proceso de aprendizaje.

Al Prof. Gerhard J. Herndl del Departamento de Limnología y Bio-Oceanografía, Universidad de Viena, por recibirme en su laboratorio para realizar los análisis de aminoácidos y a Bárbara Maehnert por su tiempo y dedicación durante mi estancia. Al Prof. Hermann Bange de la Unidad de Oc. Química del GEOMAR (Kiel, Alemania) que lamentablemente tuvimos que cancelar la estancia en el último momento debido al cierre de fronteras por la pandemia.

A mis amigas del doctorado. Lola mi gran compi de oficina, Eli e Iría, "nuestra" Cristina y "nuestra" Ana, Miriam y Eva. Gracias por los desayunos, almuerzos eternos y buenos ratos compartidos. Gracias por hacer tan ameno este tiempo. Al grupito de padres de la escuela de Salva por integrarnos enseguida, con ese carácter andaluz tan sociable, abierto y cálido, y en especial a Rocío…gracias por las tardes de parque y playa compartidas con los niños. A Xavi, Loli y sus niños. A Kike y Manuela. Cuando se está lejos se agradece cruzarse con personas tan cálidas que te hacen sentir como en casa.

A mis padres por su apoyo y ayuda incondicional y por enseñarme las herramientas que me han traído hasta aquí. A mis hermana y mi hermano, amigas y amigos, por siempre estar ahí. A los padres de Gastón, siempre dispuestos a dar una mano.

Por último, a mi equipazo. Gastón, esto no hubiese sido posible sin tu apoyo, cariño y compañerismo. A mi niño Salvador, espero que con los años recuerdes con alegría esta parte de tu infancia en la isla…de *cañailla* .. que *pechá* de parques, de bocatas, de ferias, de agua, de playa, de amiguitos y amiguitas, de viajes, que *pechá* de andar… ¡y que *jartura* de levante! A mi niña, Matilde, nuestro fichaje gaditano, compañera de todas las horas de teletrabajo, no faltó un día. ¡No se perdió una revisión! Gracias a los tres por acompañarme y vivir esta emocionante experiencia conmigo.

Cádiz, ¡Gracias…totales! Volveremos a vernos… algún día.

Agua, ¿dónde vas?
Riyendo voy por el río
a las orillas del mar.
Mar, ¿adónde vas?
Río arriba voy buscando
fuente donde descansar.

Federico García Lorca
Canciones, 1921-1924.

A Gastón, Salvador y Matilde

Organización de la Tesis

La presente Tesis Doctoral se ha estructurado en 5 partes. En la primera parte se presenta un resumen extendido del trabajo, una introducción general a la temática y se describe la zona de estudio (español). En la segunda parte se exponen hipótesis, objetivos generales y específicos del estudio. En la tercera parte se detalla la metodología empleada así como la estrategia de muestreo (español). En la cuarta parte se compilan resultados y discusión de cada uno de los cinco capítulos. Todos ellos se estructuran en formato de artículo científico y cuentan con sus correspondientes secciones de "Resumen", "Introducción", "Materiales y Métodos", "Resultados" "Discusión", "Referencias" y "Material Suplementario". Éstos reproducen los contenidos de artículos publicados en revistas científicas y en preparación, por lo que se ha optado por mantener su redacción en inglés.

A continuación se detallan los manuscritos que componen esta Tesis:

Capítulo 1: Dissolved organic matter in the Gulf of Cádiz: Distribution and drivers of chromophoric and fluorescent properties. Amaral, V., Romera-Castillo, C., & Forja, J. (2020). Publicado en *Frontiers in Marine Science*.

https://doi.org/10.3389/fmars.2020.00126

Capítulo 2: Submarine mud volcanoes as a source of chromophoric dissolved organic matter to the deep waters of the Gulf of Cádiz. Amaral, V., Romera-Castillo, C., &

Forja, J. (2021). Publicado en *Scientific reports*. https://doi.org/10.1038/s41598-021-82632-3

Capítulo 3: Distribution of dissolved organic matter in estuaries of the southern Iberian Atlantic Basin: Sources, behavior and export to the coastal zone. Amaral, V., Romera-Castillo, C., García-Delgado, M., Gómez-Parra, A., & Forja, J. (2020). Publicado en *Marine Chemistry*.

https://doi.org/10.1016/j.marchem.2020.103857

Capítulo 4: Dissolved free amino acids in estuarine systems: Sources, distribution and implication for DOM reactivity. Submitted to *Organic Geochemistry*

Capítulo 5: Linkages between greenhouse gases (CO_2, CH_4, and N_2O) and dissolved organic matter composition in a shallow estuary. Amaral, V., Ortega, T., Romera-Castillo, C., & Forja, J. (2021). Publicado en *Science of The Total Environment*. https://doi.org/10.1016/j.scitotenv.2021.147863

Por último, una quinta parte recoge las consideraciones finales y conclusiones generales de la memoria realizada (español).

Índice

List of abbreviations

a_{254} absorption coefficient at 254 nm
a_{350} absorption coefficient at 350 nm
AA-C carbon-normalized yields of amino acids
AAs amino acids
A_{ORG} Organic Alkalinity
AOU apparent oxygen utilization
AOUres AOU residuals
BIX freshness index
CDOM chromophoric dissolved organic matter
CH_4 Methane
Chl a in vivo chlorophyll a fluorescence
CO_2 carbon dioxide
CTD conductivity Temperature Depth
DCAA dissolved combined amino acids
DeepW deep water
DFAA dissolved free amino acids
DI degradation index
DIC dissolved inorganic carbon
DO dissolved oxygen
DOC dissolved organic carbon
DOCres DOC residuals
DOM dissolved organic matter
EEMs excitation-Emission matrixes
ENACW Eastern North Atlantic Central Water
$ENACW_P$ Eastern Subpolar North Atlantic Central Water
$ENACW_T$ Eastern Subtropical North Atlantic Central Water
FDOM fluorescent dissolved organic matter
GABA γ-aminobutyric acid
GD Guadalquivir
GHGs greenhouse gases
GoC Gulf of Cádiz
Gt gigaton
GU Guadiana
HCl hydrochloric acid
HIX humification index
HPLC high-pressure liquid chromatography
MAHs monocyclic aromatic hydrocarbons
MCCs methylene chain compounds
MOW Mediterranean Outflow Water
MVs mud Volcanoes

N nitrogen
N_2O nitrous oxide
NaCl sodium chloride
NACW North Atlantic Central Water
NH_4^+ ammonium
NO_2^- nitrite
NO_3^- nitrate
NPAA non-protein amino acid
ºC Degree Celsius
OCAL Integrated Oceanography of the Gulf of Cádiz in a Global Change Scenario
OMP optimum multiparametric water mass analysis
OPA ortho-phthaldialdehyde
PAH polycyclic aromatic hydrocarbon
PARAFAC parallel factor analysis
PCA principal component analysis
*p*CO2 partial pressure of carbon dioxide
Pg petagram
PO_4^{3-} phosphate
POM particulate organic matter
ppm parts per million
Py-GC-MS pyrolysis-gas chromatography-mass spectroscopy
RDOM refractory dissolved organic matter
R/V Research Vessel
rpm revolutions per minute
S salinity
$S_{275–295}$ spectral slope between 275 and 295 nm
SAW surface Atlantic Water
SD standard Deviation
SO_4^{2-} sulphate
SP Sancti Petri
St. Saint
SurfW surface water
$SUVA_{254}$ specific ultraviolet absorbance at 254 nm
SWT source water types
T temperature
TA total Alkalinity
TDAA total dissolved amino acids
TDLP9 total dissolved lignin phenol
TF Trafalgar
THAA total hydrolysable amino acids
TO Tinto-Odiel
yr year

Parte I

Resumen, introducción y zona de estudio

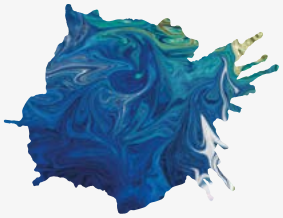

I. RESUMEN

La materia orgánica disuelta (DOM, *dissolved organic matter*) es uno de los principales reservorios de carbono orgánico del planeta y puede persistir desde cientos a miles de años en el océano, contribuyendo así al secuestro de carbono. En general, la DOM es una pieza clave en los sistemas acuáticos, donde participa además de varios procesos ecosistémicos. Sin embargo, la caracterización química de la DOM es limitada debido a que está formada por una mezcla compleja de cientos de miles de compuestos diferentes. Por otro lado, los mecanismos detrás de su estabilidad a largo plazo en el océano siguen siendo un enigma. Para entender mejor el rol que juega la DOM en los procesos en los que participa es importante conocer los procesos que determinan su distribución, dilucidar su composición y las condiciones ambientales que contribuyen a su producción y degradación.

Esta Tesis doctoral está enmarcada en las campañas oceanográficas realizadas en el marco del proyecto OCAL (Oceanografía integrada del golfo de Cádiz en un escenario de cambio global: Ciclo del carbono y flujos de gases invernadero). El golfo de Cádiz es un sistema espacialmente heterogéneo cuyas características biogeoquímicas y ecológicas están condicionadas por los intercambios entre los compartimentos ambientales que lo limitan (las cuencas mediterránea y atlántica, sistemas costeros, la atmósfera y el sedimento). El golfo de Cádiz es la única conexión entre el mar Mediterráneo y el Atlántico Norte, es decir, es una zona de transición biogeográfica entre ambas cuencas.

En este trabajo se ha estudiado la distribución y características de la DOM en la plataforma continental del golfo de Cádiz, en los principales estuarios que allí desembocan y en volcanes de fango submarinos localizados entre los 500 y 1000 m de profundidad. En la plataforma continental y en los volcanes de fango submarinos la DOM se analizó utilizando sus propiedades ópticas (absorbancia y fluorescencia). Además, se realizó un análisis de masas de agua para diferenciar el efecto de los procesos físicos de los biogeoquímicos en la distribución de la DOM en la zona mesopelágica y se estimaron los flujos bentónicos de DOM desde los volcanes hacia las aguas profundas del golfo de Cádiz. En los estuarios del golfo de Cádiz además de las propiedades ópticas para caracterizar la DOM se empleó la técnica pirólisis con cromatografía de gases y espectrometría de masas (Py-GC-MS) y se realizaron análisis de aminoácidos libres disueltos (DFAA, *dissolved free amino acids*). Se estimaron los flujos de DOC y de las distintas fracciones de la DOM desde los estuarios a la zona costera del golfo de Cádiz.

En la plataforma continental se identificaron seis componentes fluorescentes, tres del tipo húmico, dos del tipo proteico y una posible mezcla de compuestos proteicos con hidrocarburos aromáticos. La variabilidad de los componentes del tipo húmico se explica mayoritariamente por los procesos de mezcla de masas de agua, mientras que la variabilidad del carbono orgánico disuelto (DOC, *dissolved organic carbon*) y los compuestos del tipo proteico está fuertemente asociada a la estacionalidad y a los procesos biogeoquímicos que ocurren a escala local. En las capas profundas, la distribución del DOC presenta comportamientos contrastantes (eliminación/acumulación) asociado a la presencia de afloramientos costeros.

En los volcanes de fango se identificaron cuatro de los seis componentes fluorescentes encontrados en la plataforma continental, dos del

tipo húmico y dos del tipo proteico. Sin embargo, el origen de estos compuestos está relacionado con los fluidos volcánicos que provienen de los sedimentos profundos y con la actividad de las bacterias reductoras del sulfato. Los volcanes de fango representan una fuente de DOC y DOM a las aguas profundas del golfo de Cádiz.

En los estuarios de los ríos Guadalquivir, Guadiana y Tinto- Odiel se identificaron cuatro componentes fluorescentes, dos del tipo húmico y dos del tipo proteico, también encontrados en la plataforma continental. Las características químicas y moleculares de la DOM exportada desde los estuarios a la zona costera depende de las condiciones locales, como las características de la cuenca y la reactividad biogeoquímica de la DOM dentro de cada estuario. Por ejemplo, la DOM en el estuario del río Guadalquivir y Guadiana es predominantemente de origen terrestre y su distribución está influenciada por la presencia de prácticas agrícolas y marismas en sus márgenes, mientras que en el estuario del río Tinto- Odiel predomina la DOM de origen autóctono asociado a una mayor influencia marina así como a la contaminación antropogénica debido a la actividad minera e industrial que ocurre en sus márgenes. Los resultados obtenidos mediante el análisis de Py-GC-MS coincidieron con los encontrados empleando las propiedades ópticas de la DOM. Las fracciones de DOM provenientes de plantas vasculares (lignina, fenoles, hidrocarburos aromáticos) fueron más abundantes en Guadalquivir, seguido del Guadiana y Tinto-Odiel, mientras que los compuestos derivados de la producción *in situ* y contaminantes antropogénicos fueron más abundantes en Tinto- Odiel (compuestos de metileno). Además, la variabilidad de la DOM en estos estuarios está fuertemente influenciada por los ciclos mareales y transportan DOC y DOM de origen mayoritariamente húmico a la zona costera,

principalmente el estuario del Guadalquivir (1.25 kg C s^{-1} y 0.22 × 10^3 m^2 s^{-1} de DOC y CDOM, respectivamente).

Por último, en el estuario del río Guadalete, localizado en la bahía de Cádiz, evaluamos la relación entre los gases invernadero CO_2, CH_4 y N_2O y la composición de la DOM. Se identificaron cuatro componentes fluorescentes, tres del tipo húmico, de diverso origen (terrestre, microbiano y proveniente de efluentes de la agricultura y aguas tratadas) y otro del tipo proteico. El estuario del Guadalete actúa como una fuente de CO_2, CH_4 y N_2O a la atmósfera, en donde las concentraciones de estos gases están significativamente relacionas con la concentración del DOC y la composición de la DOM. La distribución del CO_2 está relacionada principalmente con compuestos del tipo húmico con mayor aromaticidad, mientras que la concentración de N_2O está mayormente influenciada por compuestos del tipo proteico derivados de efluentes. Por ultimo, la concentración de CH_4 se relaciona con ambas fracciones de la DOM, húmica y proteica de diverso origen. Además se observó que podría estar ocurriendo un acoplamiento entre el flujo bentónico de CH_4 y DOM dada la baja profundidad del estuario Guadalete. Por tanto, es importante tener en cuenta la composición de la DOM al estudiar la distribución de gases invernadero en sistemas estuarinos, y así comprender su rol y posibles respuestas asociadas al cambio climático.

I. 1. INTRODUCCIÓN GENERAL

Los principales reservorios de materia orgánica activos en el planeta son la materia orgánica en los suelos (1600 Pg C), la depositada en los sedimentos marinos en los últimos 5000 - 10000 años (1000 Pg C), la materia orgánica disuelta (DOM, *dissolved organic matter*) en el océano (662 Pg C) y la biomasa vegetal en la superficie terrestre (600 Pg C) (Hedges, 2002).

I. 1.1. ¿Qué es la materia orgánica disuelta?

La DOM se define operacionalmente como toda la materia orgánica, constituida principalmente por C, H, O, N y P, que pasa por un filtro nominal de 0.45 µm (operacionalmente entre 0.2 y 0.7 µm), mientras que la fracción retenida en el filtro se denomina materia orgánica particulada (POM, *particulate organic matter*) (Fig. 1.1).

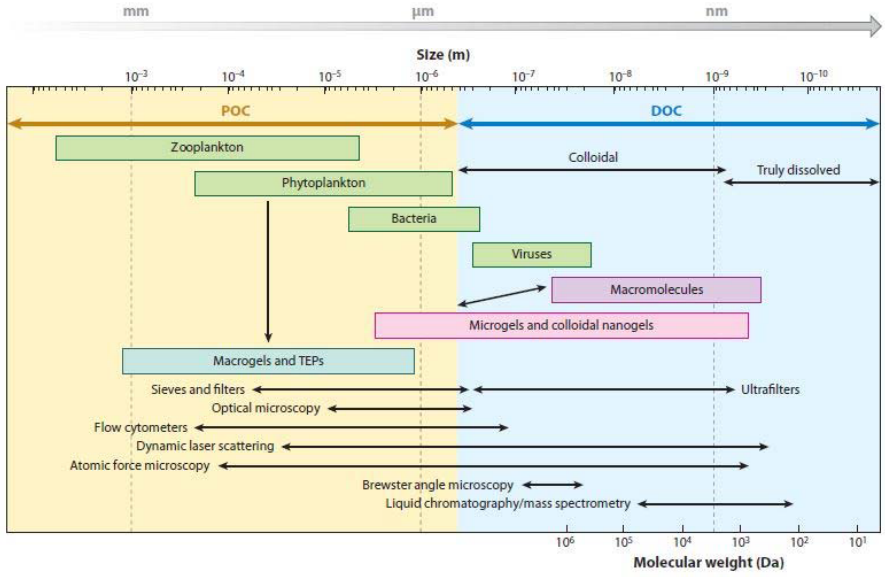

Fig. 1.1. Escala de tamaños de la materia orgánica en el agua de mar. Los recuadros verdes indican la materia orgánica viva mientras que los recuadros azules y rosados representan la materia orgánica no viva. En la parte inferior de la figura se resumen los principales métodos utilizados para el estudio de cada fracción. Tomado de Verdugo, 2012.

La DOM es una mezcla compleja y heterogénea que va desde compuestos simples (aminoácidos, azúcares, ácidos grasos) hasta biopolímeros complejos (proteínas, polisacáridos, ligninas) y productos de difícil degradación (sustancias húmicas, carbono negro). La DOM constituye un continuo de compuestos con diferente peso molecular que exhiben distintas solubilidades, reactividad y propiedades ópticas según su estructura molecular (Hedges, 2002). Según su reactividad o tiempo de residencia se puede clasificar en DOM lábil, semilábil, semirefractaria, refractaria (RDOM, *refractory dissolved organic matter*) o ultra refractaria (Fig. 1.2) (Carlson y Hansell, 2015; Hansell, 2013). La DOM lábil es una pequeña fracción de la reserva total de DOC oceánico. Incluye azúcares y aminoácidos libres disueltos y es consumida en escala de tiempo de horas o días por los microorganismos (Carlson y Hansell, 2015), es decir, es rápidamente respirada a dióxido de carbono (CO_2). La DOM semilábil es más resistente a la degradación bacteriana que la lábil y es usada por los microorganismos en escalas de tiempo de meses a años. Está compuesta principalmente por polisacáridos, azúcares y aminoácidos combinados disueltos. La DOM semirefractaria comprende compuestos de reactividad intermedia y se transforma en escalas de tiempos de décadas, mientras que la RDOM es la fracción más resistente a la degradación bacteriana y puede persistir durante cientos a miles de años en el interior del océano. Por último, la DOM ultra refractaria es una pequeña fracción de la RDOM que comprende carbono negro y puede persistir en el océano durante miles de años (Ziolkowski y Druffel, 2010). Además, la DOM también se puede clasificar atendiendo a su peso molecular como DOM de bajo peso molecular (<200 nm o <1 KDa) y DOM coloidal o de alto peso molecular (> 200-700 nm o > 1 KDa) (Fig. 1.2). Aunque esos son los rangos de tamaño

más utilizados para clasificar la DOM como de alto o bajo peso molecular, el límite entre ambas fracciones no es considerado siempre el mismo y depende del autor. En general, la DOM de alto y bajo peso molecular constituye alrededor del 25% y 75% del *pool* total de DOM, respectivamente (Benner y Amon, 2015).

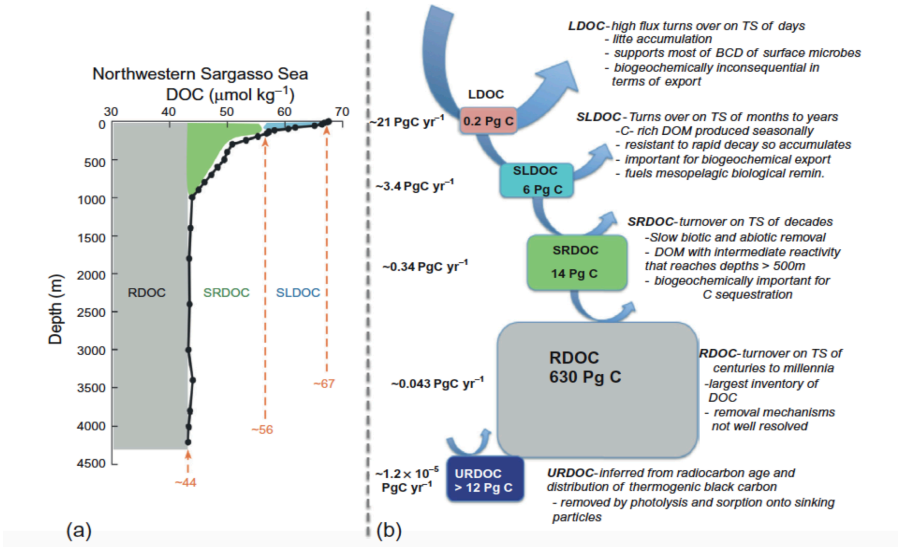

Fig. 1.2. Clasificación de las distintas fracciones de carbono orgánico disuelta (DOC) en función de su reactividad (LDOC: lábil, SLDOC: semilábil, SRDOC: semirefractaria, RDOC: refractaria, URDOC: ulrarefractaria). TS= escala de tiempo, BCD= demanda de carbono bacteriano. Tomado de Carlson y Hansell (2015).

I. 1.2. El rol de la materia orgánica disuelta en el ciclo del Carbono

El componente mayoritario de la DOM es el carbono, por lo que en general la concentración de carbono orgánico disuelto (DOC, *dissolved organic carbon*) se usa como indicador cuantitativo de DOM. La DOM representa el 96% del carbono orgánico total en los océanos, su stock es comparable en escala al CO_2 presente en la atmosfera (860 Pg C) y es casi 200 veces mayor que la cantidad de carbono que conforma la biomasa

marina (Hansell, 2013; Hansell et al., 2009). Por tanto, variaciones en el reservorio de DOC debido al cambio global, podrán tener un gran impacto en la concentración de CO_2 atmosférico y, por ende en el clima de la Tierra (Hedges, 2002; Lønborg et al., 2020). Por ejemplo, debido a que las cantidades de carbono en la DOM del océano y el CO_2 atmosférico son similares, la oxidación neta del 1% de la DOM durante 1 año sería suficiente para generar un flujo de CO_2 mayor que el producido anualmente por la combustión de combustibles fósiles (Hedges, 2002). Asimismo, se ha especulado que una gran oxidación de DOC a CO_2 pudo haber evitado una glaciación global en el período Neoproterozoico, al haber aumentado el efecto invernadero (Peltier et al., 2007).

Los océanos juegan un rol central regulando el clima en la Tierra no sólo por el intercambio de calor, sino también mediante el intercambio atmosférico de CO_2 en la interfaz agua-atmósfera y al secuestrar carbono en las profundidades del océano. La absorción neta de CO_2 por parte de los océanos es casi de 2.6 ± 0.3 Pg C $año^{-1}$ (Gruber et al., 2019). Los procesos que controlan este intercambio se han dividido en cuatro "bombas" (Sarmiento y Gruber, 2006, Jiao et al., 2010): 1) la bomba de solubilidad, 2) la bomba de carbonato, 3) la bomba de carbono orgánico y 4) la bomba microbiana de carbono (Fig. 1.3).

La bomba de solubilidad se debe a un proceso físico. La solubilidad de los gases depende de la temperatura, por lo que la disolución del CO_2 aumenta en aguas superficiales frías de latitudes altas, donde tiene lugar la formación de masas de aguas profundas. El rápido hundimiento de estas densas aguas superficiales enriquecidas en CO_2, y por tanto en carbono inorgánico disuelto (DIC, *dissolved inorganic carbon*), y su redistribución en las profundidades oceánicas a través de la circulación termohalina resulta en

un bombeo eficiente de carbono desde la atmósfera hacia las profundidades oceánicas.

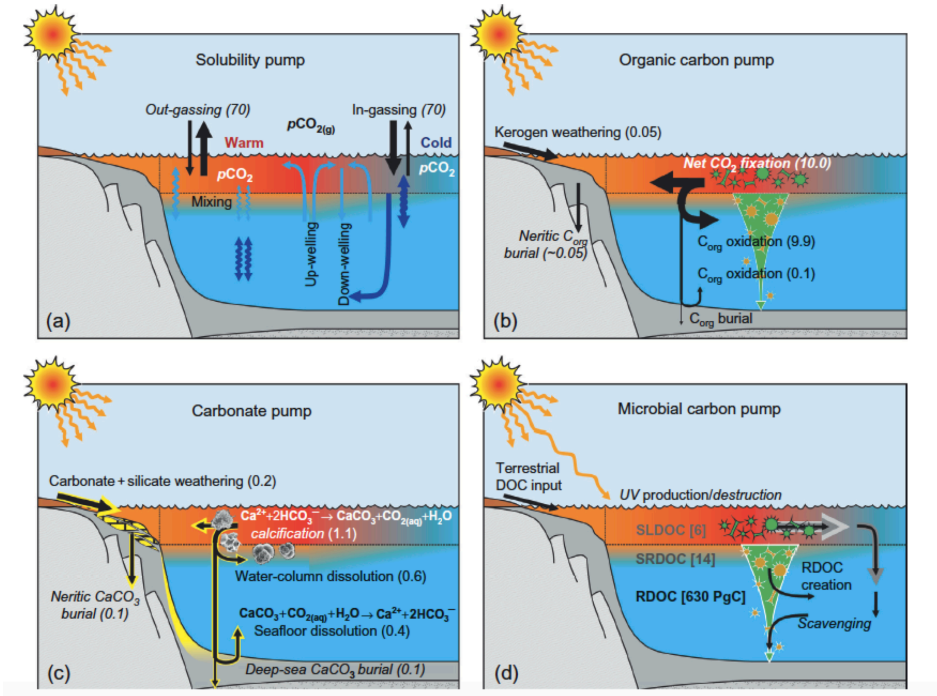

Fig. 1.3. Funcionamiento esquemático de las cuatro bombas de carbono en el océano. a) Bomba de solubilidad, b) Bomba de carbono orgánico, c) Bomba de carbonato y d) Bomba de carbono microbiana. Tomado de Ridgwell y Arndt, 2015.

La bomba de carbonato transporta carbono inorgánico particulado que se formó en la superficie hacia el fondo del océano a través de la producción del carbonato de calcio ($CaCO_3$) (y en menor medida de magnesio) por organismos calcificantes (ej. cocolitofóridos, foraminíferos, pterópodos) y su posterior disolución a grandes profundidades. Cuando estos organismos mueren sus estructuras de $CaCO_3$ son transportadas hacia el interior del océano (Elderfield, 2002). Alrededor del 50% del $CaCO_3$ se disuelve a medida que se va hundiendo (Feely et al., 2004), mientras que el resto, alcanza los sedimentos superficiales donde el 20% escapa a la

disolución y es preservado (Feely et al., 2004), formando nuevamente parte del depósito de carbono geológico.

La bomba de carbono orgánico se debe a la eliminación de CO_2 que se encuentra en aguas superficiales a través de la fotosíntesis realizada principalmente por el fitoplancton, convirtiéndolo en POM y DOM (50 Pg C $año^{-1}$, Carr et al., 2006; Chavez et al., 2011). Alrededor del 80% de este carbono es respirado rápidamente en la zona situada por encima de la termoclina mediante la acción de las bacterias y el zooplancton, volviendo a la atmósfera en forma de CO_2. El 20% restante se hunde al interior del océano, principalmente como POM pero también DOM, donde es oxidado nuevamente a CO_2 por los microorganismos heterótrofos. Entre el 1 y el 6% de este carbono llega al fondo marino, donde solo el 0.3% escapa de la degradación bentónica para ser secuestrado en los sedimentos marinos (Dunne et al., 2007). Sin embargo, trabajos recientes que revisaron los mecanismos físicos y biológicos asociados a la exportación de POM al océano profundo, sugieren que la bomba de carbono orgánico captura el doble de carbono que lo estimado hasta ahora (Buesseler et al., 2020).

La fracción de la DOM que no es utilizada por el metabolismo microbiano (~ 1% anual) se ha ido acumulando en la columna de agua durante miles de años (5000 - 8000 años) hasta alcanzar un stock de 640 Pg C, denominada RDOM, contribuyendo así al secuestro de carbono por parte de los océanos (Hansell et al., 2009; Hansell, 2013). La bomba microbiana de carbono se ha propuesto como marco conceptual para explicar los procesos y mecanismos involucrados en la generación de la RDOM (Jiao et al., 2010). Se basa en la producción de DOM resistente a la degradación bacteriana como subproducto del metabolismo microbiano (Jiao et al., 2010; Ogawa et al., 2001). Sin embargo, existe cierta controversia en cuanto a los

mecanismos responsables de la estabilidad de la DOM a largo plazo en el océano y se han propuesto varias hipótesis para explicar su existencia (Dittmar, 2015):

1) La hipótesis del continuo tamaño-reactividad (Amon y Benner, 1996; Benner y Amon, 2015), que se refiere al consumo preferencial por parte de los microorganismos de compuestos de mayor peso molecular, dando lugar a estructuras más complejas y pequeñas con menor reactividad. Esta hipótesis está fuertemente relacionada con la bomba de carbono microbiana, en donde en las profundidades del océano la degradación microbiana es la principal fuente de RDOM.

2) La teoría de la dilución, que postula que la persistencia de la DOM en el interior del océano se debe a que se trata de miles de compuestos diferentes intrínsecamente lábiles pero cada uno en concentraciones tan bajas que no compensa el coste metabólico asociado a su utilización (Arrieta et al., 2015; Dittmar, 2015).

3) La estabilidad intrínseca de la DOM, en relación a la estructura molecular de los compuestos, es decir, que los microorganismos carezcan de las vías enzimáticas necesarias para descomponer determinadas estructuras moleculares y por ende estas se acumulen en el interior del océano (Dittmar, 2015).

4) Que las condiciones ambientales sean adversas para la degradación de la DOM, por ejemplo, falta de O_2 o limitación por nutrientes (Dittmar, 2015).

Existen evidencias a favor de todas estas hipótesis y probablemente la combinación de ellas explique la acumulación de la DOM en el interior del océano (Baltar et al., 2021; Dittmar, 2015). Por otro lado, recientemente se ha propuesto que la RDOM se defina operacionalmente ya que existen varias

definiciones del término "refractario" y se han empleado diferentes enfoques para caracterizar el *pool* de DOM almacenado a largo plazo por los océanos (Baltar et al., 2021).

I. 1.3. Importancia de la DOM en diversos procesos ecosistémicos

Además de su importancia en el ciclo del carbono, la DOM participa en varios procesos ecosistémicos. Por ejemplo, es el sustrato fundamental para el desarrollo de las comunidades microbianas, es decir, se encuentra en la base de la cadena trófica (Cuss y Guéguen, 2015), regula la penetración de la luz protegiendo a los organismos de la radiación UV (Nelson y Siegel, 2013), interactúa con metales pesados (Yamashita y Jaffé, 2008) y otros contaminantes orgánicos (Chin, 2003), participa en reacciones fotoquímicas que pueden tener como producto final tanto compuestos más lábiles que quedarán disponibles para los microorganismos (Benner y Biddanda, 1998; Obernosterer y Benner, 2004) como potentes gases como el CO, CO_2 o CH_4 (Li et al., 2020; Moran y Zepp, 1997). Además, contribuye a la alcalinidad total (TA, *total alkalinity*) del agua de mar (Kim y Lee, 2009) y presenta actividad antioxidante, minimizando los efectos negativos de los radicales libres (Romera-Castillo y Jaffé, 2015).

I. 1.4 Fuentes y sumideros de la materia orgánica disuelta

En el océano la DOM es de origen autóctono o alóctono (Fig. 1.4). La DOM autóctona puede representar > 95% y deriva principalmente de la producción fitoplanctónica, mientras que la alóctona proviene principalmente de los aportes continentales, que representan entre el 2- 3% del *pool* total, aunque puede ser dominante en las zonas costeras (Opsahl y

Benner, 1997). El fitoplancton puede producir DOM mediante liberación extracelular de distintos compuestos o autolisis durante eventos de estrés.

Además, se ha observado liberación de DOM, mediada por el zooplancton, durante su alimentación (*sloppy feeding*), excreción y defecación (Hygum et al., 1997). Las bacterias, además de ser las principales consumidoras de DOM, también producen DOM durante la división celular o lisis viral (Iturriaga y Zsolnay, 1981; Kawasaki y Benner, 2006; Ogawa et al., 2001). Las macrófitas son altamente productivas y pueden ocupar grandes extensiones en las zonas costeras. Por ejemplo, se ha estimado que, globalmente, la producción de DOC por parte de las macrófitas podría ser de 0.16 Pg C $año^{-1}$ (Barrón y Duarte, 2015) es decir, más de la mitad de lo que transportan los ríos anualmente (0.25 Pg C $año^{-1}$). Adicionalmente, los sedimentos marinos también son una fuente importante de DOM. En general, la concentración de DOC en los sedimentos es un orden de magnitud mayor que lo encontrado en la columna de agua (Burdige y Gardner, 1998). En ese sentido, se ha estimado que los sedimentos liberarían 0.35 Pg C $año^{-1}$ a través de flujos difusivos (Burdige y Komada, 2015), esto es, mayor a la entrada de DOC anual a través de los ríos, y sin considerar los eventos de resuspensión que también liberan DOC (Komada y Reimers, 2001). Asimismo, varios estudios han observado que ciertas estructuras asociadas al fondo marino, como fuentes hidrotermales, hidratos de metano y volcanes de fango, actúan como fuente de DOM en el océano profundo (Dittmar y Koch, 2006; Retelletti et al., 2019; Yang et al., 2012). Sin embargo, actualmente no hay información consistente en cuanto al aporte global de DOM por parte de estas estructuras. Asimismo, las aguas subterráneas podrían ser importantes contribuyentes de DOM en las zonas

costeras (Webb et al., 2019), aunque actualmente tampoco se cuenta con estimaciones globales fiables.

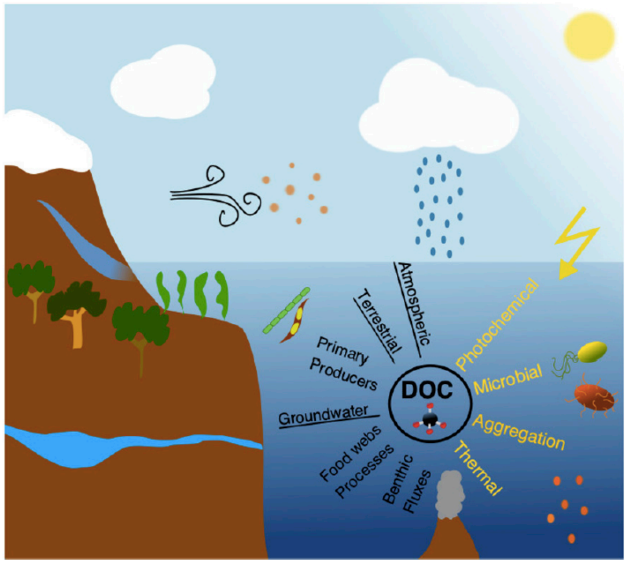

Fig. 1.4. Esquema simplificado con las principales fuentes (en negro) (subrayadas: fuentes alóctonas) y sumideros (en amarillo) de carbono orgánico disuelto (DOC). Tomado de Longborg et al., 2021.

Los principales mecanismos de eliminación de DOM en la columna de agua son la degradación microbiana y la fotoquímica (Carlson y Hansell, 2015). Además, se ha observado que durante la mezcla de agua marina y dulce puede darse un proceso abiótico de floculación (Sholkovitz, 1976). Este proceso transforma la DOM en material particulado, que luego puede sedimentar o ser consumido por otros organismos (Tranvik y Sieburth, 1989). En las aguas costeras la floculación puede eliminar entre un 3 a un 30% de la DOM, dependiendo de las condiciones del sistema (Sholkovitz et al., 1976, 1978).

I. 1.5. Dinámica de la materia orgánica disuelta en sistemas estuarinos

Las zonas costeras suponen sólo el 7% de la superficie oceánica (Gattuso et al., 1998), sin embargo, debido a su alta productividad son particularmente relevantes para el ciclo global del carbono, contribuyendo

desproporcionadamente al mismo en relación a su extensión y actuando como nexo de unión de las fases terrestres y marinas en los ciclos biogeoquímicos (Schlesinger, 1997). Los ríos y estuarios son el vínculo principal entre la tierra y los océanos, y conectan más del 87% de la superficie terrestre a sus costas (Hedges et al., 1997). Tradicionalmente, los ríos se consideraban componentes pasivos en el ciclo del carbono, es decir, simples "tuberías" (*riverine pipe*) que transportaban carbono orgánico e inorgánico desde los ecosistemas terrestres al mar (ver ref. en Cole et al., 2007). Sin embargo, los ríos son componentes activos del ciclo global del C que almacenan carbono de origen terrestre en los sedimentos y emiten CO_2 a la atmósfera, además de transportarlo (Cole et al., 2007). Anualmente, los ríos transportan ~ 0.25 Pg C por año desde los continentes al océano a través de los estuarios (Raymond y Spencer, 2015). Los estuarios son regiones de transición entre los ríos y la zona costera adyacente, por lo que son sistemas muy dinámicos caracterizados por fuertes gradientes fisicoquímicos debido a la intensa variación de salinidad, pH, actividad biológica y a la resuspensión de sedimentos (Gattusso et al., 1998). Reciben aportes de materia orgánica y nutrientes inorgánicos desde los ríos, descargas de aguas subterráneas, e intercambia especies con los sedimentos, humedales costeros y el océano (Fig. 1.5). Por tanto, la DOM en los estuarios puede tener diversos orígenes, fundamentalmente asociados a las entradas de sustancias húmicas derivadas de la biomasa terrestre y el suelo, a los aportes antropogénicos procedentes de residuos urbanos y otras actividades que ocurren en sus márgenes (agricultura, acuicultura, industrias), así como la contribución de compuestos derivados de la actividad biológica (plancton, vegetación acuática y producción secundaria) y de los aportes laterales desde zonas de marismas (Bauer y Bianchi, 2011). Asimismo, la DOM que llega a los

estuarios experimenta importantes transformaciones antes de llegar a la zona costera. Por esta razón, los estuarios se encuentran entre los sistemas acuáticos más complejos con respecto a la caracterización biogeoquímica de la DOM (Bauer y Bianchi, 2011).

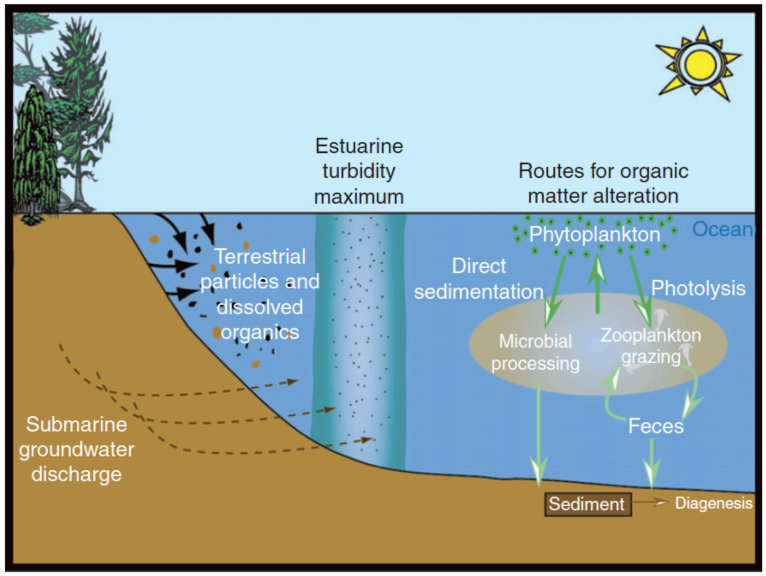

Fig. 1.5. Esquema simplificado con las principales fuentes (autóctonas y alóctonas) y sumideros en los sistemas estuarinos. Tomado de Bauer y Bianchi, 2011.

En general, se consideraba que la DOM proveniente de los ríos era recalcitrante y transportada de forma conservativa hasta la zona costera. Sin embargo, el comportamiento de la DOM durante su tránsito por los estuarios es altamente variable, lo que determina la concentración y composición que finalmente es transportada al océano. La salinidad es un componente conservativo en los estuarios y puede ser un buen indicador de mezcla de masas de aguas de distintos *endmembers* (fluvial y marina). En ese sentido, en los estuarios, los diagramas de mezcla a lo largo de un gradiente de salinidad son ampliamente usados para determinar e identificar las fuentes y sumideros de los constituyentes disueltos (Officer, 1979; Bauer y Binchi,

2011) (Fig. 1.6). Por ejemplo, un comportamiento lineal (conservativo) con la salinidad estaría indicando pocos cambios en las propiedades DOM a lo largo del estuario y su comportamiento podría ser explicado por simple dilución/mezcla de ambas masas de agua.

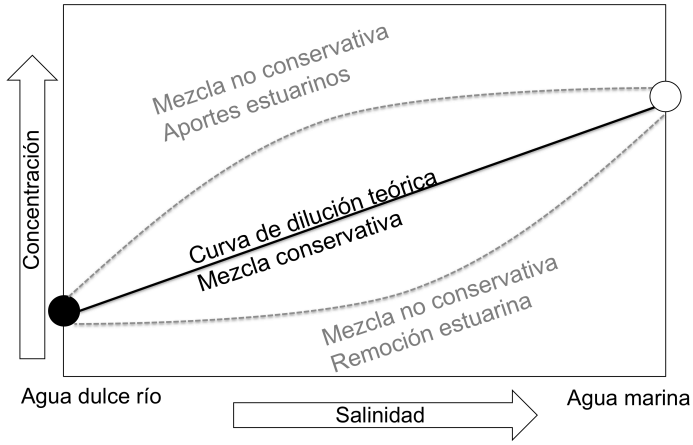

Fig. 1.6. Diagrama de mezcla esquemático para un componente disuelto en función de la salinidad. Modificado de Wolfgang et al. (1993).

Por el contrario, un comportamiento no lineal (no conservativo) podría estar indicando tanto eliminación (ej. microbiana o fotoquímica) como producción *in situ* o proveniente de aportes laterales (ej. humedales, actividades antropogénicas) (Guo et al., 2007; Raymond y Spencer, 2015; Rochelle-Newall y Fisher, 2002). Por tanto, es importante comprender los diversos factores (químicos, físicos y biológicos) que regulan el transporte de DOM hacia la zona costera, así como la composición y reactividad de la misma dentro de estos sistemas de transición tierra-océano.

I. 1.6. Caracterización química de la DOM

La caracterización química de la DOM es limitada debido a que está formada por una mezcla compleja de cientos de miles de compuestos diferentes que, además, en el agua de mar están presentes en concentraciones muy bajas con respecto al contenido de sales (Repeta, 2015). Se han desarrollado diversas técnicas y aproximaciones para estudiar su composición

a distintos niveles que incluyen el análisis elemental de la relación entre carbono, nitrógeno y fósforo, análisis de isótopos estables del C y el N (Bauer, 2002), métodos analíticos para la determinación de distintos componentes como aminoácidos, lignina, carbohidratos y lípidos (Benner, 2002, Fichot et al., 2016), empleo de las propiedades ópticas de la DOM (absorbancia y fluorescencia, Coble, 1996; Coble et al., 2014) técnicas de resolución a nivel molecular, como la resonancia magnética nuclear (Benner et al., 1992), pirólisis con cromatografía de gases y espectrometría de masas (Py-GC-MS, Kaal, 2019) y la espectrometría de masas de resonancia ciclotrónica iónica por transformada de Fourier (Hertkorn et al., 2013) que permite llegar hasta la formula elemental. Muchos de estos análisis requieren una concentración y aislamiento previo de la materia orgánica, y entre las técnicas más comunes para hacerlo están la ultrafiltración o la extracción en fase sólida.

Basándose en los análisis de compuestos específicos como carbohidratos, aminoácidos, proteínas o lípidos, menos del 10% de la composición molecular de la DOM ha sido caracterizada en los sistemas marinos (Repeta, 2015). Sin embargo, otras características de la DOM, como la distribución de los principales grupos funcionales o clases de compuestos que contribuyen a distintas fracciones de la DOM (ej. lábil/refractaria), son útiles para comprender las principales fuentes y sumideros así como el ciclo de la DOM en sistemas acuáticos. Desde esta otra perspectiva, entre el 60% y 70% de la DOM ha sido "caracterizada" (Repeta, 2015).

La fracción ópticamente activa de la DOM proporciona información sobre el origen de la materia orgánica, su estado diagenético, función ecológica, biodisponibilidad y reactividad (Coble et al., 2014). Asimismo, las

propiedades ópticas de la DOM son independientes de la concentración de DOC (Baker et al., 2008) y pueden emplearse para trazar cambios en la composición de la DOM, ya que sus características bioquímicas suelen relacionarse con sus propiedades ópticas (Hernes et al., 2009). Asimismo, las medidas de fluorescencia ofrecen información sobre el ciclo biogeoquímico de una amplia gama de moléculas no fluorescentes que aparentemente siguen el mismo gradiente que la DOM fluorescente (FDOM, *fluorescent dissolved organic matter*) en los sistemas acuáticos (Stubbins et al., 2014). Por otro lado, además de ser una técnica rápida, precisa y accesible, posibilita abordar estudios de cambios temporales y espaciales al permitir el análisis de una gran cantidad de muestras, necesario para comprender la dinámica de la DOM en estos sistemas.

I. 1.6.1. Propiedades ópticas de la materia orgánica disuelta

Una fracción variable de la DOM absorbe luz en el rango visible y ultravioleta (UV) del espectro, y se denomina DOM coloreada o cromofórica (CDOM, *chromophoric dissolved organic matter*, Coble, 2007). La absorción en el rango UV- visible involucra la excitación de un electrón a un nivel mayor de energía, proceso que depende de la estructura química de la molécula (Silverstein et al., 1974). La CDOM es uno de los componentes ópticamente activos más importantes de los sistemas acuáticos, junto con el agua pura, el fitoplancton y partículas detríticas en suspensión (Armstrong y Boalch, 1961; Nelson y Siegel, 2013, Fig. 1.7). La absorción de la CDOM es mayor en el UV y decrece exponencialmente al aumentar la longitud de onda (Kirk, 1994). A longitudes de onda < 440 nm, la CDOM puede contribuir entre un 30% y un 70% a la absorción total de la luz. El espectro de absorción de la CDOM es el producto de una mezcla compleja de compuestos, como aminoácidos e hidrocarburos aromáticos y polifenoles

(ej. flavonoides, taninos y ligninas) presentes en abundancia en la biomasa terrestre y en las algas. Por lo tanto, dicho espectro es muy amplio y solapa con el de la clorofila *a* (440 nm), pudiendo reducir la radiación fotosintética disponible, y por ende la producción primaria. Asimismo, puede interferir en las estimaciones de biomasa y actividad del fitoplancton derivadas de imágenes satelitales que emplean la absorción a 440 nm (Nelson y Siegel, 2013; Siegel et al., 2002). Por otro lado, puede atenuar los daños de la radiación UV en las poblaciones planctónicas (Herndl et al., 1993).

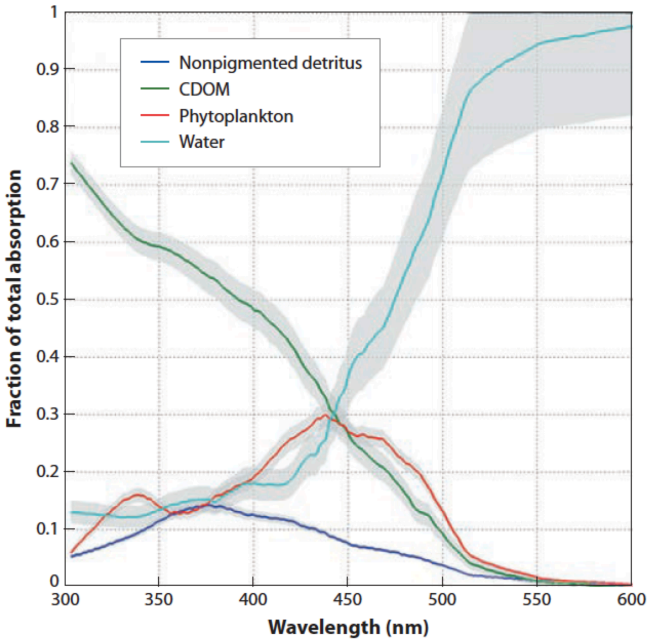

Fig. 1.7. Contribución relativa de los principales componentes ópticamente activos en el agua. Tomado de Nelson y Siegel, 2013.

La CDOM puede representar entre el 30% y el 70% del DOC dependiendo del sistema acuático, y los mayores porcentajes suelen encontrarse en las zonas costeras (Chen y Bada, 1992; Kowalczuk et al., 2010). Las principales fuentes de CDOM son los aportes terrestres (Coble, 2007), la condensación abiótica y condensación de biopolímeros (Kieber et

al., 1997) y la producción *in situ* (Ortega-Retuerta et al., 2009; Romera-Castillo et al., 2010; Steinberg et al., 2004). Tradicionalmente la CDOM ha sido relacionada con material de origen terrestre (Stedmon y Nelson, 2015), sin embargo, también puede derivar como subproducto del metabolismo microbiano (Kramer y Herndl, 2004) o ser producido por el fitoplancton (Romera-Castillo et al., 2010) y el zooplancton (Steinberg et al., 2004, Ortega-Retuerta et al., 2009). Por otro lado, la fotodegradación es el principal mecanismo de eliminación de CDOM en los sistemas acuáticos (Moran et al., 2000). Las transformaciones fotoquímicas de CDOM juegan un papel importante en los ciclos biogeoquímicos (Mopper et al., 2015; Moran et al., 2016) a través de reacciones fotoquímicas que pueden alterar la composición y concentración química de nutrientes, DOC y gases traza como por ejemplo CO, CO_2 y CH_4 (Moran y Zepp, 1997; Mopper et al., 2015; Moran et al., 2016; Li et al., 2020). La fotodegradación de la CDOM puede derivar en compuestos más lábiles y por ende con mayor biodisponibilidad para ser utilizados por los microorganismos (Obernosterer y Benner, 2004). Por otro lado, también se ha observado que la fotodegradación puede transformar ciertos compuestos en material más complejo y aromático que son más resistentes a la degradación microbiana (Berto et al., 2016; Kieber et al., 1997).

La CDOM ha sido empleada en una variedad de sistemas acuáticos para estimar la concentración de DOC (Catalá et al., 2018; Lønborg y Álvarez-Salgado, 2014; Rochelle-Newall et al., 2014). Sin embargo, dada la complejidad y variedad de compuestos que se pueden encontrar en la CDOM, no se puede cuantificar en unidades de concentración sino que depende de la intensidad de la señal óptica. Existen diversos indicadores cualitativos obtenidos a través de las medidas de absorbancia, ampliamente

usados en biogeoquímica (Coble, 2007; Helms et al., 2008; Huguet et al., 2009; Weishaar et al., 2003). Estos indicadores incluyen coeficientes de absorción a longitudes de onda específicas, como el a_{254} o el a_{350}, que además de proporcionar información sobre la composición, también se utilizan como una medida para estimar la concentración de distintas fracciones de la CDOM (Blough y Del Vecchio, 2002), así como coeficientes espectrales obtenidos al determinar la absorbancia en un rango determinado de longitudes de onda (Fichot y Benner, 2012; Helms et al., 2008). Por ejemplo, el coeficiente espectral $S_{275\text{-}295}$ es un buen indicador del peso molecular de la DOM (Helms et al., 2008). Además, se han desarrollado modelos empíricos sencillos para estimar la concentración de lignina a partir de coeficientes de absorción (Fichot et al., 2016).

La distribución de CDOM en el océano se puede evaluar utilizando algoritmos de detección remota en imágenes satelitales (e.g., Siegel et al., 2002, Nelson y Siegel, 2013) (Fig. 1.8). En el océano los niveles más altos de CDOM se encuentran en las regiones costeras, en las plataformas continentales y estuarios, debido a un mayor aporte de DOM de origen terrestre, productividad y flujos bentónicos (Nelson y Siegel, 2013, Nelson y Stedmon, 2015). En general, la CDOM disminuye al aumentar la distancia a la costa debido a los procesos de dilución (Nelson y Siegel, 2013).

En el océano abierto, los contenidos más elevados de CDOM se han observado en latitudes altas del hemisferio Norte y en zonas de afloramientos (> 0.1 m^{-1}), indicando una conexión tanto con la productividad como con las aguas profundas ricas en CDOM (Nelson y Siegel, 2013, Stedmon y Nelson, 2015). Los niveles más bajos se observaron en los giros subtropicales (≤ 0.01 m^{-1}), debido a la baja productividad, y una alta estratificación y fotodegradación en estas zonas (Nelson y Siegel, 2013, Stedmon y Nelson,

2015). En zonas más profundas se observa una relación entre CDOM y la utilización aparente de oxígeno (AOU, *apparent oxygen utilization*) en los océanos Indico y Pacífico, indicando que la CDOM es producida durante la oxidación de la DOM (Nelson et al., 2010; Nelson y Siegel, 2013). Esta correlación no se observó en el océano Atlántico, probablemente debido a que el grado de ventilación es mayor que en el Indico y Pacífico (Nelson et al., 2010). En general, los principales factores que controlan la distribución de CDOM en los océanos son la producción microbiana, la fotodegradación y la mezcla de las masas de agua (Coble, 2007; Nelson et al., 2010; Nelson y Siegel, 2013; Álvarez-Salgado et al., 2013).

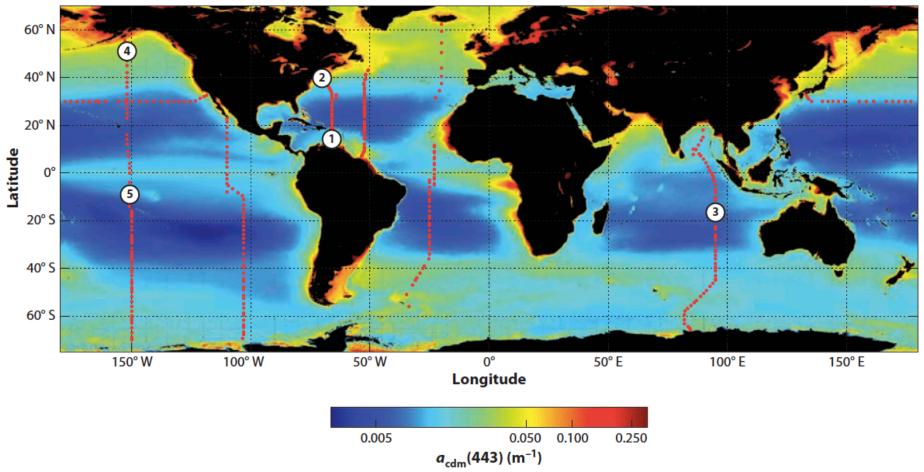

Fig. 1.8. Distribución global de la absorción de la CDOM (+ partículas detríticas) a 443 nm derivada de imágenes satelitales (1997-2010). Tomada de Nelson y Siegel (2013).

Una subfracción de la CDOM es capaz de emitir parte de la luz absorbida en forma de fluorescencia y corresponde a la FDOM (Coble 1996). La longitud de onda de excitación y emisión a la cual ocurre la fluorescencia es característica de las estructuras específicas de cada molécula. Los compuestos que re-emiten la luz absorbida como fluorescencia se denominan fluoróforos. Para el estudio de la FDOM se emplean matrices de excitación emisión (EEMs, *excitation emission matrixes*), que se obtienen

adquiriendo espectros de emisión a lo largo de una serie de longitudes de onda de excitación (Coble, 1996; Coble et al., 1990). Para su análisis, tradicionalmente se usaba la técnica "peak picking", que consiste en la clasificación de diversos máximos de emisión-excitación o picos de fluorescencia (Coble, 1996, Stedmon et al., 2003) (Tabla 1.1, Fig. 1.9). En general, la FDOM puede clasificarse en compuestos similares a proteínas, relacionados con aminoácidos aromáticos, que absorben a longitudes de onda < 300 nm, y en compuestos similares a las sustancias húmicas, relacionadas con los ácidos húmicos terrestres y marinos y los ácidos fúlvicos, que absorben a longitudes de onda > 300 nm (Coble, 2007, Coble et al., 2014). Con el desarrollo de técnicas multivariadas, como el *parallel factor analysis* (PARAFAC, Bro, 1997; Stedmon et al., 2003), la clasificación propuesta por Coble (1996) ha evolucionado hacia el modelado de la DOM presente en cada conjunto de muestras mediante la descomposición de la señal de fluorescencia en sus componentes individuales, los fluoróforos. Este tipo de análisis ha sido extensamente aplicado al estudio de la composición y dinámica de la FDOM tanto en el océano como en sistemas continentales (Coble et al., 2014).

Tabla 1.1. Máximos de excitación y emisión (Ex max y Em max) y descripción de los picos de fluorescencia tradicionales en muestras de agua (Coble, 1996, Stedmon et al., 2003). Tomado de Coble et al., 2014.

Nombre	Ex max (nm)	Em max (nm)	Descripción
B	275	305	protein-like, tirosina
T	275	340	protein-like, triptófano
A	260	400–460	humic-like
M	290–310	370–410	humic-like, marino
C	320–360	420–460	humic-like
D	390	509	fulvic-like (suelos)
E	455	521	fulvic-like (suelos)
N	280	370	plankton derived

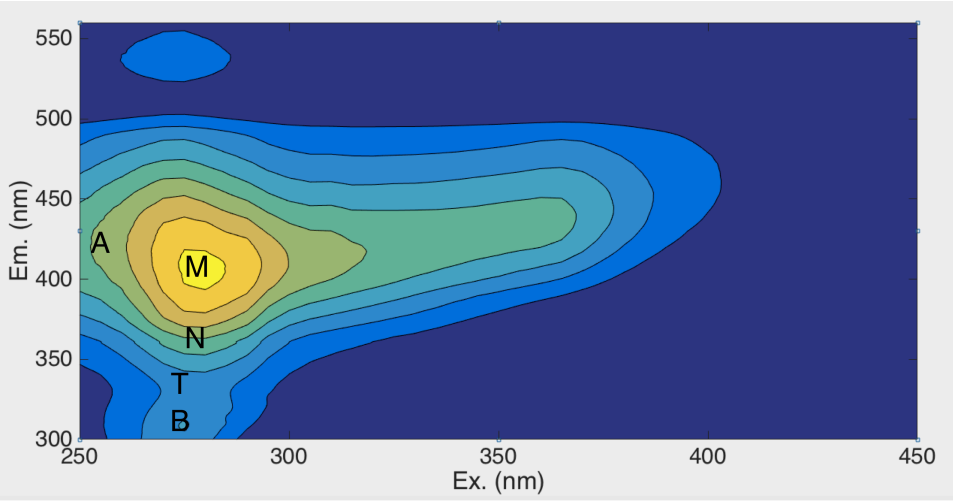

Fig. 1.9. Matriz de excitación emisión de una muestra de agua del estuario Guadalete indicando los picos de fluorescencia característicos de Coble 1996.

En las distribuciones globales de FDOM se observa un aumento de los componentes húmicos con la profundidad debido a la fotodegradación en superficie así como a la producción microbiana producto de la oxidación de la materia orgánica (Catalá et al., 2015; Jørgensen et al., 2011; Kowalczuk et al., 2013; Lønborg y Álvarez-Salgado, 2014). Por el contrario, los componentes proteicos muestran mayores valores en superficie debido a que derivan principalmente de la fotosíntesis, son más foto-resistentes que los componentes húmicos y consumidos en aguas profundas (Jørgensen et al., 2011; Catalá et al., 2015). En los estuarios se observa una predominancia de componentes del tipo húmico debido a los aportes terrestres, mientras que los de origen proteico aumentan su contribución relativa generalmente en la zona marina (Jaffé et al., 2004; Yamashita et al., 2008).

I. 1.6.2. Aminoácidos disueltos

Las proteínas están compuestas por aproximadamente 20 α-aminoácidos (AA) que se pueden dividir en diferentes categorías según sus grupos funcionales. Un α-aminoácido consta de un grupo amino, un grupo carboxilo, un átomo de H y un grupo R distintivo (cadena lateral) que está unido a un átomo de C (C α). Los AA representan una pequeña fracción de la DOM en los sistemas acuáticos (5–20% DON y 3–4% DOC, Sharp, 1983). Sin embargo, es uno de los sustratos más importantes para los microorganismos heterótrofos y representa la fracción más lábil de la DOM (Keil y Kirchman, 1991). Los AA pueden encontrarse en su forma libre o formando parte de proteínas y otros compuestos compuestos orgánicos como sustancias húmicas (Hedges y Hare, 1987). La concentración de aminoácidos disueltos ha sido medida tanto en el océano como en sistemas estuarinos desde los 70 debido a su capacidad para medirse directamente en la fase disuelta (sin extracción previa) y al desarrollo temprano de técnicas

relativamente simples para su cuantificación (Keil y Kirchman, 1991, 1993; Lindroth y Mopper, 1979).

Los aminoácidos disueltos se clasifican operativamente según el método utilizado en el procesamiento previo de las muestras. Los aminoácidos "libres" disueltos (DFAA, *dissolved free amino acids*) son medidos directamente en la muestra previamente filtrada y representan monómeros de aminoácidos libres. Por otro lado, cuando la muestra filtrada es tratada con ácido, se miden los aminoácidos totales "hidrolizables" (THAA, *total hydrolysable amino acids*, Lee y Bada, 1977, 1975). La diferencia entre los THAA y los DFAA representan los aminoácidos disueltos combinados (DCAA, *dissolved combined amino acids*), es decir, la fracción de aminoácidos unido a proteínas, péptidos y otros polímeros. Los DFAA son típicamente una orden de magnitud menor que los DCAA por lo que los estudios recientes se han enfocado principalmente en esta última fracción (Repeta, 2015) y son poco los estudios de la composición de DFAA, en particular en los sistemas estuarinos. Si bien algunos autores proponen que los DCAA son relativamente más importantes como sustratos bacteriano que los DFAA (Coffin, 1989; Keil y Kirchman, 1999), otros autores han observado que los DFAA son consumidos preferentemente por las bacterias (e.g. Keil y Kirchman, 1993). Por ejemplo, mientras que en los sistemas oligotróficos las bacterias prefieren los AA en proteínas (Keil y Kirchman, 1999) en sistemas estuarianos se ha observado que prefieren los DFAA (Coffin, 1989; Keil y Kirchman, 1993). Según Coffin (1989) es posible que las bacterias no puedan absorber fácilmente los AA unidos a compuestos húmicos, característicos de los estuarios.

En esta Tesis doctoral se analizará la concentración y distribución de los DFAA en tres estuarios del golfo de Cádiz y se emplearan distintos indicadores basados en la composición de AA para estudiar el estado diagenetico de la DOM.

En general, la concentración de DFAA en los sistemas acuáticos es del orden nanomolar con mayores concentraciones en las zonas costeras que en el océano abierto (Lee y Bada, 1977, 1975). Los estuarios reciben importantes aportes terrestres de materia orgánica y mantienen altos niveles de producción primaria (Bauer y Bianchi, 2011) así como grandes flujos de DFAA a través de la interfase sedimento-agua (Burdige y Martens, 1990) que contribuyen a la composición de estos compuestos en la columna de agua. Se ha observado que la abundancia relativa de cada aminoácido en organismos distintos (plantas vasculares, macrófitas, fitoplancton, bacterias) es bastante similar (Cowie y Hedges, 1992). Por tanto, las diferencias observadas en la composición relativa de los THAA y DFAA se ha usado como un indicador de cambios en el estado de degradación de la DOM (e.g. (Dauwe et al., 1999; Sarmento et al., 2013). Por ejemplo, los aminoácidos no proteicos como la β-alanina, el ácido γ-aminobutírico y la ornitina son producidos enzimáticamente durante procesos de descomposición a partir de sus precursores, el ácido aspártico, ácido glutámico y arginina, respectivamente. Por otro lado, los AA aromáticos (tirosina, triptófano y fenilalanina), el ácido glutámico y la arginina, son más biodegradables que algunos AA ácidos como la glicina, la serina, la alanina y la lisina (Amon y Fitznar, 2001; Cowie y Hedges, 1992). Berggren et al. (2010) encontraron que los AA derivados del material terrestre están altamente biodisponibles y sustentan el metabolismo bacteriano en sistemas acuáticos dominados por DOM de origen alóctono (Berggren et al., 2010).

La relación de los enantiómeros de cada aminoácido (D/L) ha sido ampliamente usada como indicador diagenético de la DOM y se ha correlacionado con la biodisponibilidad de la DOM (Jørgensen et al., 1999). En general, el enantiómero D se considera de origen microbiano. Durante la degradación bacteriana de la DOM se ha observado un enriquecimiento de los D-AA debido al rápido uso de los L-AA (Amon y Fitznar, 2001; Jørgensen et al., 1999). Por tanto, una alta proporción de D/L AA estaría indicando una mayor contribución de DOM de origen bacteriano así como un mayor ciclado de este material (Bianchi, 2007).

I. 1.6.3. Pirólisis con cromatografía de gases y espectrometría de masas

En las última décadas, las herramientas analíticas para determinar las características químicas de la DOM han avanzado significativamente, desde análisis elementales hasta enfoques simples a un nivel molecular empleando espectroscopias UV-Vis y de fluorescencia. Sin embargo, ampliar la caracterización a la escala molecular sigue siendo un desafío. En la mayoría de los casos es necesario realizar una preconcentración de la muestra y extracción de la DOM previa al análisis molecular, como es el caso de la Py-GC-MS. La Py-GC-MS es una técnica que escinde la materia orgánica empleando calor (500-700 °C) en fragmentos susceptibles a la cromatografía de gases (GC) que luego pueden identificarse mediante espectrometría de masas (MS) (Kaal, 2019). Por tanto, la Py-GC-MS es empleada para obtener un rastreo rápido de los compuestos macromoleculares de la DOM. A pesar de las limitaciones cuantitativas, dado que solo se pueden obtener estimaciones de proporciones relativas de productos de pirólisis, se ha demostrado que la Py-GC-MS proporciona información valiosa sobre las fuentes de DOM (Kaal, 2019; Kaal et al., 2017, 2016). Teóricamente, los

principales biopolímeros que se pueden encontrar en los sistemas acuáticos y sus productos de degradación pueden escindirse pirolíticamente en productos identificables. Por ejemplo, se pueden identificar polisacáridos, proteínas, ligninas, taninos, pigmentos fotosintéticos, quininas y peptidoglicano, varios productos alifáticos y sus productos de degradación (ver ref. en Kaal, 2019), proporcionando un cribado rápido de las posibles fuentes y estados de degradación de la DOM. La Py-GC-MS es una técnica útil para complementar y mejorar la interpretación de la caracterización de la DOM por espectroscopia de fluorescencia (Jiang et al., 2017). En esta Tesis doctoral se empleará dicha técnica para complementar la caracterización de la DOM en los estuarios del golfo de Cádiz.

I. 1.7. Gases de efecto invernadero

Los estuarios ofrecen condiciones muy favorables para la producción de gases de efecto invernadero como el CO_2, metano (CH_4) y óxido nitroso (N_2O) (Liikanen et al., 2009). Estos gases tienen una elevada capacidad de absorción de la radiación infrarroja procedente de la superficie de la Tierra (Rodhe, 1990) y desempeñan un papel fundamental en la regulación del clima del planeta. A este respecto, la presencia de estos gases de efecto invernadero permite que la temperatura en la Tierra sea de unos 15 ºC, unos 30 ºC mayor que la esperada si no existiera este proceso (Mackenzie, 1999). El CO_2 es el que presenta mayor interés debido a que tiene una mayor concentración en la atmósfera. Sin embargo, la capacidad radiactiva del CH_4 y N_2O es 25 y 298 veces más elevada que la del CO_2 (IPCC, 2013). Las emisiones antropogénicas de estos gases han aumentado considerablemente desde la era preindustrial hasta la actualidad debido al crecimiento económico y demográfico (OMM, 2019). Los principales factores responsables de este aumento son el uso de combustibles fósiles, así como los

cambios en el uso y en la gestión de los recursos de la tierra (Le Quéré et al., 2015). La concentración de CO_2 en la atmósfera ha aumentado desde 280 ppm en la era preindustrial hasta 410 ppm en 2019 (OMM 2019). En el caso del CH_4, este aumento ha sido de 700 a 1877 ppb y para el N_2O, de 275 a 332 ppb (OMM, 2019). Este aumento continuo de la concentración atmosférica de estos gases ha tenido como consecuencia un efecto de calentamiento de la superficie terrestre (IPCC, 2013). Este aumento de la temperatura afecta a la calidad de los recursos hídricos, modificando las áreas de distribución de muchas especies, cambiando, entre otros, los rendimientos de la pesca, y perjudicando, en general, el estado de los servicios ecosistémicos (IPCC, 2013).

La degradación de la materia orgánica puede dar lugar a la producción de CO_2, CH_4 y N_2O (Borges et al., 2019). Es decir, los procesos microbianos auto y heterótrofos generan estos gases en la columna de agua y los sedimentos, y provocan un intercambio entre compartimentos ambientales (Daniel et al., 2013; Liikanen et al., 2009). Los principales procesos que controlan la distribución del CO_2 en los estuarios son la fotosíntesis, la oxidación aerobia y anaerobia de la materia orgánica, el transporte lateral desde marismas y el intercambio con la atmósfera (Abril y Borges, 2005; Cai, 2011). En general, los estuarios son sistemas heterotróficos, donde la respiración total del sistema supera la producción primaria, es decir, los valores de CO_2 generalmente están por encima del equilibrio atmosférico (> 400 µatm, Cai et al., 2011). La emisión global de CO_2 a la atmósfera proveniente de los estuarios se estima que es de 0.27 Pg C $año^{-1}$ (Borges y Abril, 2011). Por otro lado, la producción de CH_4 depende tanto de la cantidad de materia orgánica como de la disponibilidad de O_2 (Borges y Abril, 2011). En los estuarios, el CH_4 es producido

principalmente por la metanogénesis, esto es, la degradación de la materia orgánica en condiciones anóxicas (Reeburgh, 2003). Sin embargo, se ha observado producción de CH_4 en presencia de oxigeno debido, por ejemplo, a la degradación de compuestos fosfatados presentes en la DOM (Donis et al., 2017; Karl et al., 2008; Repeta et al., 2016) o a la producción por las cianobacterias durante la fotosíntesis (Bižić et al., 2020). Otro factor importante para la producción de CH_4 es la concentración de sulfato, ya que la metanogénesis es la etapa final de la degradación de la materia orgánica, y tiene lugar una vez que el sulfato ha sido agotado en los procesos de sulfatorreducción. Ya que el sulfato aumenta con la salinidad, generalmente, se observa en los estuarios una disminución del CH_4 de hasta dos órdenes de magnitud hacia la zona marina (Abril y Borges, 2005). En ese sentido, las concentraciones de CH_4 en los estuarios muestran un amplio intervalo de variación con valores, por lo general, superiores al equilibrio atmosférico, y por tanto, actúan como fuentes de CH_4 a la atmósfera. Las emisiones globales de los estuarios varían entre 0.02 – 0.91 Tg CH_4 $año^{-1}$, y los flujos con la atmósfera suelen ser mayores en los sistemas antropizados debido a la entrada de materia orgánica y nutrientes procedentes de la urbanización, eutrofización y cambios en el uso de la tierra (Rosentreter et al., 2021). Por último, la producción de N_2O ocurre a través de los procesos microbianos de nitrificación autótrofa y desnitrificación heterótrofa (Bange, 2006; Bange et al., 1996), que pueden ocurrir en la columna de agua, en el sedimento o en el interior de partículas en suspensión (Bange, 2008; Nevison et al., 2003). La nitrificación consiste en la oxidación aerobia de amonio a nitrato, donde el N_2O se forma como un subproducto de la reacción a partir de la hidroxilamina (NH_2OH) o del óxido de nitrógeno (NO) (Arp y Stein, 2003). En la desnitrificación, el N_2O se forma como un producto

intermedio durante la reducción anaerobia de nitrato a nitrógeno molecular (N_2) (Christensen, 1994). La producción de N_2O depende en gran medida de la concentración de O_2 y se ve favorecida por el aumento en la carga de nutrientes y la presencia de vegetación (Murray et al., 2015). En promedio los sistemas estuarinos actúan como fuente de N_2O a la atmósfera con emisiones comprendidas entre 0.15 y 0.91 Tg de N_2O año^{-1} (Murray et al., 2015). Se estima que el 91% de las emisiones de este gas desde ríos, estuarios y márgenes continentales se deben a causas antropogénicas (Seitzinger et al., 2000).

Se ha propuesto la hipótesis de que el cambio climático influye en la composición de la DOM en los sistemas estuarinos a través de cambios en los patrones de precipitación, suministro de agua dulce y estratificación (Canuel et al., 2012). Estos cambios en la composición de la DOM podrían afectar también a las emisiones atmosféricas de los gases invernadero desde los estuarios. Por ejemplo, en lagos someros se ha observado que el aumento de la producción primaria, y la posible acumulación de DOM relativamente lábil derivada del fitoplancton, potencia la liberación de CH_4 (Zhou et al., 2019). Por otro lado, se ha descrito que el nitrógeno orgánico disuelto de origen terrestre potencia las emisiones de N_2O en lagos eutróficos (Zhou et al., 2020). Si bien en las últimas décadas la distribución de la DOM y gases invernadero en los estuarios ha recibido una atención considerable, poco se sabe sobre los vínculos que hay entre ellos. Dilucidar las conexiones entre la composición de DOM y la dinámica de los gases CO_2, CH_4 y N_2O podría proporcionar información valiosa sobre el papel y la respuesta de los estuarios al cambio global.

I. 2. ZONA DE ESTUDIO

Esta Tesis doctoral se realizó en la zona oriental de la plataforma continental del golfo de Cádiz (GoC, *Gulf of Cadiz*) y en cuatro estuarios de esta zona. El estuario del Guadalquivir, Guadiana y Tinto-Odiel que desembocan en el GoC y un estuario más pequeño, Guadalete, que desemboca en la bahía de Cádiz. En todos los trabajos se analizaron las propiedades ópticas de la DOM. En los estuarios del Guadalquivir, Guadiana y Tinto-Odiel además se caracterizó la DOM empleando la técnica Py-GC-MS y se analizaron los DFAA.

I. 2.1. Plataforma continental del golfo de Cádiz

El GoC forma una amplia cuenca semicerrada en el Atlántico Norte entre el suroeste de la península ibérica y el noroeste de África, es decir, entre el cabo de San Vicente (Portugal) y el estrecho de Gibraltar (Fig. 1.10). En esta zona, la hidrodinámica y los patrones de circulación son impulsados por el intercambio de masas de agua del océano Atlántico y del mar Mediterráneo a través del estrecho de Gibraltar e influenciados por su interacción con la costa (Bellanco y Sánchez-Leal, 2016). Las diferencias de densidad entre el agua del Atlántico, más cálida y de menor salinidad, y del Mediterráneo, de menor temperatura y mayor salinidad, dan como resultado un intercambio de dos capas: una entrada de agua superficial del Atlántico hacia el este y una salida de agua profunda del Mediterráneo hacia el oeste (Baringer y Price, 1999). Además, en el GoC circulan, principalmente, tres masas de agua, dependiendo de la profundidad (Fig. 1.11, Bellanco y Sánchez-Leal, 2016; Criado-Aldeanueva et al., 2006). El agua atlántica superficial (SAW, *surface Atlantic water*), de origen atlántico, que se extiende desde la superficie hasta la termoclina (~50 - 100 m) y se encuentra modificada por los intercambios con la atmósfera-océano. La posición de la

termoclina determina el límite de SAW, que presenta temperaturas por encima de los 16 ºC y valores de salinidad comprendidos entre 36.4 y 36.6. Por debajo de SAW, se encuentra el agua central noratlántica (eNACW, *eastern North Atlantic Central water*). Según algunos autores existen 2 variedades de NACW, una más cálida de origen subtropical ($NACW_T$) y una más fría de origen subpolar ($NACW_S$), con una temperatura promedio de 17 y 11 ºC y valores de salinidad de 35.6 y 36.5, respectivamente (Pérez et al., 2001). A partir de los ~ 400 m, por debajo de la eNACW y prácticamente hasta el fondo marino, se localiza el flujo de salida del agua mediterránea modificada (MOW, *Mediterranean Outflow Water*). La MOW presenta temperaturas inferiores a 13 ºC, una salinidad superior a 36.6 (Criado-Aldeanueva et al., 2006), y su distribución tiene una fuerte influencia de la topografía del fondo oceánico (Sánchez-Leal et al., 2017).

La circulación superficial del GoC se caracteriza por la presencia de un flujo anticiclónico desde el borde de la plataforma portuguesa hacia el este y hasta el estrecho de Gibraltar, denominada Corriente del golfo de Cádiz, muy controlada por la estacionalidad (Bellanco y Sánchez-Leal, 2016; Peliz et al., 2009). La zona central del GoC se ve afectada por la rama oriental proveniente de la corriente de las Azores (Peliz et al., 2007). Por otro lado, el GoC es una subregión del sistema de afloramiento de la corriente ibérica/canaria, pero presenta un comportamiento estacional debido a la configuración de la línea de costa y al intercambio de masas de agua con el mar Mediterráneo (Arístegui et al., 2009; Peliz et al., 2009). En consecuencia, se han identificado distintos sistemas de afloramiento*s* en la costa occidental portuguesa y en la española. Concretamente los existentes en 1) el cabo de San Vicente, de carácter casi permanente en primavera y verano, 2) el cabo de Santa María, se observa durante periodos cortos, donde

la NACW aflora favorecida por los vientos de poniente (Criado-Aldeanueva, 2004), y 3) la zona del cabo de Trafalgar, donde la interacción de la corriente de marea con la topografía del área ha sido identificada como el principal proceso responsable del transporte vertical de aguas profundas a las capas superficiales (Sala et al., 2018; Vargas-Yáñez et al., 2002). Este afloramiento es semipermanente y se encuentra favorecido por la mezcla de las capas superficiales inducida por el viento (Navarro et al., 2006; Vargas-Yáñez et al., 2002). En general, el GoC se caracteriza por condiciones oligotróficas, excepto en la zona costera, donde las concentraciones de clorofila *a* y de nutrientes son altas debido a las entradas continentales (Sala et al., 2018). Como resultado de estos procesos, el GoC se caracteriza principalmente por una elevada variabilidad fisicoquímica estacional a largo plazo (Criado-Aldeanueva et al., 2009; González-García et al., 2018).

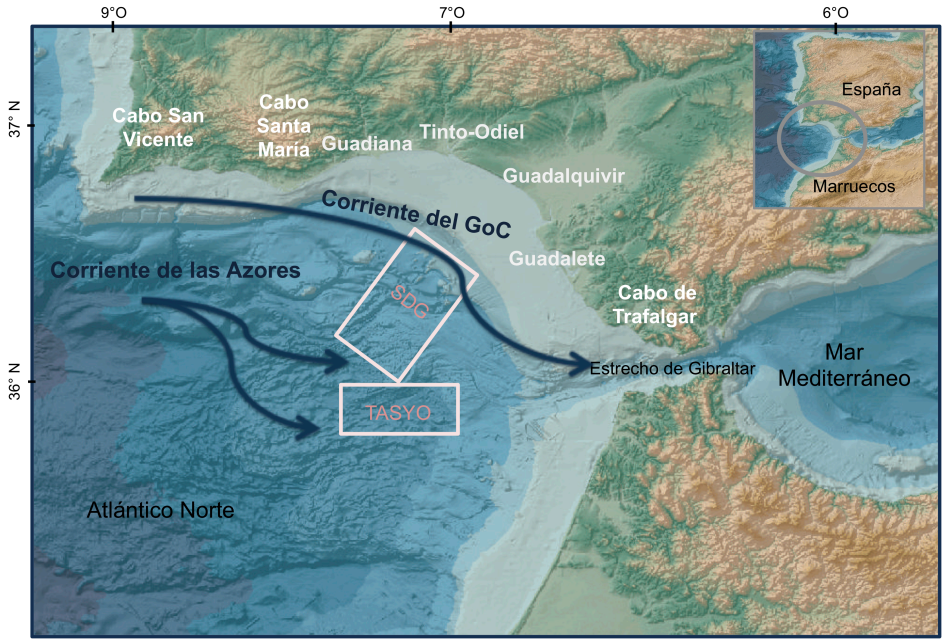

Fig. 1.10. Mapa del golfo de Cádiz indicando los principales elementos y/o fenómenos oceanográficos y geológicos que ocurren en la zona. En el límite oriental se encuentra el cabo de San Vicente y el cabo de Santa María (Portugal), seguido de los estuarios Guadiana (límite entre Portugal y España), Tinto-Odiel, Guadalquivir y Guadalete y el cabo de

Trafalgar. Se muestra la zona de influencia de la Corriente del golfo de Cádiz (costera) y de las Azores (central) así como el campo del Sistema Diapírico del Guadalquivir (SDG) y el Tasyo donde se localizan los volcanes de fango submarinos estudiados en esta tesis. Fuente: GEBCO 2020, modificado

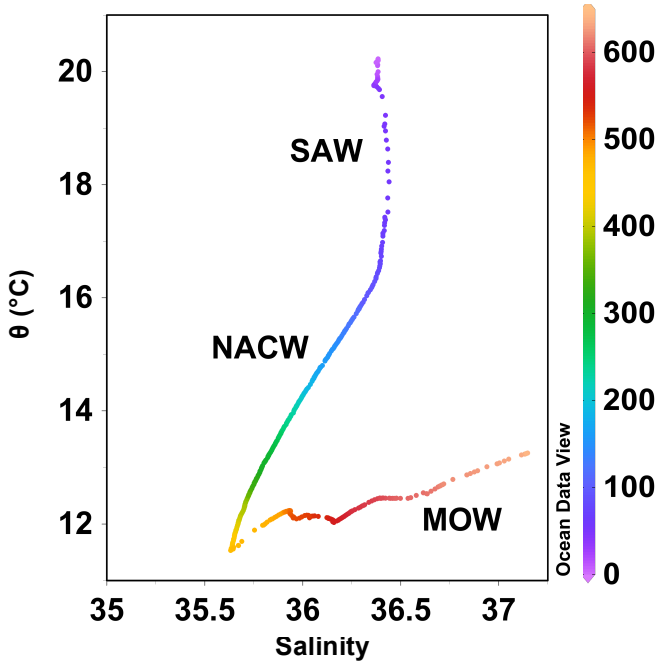

Fig. 1.11. Diagrama de salinidad y temperatura potencial (θ) indicando las principales masas de agua localizadas en el golfo de Cádiz durante los muestreos en 2016 (SAW: agua atlántica superficial, NACW: agua central noratlántica, MOW: flujo de salida del agua mediterránea).

I. 2.2. Volcanes de fango submarinos

Desde una perspectiva geológica, el GoC es una zona tectónicamente activa ubicado entre las placas de Eurasia y África, y en la parte occidental del cinturón orogénico alpino Mediterráneo, es decir, el Arco de Gibraltar (Maldonado et al., 1999). Se caracteriza por la presencia de diversas estructuras en el fondo marino del talud continental relacionadas con la emisión de fluidos ricos en hidrocarburos, como, por ejemplo, *pockmarks*, volcanes de fango, así como hidratos y carbonatos autigénicos provenientes del CH_4, como costras y chimeneas (Díaz del Río et al., 2014; Somoza et al., 2003). El origen de estas estructuras se asocia a la tectónica de compresión debido a la convergencia de las placas de Eurasia y África (Maldonado et al., 1999). Los volcanes de fango submarinos, ampliamente distribuidos en el

planeta (Milkov, 2000, 10^3 ~ 10^5), son estructuras con forma de cono, formados por la acumulación de fango y fluidos debido a erupciones periódicas provocadas por los procesos de desgasificación en depósitos más profundos (Fernández-Puga et al., 2007; Somoza et al., 2003). Las brechas de lodo contienen gases, CH_4, agua salina, lodo y, ocasionalmente petróleo, y pueden asociarse con la presencia de comunidades biológicas quimiosintéticas (Palomino et al., 2016).

En el talud continental del GoC se ha identificado más de 80 volcanes de fango submarinos (Martín-Puertas et al., 2007; Sánchez-Guillamón, 2019). En esta Tesis estudiaremos tres volcanes de fango, Anastasya, Pipoca y San Petersburgo, ubicados en dos áreas diferentes. Anastasya y Pipoca se encuentran localizados en la región del Sistema Diapírico del Guadalquivir (SDG) entre los 500 y 800 m de profundidad, mientras que el volcán San Petersburgo se sitúa en la zona Tasyo entre los 700 y 1000 m de profundidad (Fig. 1.10) (Martín-Puertas et al., 2007; Palomino et al., 2016). El volcán de fango San Petersburgo está situado a 860 m, mientras que Pipoca y Anastasya se encuentran a 500 y 460 m respectivamente. Pipoca y Anastasya presentan una estructura similar, con una base típicamente subcircular con flancos formados por depósitos de coladas de brecha fangosa, saturadas de gas y con un fuerte olor a H_2S. Anastasya mide 80 m de altura y 1.5 km de diámetro, con una depresión circular a su alrededor que alcanza unos 30 m de profundidad respecto al nivel medio del lecho marino (Fernández-Puga, 2004). Pipoca tiene una altura de 97 m y un diámetro de 2.1 km. Lo más representativo de este volcán es el conjunto de coladas que se desplazan hacia el sur a lo largo de un canal secundario a través del cual circula la MOW. Debido a esa peculiaridad, el volcán presenta flancos asimétricos y una depresión en la

parte norte de la estructura (Fernández-Puga, 2004). Por último, San Petersburgo tiene una altura de 132 m y un diámetro entre 1.8 y 2.1 km (Palomino et al., 2016).

I. 2.3. Estuarios del golfo de Cádiz: Guadalquivir, Guadiana, Tinto – Odiel y Guadalete

El GoC recibe descargas de agua dulce de los ríos Guadiana, Tinto – Odiel y Guadalquivir, que se encuentran entre el cabo de Santa María y el cabo de Trafalgar (Fig. 1.10). Las cuencas fluviales de estos ríos se encuentran en un ambiente semiárido, con periodos breves de intensas lluvias en los meses de febrero y marzo, y sequías muy marcadas con temperaturas cálidas en prácticamente la totalidad del año, típico del clima mediterráneo. Los tres estuarios están afectados por un ciclo de mareas de tipo semidiurno y de rango meso mareal. El intervalo máximo de altura durante las mareas vivas de primavera es de unos ~ 3.3 m en la desembocadura (Carro et al., 2018; Morales y Garel, 2018; Rodríguez-Ramírez et al., 2019).

Los ríos Guadalquivir y Guadiana tienen una longitud similar (680 y 810 km, respectivamente) y la descarga de agua dulce al estuario está regulado por presas. El estuario del Guadalquivir tiene una longitud de 110 km, desde la desembocadura en Sanlúcar de Barrameda hasta su límite fluvial en la presa de Alcalá del Río (Díez-Minguito et al., 2012). El ancho del estuario varía de 800 m en la desembocadura a 150 m en la cabecera (Díez-Minguito et al., 2012; Rodríguez-Ramírez et al., 2019). El río Guadalquivir es el único rio navegable de España, con una profundidad media de 7.1 m que es mantenida mediante dragados periódicos que generan episodios de elevada turbidez en el estuario (Navarro et al., 2011). La descarga del río

Guadalquivir es la más alta de la cuenca suratlántica de la península ibérica, con una media anual de 164 m^3 s^{-1} (Rodríguez-Ramírez et al., 2019), y supondrían un 90% de las entradas de aguas continentales al GoC (González-Ortegón y Drake, 2012). La cuenca del río Guadalquivir tiene una superficie de 57.527 Km^2. Una extensa zona de humedales rodea este estuario y su zona media está dominada por marismas intermareales que forman parte del Parque Nacional de Doñana (Rodríguez-Ramírez et al., 2019). Sin embargo, el Guadalquivir está sometido a una elevada presión antropogénica debido a las áreas densamente pobladas de sus márgenes (4.2 millones de personas), así como al desarrollo de las industrias agrícola y acuícola, y una alta demanda de agua dulce para riego. Los cultivos de regadío ocupan ~ 8100 Km^2 (Carrasco et al., 2010) que utilizan ~ 85% del agua extraída de este río (www.chguadalquivir.es). La construcción de embalses para satisfacer la demanda agrícola ha disminuido la entrada de agua dulce al estuario en un 60% desde 1931 al 2000, favoreciendo la paulatina salinización del río (Ruiz et al., 2015).

El Guadiana se encuentra en la frontera entre España y Portugal y su cuenca tiene una superficie de 66.960 Km^2. El estuario del Guadiana tiene una longitud de 80 km desde su desembocadura hasta la presa de Moinho dos Canais (Morales y Garel, 2019). El Guadiana es un estuario rocoso, que consta de un solo canal estrecho, que varía entre los 700 m en su desembocadura a los 70 m en la cabecera (Morales y Garel, 2019), con una profundidad promedio de 5 m que disminuye río arriba. La zona de marismas está muy reducida debido a la fuerte presión antropogénica (urbanización, agricultura, acuicultura), sin embargo, una extensa zona de humedales (~ 1000 ha) rodea su desembocadura (Ménanteau et al., 2005). Si bien la descarga anual del río Guadiana es generalmente baja (<50 m^3 s^{-1})

(Garel y Cai, 2018), es muy variable a lo largo del año con sequías severas e inundaciones episódicas en la parte baja del estuario (Garel et al., 2009). Alrededor del 70% de la descarga fluvial del Guadiana está controlada por presas (Alves et al., 2001 en Portela, 2006).

El estuario Tinto-Odiel se extiende 35 km desde su desembocadura hacia el límite de marea aguas arriba (Carro et al., 2019). Este estuario está compuesto por dos ríos, Tinto y Odiel que confluyen en una zona marina común denominada el canal del Padre Santo, que desemboca en el golfo de Cádiz. Los ríos Tinto y Odiel tienen una longitud corta de 100 y 140 km y un bajo caudal de agua dulce (5 m^3 s^{-1} y 14 m^3 s^{-1}, respectivamente). El estuario de Tinto-Odiel es un puerto industrial con una salinidad media de 37.2, considerado un brazo de mar. La cuenca fluvial de ambos ríos se encuentra principalmente sobre un área sedimentaria volcánica. Ambos ríos discurren sobre la faja pirítica ibérica, que contiene los mayores depósitos de sulfuros polimetálicos del mundo que han sido explotados desde la antigüedad (Leblanc et al., 2000). La intensa actividad minera en sus cuencas ha provocado una gran contaminación en sus aguas, que ahora contienen altas concentraciones de metales pesados (Orellana et al., 2006) y valores de pH extremadamente bajos (< 3, Grande et al., 2000). En consecuencia, la mezcla de aguas ácidas de las minas y efluentes industriales con el agua de mar conduce a cambios significativos en la composición química del agua (Carro et al., 2019).

El río Guadalete nace al norte de la Sierra de Grazalema, tiene unos 157 km de longitud y su cuenca tiene una superficie de 3766 km^2. El estuario del Guadalete tiene unos 8 km de largo, es poco profundo alcanzando una profundidad máxima de 6 m en su desembocadura en la bahía de Cádiz. Se caracteriza por la presencia de ciclos de mareas

semidiurnos, con un rango mareal promedio entre 0.98 y 3.2 m y está sujeto a una elevada presión antropogénica (Campana et al., 2005). En las proximidades del estuario se encuentra El Puerto de Santa María (88184 habitantes, año 2016) y Jerez de la Frontera (212830 habitantes, año 2016), dos de las ciudades más pobladas de la región. La estación depuradora de aguas residuales de Jerez de la Frontera descarga sus afluentes en el río. Además, recibe las descargas de granjas y extensos cultivos de regadío (remolacha azucarera, algodón, girasol, trigo y tomate) que se encuentran en sus márgenes.

Referencias

Abril, G., Borges, A.V., 2005. Carbon Dioxide and Methane Emissions from Estuaries 187–207. https://doi.org/10.1007/978-3-540-26643-38

Álvarez-Salgado, X.A., Nieto-Cid, M., Álvarez, M., Pérez, F.F., Morin, P., Mercier, H., 2013. New insights on the mineralization of dissolved organic matter in central, intermediate, and deep water masses of the northeast North Atlantic. Limnol. Oceanogr. 58, 681–696. https://doi.org/10.4319/lo.2013.58.2.0681

Amon, R.M.W., Benner, R., 1996. Bacterial Utilization of Different Size Classes of Dissolved Organc Matter. Limnol. Oceanogr. 41, 41–51.

Amon, R.M.W., Fitznar, H.P., 2001. Linkages among the bioreactivity, chemical composition, and diagenetic state of marine dissolved organic matter. Limnol. Oceanogr. 46, 287–297. https://doi.org/10.4319/lo.2001.46.2.0287

Arístegui, J., Barton, E.D., Álvarez-Salgado, X.A., Santos, A.M.P., Figueiras, F.G., Kifani, S., Hernández-León, S., Mason, E., Machú, E., Demarcq, H., 2009. Sub-regional ecosystem variability in the Canary Current upwelling. Prog. Oceanogr. 83, 33–48. https://doi.org/10.1016/j.pocean.2009.07.031

Armstrong, F.A.J., Boalch, G.T., 1961. The Ultra-Violet Absorption of Sea Water. J. mar. biol. Ass. U.K. 591–597.

Arp, D.J., Stein, L.Y., 2003. Metabolism of Inorganic N Compounds by Ammonia-Oxidizing Bacteria. Crit. Rev. Biochem. Mol. Biol. 38, 471–495. https://doi.org/10.1080/10409230390267446

Arrieta, J.M., Hansman, R.L., Herndl, G.J., Dittmar, T., Duarte, C.M., Mayol, E., 2015. Dilution limits dissolved organic carbon utilization in the deep ocean. Science. 350, 1483–1483. https://doi.org/10.1126/science.aac7249

Baker, A., Tipping, E., Thacker, S.A., Gondar, D., 2008. Relating dissolved organic matter fluorescence and functional properties. Chemosphere 73, 1765–1772. https://doi.org/10.1016/j.chemosphere.2008.09.018

Baltar, F., Alvarez-Salgado, X.A., Arístegui, J., Benner, R., Hansell, D.A., Herndl, G.J., Lønborg, C., 2021. What Is Refractory Organic Matter in the Ocean? Front. Mar. Sci. 8, 1–7. https://doi.org/10.3389/fmars.2021.642637

Bange, H.W., 2008. Gaseous Nitrogen Compounds (NO, N2O, N2, NH3) in the Ocean, Nitrogen in the Marine Environment. Elsevier Inc. https://doi.org/10.1016/B978-0-12-372522-6.00002-5

Bange, H.W., 2006. Nitrous oxide and methane in European coastal waters. Estuar. Coast. Shelf Sci. 70, 361–374. https://doi.org/10.1016/j.ecss.2006.05.042

Bange, H.W., Rapsomanik, S., Andreae, M.O., 1996. Nitrous oxide in coastal waters. Global Biogeochem. Cycles 10, 197–207. https://doi.org/10.1029/95GB03834

Baringer, M.O.N., Price, J.F., 1999. A review of the physical oceanography of the Mediterranean outflow. Mar. Geol. 155, 63–82. https://doi.org/10.1016/S0025-3227(98)00141-8

Barrón, C., Duarte, C.M., 2015. Global Biogeochemical Cycles from the coastal ocean. Global Biogeochem. Cycles 29, 1725–1738. https://doi.org/10.1002/2014GB005056.

Bauer, J.E., 2002. Chapter 8 – Carbon Isotopic Composition of DOM, in: Hansell, D.A., Carlson, C.A. (Eds.), Biogeochemistry of Marine Dissolved Organic Matter. Academic Press, San Diego, pp. 405–453. doi: 10.1016/B978–012323841–2/50010–5.

Bauer, J.E., Bianchi, T.S., 2011. Dissolved Organic Carbon Cycling and Transformation, Treatise on Estuarine and Coastal Science. Elsevier Inc. https://doi.org/10.1016/B978-0-12-374711-2.00502-7

Bellanco, M.J., Sánchez-Leal, R.F., 2016. Spatial distribution and intra-annual variability of water masses on the Eastern Gulf of Cadiz seabed. Cont. Shelf Res. 128, 26–35. https://doi.org/10.1016/j.csr.2016.09.001

Benner, R., 2002. Chapter 3 – Chemical Composition and Reactivity, in: Hansell, D.A., Carlson, C.A. (Eds.), Biogeochemistry of Marine Dissolved Organic Matter. Academic Press, San Diego, pp. 59–90. doi: 10.1016/B978–012323841–2/50005–1.

Benner, R., Amon, R.M.W., 2015. The size-reactivity continuum of major bioelements in the Ocean. Ann. Rev. Mar. Sci. 7, 185–205. https://doi.org/10.1146/annurev-marine-010213-135126

Benner, R., Biddanda, B., 1998. Photochemical transformations of surface and deep marine dissolved organic matter: Effects on bacterial growth. Limnol. Oceanogr. 43, 1373–1378. https://doi.org/10.4319/lo.1998.43.6.1373

Benner, R., Pakulski, D.J., McCarthy, M., Hedges, J.I., Hatcher, P.G., 1992. Bulk Chemical Characteristics of Dissolved Organic Matter in the Ocean. Science. 1561–1564.

Berggren, M., Laudon, H., Haei, M., Ström, L., Jansson, M., 2010. Efficient aquatic bacterial metabolism of dissolved low-molecular-weight compounds from terrestrial sources. ISME J. 4, 408–416. https://doi.org/10.1038/ismej.2009.120

Berto, S., De Laurentiis, E., Tota, T., Chiavazza, E., Daniele, P.G., Minella, M., Isaia, M., Brigante, M., Vione, D., 2016. Properties of the humic-like material arising from the photo-transformation of l-tyrosine. Sci. Total Environ. 545–546, 434–444. https://doi.org/10.1016/j.scitotenv.2015.12.047

Bianchi, T.., 2007. Biogeochemistry of estuaries.

Bižić, M., Klintzsch, T., Ionescu, D., Hindiyeh, M.Y., Günthel, M., Muro-Pastor, A.M., Eckert, W., Urich, T., Keppler, F., Grossart, H.P., 2020. Aquatic and terrestrial cyanobacteria produce methane. Sci. Adv. 6, 1–10. https://doi.org/10.1126/sciadv.aax5343

Blough, N. V., Del Vecchio, R., 2002. Chromophoric DOM in the Coastal Environment. Biogeochem. Mar. Dissolved Org. Matter 509–546. https://doi.org/10.1016/b978-012323841-2/50012-9

Borges, A. V., Abril, G., 2011. Carbon Dioxide and Methane Dynamics in Estuaries, Treatise on Estuarine and Coastal Science. https://doi.org/10.1016/B978-0-12-374711-2.00504-0

Borges, A. V., Darchambeau, F., Lambert, T., Morana, C., Allen, G., Tambwe, E., Sembaito, A.T., Mambo, T., Wabakhangazi, J.N., Descy, J.-P., Teodoru, C.R., Bouillon, S., 2019. Variations of dissolved greenhouse gases (CO2, CH4, N2O) in the Congo River network overwhelmingly driven by fluvial-wetland connectivity Alberto. Biogeosciences 16, 3801–3834. https://doi.org/10.18907/jjsre.10.22123

Bro, R., 1997. PARAFAC. Tutorial and applications. Chemom. Intell. Lab. Syst. 38, 149–171. https://doi.org/10.1016/S0169-7439(97)00032-4

Buesseler, K.O., Boyd, P.W., Black, E.E., Siegel, D.A., 2020. Metrics that matter for assessing the ocean biological carbon pump. Proc. Natl. Acad. Sci. U. S. A. 117, 9679–9687. https://doi.org/10.1073/pnas.1918114117

Burdige, D.J., Gardner, K.G., 1998. Molecular weight distribution of dissolved organic carbon in marine sediment pore waters. Mar. Chem. 62, 45–64. https://doi.org/10.1016/S0304-4203(98)00035-8

Burdige, D.J., Komada, T., 2015. Sediment Pore Waters, Biogeochemistry of Marine Dissolved Organic Matter: Second Edition. Elsevier Inc. https://doi.org/10.1016/B978-0-12-405940-5.00012-1

Burdige, D.J., Martens, C.S., 1990. Biogeochemical cycling in an organic-rich coastal marine basin: 11. The sedimentary cycling of dissolved, free amino acids. Geochim. Cosmochim. Acta 54, 3033–3052. https://doi.org/10.1016/0016-7037(90)90120-A

Cai, W.J., 2011. Estuarine and coastal ocean carbon paradox: CO 2 sinks or sites of terrestrial carbon incineration? Ann. Rev. Mar. Sci. 3, 123–145. https://doi.org/10.1146/annurev-marine-120709-142723

Campana, O., Rodríguez, A., Blasco, J., 2005. Biodisponibilidad de metales pesados en el Estuario del Río Guadalete (SO Península Ibérica). Ciencias Mar. 31, 135–147. https://doi.org/10.7773/cm.v31i12.100

Canuel, E.A., Cammer, S.S., McIntosh, H.A., Pondell, C.R., 2012. Climate change impacts on the organic carbon cycle at the land-ocean interface. Annu. Rev. Earth Planet. Sci. 40, 685–711. https://doi.org/10.1146/annurev-earth-042711-105511

Carlson, C.A., Hansell, D.A., 2015. DOM Sources, Sinks, Reactivity, and Budgets, Biogeochemistry of Marine Dissolved Organic Matter: Second Edition. https://doi.org/10.1016/B978-0-12-405940-5.00003-0

Carr, M.E., Friedrichs, M.A.M., Schmeltz, M., Noguchi Aita, M., Antoine, D., Arrigo, K.R., Asanuma, I., Aumont, O., Barber, R., Behrenfeld, M., Bidigare, R., Buitenhuis, E.T., Campbell, J., Ciotti, A., Dierssen, H., Dowell, M., Dunne, J., Esaias, W., Gentili, B., Gregg, W., Groom, S., Hoepffner, N., Ishizaka, J., Kameda, T., Le Quéré, C., Lohrenz, S., Marra, J., Mélin, F., Moore, K., Morel, A., Reddy, T.E., Ryan, J., Scardi, M., Smyth, T., Turpie, K., Tilstone, G., Waters, K., Yamanaka, Y., 2006. A comparison of global estimates of marine primary production from ocean color. Deep. Res. Part II Top. Stud. Oceanogr. 53, 741–770. https://doi.org/10.1016/j.dsr2.2006.01.028

Carrasco, J.M., Piston, J.M., Berbel, J., 2010. Evoluci.n de la productividad del agua en la Cuenca del Guadalquivir 1989-2005. Agricult. Econ. Res. 10, 59–69.

Carro, B., Borrego, J., Morales, J., 2018. Estuaries of the Huelva Coast: Odiel and Tinto Estuaries (SW Spain), in: The Spanish Coastal Systems: Dynamic Processes, Sediments and Management. p. vii. https://doi.org/10.1007/978-3-319-93169-2

Catalá, T.S., Martínez-Pérez, A.M., Nieto-Cid, M., Álvarez, M., Otero, J., Emelianov, M., Reche, I., Arístegui, J., Álvarez-Salgado, X.A., 2018. Dissolved Organic Matter (DOM) in the open Mediterranean Sea. I. Basin–wide distribution and drivers of chromophoric DOM. Prog. Oceanogr. 165, 35–51. https://doi.org/10.1016/j.pocean.2018.05.002

Catalá, T.S., Reche, I., Fuentes-Lema, A., Romera-Castillo, C., Nieto-Cid, M., Ortega-Retuerta, E., Calvo, E., Álvarez, M., Marrasé, C., Stedmon, C.A., Álvarez-Salgado, X.A., 2015. Turnover time of fluorescent dissolved organic matter in the dark global ocean. Nat. Commun. 6. https://doi.org/10.1038/ncomms6986

Chavez, F.P., Messié, M., Pennington, J.T., 2011. Marine primary production in relation to climate variability and change. Ann. Rev. Mar. Sci. 3, 227–260. https://doi.org/10.1146/annurev.marine.010908.163917

Chen, R.F., Bada, J.L., 1992. The fluorescence of dissolved organic matter in porewaters of marine sediments. Mar. Chem. 45, 31–42. https://doi.org/10.1016/0304-4203(94)90089-2

Christensen, J.P., 1994. Carbon export from continental shelves, denitrification and atmospheric carbon dioxide. Cont. Shelf Res. 14, 547–576.

https://doi.org/10.1016/0278-4343(94)90103-1
Chin, Y. P. (2003). The Speciation of Hydrophobic Organic Compounds by Dissolved Organic Matter. In S.G.E Findlay and R. L. Sinsabaugh (Eds.), Aquatic Systems: Interactivity of Dissolved Organic Matter (pp. 343-362). San Diego, CA: Academic Press.
Coble, P., 1996. Characterization of marine and terrestrial DOM in seawater using excitation-emission matrix spectroscopy. Mar. Chem. 51, 325–346.
Coble, P.G., 2007. Marine Optical Biogeochemistry: The Chemistry of Ocean Color. Chem. Rev. 107, 402–418. https://doi.org/10.1021/cr050350+
Coble, P.G., Green, S.A., Blough, N. V., Gagosian, R.B., 1990. Characterization of dissolved organic matter in the Black Sea by fluorescence spectroscopy. Nature. https://doi.org/10.1038/348432a0
Coble, P.G., Lead, J., Baker, A., Reynolds, D.M., Spencer, R.G.M., 2014. Aquatic Organic Matter Fluorescence.
Coffin, R.B., 1989. Bacterial uptake of dissolved free and combined amino acids in estuarine waters. Limnol. Oceanogr. 34, 531–542. https://doi.org/10.4319/lo.1989.34.3.0531
Cole, J.J., Prairie, Y.T., Caraco, N.F., McDowell, W.H., Tranvik, L.J., Striegl, R.G., Duarte, C.M., Kortelainen, P., Downing, J.A., Middelburg, J.J., Melack, J., 2007. Plumbing the global carbon cycle: Integrating inland waters into the terrestrial carbon budget. Ecosystems 10, 171–184. https://doi.org/10.1007/s10021-006-9013-8
Cowie, G.L., Hedges, J.I., 1992. Sources and reactivities of amino acids in a coastal marine environment. Limnol. Oceanogr. 37, 703–724. https://doi.org/10.4319/lo.1992.37.4.0703
Criado-Aldeanueva, F., 2004. Distribución y circulación de masas de agua en el Golfo de Cádiz. Variabilidad inducida por el forzamiento meteorológico. PhD Thesis, University of Málaga, Spain, 271 pp.
Criado-Aldeanueva, F., Garcia-Lafuente, J., Navarro, G., Ruiz, J., 2009. Seasonal and interannual variability of the surface circulation in the eastern Gulf of Cadiz (SW Iberia). J. Geophys. Res. Ocean. 114, 1–11. https://doi.org/10.1029/2008JC005069
Criado-Aldeanueva, F., García-Lafuente, J., Vargas, J.M., Del Río, J., Vázquez, A., Reul, A., Sánchez, A., 2006. Distribution and circulation of water masses in the Gulf of Cadiz from in situ observations. Deep. Res. Part II Top. Stud. Oceanogr. 53, 1144–1160. https://doi.org/10.1016/j.dsr2.2006.04.012
Cuss, C.W., Guéguen, C., 2015. Relationships between molecular weight and fluorescence properties for size-fractionated dissolved organic matter from fresh and aged sources. Water Res. 68, 487–497. https://doi.org/10.1016/j.watres.2014.10.013
Daniel, I., DeGrandpre, M., Farías, L., 2013. Greenhouse gas emissions from the Tubul-Raqui estuary (central Chile 36°S). Estuar. Coast. Shelf Sci. 134, 31–44. https://doi.org/10.1016/j.ecss.2013.09.019
Dauwe, B., Middelburg, J.J., Herman, P.M.J., Heip, C.H.R., 1999. Linking diagenetic alteration of amino acids and bulk organic matter reactivity. Limnol. Oceanogr. 44, 1809–1814. https://doi.org/10.4319/lo.1999.44.7.1809
Díaz del Río, V., Bruque, G., Fernandez-Salas, L.M., Rueda, J.L., Gonzalez, E., Loopez, N., Palomino, D., Lopez, F.J., Farias, C., Sanchez, R., Vazquez, J.T., Rittierott, C.C., Fernandez, A., Pablo Marina, V., 2014. Volcanes de Fango del Golfo de Cádiz 132.
Díez-Minguito, M., Baquerizo, A., Ortega-Sánchez, M., Navarro, G., Losada, M.A., 2012. Tide transformation in the Guadalquivir estuary (SW Spain) and process-based zonation. J. Geophys. Res. Ocean. 117, 1–14.

https://doi.org/10.1029/2011JC007344
Dittmar, T., 2015. Reasons Behind the Long-Term Stability of Dissolved Organic Matter, Second Edi. ed, Biogeochemistry of Marine Dissolved Organic Matter: Second Edition. Elsevier Inc. https://doi.org/10.1016/B978-0-12-405940-5.00007-8
Dittmar, T., Koch, B.P., 2006. Thermogenic organic matter dissolved in the abyssal ocean. Mar. Chem. 102, 208–217. https://doi.org/10.1016/j.marchem.2006.04.003
Donis, D., Flury, S., Stöckli, A., Spangenberg, J.E., Vachon, D., McGinnis, D.F., 2017. Full-scale evaluation of methane production under oxic conditions in a mesotrophic lake. Nat. Commun. 8. https://doi.org/10.1038/s41467-017-01648-4
Dunne, J.P., Sarmiento, J.L., Gnanadesikan, A., 2007. A synthesis of global particle export from the surface ocean and cycling through the ocean interior and on the seafloor. Global Biogeochem. Cycles 21, 1–16. https://doi.org/10.1029/2006GB002907
Elderfield, H., 2002. Carbonate Mysteries. Science. 296, 1618–1620.
Feely, R.A., Sabine, C.L., Lee, K., Berelson, W., 2004. Impact of anthropogenic CO_2 on the $CaCO_3$ system in the oceans. Science. 305, 362–366.
Fernández-Puga, M. C., 2004. Diapirismo y estructuras de expulsión de gases hidrocarburos en el talud continental del Golfo de Cádiz. PhD Thesis. Facultad de Ciencias del Mar, University of Cádiz, Spain, 336 pp.
Fernández-Puga, M.C., Vázquez, J.T., Somoza, L., Díaz del Rio, V., Medialdea, T., Mata, M.P., León, R., 2007. Gas-related morphologies and diapirism in the Gulf of Cádiz. Geo-Marine Lett. 27, 213–221. https://doi.org/10.1007/s00367-007-0076-0
Fichot, C.G., Benner, R., 2012. The spectral slope coefficient of chromophoric dissolved organic matter (S275-295) as a tracer of terrigenous dissolved organic carbon in river-influenced ocean margins . Limnol. Oceanogr. 57, 1453–1466. https://doi.org/10.4319/lo.2012.57.5.1453
Fichot, C.G., Benner, R., Kaiser, K., Shen, Y., Amon, R.M.W., Ogawa, H., Lu, C.J., 2016. Predicting dissolved lignin phenol concentrations in the coastal ocean from chromophoric dissolved organic matter (CDOM) absorption coefficients. Front. Mar. Sci. 3, 1–15. https://doi.org/10.3389/fmars.2016.00007
Garel, E., Cai, H., 2018. Effects of Tidal-Forcing Variations on Tidal Properties Along a Narrow Convergent Estuary. Estuaries and Coasts 41, 1924–1942. https://doi.org/10.1007/s12237-018-0410-y
Garel, E., Pinto, L., Santos, A., Ferreira, Ó., 2009. Tidal and river discharge forcing upon water and sediment circulation at a rock-bound estuary (Guadiana estuary, Portugal). Estuar. Coast. Shelf Sci. 84, 269–281. https://doi.org/10.1016/j.ecss.2009.07.002
Gattuso, J., Frankignoulle, M., Wollast, R., 1998. Carbon and carbonate metabolism in coastal aquatic ecosystems. Annu. Rev. Ecol. Syst. 29, 405–434.
González-García, C., Forja, J., González-Cabrera, M.C., Jiménez, M.P., Lubián, L.M., 2018. Annual variations of total and fractionated chlorophyll and phytoplankton groups in the Gulf of Cadiz. Sci. Total Environ. 613–614, 1551–1565. https://doi.org/10.1016/j.scitotenv.2017.08.292
González-Ortegón, E., Drake, P., 2012. Effects of freshwater inputs on the lower trophic levels of a temperate estuary: Physical, physiological or trophic forcing? Aquat. Sci. 74, 455–469. https://doi.org/10.1007/s00027-011-0240-5
Grande, J.A., Borrego, J., Morales, J.A., 2000. A study of heavy metal pollution in the Tinto-Odiel estuary in southwestern Spain using factor analysis. Environ. Geol. 39 (10), 1095–1101.
Gruber, N., Clement, D., Carter, B.R., Feely, R.A., van Heuven, S., Hoppema, M., Ishii, M., Key, R.M., Kozyr, A., Lauvset, S.K., Monaco, C. Lo, Mathis, J.T., Murata, A.,

Olsen, A., Perez, F.F., Sabine, C.L., Tanhua, T., Wanninkhof, R., 2019. The oceanic sink for anthropogenic CO 2 from 1994 to 2007. Science. 363, 1193–1199. https://doi.org/10.1126/science.aau5153

Guo, W., Stedmon, C.A., Han, Y., Wu, F., Yu, X., Hu, M., 2007. The conservative and non-conservative behavior of chromophoric dissolved organic matter in Chinese estuarine waters. Mar. Chem. 107, 357–366. https://doi.org/10.1016/j.marchem.2007.03.006

Hansell, D.A., 2013. Recalcitrant dissolved organic carbon fractions. Ann. Rev. Mar. Sci. 5, 421–445. https://doi.org/10.1146/annurev-marine-120710-100757

Hansell, D.A., Carlson, C.A.., Repeta, D.J.. R., Schlitzer, R., 2009. Dissolved Organic Matter in the Ocean. Oceanography 22.

Hedges, J.I., 2002. Why Dissolved Organics Matter, Biogeochemistry of Marine Dissolved Organic Matter. Elsevier Inc. https://doi.org/10.1016/b978-012323841-2/50003-8

Hedges, J.I., Hare, P.E., 1987. Amino acid adsorption by clay minerals in distilled water. Geochim. Cosmochim. Acta 51, 255–259. https://doi.org/10.1016/0016-7037(87)90237-7

Hedges, J.I., Keil, R.G., Benner, R., 1997. What happens to terrestrial organic matter in the ocean? Org. Geochem. 27, 195–212. https://doi.org/10.1016/S0146-6380(97)00066-1

Helms, J.R., Kieber, D.J., Minor, E.C., Ritchie, J.D., Stubbins, A., Mopper, K., 2008. Absorption spectral slopes and slope ratios as indicators of molecular weight, source, and photobleaching of chromophoric dissolved organic matter. Limnol. Oceanogr. 53, 955–969. https://doi.org/10.4319/lo.2008.53.3.0955

Herndl, G.J., Müller-Niklas, G., Frick, J., 1993. Major role of ultraviolet-B in controlling bacterioplankton growth in the surface layer of the ocean. Nature 361, 717–719. https://doi.org/10.1038/361717a0

Hernes, P.J., Bergamaschi, B.A., Eckard, R.S., Spencer, R.G.M., 2009. Fluorescence-based proxies for lignin in freshwater dissolved organic matter. J. Geophys. Res. Biogeosciences 114, 1–10. https://doi.org/10.1029/2009JG000938

Hertkorn, N., Harir, M., Koch, B.P., Michalke, B., Schmitt-Kopplin, P., 2013. High-field NMR spectroscopy and FTICR mass spectrometry: Powerful discovery tools for the molecular level characterization of marine dissolved organic matter. Biogeosciences 10, 1583–1624. https://doi.org/10.5194/bg-10-1583-2013

Huguet, A., Vacher, L., Relexans, S., Saubusse, S., Froidefond, J.M., Parlanti, E., 2009. Properties of fluorescent dissolved organic matter in the Gironde Estuary. Org. Geochem. 40, 706–719. https://doi.org/10.1016/j.orggeochem.2009.03.002

Hygum, B.H., Petersen, J.W., Søndergaard, M., 1997. Dissolved organic carbon released by zooplankton grazing activity - A high-quality substrate pool for bacteria. J. Plankton Res. 19, 97–111. https://doi.org/10.1093/plankt/19.1.97

IPCC [Intergovernmental Panel of Climate Change], 2013. (Stocker, T.F., Qin, D., Plattner, G.K., Tignor, M., Allen, S.K., Boschung, J., Nauels, A., Xia, Y., Bex, V., Midgley, P.M., Eds.) Climate Change 2013: The Physical Science Basis. Contribution of Working Group I to the Fifth Assessment Report of the IPCC. Cambridge University Press, Cambridge, United Kingdom and New York, NY, USA, 1535p.

Iturriaga, R., Zsolnay, A., 1981. Transformation of some dissolved organic compounds by a natural heterotrophic population. Mar. Biol. 62, 125–129. https://doi.org/10.1007/BF00388174

Jaffé, R., Boyer, J.N., Lu, X., Maie, N., Yang, C., Scully, N.M., Mock, S., 2004. Source

characterization of dissolved organic matter in a subtropical mangrove-dominated estuary by fluorescence analysis. Mar. Chem. 84, 195–210. https://doi.org/10.1016/j.marchem.2003.08.001

Jiang, T., Kaal, J., Liang, J., Zhang, Y., Wei, S., Wang, D., Green, N.W., 2017. Composition of dissolved organic matter (DOM) from periodically submerged soils in the Three Gorges Reservoir areas as determined by elemental and optical analysis, infrared spectroscopy, pyrolysis-GC–MS and thermally assisted hydrolysis and methylation. Sci. Total Environ. 603–604, 461–471. https://doi.org/10.1016/j.scitotenv.2017.06.114

Jiao, N., Herndl, G.J., Hansell, D.A., Benner, R., Kattner, G., Wilhelm, S.W., Kirchman, D.L., Weinbauer, M.G., Luo, T., Chen, F., Azam, F., 2010. Microbial production of recalcitrant dissolved organic matter: long-term carbon storage in the global ocean. Nat. Rev. Microbiol. 8, 593–599. https://doi.org/10.1038/nrmicro2386

Jørgensen, L., Stedmon, C.A., Kragh, T., Markager, S., Middelboe, M., Søndergaard, M., 2011. Global trends in the fluorescence characteristics and distribution of marine dissolved organic matter. Mar. Chem. 126, 139–148. https://doi.org/10.1016/j.marchem.2011.05.002

Jørgensen, N.O.G., Tranvik, L.J., Berg, G.M., 1999. Occurrence and bacterial cycling of dissolved nitrogen in the Gulf of Riga, the Baltic Sea. Mar. Ecol. Prog. Ser. 191, 1–18. https://doi.org/10.3354/meps191001

Kaal, J., 2019. Analytical pyrolysis in marine environments revisited. Anal. Pyrolysis Lett. 1–16.

Kaal, J., Cortizas, A.M., Biester, H., 2017. Downstream changes in molecular composition of DOM along a headwater stream in the Harz mountains (Central Germany) as determined by FTIR, Pyrolysis-GC–MS and THM-GC–MS. J. Anal. Appl. Pyrolysis 126, 50–61. https://doi.org/10.1016/j.jaap.2017.06.025

Kaal, J., Wagner, S., Jaffé, R., 2016. Molecular properties of ultrafiltered dissolved organic matter and dissolved black carbon in headwater streams as determined by pyrolysis-GC-MS. J. Anal. Appl. Pyrolysis 118, 181–191. https://doi.org/10.1016/j.jaap.2016.02.003

Karl, D.M., Beversdorf, L., Björkman, K.M., Church, M.J., Martinez, A., Delong, E.F., 2008. Aerobic production of methane in the sea. Nat. Geosci. 1, 473–478. https://doi.org/10.1038/ngeo234

Kawasaki, N., Benner, R., 2006. Bacterial release of dissolved organic matter during cell growth and decline: Molecular origin and composition. Limnol. Oceanogr. 51, 2170–2180. https://doi.org/10.4319/lo.2006.51.5.2170

Keil, R., and Kirchman, D. (1991) Contribution of dissolved free amino acids and ammonium to the nitrogen requirements of heterotrophic bacterioplankton. Mar. Ecol. Prog. Ser. 72, 1–10.

Keil, R.G., Kirchman, D.L., 1999. Utilization of dissolved protein and amino acids in the northern Sargasso Sea. Aquat. Microb. Ecol. 18, 293–300. https://doi.org/10.3354/ame018293

Keil, R.G., Kirchman, D.L., 1993. Dissolved combined amino acids: Chemical form and utilization by marine bacteria. Limnol. Oceanogr. 38, 1256–1270. https://doi.org/10.4319/lo.1993.38.6.1256

Kieber, R.J., Hydro, L.H., Seaton, P.J., 1997. Photooxidation of triglycerides and fatty acids in seawater: Implication toward the formation of marine humic substances. Limnol. Oceanogr. 42, 1454–1462. https://doi.org/10.4319/lo.1997.42.6.1454

Kim, H.C., Lee, K., 2009. Significant contribution of dissolved organic matter to seawater

alkalinity. Geophys. Res. Lett. 36, 1–5. https://doi.org/10.1029/2009GL040271
Kirk, J.T.O., 1994. Light and photosynthesis in aquatic ecosystems. Light Photosynth. Aquat. Ecosyst. https://doi.org/10.2307/2405114
Komada, T., Reimers, C.E., 2001. Resuspension-induced partitioning of organic carbon between solid and solution phases from a river - Ocean transition. Mar. Chem. 76, 155–174. https://doi.org/10.1016/S0304-4203(01)00055-X
Kowalczuk, P., Tilstone, G.H., Zabłocka, M., Röttgers, R., Thomas, R., 2013. Composition of dissolved organic matter along an Atlantic Meridional Transect from fluorescence spectroscopy and Parallel Factor Analysis. Mar. Chem. 157, 170–184. https://doi.org/10.1016/j.marchem.2013.10.004
Kowalczuk, P., Zabłocka, M., Sagan, S., Kuliński, K., 2010. Fluorescence measured in situ as a proxy of CDOM absorption and DOC concentration in the Baltic Sea. Oceanologia 52, 431–471. https://doi.org/10.5697/oc.52-3.431
Kramer, G. D., & Herndl, G. J. (2004). Photo-and bioreactivity of chromophoric dissolved organic matter produced by marine bacterioplankton. *Aquatic microbial ecology*, *36*(3), 239-246.
Le Quéré, C., Moriarty, R., Andrew, R.M., Canadell, J.G., Sitch, S., Korsbakken, J.I., Friedlingstein, P., Peters, G.P., Andres, R.J., Boden, T.A., Houghton, R.A., House, J.I., Keeling, R.F., Tans, P., Arneth, A., Bakker, D.C.E., Barbero, L., Bopp, L., Chang, J., Chevallier, F., Chini, L.P., Ciais, P., Fader, M., Feely, R.A., Gkritzalis, T., Harris, I., Hauck, J., Ilyina, T., Jain, A.K., Kato, E., Kitidis, V., Klein Goldewijk, K., Koven, C., Landschützer, P., Lauvset, S.K., Lefèvre, N., Lenton, A., Lima, I.D., Metzl, N., Millero, F., Munro, D.R., Murata, A., S. Nabel, J.E.M., Nakaoka, S., Nojiri, Y., O'Brien, K., Olsen, A., Ono, T., Pérez, F.F., Pfeil, B., Pierrot, D., Poulter, B., Rehder, G., Rödenbeck, C., Saito, S., Schuster, U., Schwinger, J., Séférian, R., Steinhoff, T., Stocker, B.D., Sutton, A.J., Takahashi, T., Tilbrook, B., Van Der Laan-Luijkx, I.T., Van Der Werf, G.R., Van Heuven, S., Vandemark, D., Viovy, N., Wiltshire, A., Zaehle, S., Zeng, N., 2015. Global Carbon Budget 2015. Earth Syst. Sci. Data 7, 349–396. https://doi.org/10.5194/essd-7-349-2015
Leblanc, M., Morales, J.A., Borrego, J., Elbaz-Poulichet, F., 2000. 4,500-year-old mining pollution in southwestern Spain: Long-term implications for modern mining pollution. Econ. Geol. 95, 655–661. https://doi.org/10.2113/gsecongeo.95.3.655
Lee, C., Bada, J.L., 1977. Dissolved amino acids in the equatorial Pacific, the Sargasso Sea, and Biscayne Bay. Limnol. Oceanogr. 22, 502–510. https://doi.org/10.4319/lo.1977.22.3.0502
Lee, C., Bada, J.L., 1975. Amino acids in equatorial Pacific Ocean water. Earth Planet. Sci. Lett. 26, 61–68. https://doi.org/10.1016/0012-821X(75)90177-6
Li, Y., Fichot, C.G., Geng, L., Scarratt, M.G., Xie, H., 2020. The Contribution of Methane Photoproduction to the Oceanic Methane Paradox. Geophys. Res. Lett. 47, 0–2. https://doi.org/10.1029/2020GL088362
Liikanen, A., Silvennoinen, H., Karvo, A., Rantakokko, P., Martikainen, P.J., 2009. Methane and nitrous oxide fluxes in two coastal wetlands in the northeastern Gulf of Bothnia, Baltic Sea. Boreal Environ. Res. 14, 351–368.
Lindroth, P., Mopper, K., 1979. High Performance Liquid Chromatographic Determination of Subpicomole Amounts of Amino Acids by Precolumn Fluorescence Derivatization with o-Phthaldialdehyde. Anal. Chem. 51, 1667–1674. https://doi.org/10.1021/ac50047a019
Lønborg, C., Álvarez-Salgado, X.A., 2014. Tracing dissolved organic matter cycling in the eastern boundary of the temperate North Atlantic using absorption and fluorescence

spectroscopy. Deep. Res. Part I Oceanogr. Res. Pap. 85, 35–46. https://doi.org/10.1016/j.dsr.2013.11.002

Lønborg, C., Carreira, C., Jickells, T., Álvarez-Salgado, X.A., 2020. Impacts of Global Change on Ocean Dissolved Organic Carbon (DOC) Cycling. Front. Mar. Sci. 7, 1–24. https://doi.org/10.3389/fmars.2020.00466

Mackenzie, F.T., 1999. Global Biogeochemical Cycles and the Physical Climate System. Global Change Instruction Program, University Corporation for Atmospheric Research (UCAR), Boulder, Colorado.

Maldonado, A., Somoza, L., Pallarés, L., 1999. The Betic orogen and the Iberian-African boundary in the Gulf of Cadiz: Geological evolution (central North Atlantic). Mar. Geol. 155, 9–43. https://doi.org/10.1016/S0025-3227(98)00139-X

Martín-Puertas, C., Mata, M.P., Fernández-Puga, M.C., Díaz del Río, V., Vázquez, J.T., Somoza, L., 2007. A comparative mineralogical study of gas-related sediments of the Gulf of Cádiz. Geo-Marine Lett. 27, 223–235. https://doi.org/10.1007/s00367-007-0075-1

Menanteau, L., C.line, C., Choblet, C., 2005. Les marais du Bas-Guadiana (Algarve, Andalousie): emprise, d.prise et reprise humaines. Aestuaria 9, 309–331.

Milkov, A. V., 2000. Worldwide distribution of submarine mud volcanoes and associated gas hydrates. Mar. Geol. 167, 29–42. https://doi.org/10.1016/S0025-3227(00)00022-0

Mopper, K., Kieber, D.J., Stubbins, A., 2015. Marine Photochemistry of Organic Matter: Processes and Impacts. Processes and Impacts., Second Edi. ed, Biogeochemistry of Marine Dissolved Organic Matter: Second Edition. Elsevier Inc. https://doi.org/10.1016/B978-0-12-405940-5.00008-X

Morales, J.A., Garel, E., 2018. The Guadiana River Delta, The Spanish Coastal Systems: Dynamic Processes, Sediments and Management. Springer International Publishing. https://doi.org/10.1007/978-3-319-93169-2

Moran, M.A., Kujawinski, E.B., Stubbins, A., Fatland, R., Aluwihare, L.I., Buchan, A., Crump, B.C., Dorrestein, P.C., Dyhrman, S.T., Hess, N.J., Howe, B., Longnecker, K., Medeiros, P.M., Niggemann, J., Obernosterer, I., Repeta, D.J., Waldbauer, J.R., 2016. Deciphering ocean carbon in a changing world. Proc. Natl. Acad. Sci. U. S. A. 113, 3143–3151. https://doi.org/10.1073/pnas.1514645113

Moran, M.A., Zepp, R.G., 1997. Role of photoreactions in the formation of biologically labile compounds from dissolved organic matter. Limnol. Oceanogr. 42, 1307–1316. https://doi.org/10.4319/lo.1997.42.6.1307

Moran Mary Ann, A., Wade M. Sheldon, J. author, Richard G. Zepp, A., 2000. Carbon Loss and Optical Property Changes during Long-Term Photochemical and Biological Degradation of Estuarine Dissolved Organic Matter. Limnol. Oceanogr. 45, 1254.

Murray, R.H., Erler, D. V., Eyre, B.D., 2015. Nitrous oxide fluxes in estuarine environments: Response to global change, Global Change Biology. https://doi.org/10.1111/gcb.12923

Navarro, G., Gutiérrez, F.J., Díez-Minguito, M., Losada, M.A., Ruiz, J., 2011. Temporal and spatial variability in the Guadalquivir estuary: A challenge for real-time telemetry. Ocean Dyn. 61, 753–765. https://doi.org/10.1007/s10236-011-0379-6

Navarro, G., Ruiz, J., Huertas, I.E., García, C.M., Criado-Aldeanueva, F., Echevarría, F., 2006. Basin-scale structures governing the position of the deep fluorescence maximum in the Gulf of Cádiz. Deep. Res. Part II Top. Stud. Oceanogr. 53, 1261–1281. https://doi.org/10.1016/j.dsr2.2006.04.013

Nelson, N.B., Siegel, D.A., 2013. The Global Distribution and Dynamics of

Chromophoric Dissolved Organic Matter. Ann. Rev. Mar. Sci. 5, 447–476. https://doi.org/10.1146/annurev-marine-120710-100751

Nelson, N.B., Siegel, D.A., Carlson, C.A., Swan, C.M., 2010. Tracing global biogeochemical cycles and meridional overturning circulation using chromophoric dissolved organic matter. Geophys. Res. Lett. 37, n/a-n/a. https://doi.org/10.1029/2009gl042325

Nevison, C., Butler, J.H., Elkins, J.W., 2003. Global distribution of N2O and the ΔN2O-AOU yield in the subsurface ocean. Global Biogeochem. Cycles 17, 1–18. https://doi.org/10.1029/2003gb002068

Obernosterer, I., Benner, R., 2004. Competition between biological and photochemical processes in the mineralization of dissolved organic carbon. Limnol. Oceanogr. 49, 117–124.

Officer, C.B., 1979. Discussion of the Behaviorur of Nonconservative Dissolved Constituents in Estuaries. Estuarine and Coastal Marine Science 9, 91-94.

Ogawa, H., Amagai, Y., Koike, I., Kaiser, K., Benner, R., 2001. Production of refractory dissolved organic matter by bacteria. Science. 292, 917–920. https://doi.org/10.1126/science.1057627

OMM [Organización Meteorológica Mundial], 2019. Boletín de la OMM sobre los gases de efecto invernadero. Estado de los gases de efecto invernadero en la atmósfera según las observaciones mundiales realizadas en 2019. Organización Meteorológica Mundial. ISSN 2078-0796

Opsahl, S., Benner, R., 1997. Distribution and cycling of terrigenous dissolved organic matter in the ocean. Nature 386, 480–482.

Orellana, F., Santillana, E., González, J., Alegre, R., 2006. De Metales Pesados Transportada Por Los Ríos Tinto Y Odiel (Huelva) 69–78.

Ortega-Retuerta, E., Frazer, T.K., Duarte, C.M., Ruiz-Halpern, S., Tovar-Sańchez, A., Arrieta, J.M., Reche, I., 2009. Biogeneration of chromophoric dissolved organic matter by bacteria and krill in the southern ocean. Limnol. Oceanogr. 54, 1941–1950. https://doi.org/10.4319/lo.2009.54.6.1941

Palomino, D., López-González, N., Vázquez, J.T., Fernández-Salas, L.M., Rueda, J.L., Sánchez-Leal, R., Díaz-del-Río, V., 2016. Multidisciplinary study of mud volcanoes and diapirs and their relationship to seepages and bottom currents in the Gulf of Cádiz continental slope (northeastern sector). Mar. Geol. 378, 196–212. https://doi.org/10.1016/j.margeo.2015.10.001

Peliz, A., Dubert, J., Marchesiello, P., Teles-Machado, A., 2007. Surface circulation in the Gulf of Cadiz: Model and mean flow structure. J. Geophys. Res. Ocean. 112, 1–20. https://doi.org/10.1029/2007JC004159

Peliz, A., Marchesiello, P., Santos, A.M.P., Dubert, J., Teles-Machado, A., Marta-Almeida, M., Le Cann, B., 2009. Surface circulation in the Gulf of Cadiz: 2. Inflow-outflow coupling and the Gulf of Cadiz slope current. J. Geophys. Res. Ocean. 114, 1–16. https://doi.org/10.1029/2008JC004771

Peltier, W.R., Liu, Y., Crowley, J.W., 2007. Snowball Earth prevention by dissolved organic carbon remineralization. Nature 450, 813–818. https://doi.org/10.1038/nature06354

Pérez, F.F., Castro, C.G., Álvarez-Salgado, X.A., Ríos, A.F., 2001. Coupling between the Iberian basin - Scale circulation and the Portugal boundary current system: A chemical study. Deep. Res. Part I Oceanogr. Res. Pap. 48, 1519–1533. https://doi.org/10.1016/S0967-0637(00)00101-1

Portela, L., 2006. Calculation of Sediment Delivery from the Guadiana Estuary to the Coastal. J. Coast. Res. 1819–1823.

Raymond, P.A., Spencer, R.G.M., 2015. Riverine DOM. Biogeochem. Mar. Dissolved Org. Matter Second Ed. 509–533. https://doi.org/10.1016/B978-0-12-405940-5.00011-X

Reeburgh, W.S., 2003. Global methane biogeochemistry. Treatise on Geochemistry 4, 65-89.

Repeta, D.J., 2015. Chemical Characterization and Cycling of Dissolved Organic Matter, Second Edi. ed, Biogeochemistry of Marine Dissolved Organic Matter: Second Edition. Elsevier Inc. https://doi.org/10.1016/B978-0-12-405940-5.00002-9

Repeta, D.J., Ferrón, S., Sosa, O.A., Johnson, C.G., Repeta, L.D., Acker, M., Delong, E.F., Karl, D.M., 2016. Marine methane paradox explained by bacterial degradation of dissolved organic matter. Nat. Geosci. 9, 884–887. https://doi.org/10.1038/ngeo2837

Retelletti, S., Kim, J.H., Ryu, J.S., Jin, Y.K., Lee, Y.K., Hur, J., 2019. Exploring sediment porewater dissolved organic matter (DOM) in a mud volcano: Clues of a thermogenic DOM source from fluorescence spectroscopy. Mar. Chem. 211, 15–24. https://doi.org/10.1016/j.marchem.2019.03.009

Ridgwell, A., Arndt, S., 2015. Why Dissolved Organics Matter: DOC in Ancient Oceans and Past Climate Change, Second Edi. ed, Biogeochemistry of Marine Dissolved Organic Matter: Second Edition. Elsevier Inc. https://doi.org/10.1016/B978-0-12-405940-5.00001-7

Rochelle-Newall, E., Hulot, F.D., Janeau, J.L., Merroune, A., 2014. CDOM fluorescence as a proxy of DOC concentration in natural waters: A comparison of four contrasting tropical systems. Environ. Monit. Assess. 186, 589–596. https://doi.org/10.1007/s10661-013-3401-2

Rochelle-Newall, E.J., Fisher, T.R., 2002. Chromophoric dissolved organic matter and dissolved organic carbon in Chesapeake Bay. Mar. Chem. 77, 23–41. https://doi.org/10.1016/S0304-4203(01)00073-1

Rodhe, H., 1990. A Comparison of the Contribution of Various Gases. Science. 248, 1217–1219.

Rodríguez-Ramírez, A., Villar.as-Robles, J.J.R., Pérez-Asensio, J.N., Celestino-Pérez, S.,2019. The Guadalquivir Estuary: Spits and Marshes. In: The Spanish Coastal Systems, pp. 517–541.

Romera-Castillo, C., Jaffé, R., 2015. Free radical scavenging (antioxidant activity) of natural dissolved organic matter. Mar. Chem. 177, 668–676. https://doi.org/10.1016/j.marchem.2015.10.008

Romera-Castillo, C., Sarmento, H., Álvarez-Salgado, X.A., Gasol, J.M., Marrasé, C., 2010. Production of chromophoric dissolved organic matter by marine phytoplankton. Limnol. Oceanogr. 55, 1466–1466. https://doi.org/10.4319/lo.2010.55.3.1466

Rosentreter, J.A., Borges, A. V., Deemer, B.R., Holgerson, M.A., Liu, S., Song, C., Melack, J., Raymond, P.A., Duarte, C.M., Allen, G.H., Olefeldt, D., Poulter, B., Battin, T.I., Eyre, B.D., 2021. Half of global methane emissions come from highly variable aquatic ecosystem sources. Nat. Geosci. 14, 225–230. https://doi.org/10.1038/s41561-021-00715-2

Ruiz, J., Polo, M. J., Díez-Minguito, M., Navarro, G., Morris, E. P., Huertas, E., Caballero, I., Contreras, E., Losada, M. A. (2015). The Guadalquivir estuary: a hot spot for environmental and human conflicts. In *Environmental Management and Governance*, p. 199-232, Springer, Cham.

Sala, I., Navarro, G., Bolado-Penagos, M., Echevarría, F., García, C.M., 2018. High-chlorophyll-area assessment based on remote sensing observations: The case study of

Cape Trafalgar. Remote Sens. 10. https://doi.org/10.3390/rs10020165
Sánchez-Guillamón, O., 2019. Deep Submarine volcanoes in two geodynamic settings (Canary Basin and Gulf of Cádiz): Morphology and shallow structure.
Sánchez-Leal, R.F., Bellanco, M.J., Fernández-Salas, L.M., García-Lafuente, J., Gasser-Rubinat, M., González-Pola, C., Hernández-Molina, F.J., Pelegrí, J.L., Peliz, A., Relvas, P., Roque, D., Ruiz-Villarreal, M., Sammartino, S., Sánchez-Garrido, J.C., 2017. The Mediterranean Overflow in the Gulf of Cadiz: A rugged journey. Sci. Adv. 1–12. https://doi.org/10.1126/sciadv.aao0609
Sarmento, H., Romera-Castillo, C., Lindh, M., Pinhassi, J., Sala, M.M., Gasol, J.M., Marrasé, C., Taylor, G.T., 2013. Phytoplankton species-specific release of dissolved free amino acids and their selective consumption by bacteria. Limnol. Oceanogr. 58, 1123–1135. https://doi.org/10.4319/lo.2013.58.3.1123
Sarmiento, J. L., & Gruber, N. Ocean Biogeochemical Dynamics
Schlesinger, W.H. (1997) Biogeochemistry: an Analysis of Global Change. New York: Academic Press.
Seitzinger, S.P., Kroeze, C., Styles, R. V., 2000. Global distribution of N2O emissions from aquatic systems: Natural emissions and anthropogenic effects. Chemosph. - Glob. Chang. Sci. 2, 267–279. https://doi.org/10.1016/S1465-9972(00)00015-5
Sharp, J.H. (1983) The distribution of inorganic nitrogen and dissolved and particulate organic nitrogen in the sea. In Nitrogen in the Marine Environment (Carpenter, E.J., and Capone, D.G., eds.), pp. 1–35, Academic Press, New York.
Sholkovitz, E.R., 1976. Flocculation of dissolved organic and inorganic matter during the mixing of river water and seawater. Geochim. Cosmochim. Acta 40, 831–845. https://doi.org/10.1016/0016-7037(76)90035-1
Sholkovitz, E. R., Boyle, E. A., and Price, N. B. (1978). The removal of dissolved humic acids and iron during estuarine mixing. Earth Planet. Sci. Lett. 40, 130–136. doi: 10.1016/0012-821X(78)90082-1
Siegel, D.A., Maritorena, S., Nelson, N.B., Hansell, D.A., Lorenzi-Kayser, M., 2002. Global distribution and dynamics of colored dissolved and detrital organic materials. J. Geophys. Res. Ocean. 107, 1–14. https://doi.org/10.1029/2001jc000965
Silverstein, R. M.; Bassler, G. C.; Morrill, T. C. Spectrometric Identification of Organic Compounds, 3rd ed.; John Wiley & Sons: New York, 1974.
Somoza, L., Díaz-del-Río, V., León, R., Ivanov, M., Fernández-Puga, M.C., Gardner, J.M., Hernández-Molina, F.J., Pinheiro, L.M., Rodero, J., Lobato, A., Maestro, A., Vázquez, J.T., Medialdea, T., Fernández-Salas, L.M., 2003. Seabed morphology and hydrocarbon seepage in the Gulf of Cádiz mud volcano area: Acoustic imagery, multibeam and ultra-high resolution seismic data. Mar. Geol. 195, 153–176. https://doi.org/10.1016/S0025-3227(02)00686-2
Stedmon, C.A., Markager, S., Bro, R., 2003. Tracing dissolved organic matter in aquatic environments using a new approach to fluorescence spectroscopy. Mar. Chem. 82, 239–254. https://doi.org/10.1016/S0304-4203(03)00072-0
Stedmon, C.A., Nelson, N.B., 2015. The Optical Properties of DOM in the Ocean. Biogeochem. Mar. Dissolved Org. Matter Second Ed. 481–508. https://doi.org/10.1016/B978-0-12-405940-5.00010-8
Steinberg, D.K., Nelson, N.B., Carlson, C.A., Prusak, A.C., 2004. Production of chromophoric dissolved organic matter (CDOM) in the open ocean by zooplankton and the colonial cyanobacterium Trichodesmium spp. Mar. Ecol. Prog. Ser. 267, 45–56. https://doi.org/10.3354/meps267045
Stubbins, A., Lapierre, J.F., Berggren, M., Prairie, Y.T., Dittmar, T., Del Giorgio, P.A.,

2014. What's in an EEM? Molecular signatures associated with dissolved organic fluorescence in boreal Canada. Environ. Sci. Technol. 48, 10598–10606. https://doi.org/10.1021/es502086e

Tranvik, L. J., and Sieburth, J. M. (1989). Effects of flocculated humic matter on free and attached pelagic microorganisms. Limnol. Oceanogr. 34, 688–699. doi: 10.4319/lo.1989.34.4.0688

Vargas-Yáñez, M., Sarhan, T., Plaza, F., Rubín, J.P., García-Martínez, M.C., 2002. The influence of tide-topography interaction on low-frequency heat and nutrient fluxes . Application to Cape Trafalgar 22, 115–139.

Verdugo, P., 2012. Marine microgels. Ann. Rev. Mar. Sci. 4, 375–400. https://doi.org/10.1146/annurev-marine-120709-142759

Webb, J.R., Santos, I.R., Maher, D.T., Tait, D.R., Cyronak, T., Sadat-Noori, M., Macklin, P., Jeffrey, L.C., 2019. Groundwater as a source of dissolved organic matter to coastal waters: Insights from radon and CDOM observations in 12 shallow coastal systems. Limnol. Oceanogr. 64, 182–196. https://doi.org/10.1002/lno.11028

Weishaar, J., Aiken, G., Bergamaschi, B., Fram, M., Fujii, R., Mopper, K., 2003. Evaluation of specific ultra-violet absorbance as an indicator of the chemical content of dissolved organic carbon. Environ. Chem. 41, 843–845. https://doi.org/10.1021/es030360x

Yamashita, Y., Jaffé, R., 2008. Characterizing the interactions between trace metals and dissolved organic matter using excitation-emission matrix and parallel factor analysis. Environ. Sci. Technol. 42, 7374–7379. https://doi.org/10.1021/es801357h

Yamashita, Y., Jaffe, R., Maie, N., Tanoue, E., 2008. Assessing the dynamics of dissolved organic matter (DOM) in coastal environments by excitation emission matrix fluorescence and parallel factor analysis (EEM-PARAFAC). Limnol. Oceanogr. 53, 1900–1908.

Yamashita, Y., Tanoue, E., 2003. Distribution and alteration of amino acids in bulk DOM along a transect from bay to oceanic waters. Mar. Chem. 82, 145–160. https://doi.org/10.1016/S0304-4203(03)00049-5

Yang, L., Hong, H., Guo, W., Chen, C.T.A., Pan, P.I., Feng, C.C., 2012. Absorption and fluorescence of dissolved organic matter in submarine hydrothermal vents off NE Taiwan. Mar. Chem. 128–129, 64–71. https://doi.org/10.1016/j.marchem.2011.10.003

Zhou, Y., Xiao, Q., Zhou, L., Jang, K.S., Zhang, Y., Zhang, M., Lee, X., Qin, B., Brookes, J.D., Davidson, T.A., Jeppesen, E., 2020. Are nitrous oxide emissions indirectly fueled by input of terrestrial dissolved organic nitrogen in a large eutrophic Lake Taihu, China? Sci. Total Environ. 722, 1–13. https://doi.org/10.1016/j.scitotenv.2020.138005

Zhou, Y., Zhou, L., Zhang, Y., Garcia de Souza, J., Podgorski, D.C., Spencer, R.G.M., Jeppesen, E., Davidson, T.A., 2019. Autochthonous dissolved organic matter potentially fuels methane ebullition from experimental lakes. Water Res. 166, 115048. https://doi.org/10.1016/j.watres.2019.115048

Ziolkowski, L.A., Druffel, E.R.M., 2010. Aged black carbon identified in marine dissolved organic carbon. Geophys. Res. Lett. 37, 4–7. https://doi.org/10.1029/2010GL043963

Parte II

Hipótesis y objetivos

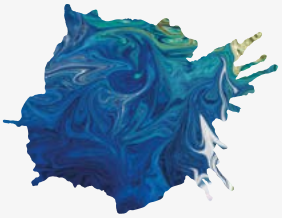

II. HIPÓTESIS Y OBJETIVOS

En respuesta a la falta de conocimiento que existe sobre la caracterización química de la DOM y su reactividad en el golfo de Cádiz, el objetivo general de esta Tesis doctoral consiste en contribuir al conocimiento de la DOM en la zona de transición costa- océano del golfo de Cádiz y los estuarios que allí desembocan.

La dinámica oceanográfica del GoC está condicionada por su cuenca semicerrada, es decir, por los intercambios entre los compartimentos ambientales que lo limitan (cuenca mediterránea, cuenca atlántica, sistemas costeros, la atmósfera y el sedimento). La **hipótesis** de partida de este trabajo considera que el GoC es un sistema espacialmente heterogéneo cuyas características biogeoquímicas están condicionadas por la presencia de estos intercambios, lo que provoca que sea una zona de transición biogeográfica entre las cuencas atlántica y mediterránea. Debido a la complejidad biogeoquímica de la región de estudio se espera que la dinámica de la DOM sea altamente variable con un marcado patrón estacional impulsado por transformaciones biológicas y fotoquímicas.

Para responder a estas preguntas se han fijado en esta Tesis doctoral los siguientes objetivos específicos:

1. Caracterizar ópticamente la DOM en la columna de agua de la zona de transición costa-océano del golfo de Cádiz, determinar su distribución espacio-temporal y evaluar los factores físicos y biogeoquímicos que influyen en su distribución (Capítulo 1).
2. Analizar la influencia de los volcanes de fango submarinos en la distribución de la DOM en el golfo de Cádiz, mediante la caracterización de la DOM en los sedimentos superficiales y el cálculo

de sus flujos difusivos hacia la zona profunda de la columna de agua (Capítulo 2).

3. Estudiar la dinámica de la DOM en los estuarios del Guadalquivir, Guadiana y Tinto-Odiel y su posible influencia en la zona costera del golfo de Cádiz a través del análisis de la composición química y molecular de la DOM, su reactividad y sus flujos desde estos estuarios hacia la zona costera (Capítulo 3 y 4).
4. Determinar la composición de la DOM y su relación con la distribución de los gases de efecto invernadero CO_2, CH_4 y N_2O en el estuario Guadalete (Capítulo 5).

Con objeto de abordar el objetivo número 1 (Capítulo 1) se ha medido la concentración de DOC y las propiedades ópticas de la DOM (absorbancia y fluorescencia) en 766 muestras de agua colectadas entre los 5 y 800 m de profundidad durante cuatro cruceros oceanográficos en el GoC. Mediante el empleo de EEMs, en combinación con el análisis multivariado PARAFAC, se han identificado los principales fluoróforos presentes en la zona de transición costa-océano del GoC y se ha realizado un análisis multiparamétrico óptimo (OMP, *optimum multiparametric water mass analysis*) para diferenciar el efecto de la mezcla de las masas de agua de los procesos biogeoquímicos en aguas profundas.

Para la consecución del objetivo número 2 (Capítulo 2) se ha medido la concentración de DOC y las propiedades ópticas de la DOM (absorbancia y fluorescencia) en el agua intersticial de tres volcanes de fango ubicados en el GoC (entre 500 y 1000 m de profundidad). Se han determinado las posibles fuentes de las diferentes fracciones de DOM y estimado los flujos bentónicos difusivos de DOC, CDOM y FDOM para comprender mejor su

efecto sobre la concentración y distribución de DOM en las aguas profundas del GoC.

Con fin de alcanzar el objetivo número 3 (Capítulo 3 y 4) se ha cuantificado la concentración de DOC y las características ópticas de DOM en transectos a lo largo de un gradiente de salinidad en los estuarios Guadalquivir, Guadiana y Tinto - Odiel. Se ha empleado el análisis multivariado PARAFAC (Murphy et al., 2013) en combinación con la técnica de alta resolución Py-GC-MS (Kaal, 2019) y análisis de DFAA para evaluar la composición de la DOM. En cada estuario se ha realizado un estudio de la influencia del ciclo de mareas y se han estimado el transporte de DOC, CDOM y de las diferentes fracciones de FDOM desde estos estuarios hacia la costa adyacente del golfo de Cádiz. Se ha partido de la hipótesis de que las diferentes características de las cuencas fluviales, la descarga de agua dulce, los ciclos de las mareas y las singularidades de cada cuenca podrían conducir a una composición y un comportamiento diferentes de la DOM entre los estuarios.

Por último, para tratar el objetivo número 4 (Capítulo 5) se ha realizado una caracterización óptica de la DOM y se ha determinado la distribución de los gases invernadero CO_2, CH_4 y N_2O en un estuario poco profundo sujeto a actividades antropogénicas (agricultura y urbanización). Para comprender mejor la importancia de la composición de DOM en la dinámica de estos gases, se han analizado las relaciones existentes entre sus concentraciones y diferentes fracciones de la DOM mediante regresiones lineales múltiples. En este caso, la hipótesis planteada es que la distribución de los tres gases podría estar significativamente relacionada con la concentración y composición de la DOM, y que estas relaciones variarían dependiendo del gas.

Se espera que los resultados de esta Tesis doctoral contribuyan al entendimiento del papel de la DOM en los ecosistemas acuáticos, estudiando un sistema tan característico como es el golfo de Cádiz por ser zona de transición Atlántico-Mediterráneo, y que hasta ahora ha sido prácticamente ignorado en términos de caracterización química de la DOM. Además, se espera contribuir a comprender la importancia de la composición de la DOM en la dinámica de los gases de efecto invernadero en los sistemas estuarinos.

Parte III

Metodología extendida

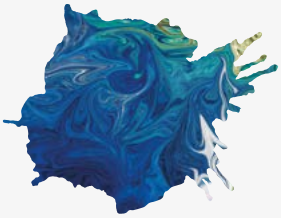

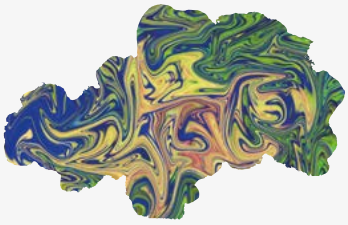

III. METODOLOGÍA GENERAL

III. 1. Estrategia de muestreo

Se realizaron 4 campañas oceanográficas en la plataforma del GoC en los meses de marzo, junio, septiembre y diciembre del 2016 a bordo de los B/O Ángeles Alvariño y Ramón Margalef. En cada una de las campañas se realizaron 5 transectos perpendiculares a costa, desde la desembocadura del Guadiana, Tinto-Odiel, Guadalquivir, caño de Sancti Petri y en el cabo de Trafalgar, con varios puntos de muestreo en cada uno y a diferentes profundidades, desde 5 m hasta el fondo. Además, se tomaron muestras en tres estaciones entre transectos localizadas en la zona más distal del estudio. En total se tomaron 766 muestras (Capítulo 1). En junio y diciembre se muestreó en la columna de agua situada encima de los tres volcanes de fango (San Petersburgo, Pipoca y Anastasya, n = 44) y se colectaron dos testigos de sedimento en cada uno de ellos (Capítulo 2).

Los muestreos en los estuarios de Guadalquivir, Guadiana y Tinto – Odiel se llevaron a cabo en julio de 2017 a bordo del B/O UCádiz. Debido a su calado, la toma de muestra en la zona más interna del Tinto – Odiel y del Guadiana se realizó con una embarcación neumática perteneciente al Servicio de embarcaciones de la Universidad de Cádiz (UCA). En cada uno de los estuarios se realizaron tres tipos de muestreos con un total de 150 muestras 1) un transecto longitudinal a lo largo del estuario, desde la desembocadura hasta la parte más interna, 2) un estudio de los ciclos mareales (24 horas) en la desembocadura, con una frecuencia de una muestra por hora y 3) un muestreo en varias estaciones costeras externas para analizar la influencia de los estuarios en la zona marina costera más próxima. Además, se tomaron muestras representativas en cada estuario para el análisis Py-GC-

MS (Capítulo 3). Por otro lado, se colectaron muestras para el análisis de DFAA a lo largo del gradiente de salinidad en cada estuario y durante el ciclo mareal con una frecuencia de 6 horas aproximadamente (n total = 40) (Capítulo 4).

Los muestreos en el estuario Guadalete se realizaron estacionalmente en una embarcación neumática perteneciente al Servicio de embarcaciones de la UCA cuando la marea comenzaba a bajar (rango de la marea = 1.8 y 2.4 m). Los muestreos se realizaron en mayo de 2016, noviembre de 2017, febrero de 2018, junio de 2018 y julio de 2018 desde la desembocadura hasta una presa que regula el caudal del río en la zona fluvial del estuario. En total se colectaron 50 muestras. En junio de 2018, el muestreo se realizó durante marea baja debido a las condiciones climáticas (Capítulo 5).

III. 2. Toma de muestras y pre procesamiento

Todas las muestras fueron tomadas en botellas Niskin de 10 L colocadas en una roseta con una CTD (Seabird CTD 911+ y Seabird CTD 25) acoplada, excepto cuando se emplearon la embarcaciones neumáticas. En ese caso, las muestras para nutrientes, concentración de DOC, propiedades ópticas de la DOM y alcalinidad se recogieron directamente en botellas de vidrio ámbar (250 mL) lavadas con HCl al 10%. La temperatura *in situ* se midió con un termómetro de mercurio (precisión de ± 0.1 °C) y la salinidad se cuantificó en el laboratorio utilizando un salinómetro de inducción Rousemount® Analytical (precisión de ± 0.001 unidades). Adicionalmente, se utilizó un mini CTD (YSI Castaway) para comprobar la homogeneidad de la columna de agua.

Las muestras para el análisis de oxígeno disuelto se tomaron en botellas Winklers, se fijaron y fueron almacenados en oscuridad hasta su análisis. En el estuario Guadalete, las muestras para CH_4 y N_2O se tomaron en botellas Winklers de 250 mL, por duplicado, evitando que se generaran burbujas en su interior. Se les añadió 250 µL de cloruro de mercurio para inhibir procesos microbianos, se sellaron con grasa Apiezon para prevenir el intercambio gaseoso y se conservaron en oscuridad para evitar reacciones fotoquímicas. Se almacenaron en el laboratorio a una temperatura constante de 25 °C (± 2 °C) hasta su análisis.

Las muestras para concentración de nutrientes (NO_3^-, NO_2^-, NH_4^+, PO_4^{3-}), alcalinidad total, concentración de DOC, propiedades ópticas de la DOM (absorbancia y fluorescencia), aminoácidos y extracción de fase sólida de la DOM fueron filtradas inmediatamente usando filtros de fibra de vidrio (GF/F Whatman 0.7 µm) previamente calcinados durante 4 horas a 450 °C. Todo el material empleado se dejó durante 24 horas en HCl al 10%, se enjuago con agua Milli-Q y posteriormente con la muestra. La absorbancia, fluorescencia y alcalinidad total se midieron inmediatamente. Las muestras para nutrientes y para concentración de DOC se tomaron por triplicado y por duplicado, respectivamente, y se almacenaron a -20 °C en oscuridad hasta su análisis, al igual que las muestras para aminoácidos.

III. 3. Análisis de muestras

III. 3.1. Materia orgánica disuelta

III. 3.1.1. Determinación de la concentración de DOC, CDOM y FDOM

La concentración de DOC se determinó mediante oxidación catalítica a alta temperatura utilizando un analizador Multi N/C 3100

Analytik Jena (Servicios periféricos INMAR), calibrado diariamente con ftalato de potasio (Panreac, 99.1%). Para evaluar la variabilidad del instrumento se midió material de referencia con bajas concentraciones de carbono proporcionado por el Prof. D. Hansell (Universidad de Miami, Material Certificado de Referencia para análisis de DOC, CRM Program, 42–45 µM) (43 ±1.8 µM, n = 5, Mar de los Sargazos, 2600 m).

La caracterización de CDOM se realizó a partir de los espectros de absorbancia medidos desde 240 a 800 nm cada 1 nm utilizando un espectrofotómetro JASCO-V750 conectado a un baño con control de temperatura fijado en 20 °C. Para las muestras de la zona costero-marina del GoC se utilizaron cubetas de cuarzo de 10 cm, mientras que para los estuarios se usaron cubetas de cuarzo de 1 cm de paso óptico. El límite de detección estimado del espectrofotómetro para cuantificar la absorción de CDOM es 0.0015 unidades de absorbancia o 0.03 m^{-1}, y el ruido es de 0.00004 unidades de absorbancia (especificaciones JASCO-750). Como blanco se empleó agua Milli-Q y se aplicó una corrección de línea de base a los espectros restándole el promedio de los valores obtenidos entre 600 y 700 nm (Green y Blough, 1994). Se midió un blanco cada seis muestras para detectar y corregir la deriva del instrumento. Finalmente, las absorbancias corregidas se convirtieron en coeficientes de absorción neperianos ($a_{(\lambda)}$, m^{-1}) multiplicando por 2.303 y dividiendo por el paso óptico de la cubeta en metros. A partir de estos datos se calcularon distintos índices espectrales que describen cuantitativa y cualitativamente la DOM y se resumen en la tabla 3.1.

La fluorescencia se midió a bordo o en el laboratorio después de la recogida de muestra usando una cubeta de cuarzo de 1 cm de paso óptico en un espectrofluorómetro (JASCO FP-8300) conectado a un porta-celdas

termostatizado mediante efecto Peltier (EHC-813) para el control de temperatura (20 °C). Las EEMs se obtuvieron mediante mediciones de fluorescencia en un rango de emisión de 300 a 580 nm, en incrementos de 1 nm, y un rango de excitación de 240 a 450 nm, en incrementos de 5 nm. Se empleó un ancho de banda de 5 nm en ambos casos y un tiempo de integración de 0.2 s. Para la corrección del blanco y el pico Raman se midió diariamente agua Milli-Q (Fig. 3.1), junto con un estándar de sulfato de quinina monohidrato (Sigma Aldrich, 98%) en H_2SO_4 para comprobar el rendimiento del sistema.

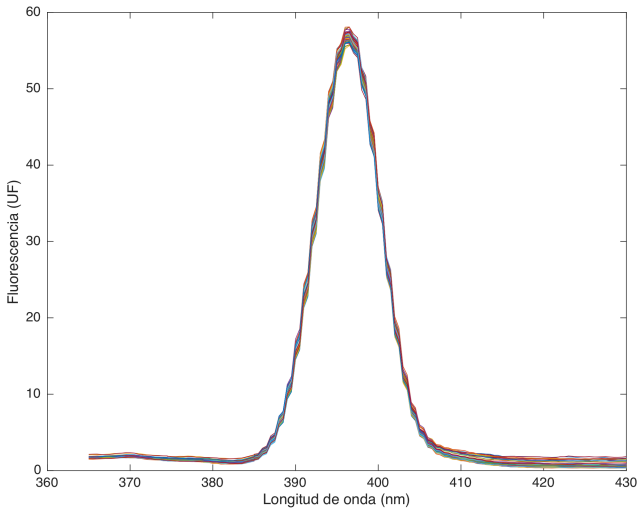

Fig. 3.1. Ejemplo de picos Raman en 64 muestras de agua Milli-Q durante la campaña oceanográfica en el golfo de Cádiz (Marzo 2016).

Tabla 3.1. Indicadores cualitativos empleados en esta Tesis doctoral para la caracterización de la DOM.

Índice Espectral	Definición	Interpretación	Referencias
a_{254} (m^{-1})	Coeficiente de absorción a 254 nm	Proporcional a la abundancia de dobles enlaces de carbono y proxy de la concentración de DOC	(Catalá et al., 2018; Lønborg y Álvarez-Salgado, 2014)
a_{350} (m^{-1})	Coeficiente de absorción a 350 nm	Indicador cuantitativo de la cantidad de CDOM.	(Coble, 2007)
$SUVA_{254}$ (mg C L^{-1})	Es el coeficiente de absorción decádico a 254 nm (m^{-1}) dividido por la concentración de DOC (mg L^{-1})	Está fuertemente correlacionado con el % de aromaticidad	(Weishaar et al., 2003)
$S_{275-295}$ (nm^{-1})	Relación entre los $a_{(\lambda)}$ de la pendiente entre las longitudes de onda 275 nm y 295 nm	Inversamente relacionado con el peso molecular de la DOM y con la cantidad de lignina.	(Fichot y Benner, 2012; Helms et al., 2008)
Total dissolved lignin phenol (TDLP9, nmol L^{-1})	Si $a_{250} < 4$ m^{-1}, ln TDLP9 = 0.7672 × a_{263} –0.3987. Si $a_{250} > 4$ m^{-1}, ln TDLP9 = –2.282 × ln (a_{350}) – 8.209 × ln (a_{275}) +11.365 × ln (a_{295}) + 2.909.	Proxy de la concentración total de lignina fenol disuelta derivada en general de DOM terrestre	(Fichot et al., 2016)

III. 3.1.2. Extracción en fase sólida de la DOM y análisis por Py-GC-MS

Para el análisis molecular de la DOM en los estuarios Guadalquivir, Guadiana y Tinto-Odiel se tomaron muestras representativas y se realizó la extracción de DOM en fase sólida utilizando cartuchos PPL, según Dittmar et al., (2008). Se filtraron 2 L de cada muestra usando filtros GF/F calcinados (4 horas, 450 °C), se acidificaron a pH 2 con HCl 25% e inmediatamente se pasaron a través de cartuchos PPL. Todo el material se lavó previamente con Milli-Q a pH 2 y los cartuchos de PPL se activaron el día anterior a la extracción empleando MeOH. Para la elución de la DOM, los cartuchos se lavaron previamente con Milli-Q pH 2 (desalinización), se secaron con N_2 gas, se llenaron con MeOH que luego se colectó y almacenó a – 20 °C en frascos ámbar previamente tratados térmicamente (4 horas, 450 °C). La eficiencia de extracción de DOM, determinada como la relación entre el DOC extraído y el DOC de la muestra, fue aproximadamente de un 60%.

Una vez extraídas, las muestras se analizaron por Py-GC-MS usando un Pyroprobe 5000 acoplado a un sistema MSD Agilent 5975. La pirólisis se realizó a 650 °C durante 20 s (velocidad de calentamiento 10 °C ms^{-1}) y para la GC-MS se usó un programa de temperatura de 10 °C min^{-1} operando en modo split 1:50. El GC estaba equipado con una columna no polar HP5-MS y el MS escaneaba en el rango m/z 50-500.

III. 3.1.3. Análisis de aminoácidos libres disueltos

El análisis de DFAA se realizó en el laboratorio del Prof. Gerhard J. Herndl en el Departamento de Limnología y Bio-Oceanografía de la Universidad de Viena. Los análisis se realizaron por duplicado empleando

cromatografía líquida de alta eficacia (HPLC, *high performance liquid chromatography*) en un Agilent 1260 Infinity Bioinert, mediante detección fluorométrica siguiendo el protocolo descripto en Taubner et al., (2019). En la Tabla 3.2 se indican los aminoácidos analizados en esta Tesis. Se realizó una derivatización, empleando un automuestreador robótico, con el reactivo o- ftalaldehído en presencia del ácido 3-mercaptopropiónico (OPA, Agilent Technologies). Los aminoácidos reaccionan con el reactivo OPA en presencia de un reductor fuerte (ácido 3-mercaptopropiónico) y en condiciones alcalinas (buffer borato, 0.4 N en agua, pH = 10.2; Agilent Technologies) para originar derivados fluorescentes. A 1 mL de muestra, se le añadieron 75 µL de tampón de borato (0.4 N en agua, pH = 10.2; Agilent Technologies), se mezclaron y se añadieron 5 µL del reactivo OPA (Agilent Technologies). Tras 2 minutos de tiempo de reacción a 27 ºC, se inyectaron 500 µL de la mezcla en el HPLC. La separación de los derivados fluorescentes (aminoácidos libres primarios disueltos) se realizó en una columna Zorbax ECLIPSE AAA (4.6 ×150 mm, 3.5 µm, Agilent Technologies) con un cartucho protector Zorbax ECLIPSE AAA (4.6 ×150 mm, 5 µm, Agilent Technologies), a una temperatura de 25 °C y un caudal de 0.8 mL min^{-1}. Se midió la excitación y emisión a una longitud de onda de 340 nm y 450 nm, respectivamente. Para crear el gradiente se utilizó MeOH y dihidrogenofosfato de sodio (NaH_2PO_4). Este método está particularmente establecido para muestras donde la concentración de amoníaco excede las concentraciones de los DFAA. La cuantificación de DFAA en muestras con altas concentraciones de amoníaco a menudo es complicada debido al exceso de sodio y la interacción con la fase estacionaria, lo que resulta en un ensanchamiento del pico. Por lo tanto, algunos de los DFAA no se pueden cuantificar, ya que están enmascarados por el pico de amoníaco. Además, se

utilizó tetrahidrofurano para lograr una mejor separación de los componentes individuales, especialmente entre metionina y valina, y se añadió ácido trifluoroacético para mejorar la resolución de los picos. El gradiente de elución se muestra en la Tabla 3.2.

Tabla 3.2 Aminoácidos disueltos medidos en este trabajo

Aminoácido	Abreviatura
Neutral R-alifático	
Glicina	Gly
Alanina	Ala
Valina	Val
Leucina	Leu
Isoleucina	Ile
Neutral R-hidroxilo y azufre	
Serina	Ser
Treonina	Thr
Metionina	Met
Aminoácidos ácidos y sus aminas	
Asparagina	Asn
Ácido aspártico	Asp
Ácido glutamico	Glu
Glutamina	Gln
Básicos	
Lysine	Lys
Arginine	Arg
Histidine	His
Aromáticos	
Lisina	Phe
Arginina	Trp
Histidina	Tyr
No-proteicos	
Ácido γ - aminobutírico	GABA
β-alanina	β- Ala
Ornitina	Orn
Orgánico sulfónico	
Taurina	Tau

Tabla 3.2. Gradiente de elución aplicado para la separación de aminoácidos libres primarios disueltos por HPLC. Eluyente A (fase polar): buffer NaH_2PO_4 40 mM (pH 7.8 ajustado con NaOH en agua Milli-Q; Sigma-Aldrich); B (fase no polar): Metanol (grado HPLC, Sigma- Aldrich)/agua Milli-Q/ácido trifluoroacético (calidad HPLC, Roth); C: tetrahidrofurano (grado HPLC; Sigma-Aldrich), tiempo total: 90 min.

Tiempo (min)	% A	% B	% C
0	90	10	0
2	90	7.5	2.5
40	68	30	2.0
42	64	35	1.0
75	35	65	0
77	0	100	0
80	90	10	0
90	90	10	0

Para la identificación y cuantificación de los picos, en cada ciclo se preparó una mezcla estándar de aminoácidos primarios (AAS18, Sigma Aldrich) a diferentes concentraciones de acuerdo con el intervalo de variación de las muestras (0.5 a 500 nM) (Fig. 3.2). Los aminoácidos asparagina, ácido glutámico, ácido γ-aminobutírico, taurina y triptófano (Sigma Aldrich) se agregaron a la mezcla estándar AAS18 en concentraciones conocidas. Para la interpretación de los cromatogramas se utilizó el software Agilent ChemStation.

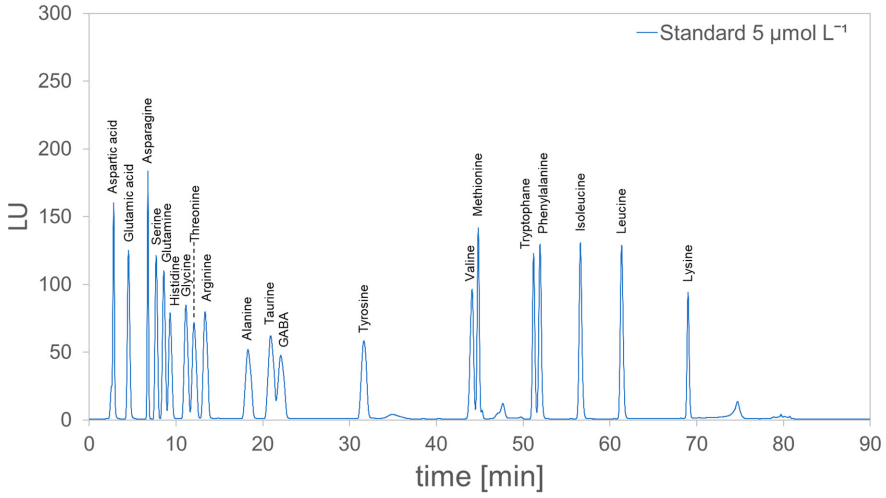

Fig. 3.2. Ejemplo de cromatograma adquirido mediante HPLC de un estándar de 5 µmol L^{-1} (AAS18, Sigma Aldrich) en agua Milli-Q mediante el método empleado en este trabajo (Tomado de Taubner et al., 2019).

III. 3.2. Concentración de gases de efecto invernadero

III. 3.2.1. Determinación de CO_2

La concentración de CO_2 se obtuvo a partir de medidas de pH y la TA, que se realizaron en un valorador potenciométrico (Metrohm 794) provisto de un electrodo combinado de vidrio que se calibró previamente en la escala total de pH usando una solución buffer de TRIS (Zeebe y Wolf-Gladrow, 2001). Se utilizó HCl 0.1 M como solución valorante que se preparó en NaCl 0.7 M para evitar cambios en la fuerza iónica durante la valoración. Para su factorización se empleó el material de referencia suministrado por A. Dickson (Scripps Institution of Oceanography, University of California, San Diego, EEUU, Batch#107). Las valoraciones potenciométricas se realizaron por duplicado en alícuotas de muestra de aproximadamente 50 g (± 0.1 mg). La TA se determinó a partir del segundo punto de equivalencia mediante la aplicación de una función de Gran a la parte ácida de la curva de valoración. El DIC y la presión parcial de CO_2

(pCO_2) se calcularon a partir de TA y pH utilizando las constantes de disociación del carbónico K1 y K2 para aguas estuarinas propuestas por Millero (2010) con el programa CO2SYS (Pierrot et al., 2006).

III. 3.2.2. Determinación de CH_4 y N_2O por cromatografía de gases

Las concentraciones de CH_4 y N_2O disueltos se determinaron por duplicado utilizando un cromatógrafo de gases Bruker® GC-450 equipado con un detector de ionización de llama (FID) para el CH_4 y un detector de captura de electrones (ECD) para el N_2O. Como gases portadores para la cuantificación de CH_4 y N_2O, se utiliza N_2 y una mezcla de Ar/CH_4 (95%/ 5%) (10 mL min^{-1}), respectivamente. Los detectores se calibraron diariamente utilizando cuatro patrones estándar de mezclas de gases certificadas por Abelló Linde, con concentraciones de CH_4 de 1952, 3078, 10064, 103829 ppbv y concentraciones de N_2O de 304, 430, 474 y 1766 ppbv. Las mezclas de gases estándar se han calibrado con el estándar SCOR (Comité Científico sobre Investigación Oceánica) disponible en España (Dra. Mercedes de la Paz, Instituto de Investigaciones Marinas, CSIC IIM, Vigo).

Para determinar la concentración de CH_4 y N_2O en cada muestra se utilizo la técnica de espacio de cabeza. Brevemente, se tomaron 25 g (± 0,01 g) de muestra mediante pesada usando una jeringa de vidrio de 50 mL (Agilent P/N 5190-1547). Para completar el volumen de la jeringa, se inyectaron 25 mL del primer patrón, con concentraciones de CH_4 y N_2O similares a los valores atmosféricos (1952 y 304 ppbv, respectivamente).

Esta operación se realizó por duplicado en cada muestra, por lo que se realizaron cuatro replicas. Las jeringas se agitaron durante cinco minutos (VIBROMATIC Selecta) para asegurar la mezcla; luego se esperó otros 5 minutos para alcanzar el equilibrio. Finalmente, la muestra se inyectó en el cromatógrafo.

III. 4. Análisis de datos

III. 4.1. Estandarización de los datos y análisis PARAFAC

Para el análisis de las EEMs se empleó la técnica de modelación multivariada PARAFAC, mediante el uso de la herramienta drEEM 0.2 para MATLAB (Murphy et al., 2013). Este análisis es un método de descomposición de tres vías (muestras × longitud de onda de excitación × longitud de onda emisión), similar al análisis de componentes principales (Fig. 3.3). Permite descomponer la señal de fluorescencia en sus componentes individuales, donde cada componente representa un fluoróforo (Bro, 1997; Murphy et al., 2013), mediante la siguiente ecuación:

$$x_{ijk} = \sum_{f=1}^{F} a_{if} b_{jf} c_{kf} + e_{ijk}$$

Donde *x* representa la muestra, *i* la intensidad de fluorescencia a una emisión *j* y excitación *k*. e_{ijk} representa la señal no explicada debido a, por ejemplo, variación no modelada, dispersión y ruido del instrumento; f corresponde a un componente PARAFAC y los parámetros *a, b y c* son los resultados del modelo y representan la concentración, los espectros de emisión y los espectros de excitación de los fluoróforos, respectivamente.

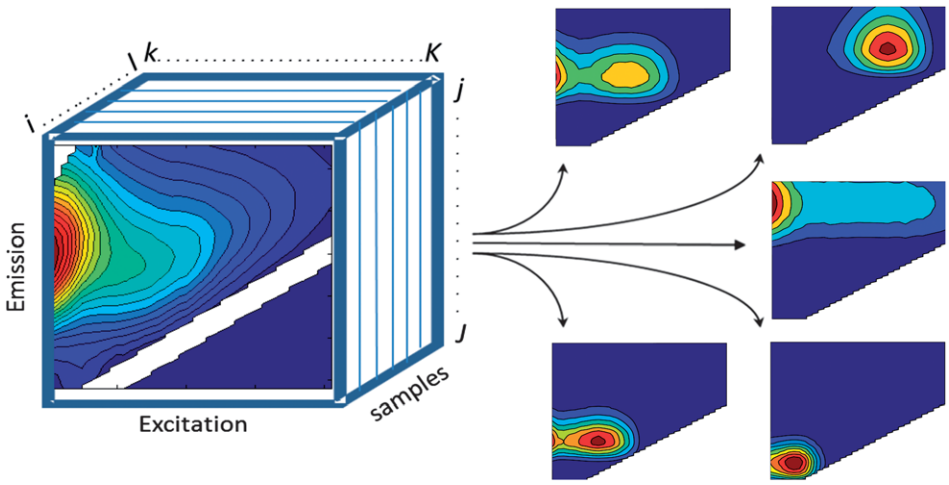

Fig. 3.3. Conjunto de matrices de excitación emisión organizado en una estructura de tres vías y descompuesto en cinco componentes (fluoróforos) PARAFAC. Tomado de Murphy et al. (2013).

Previo al modelado PARAFAC, las EEMs fueron estandarizadas empleando el tutorial desarrollado por Murphy et al. (2013). Su objetivo es corregir los datos debido a defectos introducidos por el equipo (ej. lámpara, monocromadores, fotomultiplicadores) mediante el uso de los factores de corrección del instrumento obtenidos del protocolo del fabricante utilizando rodamina A. Además, las señales no relacionadas a la fluorescencia, como por ejemplo el efecto de la absorbancia (IFE, *inner filter effect*, Lakowicz, 2006), y otros procesos asociados a la dispersión de la luz, fueron eliminados. Ya que la absorción de luz por la cubeta y la muestra disminuye al aumentar la longitud de onda, la fluorescencia se ve disminuida con distinta intensidad según la longitud de onda, es decir, el IFE es más severo a longitudes de onda más cortas, de esta forma, los espectros de emisión no sólo van a depender de los fluoróforos presentes sino de la longitudes de onda de excitación a la que son medidas. Para corregir el IFE se emplea una formula que usa el espectro de absorbancia de la muestra para calcular una matriz con factores de corrección correspondientes a cada par de longitud de onda de la

EEM (Lakowicz, 2006), mediante la ecuación:

$$F_{corr} = F_{obs} \times 10^{(Aexc+Aem)\times b}$$

donde F_{corr} es la matriz de fluorescencia corregida, F_{obs} es la observada, Aexc y Aem es la absorbancia a cada excitación y emisión medida y b es el promedio del paso óptico de la cubeta empleada. Todas las muestras fueron normalizadas dividiendo por el área del pico Raman del agua Milli-Q a 350 nm y expresadas en unidades Raman (RU) usando la herramienta drEEM. Este consiste en dividir la señal de fluorescencia de la muestra entre el área bajo la gráfica (Arp) a una excitación de 350 nm y emisión optima entre 381 y 426 nm (Lawaetz y Stedmon, 2009). Posteriormente, la fluorescencia de la muestra en cada punto fue dividida por Arp, dando como resultado una nueva unidad comparable entre equipos y con otros estudios. Además, dicha conversión compensa las fluctuaciones en la intensidad de la lámpara ocurridas durante el periodo de análisis (Lawaetz y Stedmon, 2009).

Otras de las señales no relacionadas con la fluorescencia son la dispersión de Raman y Rayleigh (Fig. 3.4). Dichas señales causan la presencia de picos de dispersión diagonal a la misma longitud de onda, pero de una magnitud mayor que la fluorescencia y es necesario eliminar la parte de datos afectada por este fenómeno. Para ello puede remplazarse la señal con ceros o interpolar la zona con los datos obtenidos a cada lado de la banda de dispersión (Zepp et al., 2004). La dispersión de Rayleigh ocurre en una región donde no hay señal química por lo que se empleó la sustitución por ceros mientras que para la dispersión de Raman se interpoló sobre la región de datos afectada, empleando la función *smootheem* en la herramienta drEEM que permite trabajar con las bandas de dispersión de

Raman y Rayleigh independientemente (Murphy et al., 2013).

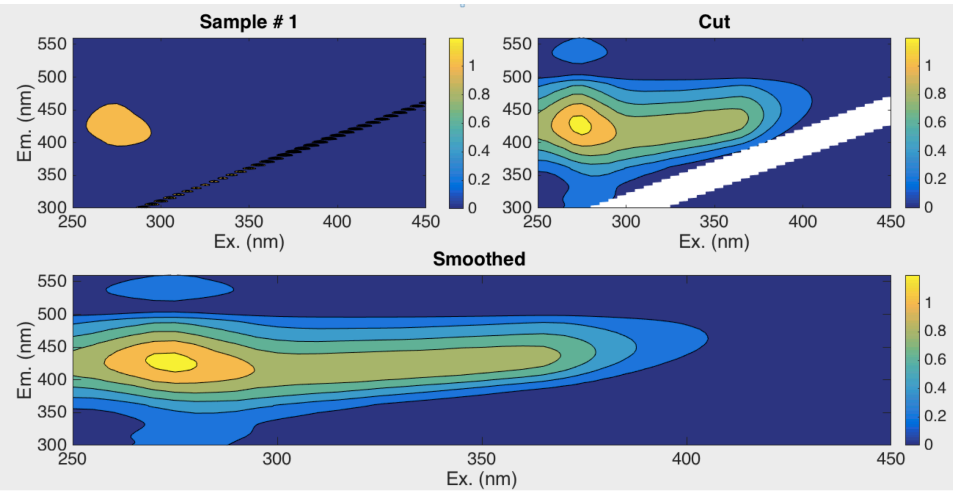

Fig. 3.4. Ejemplo de una matriz de excitación emisión. Arriba izq. Muestra #1 Guadalete sin corregir dispersión diagonal Raman y Rayleigh. Arriba derecha: Dispersión Raman y Rayleigh eliminada y abajo EEM corregida.

Por último, es necesario normalizar los datos, ya que muestras con alta concentración de DOM ejercen mayor fuerza en el modelo y los fluoróforos tienden a covariar por el efecto de la concentración. Al normalizar los datos, el modelo se enfoca en la variación química y no en la magnitud de la señal, aumentando la probabilidad de que aparezcan picos pequeños.

Después de esto se generó un conjunto de datos corregidos listos para el modelado PARAFAC mediante el uso de la herramienta drEEM 0.2.0. En la fase exploratoria se generaron modelos preliminares con distintos números de componentes (en general entre 3 y 7), con el fin de explorar la cantidad de componentes que podrían llegar a tener los modelos en base a los espectros obtenidos para cada uno. Se descartan componentes con espectros atípicos como cambios espectrales abruptos (Murphy et al., 2013). Para cada modelo preliminar se chequearon muestras *outlie*r que tenían un peso en el modelo mayor al promedio (*leverage* 0-1) y que por ende ejercían una mayor

influencia en el modelado. Lo mismo se realizó con las longitudes de onda de excitación y emisión. De esta forma, se volvieron a generar los modelos preliminares sin los *outlier* observados en cada caso. Asimismo, se chequearon los residuales para cada muestra en cada modelo preliminar, los cuales no debían presentar información importante que no estuviera siendo modelada, es decir, no deben observarse patrones sistemáticos y deben caracterizarse por ruido que contenga poca estructura (Murphy et al., 2013; Stedmon y Bro, 2008). En caso contrario, el número de componentes no sería el adecuado para modelar el conjunto de medidas.

El modelado se realizó empleando la restricción del uso de datos negativos (*nonnegativity*) y se chequearon las correlaciones entre los componentes obtenidos para cada modelo. Cuando las puntuaciones (*scores*) de dos componentes PARAFAC están altamente correlacionados, es muy difícil resolver posteriormente el espectro de emisión y excitación de cada uno, por lo que es necesario normalizar el conjunto de datos, lo que reduce el efecto concentración dándole la oportunidad a las muestras con baja concentración de entrar en el modelo. La normalización de los datos se realizó mediante la división de cada punto por la suma del cuadrado de todos los valores. Tras ser ajustado y validado el modelo y adquiridos los espectros de emisión y excitación de cada componente esta transformación fue revertida para obtener los valores reales.

Con el conjunto de datos normalizados se procedió a la validación del modelo que mejor se ajustaba a los datos, mediante el análisis *Split half validation*, esto es, el conjunto de datos es dividido al azar en varias fracciones para ver si se obtiene el mismo modelo cuando se modelan distintos grupos de muestras (Fig. 3.5). Esto implica división alternante. Empezando por la primera muestra del conjunto de datos cada una es

asignada a 1 de los 4 *split*, los cuales van a contener 1/4 del conjunto de datos y luego son combinados en 6 formas diferentes para generar nuevas mitades del conjunto de datos. Por ejemplo, divisiones-4, combinaciones-6, pruebas-3 (Stedmon y Bro, 2008; Murphy et al., 2013).

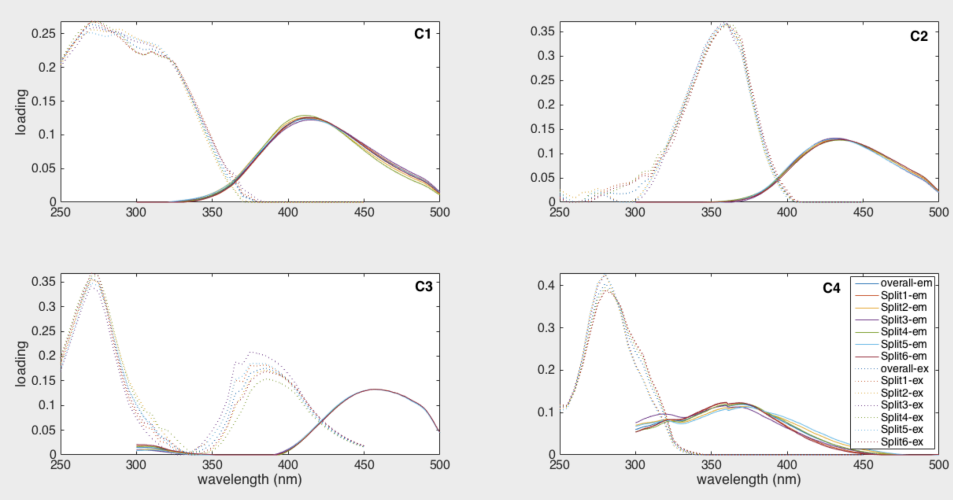

Fig. 3.5. Ejemplo de validación del modelo de 4 componentes PARAFAC mediante *Split half validation* para el set de datos del estuario Guadalete (Capítulo 5).

III. 4.2 Calculo Índices de Fluorescencia

A partir de las EEMs estandarizadas se calculó el índice de humificación (HIX) y el de frescura (BIX). El índice HIX se calculó como el área bajo los espectros de emisión entre 435 nm y 480 nm divida por el área del pico entre 300-345 nm + 435-480 nm, a una excitación de 254 nm. Los valores de HIX varían entre 0 y 1, indicando los valores más altos un mayor grado de humificación (Ohno, 2002). El índice BIX se calculó como la relación entre la fluorescencia emitida a 380 nm y 430 nm, obtenida a una excitación de 310 nm (Huguet et al., 2009). Los valores de BIX > 1 corresponden a DOM recién liberado, mientras que los valores < 0.7 corresponden a la presencia de DOM más procesada (Huguet et al., 2009).

III. 4.3 Flujos bentónicos difusivos sedimento-agua

En el capítulo 2 de esta tesis se estimaron los flujos difusivos a través de la interfase sedimento-agua de DOC, CDOM y los componentes fluorescentes identificados en los sedimentos de los volcanes de fango. Para ello se empleó la primera ley de Fick (Berner, 1980):

$$J = \phi D_s \left(\frac{\partial C}{\partial Z}\right)$$

donde J es el flujo difusivo, ϕ es la porosidad del sedimento, Ds es el coeficiente de difusión en el sedimento corregido por la tortuosidad del sedimento (θ^2) de acuerdo con la expresión D_0/θ^2, D_0 es el coeficiente de difusión a dilución infinita (1.585×10^{-6} cm^2 s^{-1} para DOM, Komada et al., 2013) y θ^2 se estimó utilizando la ecuación propuesta por Boudreau (1997): $\theta^2 = [1 - 2 \text{ Ln } (\phi)]$). Finalmente, $\partial C / \partial Z$ se calculó a partir de la diferencia entre la concentración a 5 metros por encima del volcán de fango y la encontrada en el agua intersticial de los sedimentos más superficiales (0- 1 cm).

III. 4.4. Transporte de DOM con las mareas

En el capítulo 3 se estimaron los flujos de DOC, CDOM y los componentes de la FDOM desde los estuarios Guadalquivir, Guadiana y Tinto-Odiel hacia la zona costera adyacente. Durante los estudios de intercambio con las mareas, la velocidad de corriente y la altura de marea fueron medidas cada 5 minutos empleando un Nortek Aquapro Current Meter. La velocidad de corriente fue registrada desde el fondo hasta la superficie en capas de 1 m de agua. La sección de los estuarios se ha

calculado durante la bajamar mediante embarcaciones ligeras provistas de una sonda de profundidad en el estuario del Guadalquivir o utilizando cartas naúticas para los estuarios del Guadiana y Tinto-Odiel (https://www.navionics.com). En este caso, la altura de marea en bajamar fue corregida teniendo en cuenta la intensidad de la marea en los días en los que se realizó el estudio.

A partir de un balance hídrico se estimaron los caudales de los ríos:

$$\int_{t_0}^{t_F} Q_i \, dt = \; Q_R \, (t_F - \; t_0)$$

donde $t_F - t_0$ incluye dos ciclos de mareas consecutivos (25 horas) y Q_i es el flujo de agua instantáneo calculado a partir de la velocidad de corriente y el área de la sección de los estuarios (Chen et al., 2012; Gardner y Kjerfve, 2006).

El transporte neto con las mareas se ha calculado mediante un balance de masas según las siguientes ecuaciones:

$$Tidal\ transport = \int_{t_0}^{t_F} Q_i \, C_i \, dt$$

$$River\ transport = Q_R \, C_R \, (t_F - \; t_0)$$

Donde C_i y C_R son las concentraciones durante el ciclo mareal y en el río, respectivamente. Valores positivos corresponden a un transporte del componente analizados desde el río al estuario y del estuario a la zona costera.

III.4.5. Análisis de los pirocromatogramas

Los picos más relevantes en los pirocromatogramas obtenidos mediante Py-GC-MS en las muestras de los estuarios Guadalquivir, Guadiana y Tinto-Odiel se identificaron mediante el uso de la biblioteca de espectros de masas NIST 2014 y la literatura (Fig. 3.6). Por último, se calcularon las proporciones relativas para una serie de productos de interés que reflejan la fracción macromolecular de la DOM (Tabla 3.3).

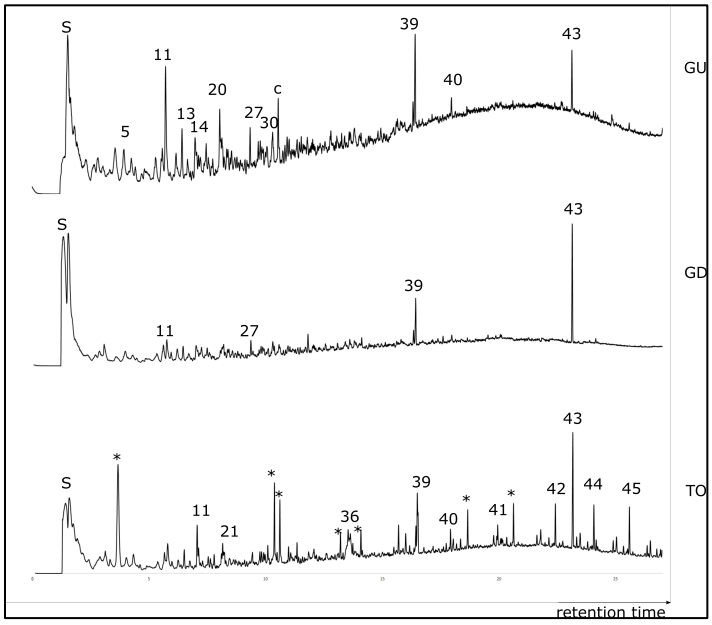

Fig. 3.6. Cromatogramas de la Py-MS-GC para Guadiana (GU), Guadalquivir (GD) y Tinto-Odiel (TO). La etiqueta de los picos corresponden a los números de productos de pirólisis en la Tabla 3.3. RT = tiempo de retención, S = azufre inorgánico, c = contaminación del sistema, * = otros compuestos no enumerados.

Tabla 3.3. Lista de productos de pirólisis, con tiempo de retención (RT), relación masa carga (m/z) y clases de compuestos (N-compounds = compuestos nitrogenados, MAH/PAH = hidrocarburos aromáticos monocíclicos y policíclicos, MCC = compuestos de cadena de metileno). N° picos figura 3.6.

N°	Producto de pirólisis	RT (min)	m/z	Clase
1	pyridine	2.713	79	N-compounds
2	pyrrole	2.780	67	N- compounds
3	toluene	2.895	91+92	MAH
4	acetamide	3.307	59	N- compounds
5	C2-benzene	4.015	91+106	MAH
6	propionamide/alkanoic acid	4.332	73	Other
7	C2-benzene	4.335	91+106	MAH
8	2-methyl-2-cyclopentenone	4.508	67 (96)	Carbohydrate
9	C3-benzene	5.232	105+120	MAH
10	phenol	5.634	94+66	Phenol
11	C3-benzene	5.790	105+120	MAH
12	C3-benzene	6.240	105+120	MAH
13	2,3-dimethyl-2-cyclopentenone	6.505	67 (110)	Carbohydrate
14	C1-phenol	6.739	107+108	Phenol
15	trimethylcyclopentenone	6.854	109+124	Carbohydrate
16	C1-phenol	7.066	107+108	Phenol
17	guaiacol (T)	7.279	124+109	Lignin
18	unidentified cyclopentenone	7.528	67 (X)	Carbohydrate
19	C2-phenol	8.166	107+122	Phenol
20	C1-indene	8.191	130+115	PAH
21	C4-benzene	8.234	119+134	MAH
22	C1-indene	8.291	130+115	PAH
23	C2-phenol	8.472	107+122	Phenol
24	C2-phenol	8.618	107+122	Phenol
25	naphthalene	8.747	128	PAH
26	C2-phenol	8.851	107+122	Phenol
27	C3-1H-pyrrole-2,5-dione	9.401	67 (139)	Carbohydrate
28	C1-naphthalene	10.330	142+115	PAH
29	indole	10.340	117+90	N- compounds
30	C1-naphthalene	10.584	142+115	PAH
31	C4-phenol (T)	11.202	135+150	Phenol
32	trimethylindene	11.404	143+158	PAH
33	trimethylindene	11.497	143+158	PAH

34	trimethylindene	11.715	143+158	PAH
35	4-vinylguaiacol (T)	12.110	135+150	Lignin
36	dichlorobenzoic acid	13.531	173+192	Other
37	diketodipyrrole	15.550	186+93	N-compounds
38	C14 fatty acid	15.984	60+73	MCC
39	N-butylbenzenesulfonamide	16.349	141+170	Plasticizer
40	C16 fatty acid	17.999	60+73	MCC
41	C18 fatty acid	19.867	60+73	MCC
42	alkyl compound	22.419	69+83	MCC
43	isooctylphthalate	23.146	149+167	Plasticizer
44	alkyl compound	24.069	69+83	MCC
45	alkyl compound	25.595	69+83	MCC
46	alkyl compound	27.011	69+83	MCC
47	alkyl compound	28.350	69+83	MCC
48	alkyl compound	29.882	69+83	MCC

III. 4.6 Indicadores moleculares del estado de la DOM basados en aminoácidos

En el capítulo 3 se calcularon diversos indicadores moleculares basados en el análisis de aminoácidos. Por ejemplo, el rendimiento de AA normalizado por carbono se calculó como la concentración de DFAA (nM) dividida por la concentración de DOC (nM), en donde valores mayores se asocian a DOM más fresca (Davis et al., 2009). La abundancia relativa de cada AA se calculó como el % relativo de contribución al *pool* total de DFAA. La abundancia relativa de los AA individuales cambia durante la descomposición de la materia orgánica y se ha utilizado para describir el estado diagenético relativo de la DOM (Dauwe et al., 1999; Dauwe y Middelburg, 1998; Yamashita y Tanoue, 2003). Además, se calculó el índice de degradación (DI) que es una medida del estado general de degradación de la materia orgánica (Dauwe y Middelburg, 1998, Dauwe et al., 1999, Kaiser y Benner, 2009) según la siguiente ecuación:

$$DI = \sum_{i} \left(\frac{var\ (i) - AVGvar\ (i)}{STDvar\ (i)}\right) \times fact.coef\ (i)$$

donde var, AVG_{var} y STD_{var} son la abundancia relativa de cada AA, la abundancia relativa promedio y la desviación estándar del AA en la muestra, y se utilizaron los factores determinados para cada AA mediante el análisis de PCA para DOM marina reportados en Kaiser y Benner, (2009)l. Los aminoácidos (*i*) empleados para el calculo de DI fueron Asp, Glu, Ser, His, Gly, Thr, Arg, Ala, Tyr, Val, Phe, Ile, Leu. Lys y Asn. Cuanto menor sea el DI, mayor es el grado de descomposición de la DOM.

Se empleó la abundancia relativa de los aminoácidos no proteicos Orn, GABA y β- Ala como indicadores de DOM relativamente envejecida y diagénesis avanzada (Cowie and Hedges, 1992). Por último, se calculó la relación de los enantiómeros D y L de los aminoácidos cuando se detectó la forma D-AA.

Referencias

Bro, R., 1997. PARAFAC. Tutorial and applications. Chemom. Intell. Lab. Syst. 38, 149–171. https://doi.org/10.1016/S0169-7439(97)00032-4

Catalá, T.S., Martínez-Pérez, A.M., Nieto-Cid, M., Álvarez, M., Otero, J., Emelianov, M., Reche, I., Arístegui, J., Álvarez-Salgado, X.A., 2018. Dissolved Organic Matter (DOM) in the open Mediterranean Sea. I. Basin–wide distribution and drivers of chromophoric DOM. Prog. Oceanogr. 165, 35–51. https://doi.org/10.1016/j.pocean.2018.05.002

Chen, S.N., Geyer, W.R., Ralston, D.K., Lerczak, J.A., 2012. Estuarine Exchange Flow Quantified with Isohaline Coordinates: Contrasting Long and Short Estuaries. J. Phys. Oceanogr. 42, 748–763. https://doi.org/10.1175/JPO-D-11-086.1

Coble, P.G., 2007. Marine Optical Biogeochemistry: The Chemistry of Ocean Color. Chem. Rev. 107, 402–418. https://doi.org/10.1021/cr050350+

Cowie, G.L., Hedges, J.I., 1992. Sources and reactivities of amino acids in a coastal marine environment. Limnol. Oceanogr. 37, 703–724. https://doi.org/10.4319/lo.1992.37.4.0703

Dauwe, B., Middelburg, J.J., 1998. Amino acids and hexosamines as indicators of organic matter degradation state in North Sea sediments. Limnol. Oceanogr. 43, 782–798. https://doi.org/10.4319/lo.1998.43.5.0782

Dauwe, B., Middelburg, J.J., Herman, P.M.J., Heip, C.H.R., 1999. Linking diagenetic alteration of amino acids and bulk organic matter reactivity. Limnol. Oceanogr. 44, 1809–1814. https://doi.org/10.4319/lo.1999.44.7.1809

Davis, J., Kaiser, K., Benner, R., 2009. Amino acid and amino sugar yields and compositions as indicators of dissolved organic matter diagenesis. Org. Geochem. 40, 343–352. https://doi.org/10.1016/j.orggeochem.2008.12.003

Dittmar, T., Koch, B., Hertkorn, N., Kattner, G., 2008. A simple and efficient method for the solid-phase extraction of dissolved organic matter (SPE-DOM) from seawater. Limnol. Oceanogr. Methods 6, 230–235.

Fichot, C.G., Benner, R., 2012. The spectral slope coefficient of chromophoric dissolved organic matter (S 275-295) as a tracer of terrigenous dissolved organic carbon in river-influenced ocean margins . Limnol. Oceanogr. 57, 1453–1466. https://doi.org/10.4319/lo.2012.57.5.1453

Fichot, C.G., Benner, R., Kaiser, K., Shen, Y., Amon, R.M.W., Ogawa, H., Lu, C.J., 2016. Predicting dissolved lignin phenol concentrations in the coastal ocean from chromophoric dissolved organic matter (CDOM) absorption coefficients. Front. Mar. Sci. 3, 1–15. https://doi.org/10.3389/fmars.2016.00007

Gardner, L.R., Kjerfve, B., 2006. Tidal fluxes of nutrients and suspended sediments at the North Inlet-Winyah Bay National Estuarine Research Reserve. Estuar. Coast. Shelf Sci. 70, 682–692. https://doi.org/10.1016/j.ecss.2006.06.034

Green, S.A., Blough, N. V, 1994. Optical absorption and fluorescence of chromophoric properties dissolved organic matter in natural waters. Limnology 39, 1903–1916.

Helms, J.R., Kieber, D.J., Minor, E.C., Ritchie, J.D., Stubbins, A., Mopper, K., 2008. Absorption spectral slopes and slope ratios as indicators of molecular weight, source, and photobleaching of chromophoric dissolved organic matter. Limnol. Oceanogr. 53, 955–969. https://doi.org/10.4319/lo.2008.53.3.0955

Huguet, A., Vacher, L., Relexans, S., Saubusse, S., Froidefond, J.M., Parlanti, E., 2009. Properties of fluorescent dissolved organic matter in the Gironde Estuary. Org.

Geochem. 40, 706–719. https://doi.org/10.1016/j.orggeochem.2009.03.002
Kaiser, K., Benner, R., 2009. Biochemical composition and size distribution of organic matter at the Pacific and Atlantic time-series stations. Mar. Chem. 113, 63–77. https://doi.org/10.1016/j.marchem.2008.12.004
Kaiser, K., Benner, R., 2008. Major bacterial contribution to the ocean reservoir of detrital organic carbon and nitrogen. Limnol. Oceanogr. 53, 99–112. https://doi.org/10.4319/lo.2008.53.1.0099
Komada, T., Burdige, D.J., Crispo, S.M., Druffel, E.R.M., Griffin, S., Johnson, L., Le, D., 2013. Dissolved organic carbon dynamics in anaerobic sediments of the Santa Monica Basin. Geochim. Cosmochim. Acta 110, 253–273. https://doi.org/10.1016/j.gca.2013.02.017
Lawaetz, A.J., Stedmon, C.A., 2009. Fluorescence intensity calibration using the Raman scatter peak of water. Appl. Spectrosc. 63, 936–940. https://doi.org/10.1366/000370209788964548
Lønborg, C., Álvarez-Salgado, X.A., 2014. Tracing dissolved organic matter cycling in the eastern boundary of the temperate North Atlantic using absorption and fluorescence spectroscopy. Deep. Res. Part I Oceanogr. Res. Pap. 85, 35–46. https://doi.org/10.1016/j.dsr.2013.11.002
Millero, F.J., 2010. Carbonate constants for estuarine waters.pdf. Mar. Freshw. Res. 61, 139–142.
Murphy, K.R., Stedmon, C.A., Graeber, D., Bro, R., 2013. Fluorescence spectroscopy and multi-way techniques. PARAFAC. Anal. Methods 5, 6557–6566. https://doi.org/10.1039/c3ay41160e
Stedmon, C., Bro, R., 2008. Characterizing dissolved organic matter fluorescence with parallel factor analysis: a tutorial. Limnol. Oceanogr. Methods 6, 572–579. https://doi.org/doi:10.4319/lom.2008.6.572b
Taubner, R.S., Baumann, L.M.F., Bauersachs, T., Clifford, E.L., Mähnert, B., Reischl, B., Seifert, R., Peckmann, J., Rittmann, S.K.M.R., Birgel, D., 2019. Membrane lipid composition and amino acid excretion patterns of Methanothermococcus okinawensis grown in the presence of inhibitors detected in the enceladian plume. Life 9. https://doi.org/10.3390/life9040085
Weishaar, J., Aiken, G., Bergamaschi, B., Fram, M., Fujii, R., Mopper, K., 2003. Evaluation of specific ultra-violet absorbance as an indicator of the chemical content of dissolved organic carbon. Environ. Chem. 41, 843–845. https://doi.org/10.1021/es030360x
Yamashita, Y., Tanoue, E., 2003. Distribution and alteration of amino acids in bulk DOM along a transect from bay to oceanic waters. Mar. Chem. 82, 145–160. https://doi.org/10.1016/S0304-4203(03)00049-5
Zepp, R.G., Sheldon, W.M., Moran, M.A., 2004. Dissolved organic fluorophores in southeastern US coastal waters: Correction method for eliminating Rayleigh and Raman scattering peaks in excitation-emission matrices. Mar. Chem. 89, 15–36. https://doi.org/10.1016/j.marchem.2004.02.006

Parte IV

Resultados y Discusión

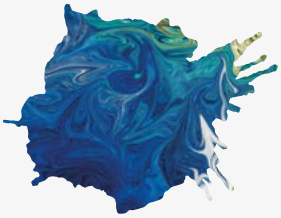

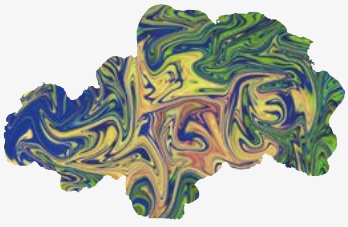

Capítulo 1

"No ocean, no life. No blue, no green. No ocean, no us".
Sylvia Earle

Dissolved Organic Matter in the Gulf of Cádiz: Distribution and Drivers of Chromophoric and Fluorescent Properties*

Valentina Amaral[1,2*], Cristina Romera-Castillo[3], Jesús Forja[1]

[1]Departamento de Química-Física, INMAR, Facultad de Ciencias del Mar y Ambientales, Universidad de Cádiz, Campus Río San Pedros/n, Puerto Real, Cádiz, España.
[2] Ecología Funcional de Sistemas Acuáticos, Centro Universitario Regional Este, Universidad de la República, Uruguay.
[3] Instituto de Ciencias del Mar-CSIC, Barcelona, España.

Publicado en *Frontiers in Marine Science

Abstract

The Gulf of Cádiz (GoC) connects the Mediterranean Sea with the Atlantic Ocean through the Strait of Gibraltar. Particular hydrographic processes take place in the GoC, such as riverine discharges and surface circulation marked by wind-induced seasonal upwelling. Although physical processes have been widely studied, little is known about the biogeochemical processes that occur in the basin, especially those involving organic matter. Therefore, vertical and seasonal dynamics of dissolved organic carbon (DOC) and dissolved organic matter (DOM) optical properties (absorption and fluorescence) were measured in 766 samples collected between 5 and 800 m depth during 4 oceanographic cruises to obtain quantitative and qualitative information about DOM in the GoC. We performed parallel factor analysis (PARAFAC) to identify the main fluorophores present in the GoC, and an optimum multiparameter water mass analysis to differentiate the effect of water mass mixing from the biogeochemical processes in deep waters. PARAFAC analysis validated six fluorescent components; three humic-like, two protein-like, and a possible mixture of polycyclic aromatic hydrocarbon-like with protein-like material. DOC average concentration was 77.0 ± 12.7 μM, with higher values in surface and coastal waters during summer, mainly related to primary production. Linear relationships between DOC and apparent oxygen utilization indicate differences in oxygen consumption within the deep waters, which could be related to upwelling zones. Seasonal and spatial differences were also observed in fluorescent DOM distribution. Protein-like components were the most abundant fraction, with an average contribution of 64.75 % ± 7.85 %, being higher in summer and surface waters, associated with an increase in biological activity. Our results indicate

that water mass mixing is the main driver of the major humic-like components, while biogeochemical processes at a local scale explain DOC and protein-like components distribution. Our findings suggest that modeling DOM dynamics in the GoC is complicated due to its complex hydrography and the presence of multiple sources and sinks of DOM.

IV. 1. Introduction

The Gulf of Cádiz (GoC) is the only connection between the Mediterranean Sea and the Atlantic Ocean through the Strait of Gibraltar. Consequently, it plays an important role in the North Atlantic circulation and climate in general (Price and O'Neil Baringer, 1994, Mauritzen et al., 2001). The GoC is also involved in the carbon cycle of the Eastern North Atlantic Ocean (Parrilla, 1998) and the Mediterranean Sea (Dafner et al., 2001). Physical processes in the GoC have been widely studied (Bellanco and Sánchez-Leal, 2016; Criado-Aldeanueva et al., 2006) as well as biogeochemical processes mainly focused on the inorganic carbon dynamics (Dafner et al., 2001; Ribas-Ribas et al., 2011). However, less is known about the processes involving the organic carbon pool. A gap of knowledge that should be filled to better understand the role of the GoC in the carbon cycle of both Atlantic and Mediterranean waters.

Marine dissolved organic matter (DOM) is one of the largest and most dynamic reservoirs of reduced carbon on the Earth (Hedges, 2002), with an estimated stock of 662 Pg (Hansell et al., 2009). The main source of oceanic DOM is primary production, while terrestrial inputs only account for 2-3% of the total pool, although they can dominate in coastal zones (Opsahl and Benner, 1997). The DOM fraction absorbing light at both ultraviolet (UV) and visible wavelengths is referred to as chromophoric

dissolved organic matter (CDOM; Coble, 2007). It is one of the major absorption components in the ocean, and a tracer for biogeochemical processes and oceanic circulation (Nelson and Siegel, 2013). The sub-fraction of CDOM that fluoresces is called fluorescent dissolved organic matter (FDOM; Coble, 2007) and can represent between 20 and 70 % of the DOC, depending on the aquatic system, being higher in coastal areas (Coble, 2007). Optical properties (absorption and fluorescence) can yield qualitative information about the origin and chemical quality of the DOM pool, such as DOM's molecular weight and aromaticity (Weishaar et al., 2003; Helms et al., 2008).

Chemical characterization of DOM has been inferred from its optical properties in both the Mediterranean (Galletti et al., 2019; Martínez-Pérez et al., 2019) and North Atlantic waters (Jørgensen et al., 2011; Álvarez-Salgado et al., 2013). However, little is known in the confluence of these two basins, the GoC. González-Ortegón et al. (2018) measured FDOM using an EXO FDOM sensor, but the measurements were limited to humic-like substances (Ex 365/Em 480) and samples shallower than 150 m depth. Another study determined CDOM and FDOM but only at three stations in the Bay of Cádiz, located in the northeast zone of the GoC (Catalá et al., 2013).

This work aims to understand the DOM dynamics in the whole GoC, from the surface to the bottom, and its seasonal changes. During one year, we have studied the DOC and DOM optical properties (both absorption and fluorescence) along the entire basin to understand the physical and biogeochemical drivers of their distribution. DOM dynamics were expected to be highly variable due to the biogeochemical complexity of the study region. We hypothesized that FDOM distribution depended on the source of the organic matter (terrestrial vs. marine). We also

hypothesized that FDOM followed a marked seasonal pattern driven by biological and photochemical transformations.

IV. 2. Material and methods

IV. 2.1. Study area

This study was carried out in the GoC, located in the Southwestern Iberian Peninsula. The GoC is a semi-enclosed basin where oceanographic dynamics and water mass circulation patterns are driven by the interaction between Atlantic and Mediterranean waters masses and influenced by the coastal system (Bellanco and Sánchez-Leal, 2016).

Three main water masses circulate in the GoC (Criado-Aldeanueva et al., 2006; Bellanco and Sánchez-Leal, 2016) (Fig. S1). The Surface Atlantic Water extends from the surface to the seasonal thermocline and has an Atlantic origin modified by atmospheric interaction. The North Atlantic Central Water (NACW) flows below 100 m depth in two different varieties (Pérez et al., 2001): a warmer one of subtropical origin ($NACW_T$) and a colder one of subpolar origin ($NACW_S$). Lastly, the denser and saltier modified Mediterranean Outflow Water (MOW) flows between 300-400 m depth and the seafloor. Density differences between NACW and MOW result in a bi-layer exchange: an inflow of Atlantic water at the surface towards the Mediterranean basin, and a deeper outflow of Mediterranean water to the Atlantic Ocean (Baringer and Price, 1999).

Three upwelling areas have been identified in the GoC: Cape St. Vincent and Cape Sta. María, where the NACW upwells favored by winds, and Cape of Trafalgar, where the tidal–topographical interaction has been identified as the main process responsible for the vertical transport of deep waters to the surface layers (Vargas-Yáñez et al., 2002; Sala et al., 2018).

Furthermore, between Cape of Sta. María and Cape of Trafalgar, three major estuaries, Guadalquivir, Guadiana, and Tinto-Odiel systems (Fig. 1), discharge freshwater into the GoC. Riverine inflows to these estuaries are located in a semiarid environment and are regulated by dams. The Tinto-Odiel estuary is an industrial port with a low flow rate of freshwater and an average salinity of 37.2 ± 0.7. Guadalquivir and Guadiana show a salinity gradient (0.3-36.6) with a mean flow rate of 1811 $m^3 s^{-1}$ (2016) and 74 $m^3 s^{-1}$ (1984-2015), respectively (http://www.chguadalquivir.es/ and https://www.chguadiana.es). The high demand for freshwater for crop irrigation, along with frequent drought events, usually leads to long water residence times in the two rivers (de la Paz et al., 2007; Vasconcelos et al., 2007). In general, the GoC is characterized by oligotrophic conditions (Navarro et al., 2012) except for the coastal zone, where Chl *a* and nutrient concentrations are high due to continental runoff (Sala et al., 2018). As a result of these spatial and temporal variable processes, the GoC is mainly characterized by long-term seasonal physicochemical variability (Criado-Aldeanueva et al., 2009; González-García et al., 2018).

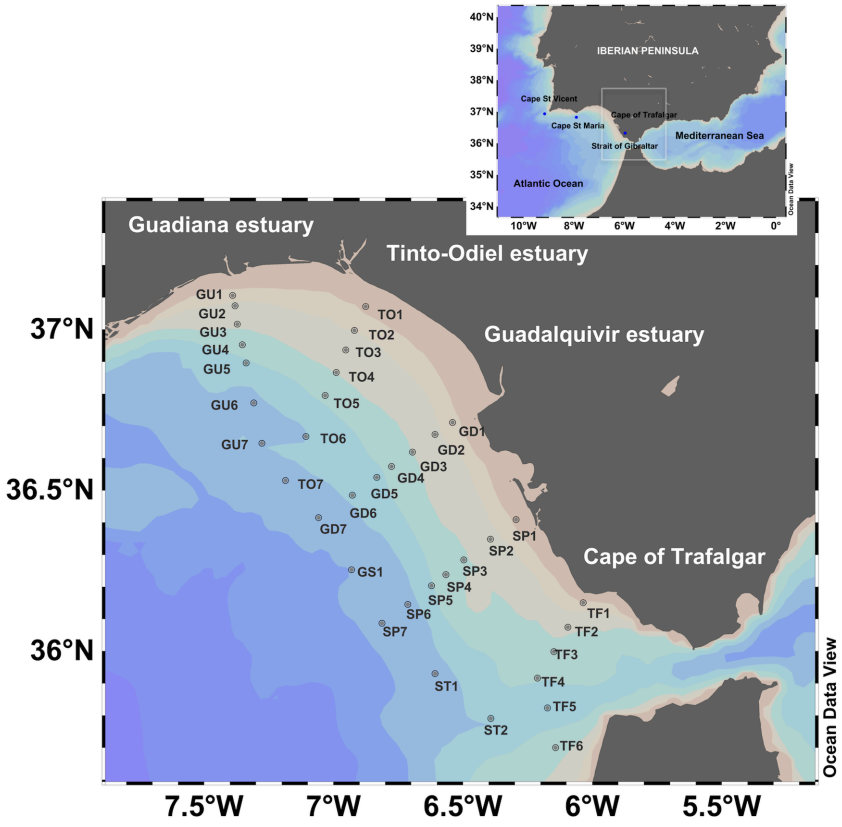

Fig. 1. Sampling stations in the Gulf of Cádiz: Guadiana (GU), Tinto-Odiel (TO), Guadalquivir (GD), Sancti Petri (SP), Trafalgar (TF) and external stations (GS1, ST1 and ST2).

IV. 2.2 Sampling strategy and analytical methods

Four cruises were conducted on board of B/O Angeles Alvariño and B/O Ramón Margalef vessels at the beginning of each season (March, June, September, and December 2016). Samples were collected at different depths, from 5 m to the bottom, and perpendicular to the coastline on five different transects designated as Guadiana (GU), Tinto-Odiel (TO), Guadalquivir (GD), Sancti Petri (SP) and Trafalgar (TF). Additionally, three off-shore stations were sampled (GS1, ST1, and ST2; Fig. 1).

Seawater samples were collected using Niskin bottles (10 L) mounted

on a rosette-sampler coupled to a Seabird CTD 911+, which measured salinity (S), temperature (T), dissolved oxygen (DO) and in vivo chlorophyll *a* fluorescence (Chl *a*). For the calibration of the Chl *a* fluorescence, data from González-García et al. (in prep.) was used. Apparent oxygen utilization (AOU) was calculated as the difference between DO at saturation and measured DO concentrations, where DO saturation was calculated from salinity and temperature following Benson and Krause (1984). Nitrate analyses were performed in a segmented flow autoanalyzer (Skalar, San Plus) based on classic spectrophotometric methods (Grasshoff and Ehrhardt, 1983) with an accuracy of ± 0.10 µM). Complementary variables such as cumulative rainfall and monthly UV solar radiation were obtained from http://www.chguadalquivir.es and http://www.soda-pro.com, respectively. Wind speed data (Sensor 2740 situated at 10 m height) were sourced from the Aanderaa Automatic Weather Station.

IV. 2.3 Determination of DOC, CDOM, and FDOM

Samples for DOC, CDOM, and FDOM analyses were collected in 0.25 L acid-cleaned amber glass bottles. Seawater was filtered through combusted Whatman GF/F filters (450 °C, 4 h) with an acid-cleaned glass filtration system, previously rinsed with the sample. Samples for DOC were taken in duplicate and kept in the dark at -20 °C until analysis. DOC concentration was determined by high-temperature catalytic oxidation using a Multi N/C 3100 Analytik Jena analyzer, calibrated daily using potassium hydrogen phthalate (Panreac, 99.1 %). Deep seawater and low carbon reference waters (Hansell CRM Program, 42-45 µM) were measured to assess instrument variability (n = 5, 43 ± 1.8 µM).

UV-visible absorption spectra of CDOM (250-800 nm) was measured on board at a 1-nm interval using a JASCO-V750 spectrometer connected to a programmable temperature control system set at 20 °C. A 10-cm path length quartz cuvette was used. Samples were blank corrected by subtracting the absorbance of daily Milli-Q water from the spectra, and a baseline correction was applied by subtracting the average absorbance between 600 and 800 nm to the measured absorption spectrum (Green and Blough, 1994). The corrected absorbance was converted into Napierian absorption coefficients (a_{λ}, m^{-1}) by multiplying by 2.303 and dividing by the cuvette path length (0.1 m) (Blough and Del Vecchio, 2002). In this study, we focused on the absorption coefficients at 254 (a_{254}), since a strong relationship with the absorption coefficient at 350 nm was observed (R^2 = 0.74, $p < 0.05$). a_{254} is proportional to the abundance of conjugated carbon double bonds and proposed as a proxy of DOC concentration (Lønborg and Álvarez-Salgado, 2014; Catalá et al., 2018). The specific ultraviolet absorbance at 254 nm ($SUVA_{254}$) is strongly correlated with aromaticity percentage and was calculated by dividing the decadic absorption coefficient at 254 (m^{-1}) by the concentration of DOC (mg C L^{-1}) (Weishaar et al., 2003). The spectral slope between 275 nm and 295 nm ($S_{275–295}$), related to DOM molecular weight, was determined according to Helms et al. (2008).

Fluorescence was measured on board in a 1-cm quartz cuvette, using a spectrofluorometer (JASCO FP-8300) connected to a Peltier Thermostatted Cell Holder with Stirrer accessory (EHC-813) for temperature control (20 °C). Excitation-Emission matrices (EEMs) were obtained for emission wavelengths from 300 nm to 560 nm (1 nm steps) and excitation wavelengths from 240 nm to 450 nm (5 nm steps) with a bandwidth of 5 nm and an integration time of 0.2 s. Raman peak at 350

nm, using Milli-Q water, was measured daily for sample blank correction together with a standard of quinine sulfate monohydrate (Sigma Aldrich, 98%) in H_2SO_4 to check system performance.

The drEEM 0.2.0 toolbox was used to standardize the EEMs (Murphy et al., 2013). Spectra were improved by the instrument correction factors obtained from the manufacturer's protocol using Rhodamine A. Inner filter effect was addressed by correcting EEMs using the absorbance-based approach (Kothawala et al., 2013), data was standardized and normalized to Raman Units (RU) based on measurements of Raman peak at 350 nm (Lawaetz and Stedmon, 2009).

IV. 2.4 PARAFAC Modeling

Multivariate parallel factor analysis (PARAFAC) was employed to identify the different fluorescent components (fluorophores) that comprise the EEMs. PARAFAC was performed using the drEEM toolbox (version 0.2.0; Murphy et al., 2013) for Matlab (R2015b). Briefly, Raman and Rayleigh scatter bands (first and second order) were trimmed in each EEM. Corrected EEMs were normalized by their intensities, along with using non-negative constraint. Six independent components were identified using split-half validation with a convergence criterion of 10^{-8}, random-initialization analysis, and thorough examination of outliers and model's residuals (Stedmon and Bro, 2008). The online repository OpenFluor database (Murphy et al., 2014), along with published literature, were used for the identification of the PARAFAC components.

Given the major variation between allochthonous and autochthonous DOM in water samples, a misleading artifact may arise when modeling all samples together, hindering the accurate identification of

biogeochemical facts regarding fluorescent components and their respective mechanisms (Mostofa et al., 2019). We performed individual seasonal models (n = 185-191) to assess whether PARAFAC modeling using all water samples together leads to information loss, such as masking seasonal variation of FDOM sources and therefore missing the underlying biogeochemical process. Nevertheless, we found that the components in the global model (n = 766) encompassed all components in individual seasonal models. In spring and winter, the same three-component models were obtained with one humic and two protein-like components (Fig. S3). In autumn and summer, PARAFAC validated a six-component model with the same components identified in the global model, except for C5 that showed slightly different Ex/Em peaks in the summer model (Fig. S3). Therefore, for simplicity and a better understanding of FDOM distribution in the GoC, only components of the global model will be described.

IV. 2.5 Optimum multiparameter water mass analysis

The variability of DOC, CDOM, and FDOM depends on water mass mixing and biogeochemical processes. To remove the variability caused by physical processes, we performed an optimum multiparameter water mass analysis (OMP, Poole and Tomczak, 1999). We obtained the mixing proportion of the different water masses found in the GoC for each water sample. Temperature and salinity, previously described in Flecha et al. (2012), were used as parameters to define the source water typeqws (SWT). The analysis was carried out following Álvarez et al. (2014) using samples below 100 m depth (n = 256) since the influence of atmospheric interaction on T and S was observed in data above that depth. Once the water mass proportions were obtained for each sample, predicted variables (T, S, AOU, NO_3, DOC, CDOM and FDOM) were back-calculated through the linear

regression between the SWT matrix and the observed variable. The high determination coefficients ($R^2 > 0.99$) between the measured and predicted variables for T and S, as well as the low standard deviation of the corresponding residuals ($<10^{-6}$), show that OMP results were reliable.

IV. 2.6 Statistical Analysis

Permutational analysis of variance (PERMANOVA) was performed to assess seasonal, vertical, and spatial differences between physicochemical variables (T, S, AOU, and Chl *a*).

To determine seasonal, vertical and spatial significant differences for DOC, CDOM, and PARAFAC components, and given the data structure, Kruskal Wallis non-parametric analysis of variance and post hoc pairwise Wilcoxon test (using Bonferroni to adjust p-value) were performed. A significance level of 0.05 was selected.

Linear regression models were developed to assess the effect of environmental conditions on the variability of DOC, CDOM and PARAFAC fluorescent components in the surface water of the GoC, and were considered statistically significant when $p < 0.01$. T and S were used as explanatory variables to assess the influence of physical conditions. All analyses were performed in R 3.5 software (R Development Core Team, 2018) using 'stats' and 'vegan' packages.

IV. 3. Results

IV. 3. 1. Fluorescent DOM components in the Gulf of Cádiz

Six fluorescent components were statistically obtained from the global PARAFAC model (Murphy et al., 2013, Fig. S2, Table S2). Components 1 (C1) and 3 (C3) have been classified as humic-like (Coble,

1996), described in almost all aquatic environments. C1 presented similar spectral characteristics to Coble's marine peak-M (Coble, 1996). However, it has been reported to have ubiquitous, allochthonous, and autochthonous origins and described for non-marine environments. C3 seems a mixture of the traditional peaks A and C (Coble, 1996). Component 4 (C4) has also been described as a common terrestrially derived component or produced after DOM exposure to UV radiation. Component 2, 5, and 6 (C2, C5, and C6) have been classified as fluorescent protein-like compounds, with narrow excitation bands and emission maxima below 400 nm, containing a fraction of autochthonous DOM. Components similar to C2 and C6 have been associated with Coble's peak-T and peak-B, respectively (Coble, 1996), while C5 shows emission and excitation maxima similar to peak-N (Coble et al., 2014). However, C5 had the lowest Tucker congruence in the Openfluor database, and the peculiar spectra of this component could be related to the presence of polycyclic aromatic hydrocarbon (PAH) which fluoresces in the same region as protein-like groups (Coble et al., 2014). Nevertheless, it could also be a mixture of PAH and protein-like compounds, as it has been previously suggested for similar components.

IV. 3.2. Physicochemical characteristics

Temperature in 2016 ranged from 11.4 to 22.9 °C, with the lowest values in March and the highest ones in September. S showed low variability, with an average value of 36.27 ± 0.34. T and S revealed a marked stratification of the water column during autumn and summer with an average thermocline depth of 39.4 ± 15.6 m (Table S1). During spring and winter, a strong mixing was observed with an average thermocline depth of 71.4 ± 34.5 m (Table S1). Chl *a* showed an average value of 0.31 ± 0.39 μg L^{-1} with maxima around 3.5 μg L^{-1} in spring and summer in the coastal zone.

This was probably due to the influence of St. Vincent upwelling and, to a lesser extent, to the riverine nutrients input. AOU was also highly variable, with values > 100 µM, characteristic of MOW, and minimum values < -80 µM corresponding to Chl *a* maxima in coastal stations.

PERMANOVA analyses showed that physicochemical variables (T, S, AOU, and Chl *a*) were statistically different ($p < 0.001$) and dependent on the season ($p < 0.001$) when comparing data from above and below the thermocline. Therefore, the dataset was split into data above (surface water, SurfW) and below the thermocline (deep water, DeepW) (Table 1). Figure S4 shows T, S, AOU, Chl *a*, and DOC profiles in GD transect during the mixed and stratified period as an example of vertical distribution.

In spring and winter, westerly winds with high average speed were predominant, while in summer and autumn, easterly winds with lower speed prevailed (Table S1). During spring, strong west winds favored the occurrence of the "Huelva Front" (Fig 3A and 3E). This was characterized by upwelled NACW extending cold water onto the coastal zone up to SP (Stevenson, 1977) and the warmer water carried by the Azores current towards the east, in the oceanic zone. During summer, the upwelling extension eastward from Cape St. Vincent lost intensity due to the easterly winds, still with a signature of cold, less salty waters, and relatively high Chl *a* (Fig. 2B, 2F and 2N). The semipermanent Trafalgar upwelling was clearly observed during autumn (Fig. 2C). In summer and winter, water with lower salinity was observed along the entire coastline ($p < 0.05$), probably due to the influence of accumulated rainfalls before the sampling dates (Table S1). Coastal stations showed higher Chl *a* values than off-shore stations for all the seasons ($p < 0.05$), and no differences were observed in AOU ($p > 0.05$). Here we define coastal stations as the stations with a maximum depth of 60

m (Bellanco and Sánchez-Leal, 2016) (Fig. 1, stations 1 and 2), and off-shore stations as those with a bottom depth > 60 m (Fig. 1, stations 3 to 7 and external stations).

Table 1. Average ± standard deviation values of temperature (T, °C), salinity (S), apparent oxygen utilization (AOU, µM), chlorophyll *a* (Chl *a*, µg/L), dissolved organic carbon (DOC, µM), CDOM absorption coefficient at 254 (a_{254}, m^{-1}), $SUVA_{254}$ index (L mg^{-1} m^{-1}) and the spectral slope $S_{275-295}$ (nm^{-1}) from surface (SurfW) and deep water (DeepW).

	Spring		Summer		Autumn		Winter	
	SurfW	DeepW	SurfW	DeepW	SurfW	DeepW	SurfW	DeepW
T	14.9 ± 0.9	13.6 ± 0.8	18.1 ± 1.9	13.9 ± 1.0	19.2 ± 2.5	14.2 ± 1.1	18.1 ± 1.0	14.2 ± 1.1
S	36.17 ± 0.16	36.19 ± 0.53	36.23 ± 0.18	36.19 ± 0.51	36.42 ± 0.13	36.25 ± 0.45	36.39 ± 0.12	36.25 ± 0.45
AOU	24.3 ± 16.1	60.9 ± 19.9	-1.7 ± 20.9	53.3 ± 14.5	-0.6 ± 14.9	46.2 ± 17.3	11.6 ± 10.9	46.2 ± 17.3
Chl *a*	0.5 ± 0.5	-	0.6 ± 0.6	-	0.4 ± 0.3	-	0.3 ± 0.1	-
DOC	73.6 ± 14.9	72.9 ± 17.6	86.4 ± 13.1	72.9 ± 6.1	80.6 ± 7.7	69.4 ± 7.5	72.2 ± 8.8	63.5 ± 8.9
a_{254}	1.38 ± 0.31	1.25 ± 0.27	1.75 ± 0.31	1.24 ± 0.25	1.44 ± 0.23	1.16 ± 0.17	1.47 ± 0.27	1.22 ± 0.23
SUVA	0.65 ± 0.14	0.63 ± 0.16	0.74 ± 0.19	0.59 ± 0.12	0.63 ± 0.09	0.59 ± 0.10	0.71 ± 0.13	0.67 ± 0.14
$S_{275-295}$	0.030 ± 0.008	0.027 ± 0.005	0.026 ± 0.006	0.025 ± 0.005	0.033 ± 0.004	0.030 ± 0.004	0.032 ± 0.06	0.027 ± 0.005

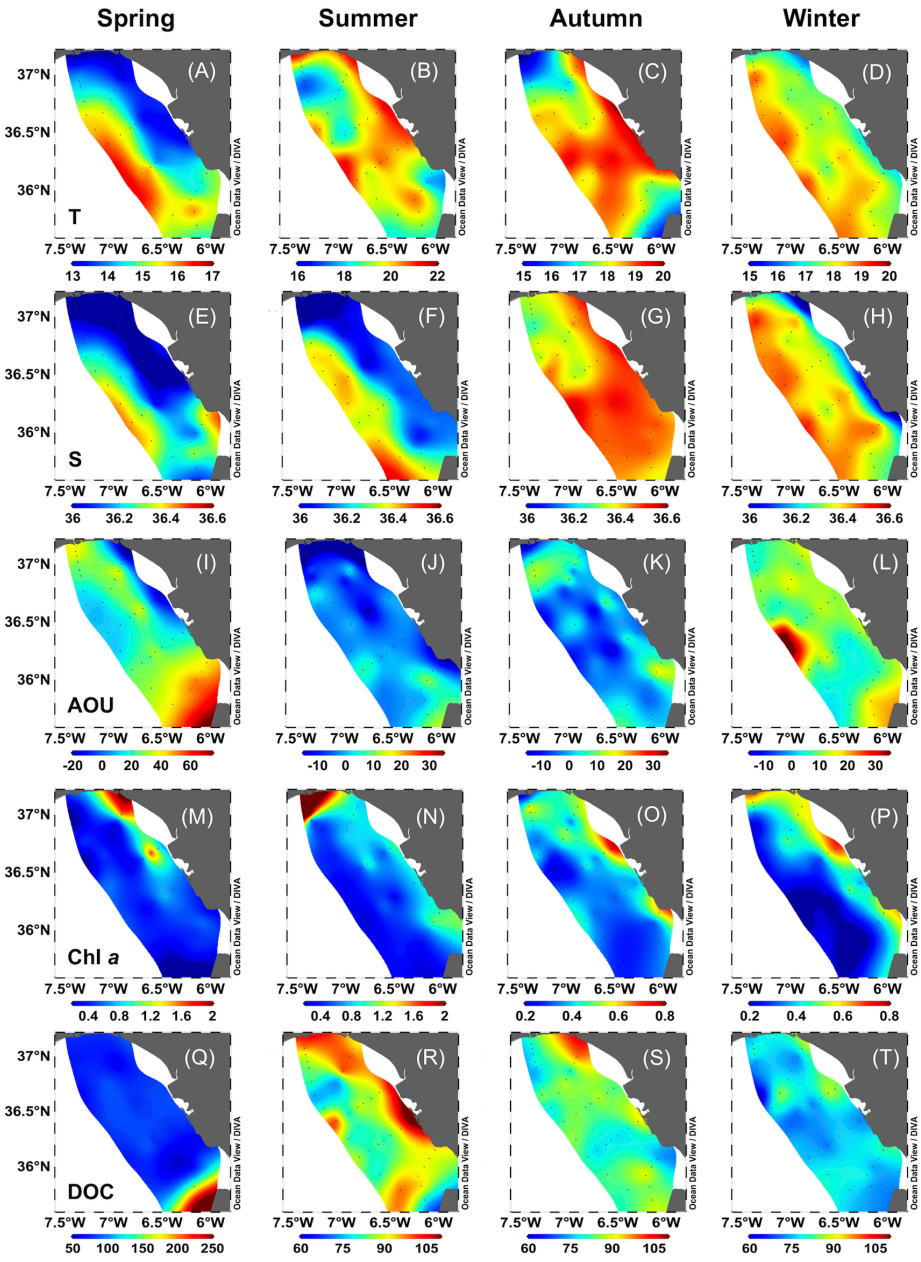

Fig. 2. Surface water distribution of temperature (T, °C), salinity (S), apparent oxygen utilization (AOU, µM), dissolved organic carbon (DOC, µM) and chlorophyll *a* (Chl *a*, µg L^{-1}) during spring, summer, autumn and winter 2016 in the Gulf of Cádiz.

IV. 3.3 Distribution of DOC, CDOM, and FDOM in the Gulf of Cádiz

DOC ranged from 67.0 to 175.7 µM, which falls within the range of previously reported values for the area (Ribas-Ribas et al., 2011b). Lower average values were observed in spring and winter and higher during autumn and summer ($p < 0.05$). a_{254} ranged between 0.76 and 3.73 m^{-1}, excluding maximum values found in SurfW during spring in TF (4.01-5.68 m^{-1}, n = 5) that matched elevated DOC values (> 150 µM, Fig. 2Q). $SUVA_{254}$ index ranged between 0.29 and 1.36 L mg^{-1} m^{-1}, while $S_{275-295}$ ranged between 0.014 and 0.059 nm^{-1}. Summer showed the highest values of $SUVA_{254}$ ($p < 0.05$) and the lowest of $S_{275-295}$ ($p < 0.05$).

Unexpectedly, high values for protein-like C2 were observed in summer samples from SP6 and SP7 between 150 and 650 m depth and TF6 between 75 and 90 m depth. These values (n = 9) were three orders of magnitude higher than the average (> 0.90 RU) and therefore excluded from the analyses. Other sources of the anomaly are discussed in section 4.3. The two major humic-like components, C1 and C3, were highly correlated with each other (n = 753, $R^2 = 0.75$, $p < 0.001$) and displayed the same distribution pattern, thus, for simplicity we will report only C1.

Humic-like C1 ranged from 0.003 to 0.024 RU (Fig. 3A), while C4 ranged between 0 and 0.21 RU, with the highest values during summer and autumn ($p < 0.05$, Fig. 3B). Protein-like C2 displayed the highest seasonal variability among all components ranging from 0.00048 to 0.69 RU (Fig. 3C and 3D). In summer, C2 mean values were ten times higher than in the rest of the seasons. C5 varied between 0 and 0.086 RU and C6 between 0 and 0.097 RU (Fig. 3E and 3F).

We observed variability in the vertical distribution of DOC with higher values occurring in SurfW than in DeepW, especially during the stratified period (summer and autumn, $p < 0.05$, Table 1). Similar to DOC concentrations, average measurements of a_{254}, $SUVA_{254,}$ and $S_{275-295}$ were higher in SurfW than in DeepW for all seasons ($p < 0.05$, Table 1). Vertical profiles of FDOM during the mixed and stratified period in the GD transect are presented as an example of vertical distribution (Fig. S5). Humic-like C1 increased with depth and presented seasonal variability in SurfW, with lower values during the mixed period (spring and winter). Instead, in DeepW, C1 remained constant during the four sampling periods. C2 and C4 showed similar values between layers along seasons ($p > 0.05$), while C5 and C6 showed higher intensities at the surface during the stratified period ($p < 0.05$).

We also observed spatial variability in DOC, CDOM, and FDOM distribution. Coastal stations showed higher values of DOC, $a_{254,}$ and $SUVA_{254}$ and lower of $S_{275-295}$ than off-shore stations ($p < 0.05$, Table 2). They also showed higher values of C1, C5, and C6 than off-shore stations ($p < 0.05$, Fig. 4A-D, Fig. 4M-P and Fig. 4Q-T, respectively). Conversely, C2 and C4 showed no spatial differences ($p > 0.05$, Fig. 4E-H and Fig. 4I-L, respectively).

The relative contribution (%) of each fluorophore was determined to assess the dominant fraction of FDOM (Tanaka et al., 2016). Protein-like C6 was the dominant fraction in spring, autumn and winter, contributing with 37.43 % ± 7.43 % to the total FDOM. In summer, protein-like C2 was the most abundant, accounting for 56.94 % ± 26.28 % and decreasing to 6.22 % ± 3.83 % in other seasons. Thus, the sum of protein-like

components (C2+C5+C6) dominated the FDOM pool during the study period (64.75 % ± 7.85 %).

Table 2. Average ± standard deviation values of dissolved organic carbon (DOC, µM), CDOM absorption coefficient at 254 (a_{254}, m^{-1}), $SUVA_{254}$ index (L mg^{-1} m^{-1}), the spectral slope $S_{275-295}$ (nm^{-1}), and fluorescent components (C1-C6, RU) from surface coastal and off-shore stations. * Indicate significant difference between zones, $p < 0.05$.

Variable	Coastal stations	Off-Shore stations
DOC*	81.1 ± 13.0	77.3 ± 12.1
a_{254}*	1.79 ± 0.54	1.49 ± 0.46
$SUVA_{254}$*	0.76 ± 0.19	0.66 ± 0.12
$S_{275-295}$*	0.027 ± 0.006	0.031 ± 0.007
C1*	0.010 ± 0.003	0.007 ± 0.002
C2	0.034 ± 0.038	0.028 ± 0.034
C4	0.009 ± 0.003	0.008 ± 0.003
C5*	0.013 ± 0.005	0.010 ± 0.004
C6*	0.027 ± 0.010	0.020 ± 0.009

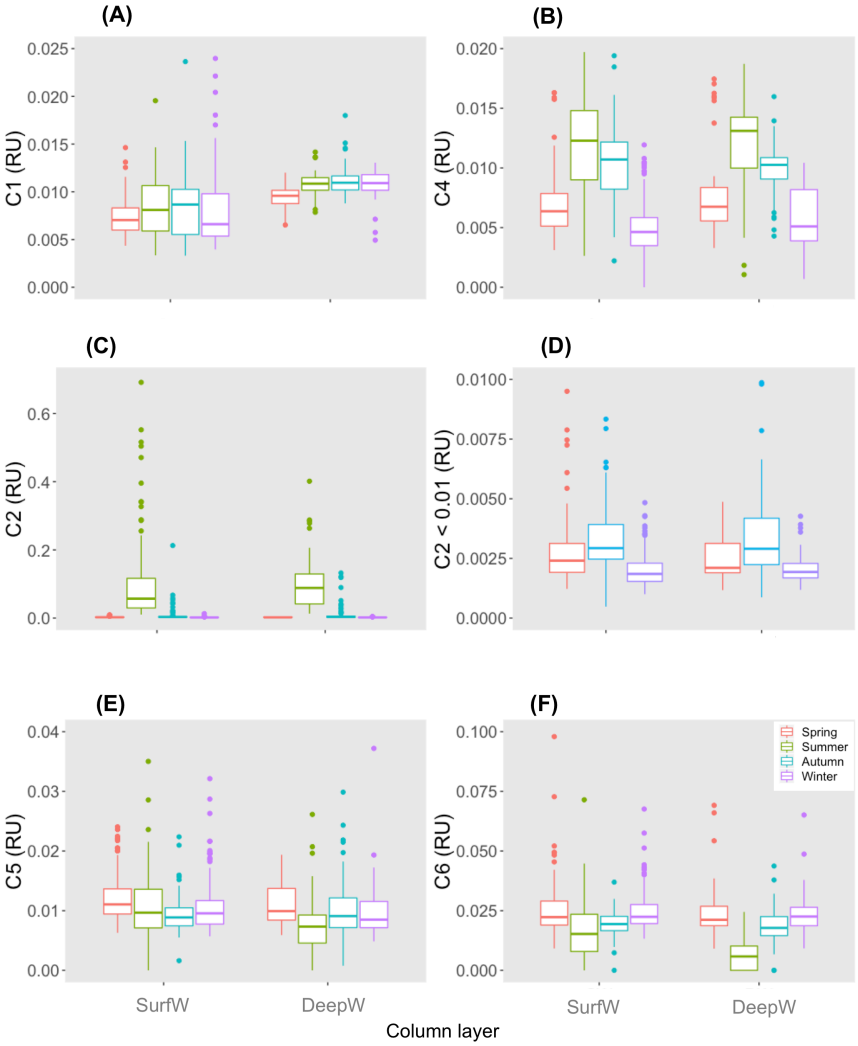

Fig. 3. Average intensities of PARAFAC components- **(A)**: C1, **(B)**: C4, **(C y D)**: C2, **(E)**: C5 and **(F)**: C6- for each season at surface water (SurfW) and deep water (DeepW) in the Gulf of Cádiz.

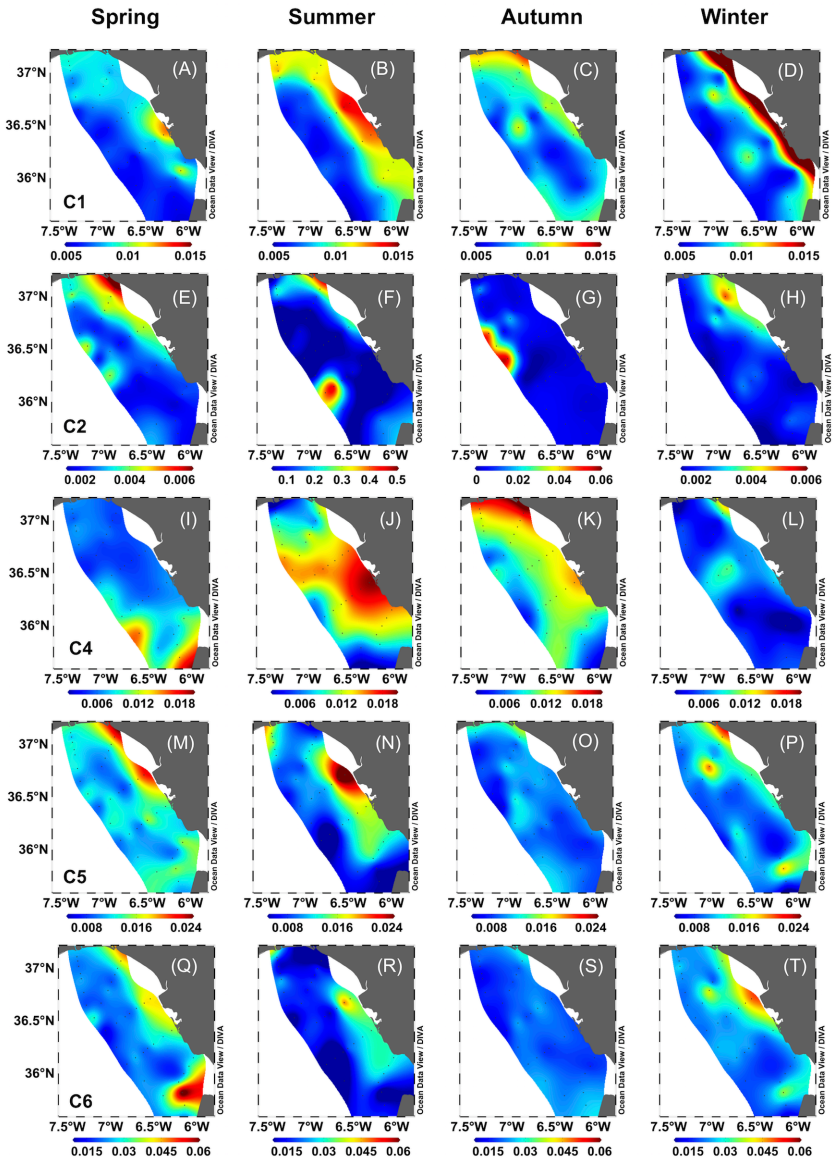

Fig. 4. Surface water distribution of fluorescent components for each season: **(A-D)**: C1, **(E-H)**: C2, **(I-L)**: C4, **(M-P)**: C5, **(Q-T)**: C6. Units are in RU. Note that C2 shows different scales in summer and autumn.

IV. 3.3.1 DOC, CDOM and FDOM drivers in the surface layer

Multiple linear regressions with T and S were applied to determine the contribution of water mass mixing to DOM surface distribution (Table S3). DOC and a_{254} showed weak but significant relationships with T and S, with highest and lowest explained variation occurring in autumn ($R^2 = 0.36$, $p < 0.001$) and spring ($R^2 = 0.09$, $p < 0.001$), respectively.

Among fluorescent components, the highest relationship with T and S was found for humic-like C1, with the highest explained variation in summer and winter ($R^2 = 0.69$ and 0.79, respectively, $p < 0.001$) and the lowest in spring and autumn ($R^2 = 0.50$ and 0.59, respectively, $p < 0.001$). Protein-like fluorescent components showed lower relationship with T and S than humic-like components ($R^2 < 0.36$; $p < 0.001$). Terrestrial photoproduct C4 showed a significant correlation with T and S only in spring ($R^2 = 0.27$, $p < 0.01$).

IV. 3.3.2. DOM drivers in deep waters: OMP analysis

A strong relationship was observed between calculated and observed values for AOU and nitrate ($R^2 = 0.82$ and 0.87, respectively, $p < 0.001$, $n = 256$), with typical values coinciding with previous reports in the GoC (Table 3, Flecha et al., 2012). DOC and a_{254} were weakly correlated with water mass mixing ($R^2 = 0.27$ and 0.18, respectively, $p < 0.01$, $n = 254$). Unlike protein-like components, humic-like C1 and C4 presented a strong linear relationship with water mass mixing proportions ($R^2 = 0.68$, and 0.66, respectively, $p < 0.001$).

Table 3. Biogeochemical and fluorescence typical values of selected water mass in OMP analyses in deep water. Results are presented as the seasonal average ± standard deviation. Temperature (T, °C), salinity (S), apparent oxygen utilization (AOU, µM), nitrate (µM), dissolved organic carbon (DOC, µM), absorption coefficient a_{254} in m^{-1}, marine humic-like (C1, RU) and terrestrial photoproduct (C4, RU) fluorescent components are presented.

SWT	T	S	AOU	Nitrate	DOC	a_{254}	C1	C4
$NACW_T$	17.3 ± 0.03	36.49 ± 0.01	8.7 ± 5.5	0.9 ± 0.7	75.9 ± 7.7	1.35 ± 0.16	0.0081 ± 0.0021	0.0080 ± 0.0030
$NACW_S$	11.3 ± 0.03	35.56 ± 0.01	84.0 ± 5.5	12.5 ± 1.2	67.7 ± 6.8	1.10 ± 0.06	0.0122 ± 0.0003	0.0097 ± 0.0028
MOW	13.1 ± 0.01	38.50 ± 0.01	90.8 ± 14.5	9.1 ± 0.9	66.9 ± 7.7	1.16 ± 0.11	0.0115 ± 0.0018	0.0084 ± 0.0024

IV. 4. Discussion

IV. 4.1. PARAFAC model: Fluorescent components in the GoC

All the six fluorescent components found in the GoC have been previously described in other marine and freshwater systems (Table S2). Among the humic-like components, C1 has been associated with microbial activity mixed with old humic material in coastal waters (Coble et al., 2014). It has been reported as ubiquitous, found in almost all environments, and derived from both autochthonous and allochthonous sources. C4 follows the same trend as UV radiation, increasing in summer and autumn and decreasing in winter and spring (Fig. S6, $R^2 = 0.98$, $p < 0.001$), supporting previous suggestions that it is produced during the exposure of DOM to UV radiation (Table S2). Protein-like C2 and C6 resemble the amino acids tryptophan and tyrosine, respectively. Finally, C5 is less common than other components and can be a combination of fluorophores containing both protein fluorescent structures and PAH substances. Abundant UV-A signals (Em < 400 nm, "protein-like"), as in our case, could be challenging for PARAFAC since spectra are shorter and steeper and affected by Raman and Rayleigh scatter (Murphy et al., 2018). Gonnelli et al. (2016) found a mixture of PAH and protein-like components with similar fluorescent characteristics as our C5 in surface water affected by oil spills. Their samples showed single fluorescence spectra with excitation at 255 nm and characteristic emission peaks of main oil components: fluorene (316 nm) and pyrene (372 nm). Both peaks were also observed in our C5. The GoC is located in one of the most important maritime crossroads in the world. More than 10% of international maritime traffic crosses the Strait of Gibraltar (145-192 ships per day), a percentage that rises in the case of oil

tankers, as it is a key connection point with the greatest oil producers (http://www.juntadeandalucia.es). Oil contaminated ballast water and bunkering (refueling) represent an important source of marine pollution in the GoC (http://www.marineplan.es). Thereby, in this work, C5 could be a yet unresolved fluorescent group consisting of a mixture of protein-like material and oil-derived compounds. However, further analysis will be necessary to confirm such origin.

IV. 4.2. DOM distribution in Surface Water

DOC and CDOM concentrations in the GoC fall within the range previously described for coastal and marine systems (Romera-Castillo et al., 2011; Nelson and Siegel, 2013). Nevertheless, the average annual mean concentration of surface DOC and CDOM are slightly lower than those observed in other oligotrophic coastal systems (Romera-Castillo et al., 2013). DOC has shown to be negatively correlated with salinity in the coastal zone (Cauwet, 2002); however, in this work, a strong relationship was not observed, in agreement with previous studies in this area (Ribas-Ribas et al., 2011b). In our study, water samples were collected between 7 and 16 km of the river mouth, and thus were likely too far from the river to observe a strong influence of terrestrial inputs. This is consistent with the low salinity range found here (35.8-36.6), and could also be the reason for water mass mixing explaining less than 36 % of DOC and CDOM surface distribution (Table S3). Another explanation for the low relationship between DOC and salinity could be the complexity of this transitional coastal-ocean system, where DOM is a mixture of allochthonous and autochthonous components.

CDOM is a reliable proxy for DOC in several aquatic systems (Lønborg and Álvarez-Salgado, 2014; Rochelle-Newall et al., 2014, Catalá et

al., 2018). However, this relationship can be weak in coastal regions not strongly influenced by riverine inputs (Del Castillo et al., 2000; Ferrari, 2000). Again, the long distance between the coast and the first stations sampled here could explain the low relationship between DOC and CDOM in SurfW (R^2 = 0.48, p < 0.001, n = 460). Another possibility is that the inner shelf coastal counter-current that transports water westward during most of the year (Garel et al., 2016), removes continental inputs, resulting in a weak terrestrial DOM signal. Additionally, that relationship can also be altered by the photodegradation of the CDOM (Blough and Del Vecchio, 2002) and microbial processing (Helms et al., 2008) during its transport along the estuaries.

In the open ocean, a strong relationship between CDOM and DOC concentrations is not usually observed (Nelson and Siegel, 2013). In the GoC, the relationship between CDOM and DOC was lower than in other open-ocean systems (R^2= 0.46, p < 0.001, n= 751) such as the Northeast Atlantic Ocean (R^2 = 0.80, n = 233, Lønborg and Álvarez-Salgado 2014), and the Mediterranean Sea (R^2 = 0.87, n = 273 Catalá et al., 2018). In our study, the intercept of this relationship indicates that 33.8 µM of DOC vary independently of a_{254}. This value is higher than the 10 µM found in the Northeast Atlantic Ocean and Mediterranean Sea (Catalá et al., 2018; Lønborg and Álvarez-Salgado 2014). This shows that equations for DOC predictions using a_{254} had to be site-specific (Catalá et al., 2018) and that this method should not be used in ecosystems with highly variable DOC and CDOM sources (Rochelle-Newall et al., 2014).

The great variability observed in $S_{275\text{-}295}$ (0.014-0.059 nm^{-1}) covers values frequently observed in rivers (0.013 -0.017 nm^{-1}, Shen et al., 2012) and oligotrophic seawaters (0.04 nm^{-1}, Aurin and Mannino, 2012). This

result suggests that the DOM pool in the GoC comprises a wide range of molecules with different molecular weights. On the other hand, according to $SUVA_{254}$ values identified by Weishaar et al. (2003), DOM in the GoC is more similar to DOM found in the ocean than in freshwater environments. Noteworthy, the average value found in our work (0.8 ± 0.1 L mg C^{-1} m^{-1}) was lower than the one found by Massicotte et al., 2017 for the open ocean (1.7 ± 0.2 L mg C^{-1} m^{-1}). In summer and winter, high molecular weight and aromatic compounds dominated the DOM pool, indicated by high $SUVA_{254}$ and low $S_{275-295}$ values, respectively (Weishaar et al., 2003; Helms et al., 2008).

Average seasonal deep DOC maximum and deep fluorescence maximum (DFM) from CTD showed the same pattern, increasing from autumn to spring (Fig. 5). That, together with the strong linear relationship observed between them ($R^2 = 0.95$, $p < 0.05$), suggests that phytoplankton release may be the most important source of DOC, as it has been previously suggested for this area (Huertas et al., 2005; Ribas-Ribas et al., 2011b). Huertas et al. (2005) found the DOC maxima matching the highest Chl *a* concentrations indicating that seasonal distribution of DOC in the GoC is related to phytoplankton biomass variation. However, we found a low correlation between DOC and CDOM with Chl *a*. In the GoC, pico and nanophytoplankton are the dominant fraction of phytoplankton and have been associated with the DFM (González-García et al., 2018). A lack of direct relationship between Chl *a* and picoplankton biomass was attributed to a low Chl *a*/cell ratio, distinctive of oligotrophic systems (Echevarría et al., 2009).

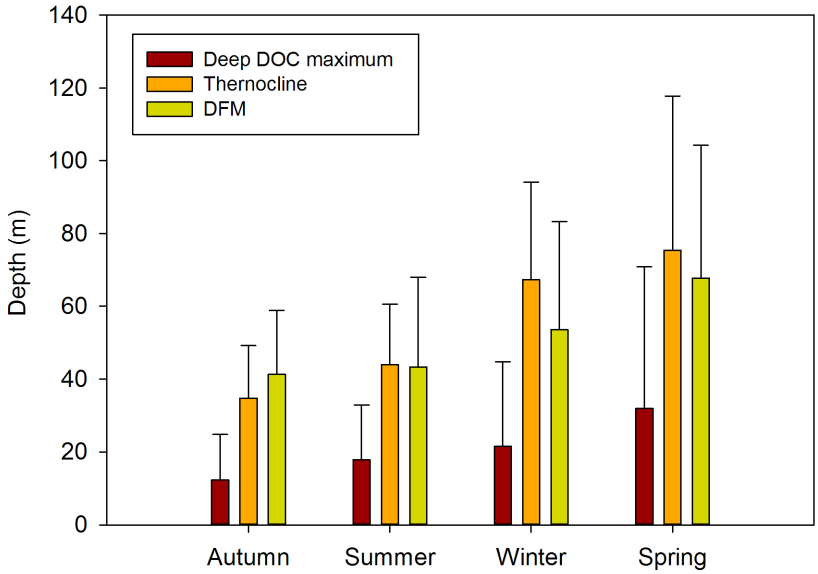

Fig. 5. Deep DOC maximum, thermocline and deep fluorescence maximum (DFM) averages for each season.

FDOM variation in the GoC showed a humic-like C1 distribution mostly explained by water mass mixing, especially in winter (80%) and summer (70%) when higher monthly accumulated precipitation took place (Table S1). Coastal stations showed higher fluorescence of C1 during these seasons, probably due to the supply of terrestrial DOM, which plays a major role in the distribution of humic-like material in the ocean (Jørgensen et al., 2011). González-Ortegón et al. (2018) found that the GoC is receiving large amounts of humic FDOM through riverine inputs with salinity as the main factor explaining FDOM variability within the Guadalquivir and Guadiana rivers and in the inner shelf of the GoC. Although in our work a strong influence of terrestrial inputs along the year was not observed, the signature of humic-like C1 during winter was evident across the coastal stations (Fig. 4D). That could be associated with the combination of continental inputs and a lower degree of photodegradation during this

season. Moreover, C1 was lower in SurfW than DeepW (Fig. 3A) in agreement with other works suggesting that photochemical degradation is the major removal mechanism of humic-like components at surface in aquatic systems (Nieto-Cid et al., 2006; Jørgensen et al., 2011). Finally, in spring, 50 % of the distribution of C1 was also explained by water mass mixing; however, it could be associated with the upwelling characterized by the "Huelva Front" (Fig. 2A and 2E) favored by intense west winds during this season (Table S1). On the other hand, the strong relationship observed between average C1 maxima depth and DFM in off-shore SurfW stations ($R^2 = 0.70$, $p < 0.05$) supports the hypothesis that phytoplankton is the main producer of humic-like FDOM in the outer shelf of the GoC, as proposed by González-Ortegón et al. (2018). Finally, C4 seems to have a relatively constant vertical and spatial distribution along the upper column with no changes during the stratified period (Fig. 3D). Its variability would be better linked to seasonality due to changes in UV radiation (Fig. S6).

Distribution patterns were different between protein-like C2 and C6 and the relationship between them was low ($R^2 = 0.2$, $p < 0.001$, $n = 460$). This suggests that the sources and sinks for both components were not the same. On the other hand, C5 follows a pattern more similar to tyrosine-like C6 than to tryptophan-like C2 ($R^2 = 0.50$ and 0.02, respectively, $p < 0.001$, $n = 460$). In general, water mass mixing explained less than 36 % of the protein-like surface distribution. In coastal environments, a major source of protein-like components is autochthonous production by phytoplankton (Coble, 2007). C6 was higher at surface in agreement with the observed decrease of this component with depth in the ocean (Catalá et al., 2015). That is the same general pattern observed for DOC and Chl *a* (coastal and surface) linked to primary production in the surface layer. On the other

hand, tryptophan fluorescence has been related to heterotrophic bacteria (Determann et al., 1998; Amaral et al., 2016) and associated with phytoplankton blooms in coastal environments (Para et al., 2010), which could explain the higher fraction of C2 found in summer after the spring bloom. However, no clear spatial distribution pattern was observed for this component. Maie et al. (2007) found that a large portion of peak-T was associated with non-proteinaceous material, and they proposed that such fluorescence could be attributed to tannin-associated phenols. They suggested that the tryptophan-like component is composed of a mixture of proteinaceous and presumably phenolic materials in humic-like substances with different chemical structures and ecological roles. Furthermore, polyphenolic compounds are also produced by brown algae (Geiselman and McConnell, 1981), which have massively expanded over the GoC in recent years (García-Gómez et al. 2018). The diverse sources of the protein-like C2 may explain the lack of a clear pattern on its spatial distribution in this work.

IV. 4.3. DOM distribution in Deep Water

DOC concentration in the DeepW of the GoC was not dependent on the water mass mixing since it only explained 27 % of DOC distribution. This result contrasts with the Mediterranean Sea, where water mass mixing explains 83 % of DOC variation (Catalá et al., 2018). This could be due to the multiple DOC sources found in the GoC, as it has been proposed for other coastal-ocean transitional systems (Liu et al., 2010). The intercept of the linear regression between the observed and calculated values from the OMP analysis showed that 54.3 µM of DOC vary independently of water mass mixing. CDOM was not dependent on the water mass mixing either, showing a non-conservative behavior. Therefore, DOC and CDOM variability are associated with biogeochemical processes occurring in the

water masses from their origin to the sampling site at a local scale. Conversely, around 70 % of humic-like compounds variability was dependent on the water mass mixing, in agreement with other studies (Álvarez-Salgado et al., 2013; Catalá et al., 2015; Martínez-Pérez et al., 2019).

The relative importance of microbial respiration on DOC and CDOM distribution can be obtained through a linear relationship between the residuals of those variables and AOU residuals (Romera-Castillo et al., 2011b). The AOU reflects the net ecosystem metabolism, i.e., the net production of dissolved oxygen due to primary producers minus the net consumption by respiration (Smith and Hollibaugh, 1997). The difference between the observed and the OMP analyses back-calculated variables yielded the residuals of such variables, which variation is due to biogeochemical processes (Romera-Castillo et al., 2019). Although the relationship between AOU residuals (AOU_{res}) and DOC residuals (DOC_{res}) in the whole dataset was low and not significant (n = 256), when the dataset was sorted by upwelling affected stations, we found different relationships between these variables. Specifically, AOU_{res} and DOC_{res} showed a negative linear relationship in the stations less affected by the upwelling (TO, GD, SP and external stations, $R^2 = 0.17$, $\beta = -0.47$, $p < 0.001$, n = 168). This result indicates that DOC supports 17 % of heterotrophic metabolism. This value is within the range found by Arísteguí et al. (2002) of 10 - 20 % in the mesopelagic ocean (200–1000 m). On the contrary, in the stations affected by upwelling (TF and GU), a positive linear relationship was observed between AOU_{res} and DOC_{res} ($R^2 = 0.28$, $\beta = 0.59$, $p < 0.001$, n = 74). This result indicates that 28 % of DOC production may be linked to microbial oxidation of particulate organic carbon to DOC (Dileep Kumar et al.,

1990). This has also been proposed for the Tyrrhenian Deep Water and Western Mediterranean Deep Water (Santinelli et al., 2002). There is evidence that Mediterranean Water carries high loads of suspended particles to the North Atlantic Ocean, with higher abundance in the continental slope than off-shore (Freitas and Abrantes, 2002). The authors found higher values of suspended particle materials in Gibraltar and the western GoC near Cape of St. Vincent, while in the eastern GoC, mixing of MOW with NACW resulted in a decrease of particle abundance. Cape of Trafalgar and Cape of Sta. María (TF and GU) are influenced by a nutrient-rich upwelling, which enhances primary production in the SurfW and increases particle sinking. We hypothesized that the influence of the upwelling together with the higher load of particle material in this zone might be responsible for the spatial differences in oxygen consumption in the Deep GoC waters. Moreover, recent work found contrasting behaviors of net removal/accumulation of DOC in the deep Atlantic Ocean when increasing the spatial resolution (Romera-Castillo et al., 2019). Thus, our results highlight the importance of local conditions in DOC dynamics.

Although not a strong relationship was observed between residuals of FDOM components with AOU_{res} ($R^2 < 0.1$, $p > 0.05$), the positive slope between humic-like C1 and AOU_{res} ($1.5 \pm 0.9*10^{-5}$ RU µmol O_2^{-1} Kg) obtained in this work was quite similar to that observed in the West Mediterranean Sea ($1.6 \pm 0.4*10^{-5}$ RU µmol O_2^{-1} Kg, Martínez-Pérez et al., 2019). This result indicates the release of humic-like FDOM as a byproduct of organic matter mineralization (Nieto-Cid et al., 2006; Jørgensen et al., 2011). Furthermore, higher typical values of C1 were found in $NACW_S$ and MOW, matching the highest AOU values (Table 3). On the contrary, the slope between residuals of protein-like C2 and AOU_{res} was negative with the

same slope value as the West Mediterranean Sea (-2.7 ± 1.3*10^{-5} RU µmol O_2^{-1} Kg), suggesting a decay of C2 fluorescence in parallel with water mass aging (Martínez-Pérez et al., 2019). The lack of correlation between tryptophan-like components and AOU has been previously reported in the global dark ocean (Catalá et al., 2015). The authors suggested that this is caused by the low fluorescence of the relatively young central water found in their study with AOU values lower than 75 µM. Our results are in agreement with this hypothesis since the typical value of AOU for $NACW_T$ was 8.71 ± 4.48 µM (Table 3) with a typical fluorescence of 0.0010 ± 0.0002 RU, even lower than those observed in Catalá et al. (2015).

Finally, it is worth mentioning the presence of distinct absorption spectra with a shoulder at ~ 300 nm during summer in off-shore stations (SP6 and SP7) between 300 and 650 m depth (Fig. S7). Those samples also present unusual values of protein-like C2 that increase with depth (1.8-5.8 RU, data excluded). One explanation is that these signals could be related to the secondary absorption nitrate peak centered at 302 nm (Catalá et al., 2016). The authors found that when the a_{302}: nitrate ratio is > than 70 µM, the impact of this peak is significant in CDOM absorption. However, in our samples, it was not the case. Another possibility is the production of CDOM by plankton, as it has been previously documented (e.g., Steinberg et al., 2004; Romera-Castillo et al., 2011b). Furthermore, Steinberg et al. (2004) found that the different major groups of plankton (including zooplankton and protozoans) have distinctive absorption spectra. The absorption spectra from CDOM exuded by gelatinous zooplankton with vertical migration (pelagic tunicates) and colonial radiolarians showed a large peak at ~297 nm and 300 nm, respectively, similar to those found in this work (Fig. S7). These plankton groups are ubiquitous, and most of the pelagic tunicates are

benthic (Gershwin et al. 2014), thus explaining the increase of C2 with depth. However, further work—including molecular characterization of DOM—is needed to establish the possible source of this FDOM.

IV. 5. Conclusions

PARAFAC modeling identified six fluorescent components in the GoC. Two were humic-like and two protein-like components widely distributed in coastal and marine waters. The other two have been less observed; a terrestrial derived DOM photoproduct and a possible mixture of PAH and protein-like compounds. The GoC showed a complicated hydrographic situation where different water masses are affected by continental inputs from riverine discharges, coastal upwelling, and currents comprised in the Strait of Gibraltar. Therefore, mesoscale processes from water mass circulation patterns were not suitable to explain DOM, except for the major humic-like components. The biogeochemical processes at a local scale explained DOC, CDOM, and protein-like components. Lower values of DOC and protein-like components were observed during spring and winter when the lowest temperatures were observed, and the water column was strongly mixed. While for CDOM, the lowest values occurred in autumn, when the water column was highly stratified, indicating the importance of photodegradation as a sink of CDOM. Humic-like C1 showed more constant average fluorescence along seasons, while the terrestrially derived photoproduct C4 and protein-like components exhibited marked seasonal changes. The tenfold higher intensity of protein-like C2 during summer that accounts for the 56.94 % ± 26.28 % of the total pool of FDOM seems to be linked to biological activity. In deep water, the relationship between AOU_{res} with DOC_{res} showed spatial differences. Near the upwelling zones (TF and GU), DOC is produced in parallel with water

mass aging due to microbial oxidation of particulate organic carbon to DOC. However, in the rest of the GoC, microbial DOC mineralization predominates. Finally, the relationship between FDOM residuals and AOU_{res} suggested the production of humic-like C1 (positive slope) and consumption of protein-like C2 (negative slope) in the deep waters of the GoC. Overall, our results highlight the importance of local hydrographic and biogeochemical features in DOM dynamics in coastal ocean systems.

Acknowledgments

This work was funded by the Spanish CICYT (Spanish Program for Science Technology) under the contract CTM2014-59244-C3-1-R and RTI2018-100865-B-C21. VA was financed by the Uruguayan Agency for Research and Innovation (ANII) with a Ph.D. fellowship (POS_EXT_2015_1_122780). CRC was funded by a Juan de la Cierva-Incorporación Postdoctoral Fellowship from the Spanish "Ministerio de Economía y Competitividad". The author would like to thanks the crews of the R/V's Angeles Alvariño and Ramón Margalef for their assistance during fieldwork. Ana Sierra and Dolores Jiménez-López for their assistance in data acquisition. Gastón Pereyra and Maria Vilas performed the final language revision.

References

Álvarez-Salgado, X. A., Nieto-Cid, M., Álvarez, M., Pérez, F. F., Morin, P., and Mercier, H. (2013). New insights on the mineralization of dissolved organic matter in central, intermediate, and deep water masses of the northeast North Atlantic. *Limnol. Oceanogr.* 58, 681–696. doi:10.4319/lo.2013.58.2.0681.

Álvarez, M., Brea, S., Mercier, H., and Álvarez-Salgado, X. A. (2014). Mineralization of biogenic materials in the water masses of the South Atlantic Ocean. I: Assessment and results of an optimum multiparameter analysis. *Prog. Oceanogr.* 123, 1–23. doi:10.1016/j.pocean.2013.12.007.

Amaral, V., Graeber, D., Calliari, D., and Alonso, C. (2016). Strong linkages between DOM optical properties and main clades of aquatic bacteria. *Limnol. Oceanogr.* 61, 906–918. doi:10.1002/lno.10258.

Arístegui, J., Duarte, C. M., Agustí, S., Doval, M., Álvarez-Salgado, X. A., and Hansell, D. A. (2002). Oceanography: Dissolved organic carbon support of respiration in the dark ocean. *Science (80-.).* 298, 1967. doi:10.1126/science.1076746.

Aurin, D., and Mannino, A. (2012). A database for developing global ocean color algorithms for colored dissolved organic material, CDOM spectral slope, and dissolved organic carbon. *Ocean Opt. XXI*, 121257.

Baringer, M. O. N., and Price, J. F. (1999). A review of the physical oceanography of the Mediterranean outflow. *Mar. Geol.* 155, 63–82. doi:10.1016/S0025-3227(98)00141-8.

Bellanco, M. J., and Sánchez-Leal, R. F. (2016). Spatial distribution and intra-annual variability of water masses on the Eastern Gulf of Cadiz seabed. *Cont. Shelf Res.* 128, 26–35. doi:10.1016/j.csr.2016.09.001.

Benson, B.B., Krause, D.J., 1984. The concentration and isotopic fractionation of oxygen dissolved in freshwater and seawater in equilibrium with the atmosphere. *Limnol. Oceanogr.* 29 (3), 620–632.

Blough, N. V. and Del Vecchio, R. (2002). Chromophoric DOM in the coastal environment. *Biogeochemistry of marine dissolved organic matter*, 509-546.

Catalá, T. S., Martínez-Pérez, A. M., Nieto-Cid, M., Álvarez, M., Otero, J., Emelianov, M., et al. (2018). Dissolved Organic Matter (DOM) in the open Mediterranean Sea. I. Basin–wide distribution and drivers of chromophoric DOM. *Prog. Oceanogr.* 165, 35–51. doi:10.1016/j.pocean.2018.05.002.

Catalá, T. S., Mladenov, N., Echevarría, F., and Reche, I. (2013). Positive trends between salinity and chromophoric and fluorescent dissolved organic matter in a seasonally inverse estuary. *Estuar. Coast. Shelf Sci.* 133, 206–216. doi:10.1016/j.ecss.2013.08.030.

Catalá, T. S., Reche, I., Fuentes-Lema, A., Romera-Castillo, C., Nieto-Cid, M., Ortega-Retuerta, E., et al. (2015). Turnover time of fluorescent dissolved organic matter in the dark global ocean. *Nat. Commun.* 6, 1–8. doi:10.1038/ncomms6986.

Catalá, T. S., Reche, I., Ramón, C. L., López-sanz, À., Álvarez, M., Calvo, E., et al. (2016). Chromophoric signatures of microbial by-products in the dark ocean. *Geophys. Res. Lett.* 43, 7639–7648. doi:10.1002/2016GL069878.

Coble, P. (1996). Characterization of marine and terrestrial DOM in seawater using excitation-emission matrix spectroscopy. *Mar. Chem.* 51, 325–346.

Coble, P. G. (2007). Marine Optical Biogeochemistry: The Chemistry of Ocean Color. *Chem. Rev.* 107, 402–418. doi:10.1021/cr050350+.

Coble, P. G., Lead, J., Baker, A., Reynolds, D. M., and Spencer, R. G. M. (2014). *Aquatic*

Organic Matter Fluorescence. , eds. P. G. Coble, J. Lead, A. Baker, D. M. Reynolds, and R. G. M. Spencer.

Criado-Aldeanueva, F., Garcia-Lafuente, J., Navarro, G., and Ruiz, J. (2009). Seasonal and interannual variability of the surface circulation in the eastern Gulf of Cadiz (SW Iberia). *J. Geophys. Res. Ocean.* 114, 1–11. doi:10.1029/2008JC005069.

Criado-Aldeanueva, F., García-Lafuente, J., Vargas, J. M., Del Río, J., Vázquez, A., Reul, A., et al. (2006). Distribution and circulation of water masses in the Gulf of Cadiz from in situ observations. *Deep. Res. Part II Top. Stud. Oceanogr.* 53, 1144–1160. doi:10.1016/j.dsr2.2006.04.012.

Dafner, E., González-Dávila, M., Magdalena Santana-Casiano, J., and Sempéré, R. (2001). Total organic and inorganic carbon exchange through the Strait of Gibraltar in September 1997. *Deep. Res. Part I Oceanogr. Res. Pap.* 48, 1217–1235. doi:10.1016/S0967-0637(00)00064-9.

de la Paz, M., Gómez-Parra, A., and Forja, J. (2007). Inorganic carbon dynamic and air-water CO2 exchange in the Guadalquivir Estuary (SW Iberian Peninsula). *J. Mar. Syst.* 68, 265–277. doi:10.1016/j.jmarsys.2006.11.011.

Del Castillo, C., Gilbes, F., Goble, P. G., and Muller-Karger, F. E. (2000). On the Seasonal Dispersal of Riverine Colored Dissolved Organic Matter(CDOM) on the West Florida Shelf. *Limnol.Oceanogr.(submitted)*, 87–92.

Determann, S., Lobbes, J. örg M., Reuter, R., and Rullkötter, J. ürgen (1998). Ultraviolet fluorescence excitation and emission spectroscopy of marine algae and bacteria. *Mar. Chem.* 62, 137–156. doi:10.1016/S0304-4203(98)00026-7.

Dileep Kumar, M., Rajendran, A., Somasundar, K., Haake, B., Jenisch, A., Shuo, Z., et al. (1990). Dynamics of dissolved organic carbon in the northwestern Indian Ocean. *Mar. Chem.* 31, 299–316. doi:10.1016/0304-4203(90)90044-D.

Echevarría, F., Zabala, L., Corzo, A., Navarro, G., Prieto, L., and Macías, D. (2009). Spatial distribution of autotrophic picoplankton in relation to physical forcings: The Gulf of Cádiz, Strait of Gibraltar and Alborán Sea case study. *J. Plankton Res.* 31, 1339–1351. doi:10.1093/plankt/fbp070.

Ferrari, G. M. (2000). The relationship between chromophoric dissolved organic matter and dissolved organic carbon in the European atlantic coastal area and in the West Mediterranean Sea (Gulf of Lions). *Mar. Chem.* 70, 339–357. doi:10.1016/S0304-4203(00)00036-0.

Flecha, S., Pérez, F. F., Navarro, G., Ruiz, J., Olivé, I., Rodríguez-Gálvez, S., et al. (2012). Anthropogenic carbon inventory in the Gulf of Cádiz. *J. Mar. Syst.* 92, 67–75. doi:10.1016/j.jmarsys.2011.10.010.

Freitas, P. S., and Abrantes, F. (2002). Suspended particulate matter in the Mediterranean water at the Gulf of Cadiz and off the southwest coast of the Iberian Peninsula. *Deep. Res. Part II Top. Stud. Oceanogr.* 49, 4245–4261. doi:10.1016/S0967-0645(02)00153-4.

Galletti, Y., Gonnelli, M., Retelletti Brogi, S., Vestri, S., and Santinelli, C. (2019). DOM dynamics in open waters of the Mediterranean Sea: New insights from optical properties. *Deep. Res. Part I Oceanogr. Res. Pap.*, 1–20. doi:10.1016/j.dsr.2019.01.007.

García-Gómez, J. C., Sempere-Valverde, J., Ostalé-Valriberas, E., Martínez, M., Olaya-Ponzone, L.,González, A. R., et al. (2018). Rugulopterix okamurae (EY Dawson) IK Hwang, WJ Lee & HS Kim (Dictyotales, Ochrophyta), alga exótica "explosiva" en el estrecho de Gibraltar. Observaciones preliminares de su distribución e impacto. Almoraima , 48.

Garel, E., Laiz, I., Drago, T., and Relvas, P. (2016). Characterisation of coastal counter-currents on the inner shelf of the Gulf of Cadiz. 155, 19–34.

Geiselman, J. A., and McConnell, O. J. (1981). Polyphenols in brown algae Fucus vesiculosus and Ascophyllum nodosum: Chemical defenses against the marine herbivorous snail, Littorina littorea. *J. Chem. Ecol.* 7, 1115–1133. doi:10.1007/BF00987632.

Gonnelli, M., Galletti, Y., Marchetti, E., Mercadante, L., Retelletti Brogi, S., Ribotti, A., et al. (2016). Dissolved organic matter dynamics in surface waters affected by oil spill pollution: Results from the Serious Game exercise. *Deep. Res. Part II Top. Stud. Oceanogr.* 133, 88–99. doi:10.1016/j.dsr2.2016.05.027.

González-García, C., Forja, J., González-Cabrera, M. C., Jiménez, M. P., and Lubián, L. M. (2018). Annual variations of total and fractionated chlorophyll and phytoplankton groups in the Gulf of Cadiz. *Sci. Total Environ.* 613–614, 1551–1565. doi:10.1016/j.scitotenv.2017.08.292.

González-Ortegón, E., Amaral, V., Baldó, F., Sánchez-Leal, R. F., Bellanco, M. J., Jiménez, M. P., et al. (2018). Sources and coastal distribution of dissolved organic matter in the Gulf of Cadiz. *Sci. Total Environ.* 630, 1583–1595. doi:10.1016/j.scitotenv.2018.02.293.

Green, S. A., and Blough, N. V (1994). Optical absorption and fluorescence of chromophoric properties dissolved organic matter in natural waters. *Limnology* 39, 1903–1916.

Hansell, D. A., Carlson, C. A. ., Repeta, D. J. . R., and Schlitzer, R. (2009). Dissolved Organic Matter in the Ocean. *Oceanography* 22.

Hedges, J. I. (2002). *Why Dissolved Organics Matter*. Elsevier Inc. doi:10.1016/b978-012323841-2/50003-8.

Helms, J. R., Kieber, D. J., Minor, E. C., Ritchie, J. D., Stubbins, A., and Mopper, K. (2008). Absorption spectral slopes and slope ratios as indicators of molecular weight, source, and photobleaching of chromophoric dissolved organic matter. *Limnol. Oceanogr.* 53, 955–969. doi:10.4319/lo.2008.53.3.0955.

Huertas, E., Navarro, G., Rodríguez-Gálvez, S., and Prieto, L. (2005). The influence of phytoplankton biomass on the spatial distribution of carbon dioxide in surface sea water of a coastal area of the Gulf of Cádiz (southwestern Spain). *Can. J. Bot.* 83, 929–940. doi:10.1139/b05-082.

Jørgensen, L., Stedmon, C. A., Kragh, T., Markager, S., Middelboe, M., and Søndergaard, M. (2011). Global trends in the fluorescence characteristics and distribution of marine dissolved organic matter. *Mar. Chem.* 126, 139–148. doi:10.1016/j.marchem.2011.05.002.

Kothawala, D. N., Murphy, K. R., Stedmon, C. A., Weyhenmeyer, G. A., and Tranvik, L. J. (2013). Inner filter correction of dissolved organic matter fluorescence. *Limnol. Oceanogr. Methods* 11, 616–630. doi:10.4319/lom.2013.11.616.

Lawaetz, A. J., and Stedmon, C. A. (2009). Fluorescence intensity calibration using the Raman scatter peak of water. *Appl. Spectrosc.* 63, 936–940. doi:10.1366/000370209788964548.

Liu, K. K., Atkinson, L., Quiñones, R., & Talaue-McManus, L. (Eds.). (2010). *Carbon and nutrient fluxes in continental margins: a global synthesis*. Springer Science & Business Media.

Lønborg, C., and Álvarez-Salgado, X. A. (2014). Tracing dissolved organic matter cycling in the eastern boundary of the temperate North Atlantic using absorption and fluorescence spectroscopy. *Deep. Res. Part I Oceanogr. Res. Pap.* 85, 35–46.

doi:10.1016/j.dsr.2013.11.002.

Massicotte, P., Asmala, E., Stedmon, C., & Markager, S. (2017). Global distribution of dissolved organic matter along the aquatic continuum: Across rivers, lakes and oceans. *Science of the Total Environment*, *609*, 180-191.

Maie, N., Scully, N. M., Pisani, O., and Jaffé, R. (2007). Composition of a protein-like fluorophore of dissolved organic matter in coastal wetland and estuarine ecosystems. *Water Res.* 41, 563–570. doi:10.1016/j.watres.2006.11.006.

Martínez-Pérez, A. M., Catalá, T. S., Nieto-Cid, M., Otero, J., Álvarez, M., Emelianov, M., et al. (2019). Dissolved organic matter (DOM) in the open Mediterranean Sea. II: Basin–wide distribution and drivers of fluorescent DOM. *Prog. Oceanogr.* 170, 93–106. doi:10.1016/j.pocean.2018.10.019.

Mauritzen, C., Morel, Y., and Paillet, J. (2001). On the influence of Mediterranean Water on the Central Waters of the North Atlantic Ocean. *Deep. Res. Part I Oceanogr. Res. Pap.* 48, 347–381. doi:10.1016/S0967-0637(00)00043-1.

Mostofa, K. M. G., Jie, Y., Sakugawa, H., and Liu, C. Q. (2019). Equal Treatment of Different EEM Data on PARAFAC Modeling Produces Artifact Fluorescent Components That Have Misleading Biogeochemical Consequences. *Environ. Sci. Technol.* 53, 561–563. doi:10.1021/acs.est.8b06647.

Murphy, K. R., Stedmon, C. A., Graeber, D., and Bro, R. (2013). Fluorescence spectroscopy and multi-way techniques. PARAFAC. *Anal. Methods* 5, 6557–6566. doi:10.1039/c3ay41160e.

Murphy, K. R., Stedmon, C. A., Wenig, P., and Bro, R. (2014). OpenFluor- An online spectral library of auto-fluorescence by organic compounds in the environment. *Anal. Methods* 6, 658–661. doi:10.1039/c3ay41935e.

Navarro, G., Caballero, I., Prieto, L., Vázquez, A., Flecha, S., Huertas, I. E., et al. (2012). Seasonal-to-interannual variability of chlorophyll-a bloom timing associated with physical forcing in the Gulf of Cádiz. *Adv. Sp. Res.* 50, 1164–1172. doi:10.1016/j.asr.2011.11.034.

Nelson, N. B., and Siegel, D. A. (2013). The Global Distribution and Dynamics of Chromophoric Dissolved Organic Matter. *Ann. Rev. Mar. Sci.* 5, 447–476. doi:10.1146/annurev-marine-120710-100751.

Nieto-Cid, M., Alvarez-Salgado, X. A., and Perez, F. F. (2006). Microbial and photochemical reactivity of fluorescent dissolved organic matter in a coastal upwelling system. *Limnol. Oceanogr.* 51, 1391–1400.

Opsahl, S., and Benner, R. (1997). Distribution and cycling of terrigenous dissolved organic matter in the ocean. *Nature* 386, 480–482.

Para, J., Coble, P. G., Charrière, B., Tedetti, M., Fontana, C., and Sempéré, R. (2010). Fluorescence and absorption properties of chromophoric dissolved organic matter (CDOM) in coastal surface waters of the northwestern Mediterranean Sea, influence of the Rhone River. *Biogeosciences* 7, 4083–4103. doi:10.5194/bg-7-4083-2010.

Pérez, F. F., Castro, C. G., Álvarez-Salgado, X. A., and Ríos, A. F. (2001). Coupling between the Iberian basin - Scale circulation and the Portugal boundary current system: A chemical study. *Deep. Res. Part I Oceanogr. Res. Pap.* 48, 1519–1533. doi:10.1016/S0967-0637(00)00101-1.

Poole, R., and Tomczak, M. (1999). Optimum multiparameter analysis of the water mass structure in the western North Atlantic Ocean. *J. Geophys. Res.* 98, 10155. doi:10.1029/93jc00180.

Price, J. F., and O'Neil Baringer, M. (1994). Outflows and deep water production by marginal seas. *Prog. Oceanogr.* 33, 161–200. doi:10.1016/0079-6611(94)90027-2.

Ribas-Ribas, M., Gómez-Parra, A., and Forja, J. M. (2011a). Air-sea CO2 fluxes in the north-eastern shelf of the Gulf of Cádiz (southwest Iberian Peninsula). *Mar. Chem.* 123, 56–66. doi:10.1016/j.marchem.2010.09.005.

Ribas-Ribas, M., Gómez-Parra, A., and Forja, J. M. (2011b). Spatio-temporal variability of the dissolved organic carbon and nitrogen in a coastal area affected by river input: The north eastern shelf of the Gulf of Cádiz (SW Iberian Peninsula). *Mar. Chem.* 126, 295–308. doi:10.1016/j.marchem.2011.07.003.

Rochelle-Newall, E., Hulot, F. D., Janeau, J. L., and Merroune, A. (2014). CDOM fluorescence as a proxy of DOC concentration in natural waters: A comparison of four contrasting tropical systems. *Environ. Monit. Assess.* 186, 589–596. doi:10.1007/s10661-013-3401-2.

Romera-Castillo, C., Álvarez-Salgado, X. A., Galí, M., Gasol, J. M., and Marrasé, C. (2013). Combined effect of light exposure and microbial activity on distinct dissolved organic matter pools. A seasonal field study in an oligotrophic coastal system (Blanes Bay, NW Mediterranean). *Mar. Chem.* 148, 44–51. doi:10.1016/j.marchem.2012.10.004.

Romera-Castillo, C., Álvarez, M., and Pelegrí, J. L. (2019). Net Additions of Recalcitrant Dissolved Organic Carbon in the Deep Atlantic Ocean Global Biogeochemical Cycles. 1–12.

Romera-Castillo, C., Nieto-Cid, M., Castro, C. G., Marrasé, C., Largier, J., Barton, E. D., et al. (2011a). Fluorescence: Absorption coefficient ratio - Tracing photochemical and microbial degradation processes affecting coloured dissolved organic matter in a coastal system. *Mar. Chem.* 125, 26–38. doi:10.1016/j.marchem.2011.02.001.

Romera-Castillo, C., Sarmento, H., Alvarez-Salgado, X. A. Á., Gasol, J. M., and Marrasé, C. (2011b). Net production and consumption of fluorescent colored dissolved organic matter by natural bacterial assemblages growing on marine phytoplankton exudates. *Appl. Environ. Microbiol.* 77, 7490–7498. doi:10.1128/AEM.00200-11.

Sala, I., Navarro, G., Bolado-Penagos, M., Echevarría, F., and García, C. M. (2018). High-chlorophyll-area assessment based on remote sensing observations: The case study of Cape Trafalgar. *Remote Sens.* 10. doi:10.3390/rs10020165.

Santinelli, C., Gasparini, G., Nannicini, L., and Seritti, A. (2002). Vertical distribution of dissolved organic carbon (DOC) in the Mediterranean Sea. *Deep Sea Res. Part I Oceanogr. Res. Pap.* 49, 2203–2219. doi:10.3354/cr031205.

Shen, Y., Fichot, C. G., and Benner, R. (2012). Floodplain influence on dissolved organic matter composition and export from the Mississippi–Atchafalaya river system to the Gulf of Mexico. *Limnol. Oceanogr.* 57, 1149–1160. doi:10.4319/lo.2012.57.4.1149.

Smith, S. V., and Hollibaugh, J. T. (1997). Annual cycle and interannual variability of ecosystem metabolism in a temperate climate embayment. *Ecol. Monogr.* 67, 509–533. doi:10.1890/0012-9615(1997)067[0509:ACAIVO]2.0.CO;2.

Stedmon, C., and Bro, R. (2008). Characterizing dissolved organic matter fluorescence with parallel factor analysis: a tutorial. *Limnol. Oceanogr. Methods* 6, 572–579. doi:doi:10.4319/lom.2008.6.572b.

Steinberg, D. K., Nelson, N. B., Carlson, C. A., and Prusak, A. C. (2004). Production of chromophoric dissolved organic matter (CDOM) in the open ocean by zooplankton and the colonial cyanobacterium Trichodesmium spp. *Mar. Ecol. Prog. Ser.* 267, 45–56. doi:10.3354/meps267045.

Stevenson, R. E. (1977). Huelva Front and Malaga, Spain, eddy chain as defined by satellite and oceanographic data. *Dtsch. Hydrogr. Zeitschrift* 30, 51–53. doi:10.1007/BF02226082.

Tanaka, K., Takesue, N., Nishioka, J., Kondo, Y., Ooki, A., Kuma, K., et al. (2016). The conservative behavior of dissolved organic carbon in surface waters of the southern Chukchi Sea, Arctic Ocean, during early summer. *Sci. Rep.* 6, 1–10. doi:10.1038/srep34123.

Vargas-Yáñez, M., Sarhan, T., Plaza, F., Rubín, J. P., and García-Martínez, M. C. (2002). The influence of tide-topography interaction on low-frequency heat and nutrient fluxes . Application to Cape Trafalgar. 22, 115–139.

Vasconcelos, R. P., Reis-Santos, P., Fonseca, V., Maia, A., Ruano, M., França, S., et al. (2007). Assessing anthropogenic pressures on estuarine fish nurseries along the Portuguese coast: A multi-metric index and conceptual approach. *Sci. Total Environ.* 374, 199–215. doi:10.1016/j.scitotenv.2006.12.048.

Weishaar, J., Aiken, G., Bergamaschi, B., Fram, M., Fujii, R., and Mopper, K. (2003). Evaluation of specific ultra-violet absorbance as an indicator of the chemical content of dissolved organic carbon. *Environ. Chem.* 41, 843–845. doi:10.1021/es030360x.

Supplementary Material

Supplementary Figures

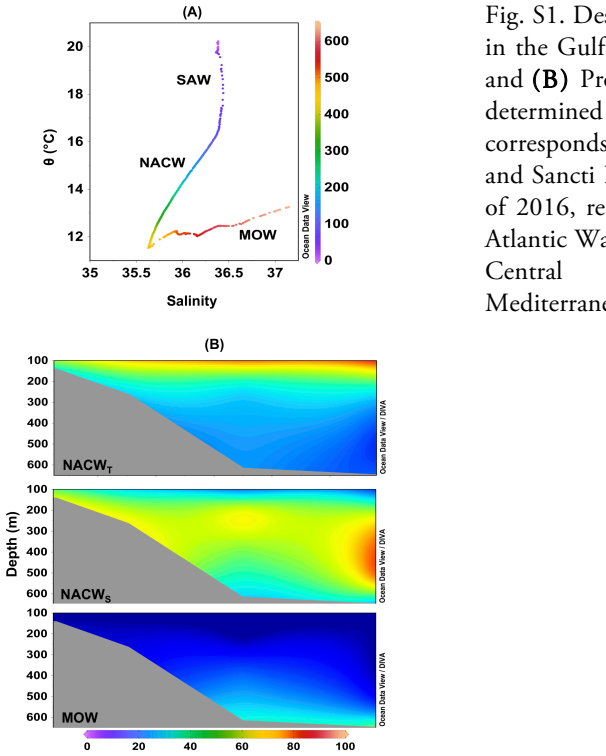

Fig. S1. Description of the water masses in the Gulf of Cádiz, **(A)** T-S diagram and **(B)** Proportion of the water masses determined by the OMP analysis. Data corresponds to the deepest station (SP7) and Sancti Petri section during summer of 2016, respectively. SAW: Superficial Atlantic Water, NACW: North Atlantic Central Water and MOW: Mediterranean Outflow Water.

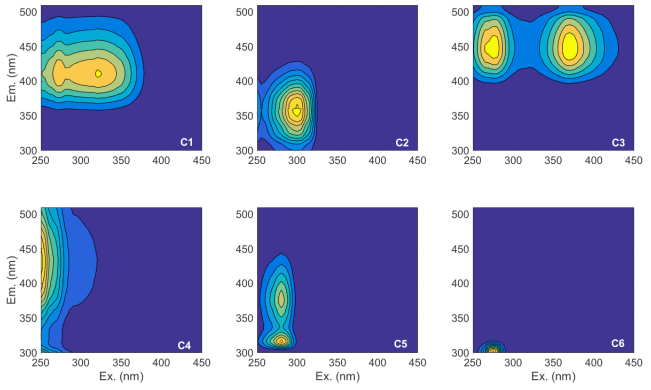

Fig. S2. Fluorescence characteristics of the six components identified by the PARAFAC global analysis.

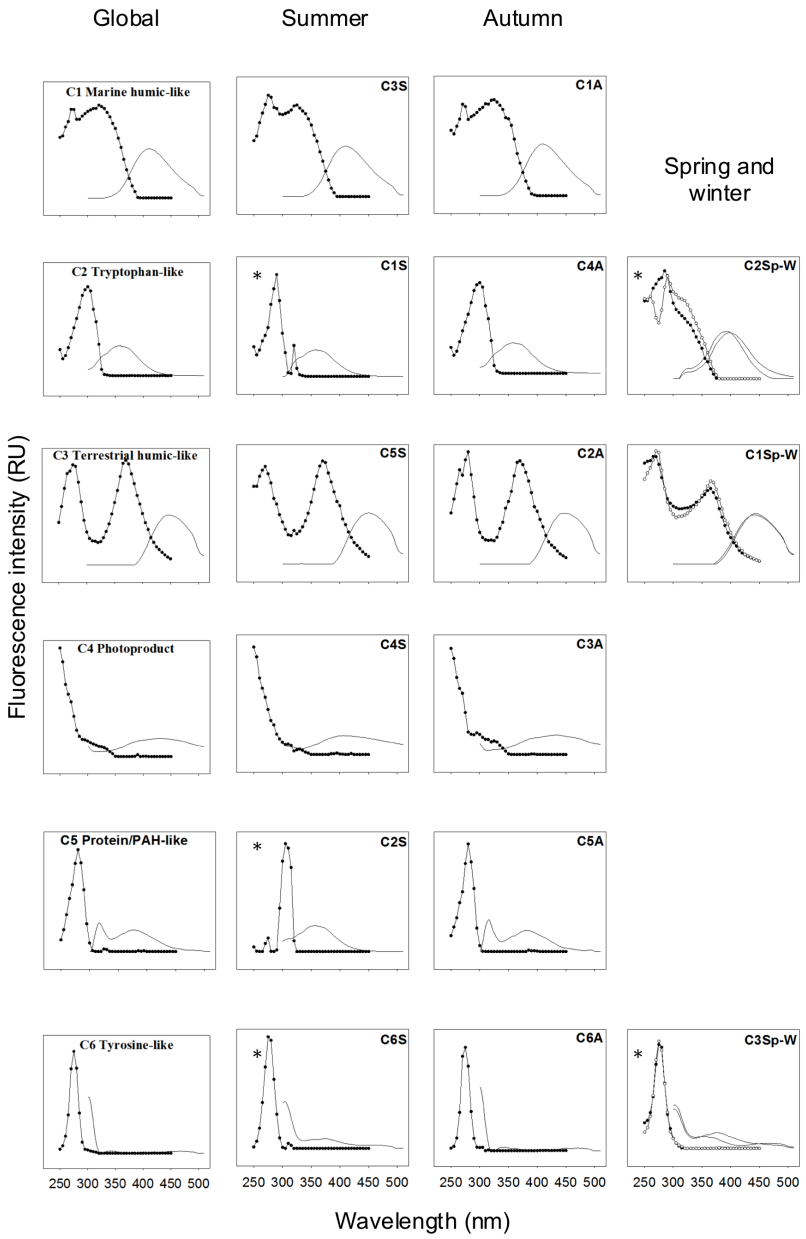

Fig. S3. Excitation (solid line) and emission (dotted line) spectra of the six-components for the global model and the same components for the individual models (components were numbered arbitrarily by the PARAFAC models) for summer (C1S - C6S), autumn (C1A - C6A), spring and winter (C1Sp-W -C3Sp-W). The * denotes comparisons between components with a Tucker congruence values < 0.98.

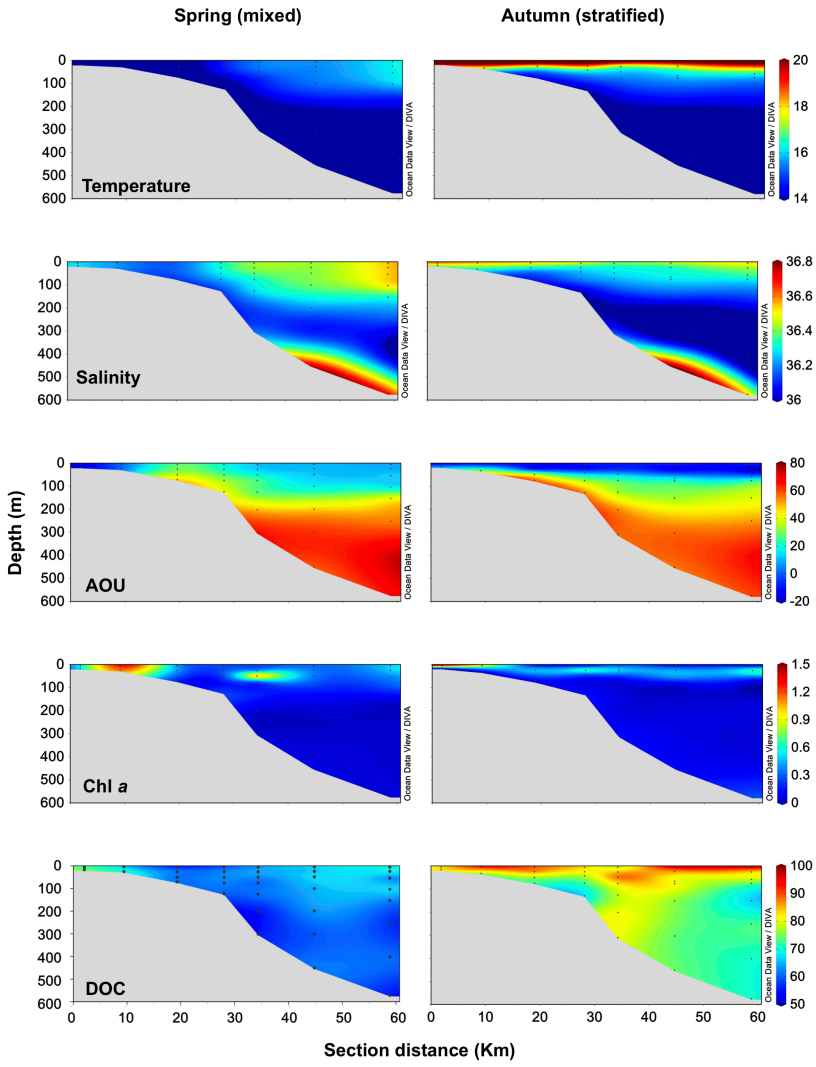

Fig. S4. Vertical profiles of temperature (°C), salinity, apparent oxygen utilization (AOU, µM), chlorophyll a (Chl *a*, µg L^{-1}) and dissolved organic carbon (DOC, µM) from Guadalquivir transect during the stratified (spring) and mixed (autumn) period.

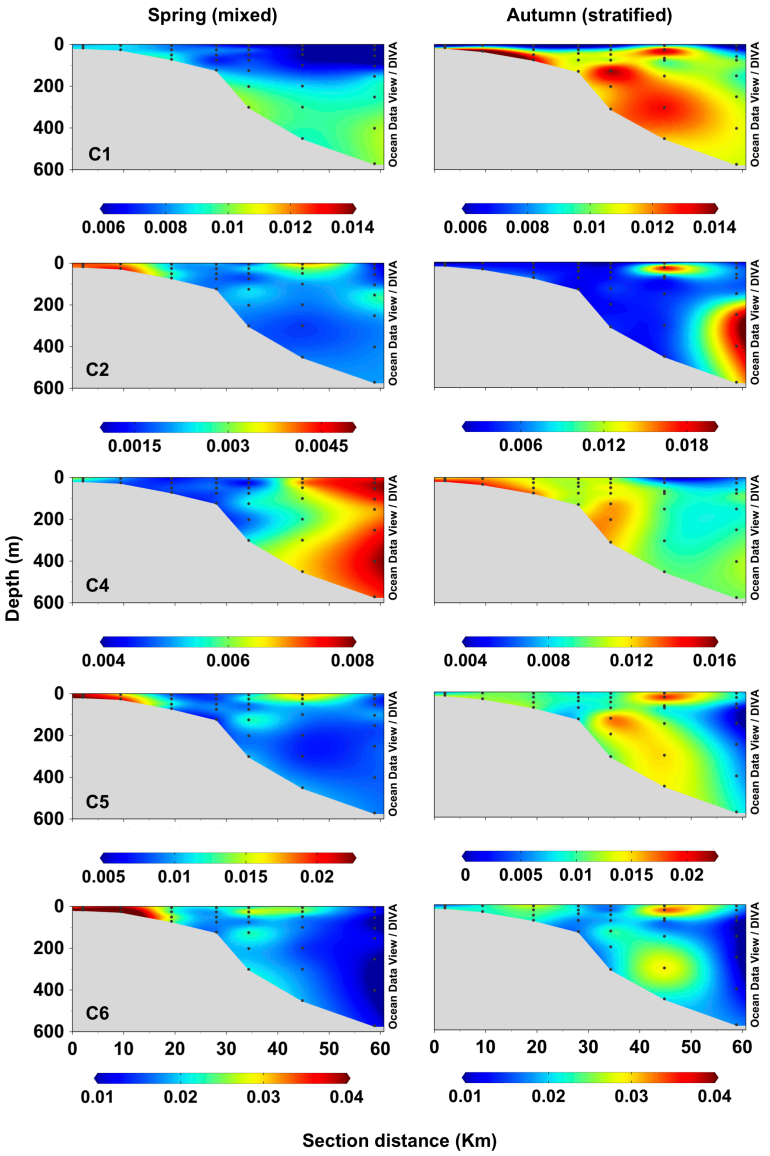

Fig. S5. Vertical profiles of fluorescence components C1-C6 during the stratified (spring) and mixed (autumn) period in the Guadalquivir transect.

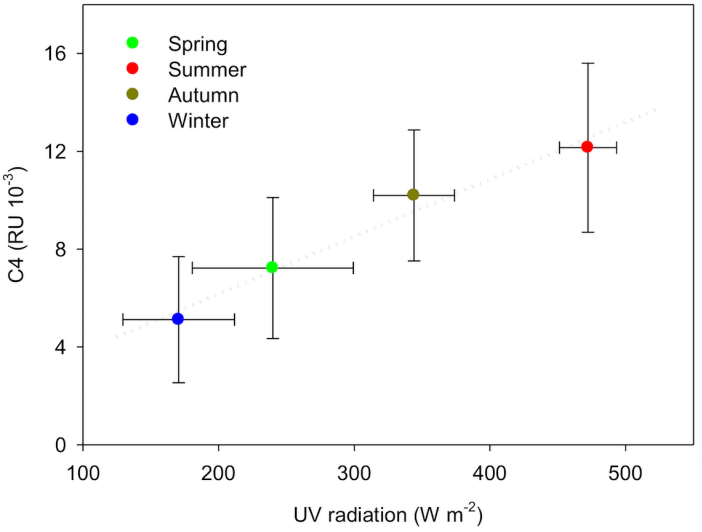

Fig. S6. Relationship between average seasonal values of UV radiation (UVA+UVB) and fluorescent intensity of component 4 (C4).

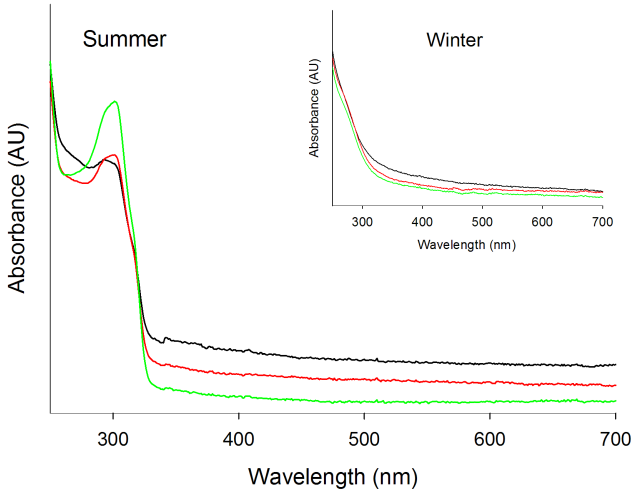

Fig. S7. Absorbance spectra for station SP7 during summer and winter at different depths: black 300 m, red 500 m and green 650 m.

Supplementary Tables

Table S1. Complementary information about oceanographic and meteorological settings in the Gulf of Cádiz during the study period. * Correspond to the accumulated precipitations 30 days prior to the sampling dates.

Variable	March	June	September	December
Thermocline depth (m)	75.4 ± 42.3	43.9 ± 16.8	34.8 ± 14.4	67.3 ± 26.9
Accumulative precipitations (L m^{-2})*	40.2	74.9	8.8	59.2
UV radiation (W m^{-2})	247.7 ± 3.3	466.8 ± 10.2	338.7 ± 14.8	166.9 ± 12.4
Wind speed (m s^{-1})	8.4 ± 4.3	7.8 ± 3.8	5.9 ± 2.9	8.0 ± 4.1

Table S2. Spectral properties of the six PARAFAC components from the global model in the Gulf of Cádiz (n = 766) and correspondence with previously identified components in different environments using OpenFluor database and literature*.

	Ex/Em	OpenFluor (Tucker congruency)	Ex/Em	Description	Environment
C1	270 (320)/411	C2, (Chen et al., 2018) (0.99)	260 (305)/404	Marine humic-like	Arctic Sea water
		C2, (Murphy et al., 2006) (0.98)	320/414	Marine humic-like	Atlantic and Pacific Ocean
		C3, (Yamashita et al., 2010b)(0.98)	> 260 (> 315)/421	Microbial humic-like	Tropical rivers
		C2, (Catalá et al., 2015)(0.98)	270 (326)/402	In situ, Microbial	Global dark ocean
		C1, (Yamashita et al., 2011)(0.97)	260 (320)/ 425	Humic-like enrinched in fulvic acids	Watersheds
				Ubiquitous, autochthonous and allochthonous	Antarctic lakes
				Peak A+M, terrestrial	Mountain streams
			-	Terrestrial	Streams riparian forest
		C415, (Kida et al., 2019)(0.97)		Terrestrial	Lakes
			240 (310)/429	Terrestrial (humic and fulvic)	Everglades
		C1, (Garcia et al., 2015) (0.97)	252 (321)/ 408	Ubiquitous	Pantanal
		C2, (Dalmagro et al., 2019)(0.97)	- 260 (305)/ 416	Marine/microbial	Artic porewater
		C2, (Li et al., 2016) (0.97)		Peak A	Mesocosm experiment
				-	Coastal zone
					Groundwater
					Lake

		C3, (Yamashita et al., 2010c) (0.97)	260 (311)/411	Terrestrial Marine humic-like	Lena River
		C1, (Murphy et al., 2018) (0.97)	318/410 240	Humic-like	Pacific and Atlantic Ocean Groundwater
		C2, (Chen et al., 2016) (0.97)	(340)/398	Marine and terrestrial, peak M.	
		C2, (Stedmon and Markager, 2005)(0.97)	- 240/308	Humic-like, terrestrial	
		C2, (Asmala et al., 2018) (0.96)	240 (310)/396		
		C1, (Kulkarni et al., 2019)(0.96)	-		
		C1, (Borisover et al., 2009) (0.96)	(>260) 310/414		
		C1, (Gonçalves-Araujo et al., 2015) (0.96)	240 (329)/400		
		P1, (Murphy et al., 2008) (0.96)			
		C2, (Kulkarni et al., 2017) (0.96)			
C2	300/359	C4, (Schittich et al., 2018) (0.97)	300/350 298/343	Protein like Tryptophan-like	Groundwater Global dark ocean

		C3, (Catalá et al., 2015) (0.97) C3, (Amaral et al., 2016) (0.96) C4, (Chen et al., 2017) 0.96) C6, (Murphy et al., 2011) (0.96)	300/340 300/338 290/352	Tryptophan-like Bound proteins Protein, Tryptophan-like	Coastal subtropical lagoon Sediments Recycled wastewaters
C3	275-370/446	C3, (Chen et al., 2016) (0.97) C3, (Graeber et al., 2012) 0.97) C1, (Yamashita et al., 2010a)(0.96)	275 (370)/ 452 255 (370)/432 260 (370)/466	Terrestrial humic-like Humic-like, ubiquitous Mix A/C, higher plant derived and microbial reworked	Artic porewater Central European streams Okhotsk Sea and the North Pacific Ocean
C4	250/430	C2, (Walker et al., 2009) (0.98) C3, (Osburn et al., 2011) (0.98) C4, (Lambert et al., 2016a) (0.98)	< 240/404 < 250/434 <260/444 <260/434	Humic-like, terrestrially, exposed to UVA Terrestrial, Peak A Terrestrial and photochemically degraded	Canadian Artic surface water Lakes Tropical rivers, Africa Sediments

			<240/434	Terrestrial,	Streams
		C2, (Chen et al., 2017)		photoproduct and/or	
		(0.98)	240(305)/425	photorefractory	Lakes
				Terrestrial and	
		C4, (Lambert et al.,		photochemical	Pacific and Atlantic Ocean
		2016b)(0.98)	250(320)/370	degradation	Artic Ocean porewater
				Humic substances	Gulf of Maine
		C3, (Osburn et al., 2017)	265/422	after degradation	Coastal waters
		(0.98)	250/436	Unknown,	South Atlantic Bight
			250/436	anthropogenic	Lakes
		C4, (Murphy et al., 2008)	250/420	Terrestrial	
		(0.97)	-	Terrestrial, Peak A	
		C1, (Chen et al., 2016)		Terrestrial humic-like	
		(0.97)		Terrestrial humic-like	
		C1, (Cawley et al., 2012)		Peak A	
		(0.97)			
		C3, (Osburn et al.,			
		2016a)(0.96)			
		C2, (Kowalczuk et al.,			
		2009) (0.96)			
		C3, (Li et al., 2016) (0.96)			
C5	280/317	C3, (Kowalczuk et al.,	275/325	Bound to proteins	Atlantic Ocean

	(378)	2013) (0.92) C1, (Gonnelli et al., 2016)* C3, (Margolin et al., 2018)* C2, (Garcia et al., 2018) (0.92) $C_{275/350}$, (Murphy et al., 2014) (0.91) C8, (Asmala et al., 2018) (0.91) C4 dwh10, (D'Sa et al., 2016) *	(349) 270/342 290/367 275/350 275/350 - 275/320	Mixture of PAH and aromatic amino acids Peak N, PAH, origin unclear Peak T, leaching of polyphenols from senescent plants Similar to free dissolved tryptophan - Oil-related	Italian coast Black Sea Headwater catchments Marine, streams, wastewaters Estuaries Oil spill
C6	275/303	C1, (Murphy et al., 2006) (0.93) C5, (Osburn et al., 2016b)(0.91)		Protein-like Tyrosine	Atlantic and Pacific Ocean Atlantic coastal plain

Table S3. Parameters of the multiple linear regressions model between dissolved organic carbon (DOC), absorption coefficient a_{254} and fluorescent components with temperature (T) and salinity (S) for surface water. Fitting parameter of the relationship with T ($ß_1$) and S ($ß_2$), standard error and the determination coefficient (R^2) are presented. The significance levels of the estimation are included ($p < 0.0001$ ***, $p < 0.001$ ** and $p < 0.01$ *). Results are described for each campaign and only cases with p-values higher than 0.01 are described.

	Season	$ß_1$ (T)	$ß_2$ (S)	Std. Error	R^2
DOC	Spring	-3.2*	41.4**	11.9	0.09
	Summer	1.9***	-30.0***	8.9	0.28
	Autumn	2.2***	-9.2	6.2	0.36
	Winter	5.7***	-32.8***	5.5	0.22
a_{254}	Spring	-0.643***	4.085***	0.301	0.16
	Summer	0.097***	-1.498***	0.378	0.30
	Autumn	0.085***	-0.870**	0.185	0.34
	Winter	0.164***	-2.070***	0.211	0.30
C1	Spring	-0.0011 **	-0.0011	0.0011	0.50
	Summer	-0.0005 ***	-0.0092***	0.0016	0.69
	Autumn	-0.0004 **	-0.0082**	0.0017	0.59
	Winter	0.0011 ***	-0.0344***	0.0017	0.79
C2	Spring	-0.0011*	0.0040	0.0009	0.24
	Winter	-0.0001	-0.0025*	0.0005	0.31
C4	Spring	-0.0019	0.0204**	0.0022	0.27
C5	Spring	-0.0082***	0.0461***	0.0030	0.28
	Summer	0.0006*	-0.0199***	0.0043	0.36
	Winter	0.0004	-0.0137**	0.0031	0.16
C6	Spring	-0.0183***	0.1034***	0.0071	0.26
	Summer	0.0015**	-0.0235***	0.0100	0.13

References

Amaral, V., Graeber, D., Calliari, D., and Alonso, C. (2016). Strong linkages between DOM optical properties and main clades of aquatic bacteria. *Limnol. Oceanogr.* 61, 906–918. doi:10.1002/lno.10258.

Asmala, E., Haraguchi, L., Markager, S., Massicotte, P., Riemann, B., Staehr, P. A., et al. (2018). Eutrophication Leads to Accumulation of Recalcitrant Autochthonous Organic Matter in Coastal Environment. *Global Biogeochem. Cycles* 32, 1673–1687. doi:10.1029/2017GB005848.

Borisover, M., Laor, Y., Parparov, A., Bukhanovsky, N., and Lado, M. (2009). Spatial and seasonal patterns of fluorescent organic matter in Lake Kinneret (Sea of Galilee) and its catchment basin. *Water Res.* 43, 3104–3116. doi:10.1016/j.watres.2009.04.039.

Catalá, T. S., Reche, I., Fuentes-Lema, A., Romera-Castillo, C., Nieto-Cid, M., Ortega-Retuerta, E., et al. (2015). Turnover time of fluorescent dissolved organic matter in the dark global ocean. *Nat. Commun.* 6, 1–8. doi:10.1038/ncomms6986.

Cawley, K. M., Butler, K. D., Aiken, G. R., Larsen, L. G., Huntington, T. G., and McKnight, D. M. (2012). Identifying fluorescent pulp mill effluent in the Gulf of Maine and its watershed. *Mar. Pollut. Bull.* 64, 1678–1687. doi:10.1016/j.marpolbul.2012.05.040.

Chen, M., Jung, J., Lee, Y. K., and Hur, J. (2018). Surface accumulation of low molecular weight dissolved organic matter in surface waters and horizontal off-shelf spreading of nutrients and humic-like fluorescence in the Chukchi Sea of the Arctic Ocean. *Sci. Total Environ.* 639, 624–632. doi:10.1016/j.scitotenv.2018.05.205.

Chen, M., Kim, J. H., Nam, S. Il, Niessen, F., Hong, W. L., Kang, M. H., et al. (2016). Production of fluorescent dissolved organic matter in Arctic Ocean sediments. *Sci. Rep.* 6, 1–10. doi:10.1038/srep39213.

Chen, M., Kim, S. H., Jung, H. J., Hyun, J. H., Choi, J. H., Lee, H. J., et al. (2017). Dynamics of dissolved organic matter in riverine sediments affected by weir impoundments: Production, benthic flux, and environmental implications. *Water Res.* 121, 150–161. doi:10.1016/j.watres.2017.05.022.

D'Sa, E. J., Overton, E. B., Lohrenz, S. E., Maiti, K., Turner, R. E., and Freeman, A. (2016). Changing Dynamics of Dissolved Organic Matter Fluorescence in the Northern Gulf of Mexico Following the Deepwater Horizon Oil Spill. *Environ. Sci. Technol.* 50, 4940–4950. doi:10.1021/acs.est.5b04924.

Dalmagro, H. J., Lathuillière, M. J., Sallo, F. da S., Guerreiro, M. F., Pinto, O. B., de Arruda, P. H. Z., et al. (2019). Streams with riparian forest buffers versus impoundments differ in discharge and DOM characteristics for pasture catchments in Southern Amazonia. *Water (Switzerland)* 11, 1–20. doi:10.3390/w11020390.

Garcia, R. D., Diéguez, M. del C., Gerea, M., Garcia, P. E., and Reissig, M. (2018). Characterisation and reactivity continuum of dissolved organic matter in forested headwater catchments of Andean Patagonia. *Freshw. Biol.* 63, 1049–1062. doi:10.1111/fwb.13114.

Garcia, R. D., Reissig, M., Queimaliños, C. P., Garcia, P. E., and Dieguez, M. C. (2015). Climate-driven terrestrial inputs in ultraoligotrophic mountain streams of Andean Patagonia revealed through chromophoric and fluorescent dissolved organic matter. *Sci. Total Environ.* 521–522, 280–292.

doi:10.1016/j.scitotenv.2015.03.102.

Gonçalves-Araujo, R., Stedmon, C. A., Heim, B., Dubinenkov, I., Kraberg, A., Moiseev, D., et al. (2015). From fresh to marine waters: Characterization and fate of dissolved organic matter in the Lena River Delta Region, Siberia. *Front. Mar. Sci.* 2, 1–13. doi:10.3389/fmars.2015.00108.

Gonnelli, M., Galletti, Y., Marchetti, E., Mercadante, L., Retelletti Brogi, S., Ribotti, A., et al. (2016). Dissolved organic matter dynamics in surface waters affected by oil spill pollution: Results from the Serious Game exercise. *Deep. Res. Part II Top. Stud. Oceanogr.* 133, 88–99. doi:10.1016/j.dsr2.2016.05.027.

Graeber, D., Gelbrecht, J., Pusch, M. T., Anlanger, C., and von Schiller, D. (2012). Agriculture has changed the amount and composition of dissolved organic matter in Central European headwater streams. *Sci. Total Environ.* 438, 435–446. doi:10.1016/j.scitotenv.2012.08.087.

Kida, M., Kojima, T., Tanabe, Y., Hayashi, K., Kudoh, S., Maie, N., et al. (2019). Origin, distributions, and environmental significance of ubiquitous humic-like fluorophores in Antarctic lakes and streams. *Water Res.* 163, 0–2. doi:10.1016/j.watres.2019.114901.

Kowalczuk, P., Durako, M. J., Young, H., Kahn, A. E., Cooper, W. J., and Gonsior, M. (2009). Characterization of dissolved organic matter fluorescence in the South Atlantic Bight with use of PARAFAC model: Interannual variability. *Mar. Chem.* 113, 182–196. doi:10.1016/j.marchem.2009.01.015.

Kowalczuk, P., Tilstone, G. H., Zabłocka, M., Röttgers, R., and Thomas, R. (2013). Composition of dissolved organic matter along an Atlantic Meridional Transect from fluorescence spectroscopy and Parallel Factor Analysis. *Mar. Chem.* 157, 170–184. doi:10.1016/j.marchem.2013.10.004.

Kulkarni, H., Mladenov, N., and Datta, S. (2019). Effects of acidification on the optical properties of dissolved organic matter from high and low arsenic groundwater and surface water. *Sci. Total Environ.* 653, 1326–1332. doi:10.1016/j.scitotenv.2018.11.040.

Kulkarni, H. V., Mladenov, N., Johannesson, K. H., and Datta, S. (2017). Contrasting dissolved organic matter quality in groundwater in Holocene and Pleistocene aquifers and implications for influencing arsenic mobility. *Appl. Geochemistry* 77, 194–205. doi:10.1016/j.apgeochem.2016.06.002.

Lambert, T., Bouillon, S., Darchambeau, F., Massicotte, P., and Borges, A. V. (2016a). Shift in the chemical composition of dissolved organic matter in the Congo River network. *Biogeosciences* 13, 5405–5420. doi:10.5194/bg-13-5405-2016.

Lambert, T., Teodoru, C. R., Nyoni, F. C., Bouillon, S., Darchambeau, F., Massicotte, P., et al. (2016b). Along-stream transport and transformation of dissolved organic matter in a large tropical river. *Biogeosciences* 13, 2727–2741. doi:10.5194/bg-13-2727-2016.

Li, P., Lee, S. H., Lee, S. H., Lee, J. B., Lee, Y. K., Shin, H. S., et al. (2016). Seasonal and storm-driven changes in chemical composition of dissolved organic matter: a case study of a reservoir and its forested tributaries. *Environ. Sci. Pollut. Res.* 23, 24834–24845. doi:10.1007/s11356-016-7720-z.

Margolin, A. R., Gonnelli, M., Hansell, D. A., and Santinelli, C. (2018). Black Sea dissolved organic matter dynamics: Insights from optical analyses. *Limnol. Oceanogr.* 63, 1425–1443. doi:10.1002/lno.10791.

Murphy, K. R., Hambly, A., Singh, S., Henderson, R. K., Baker, A., Stuetz, R., et al. (2011). Organic matter fluorescence in municipal water recycling schemes:

Toward a unified PARAFAC model. *Environ. Sci. Technol.* 45, 2909–2916. doi:10.1021/es103015e.

Murphy, K. R., Ruiz, G. M., Dunsmuir, W. T. M., and Waite, T. D. (2006). Optimized parameters for fluorescence-based verification of ballast water exchange by ships. *Environ. Sci. Technol.* 40, 2357–2362. doi:10.1021/es0519381.

Murphy, K. R., Stedmon, C. A., Waite, T. D., and Ruiz, G. M. (2008). Distinguishing between terrestrial and autochthonous organic matter sources in marine environments using fluorescence spectroscopy. *Mar. Chem.* 108, 40–58. doi:10.1016/j.marchem.2007.10.003.

Murphy, K. R., Stedmon, C. A., Wenig, P., and Bro, R. (2014). OpenFluor- An online spectral library of auto-fluorescence by organic compounds in the environment. *Anal. Methods* 6, 658–661. doi:10.1039/c3ay41935e.

Murphy, K. R., Timko, S. A., Gonsior, M., Powers, L. C., Wünsch, U. J., and Stedmon, C. A. (2018). Photochemistry Illuminates Ubiquitous Organic Matter Fluorescence Spectra. *Environ. Sci. Technol.* 52, 11243–11250. doi:10.1021/acs.est.8b02648.

Osburn, C. L., Anderson, N. J., Stedmon, C. A., Giles, M. E., Whiteford, E. J., McGenity, T. J., et al. (2017). Shifts in the Source and Composition of Dissolved Organic Matter in Southwest Greenland Lakes Along a Regional Hydro-climatic Gradient. *J. Geophys. Res. Biogeosciences* 122, 3431–3445. doi:10.1002/2017JG003999.

Osburn, C. L., Boyd, T. J., Montgomery, M. T., Bianchi, T. S., Coffin, R. B., and Paerl, H. W. (2016a). Optical proxies for terrestrial dissolved organic matter in estuaries and coastal waters. *Front. Mar. Sci.* 2. doi:10.3389/fmars.2015.00127.

Osburn, C. L., Handsel, L. T., Peierls, B. L., and Paerl, H. W. (2016b). Predicting Sources of Dissolved Organic Nitrogen to an Estuary from an Agro-Urban Coastal Watershed. *Environ. Sci. Technol.* 50, 8473–8484. doi:10.1021/acs.est.6b00053.

Osburn, C. L., Wigdahl, C. R., Fritz, S. C., and Saros, J. E. (2011). Dissolved organic matter composition and photoreactivity in prairie lakes of the U.S. Great Plains. *Limnol. Oceanogr.* 56, 2371–2390. doi:10.4319/lo.2011.56.6.2371.

Schittich, A. R., Wünsch, U. J., Kulkarni, H. V., Battistel, M., Bregnhøj, H., Stedmon, C. A., et al. (2018). Investigating Fluorescent Organic-Matter Composition as a Key Predictor for Arsenic Mobility in Groundwater Aquifers. *Environ. Sci. Technol.* 52, 13027–13036. doi:10.1021/acs.est.8b04070.

Stedmon, C. A., and Markager, S. A. (2005). Tracing the Production and Degradation of Autochthonous Fractions of Dissolved Organic Matter by Fluorescence Analysis. *Limnol. Oceanogr.* 50, 1415. Available at: http://search.ebscohost.com/login.aspx?direct=true&db=edsjsr&AN=edsjsr.3597686&authtype=sso&custid=s8993828&site=eds-live&scope=site.

Walker, S. A., Amon, R. M. W., Stedmon, C., Duan, S., and Louchouarn, P. (2009). The use of PARAFAC modeling to trace terrestrial dissolved organic matter and fingerprint water masses in coastal Canadian Arctic surface waters. *J. Geophys. Res. Biogeosciences* 114, 1–12. doi:10.1029/2009JG000990.

Yamashita, Y., Cory, R. M., Nishioka, J., Kuma, K., Tanoue, E., and Jaffé, R. (2010a). Fluorescence characteristics of dissolved organic matter in the deep waters of the Okhotsk Sea and the northwestern North Pacific Ocean. *Deep Sea Res. Part II Top. Stud. Oceanogr.* 57, 1478–1485.

Yamashita, Y., Kloeppel, B. D., Knoepp, J., Zausen, G. L., and Jaffé, R. (2011). Effects

of Watershed History on Dissolved Organic Matter Characteristics in Headwater Streams. *Ecosystems* 14, 1110–1122. doi:10.1007/s10021-011-9469-z.

Yamashita, Y., Maie, N., Briceño, H., and Jaffé, R. (2010b). Optical characterization of dissolved organic matter in tropical rivers of the Guayana Shield, Venezuela. *J. Geophys. Res. Biogeosciences* 115. doi:10.1029/2009JG000987.

Yamashita, Y., Scinto, L. J., Maie, N., and Jaffé, R. (2010c). Dissolved Organic Matter Characteristics Across a Subtropical Wetland's Landscape: Application of Optical Properties in the Assessment of Environmental Dynamics. *Ecosystems* 13, 1006–1019. doi:10.1007/s10021-010-9370-1.

Capítulo 2

"Siempre veo constante, incesante y a la deriva, la baja de los materiales desde arriba... - una deriva que se ha mantenido durante cientos de millones de años, que continuará en el tiempo mientras haya mares y continentes… Para los sedimentos es la nevadas más estupenda que se ha visto en la Tierra...".
Rachel Carson, "The Sea Around Us", 1951.

Submarine mud volcanoes as a source of chromophoric dissolved organic matter to the deep waters of the Gulf of Cádiz*

Amaral, V.[1,2*], Romera-Castillo, C.[3], Forja, J.[1]

[1]Departamento de Química-Física, INMAR, Universidad de Cádiz, Puerto Real, España.
[2]Ecología Funcional de Sistemas Acuáticos, Centro Universitario Regional Este, Universidad de la República, Rocha, Uruguay.
[3]Instituto de Ciencias del Mar-CSIC, Barcelona, España.

Publicado en *Scientific Report

Abstract

Seafloor structures related to the emission of different fluids, such as submarine mud volcanoes (MVs), have been recently reported to largely contribute with dissolved organic matter (DOM) into the oceans. Submarine MVs are common structures in the Gulf of Cádiz. However, little is known about the biogeochemical processes that occur in these peculiar environments, especially those involving DOM. Here, we report DOM characterization in the sediment pore water of three MVs of the Gulf of Cádiz. Estimated benthic fluxes of dissolved organic carbon (DOC) and chromophoric DOM (CDOM) were higher than in other marine sediments with an average of 0.11 ± 0.04 mmol m^{-2} d^{-1} for DOC and ranging between 0.11 and 2.86 m^{-1} L m^{-2} d^{-1}, for CDOM. Protein-like components represented ~ 70 % of the total fluorescent DOM (FDOM). We found that deep fluids migration from MVs (cold seeps) and anaerobic production via sulfate-reducing bacteria represent a source of DOC and FDOM to the overlying water column. Our results also indicate that fluorescent components can have many diverse sources not captured by common classifications. Overall, MVs act as a source of DOC, CDOM, and FDOM to the deep waters of the Gulf of Cádiz, providing energy to the microbial communities living there.

IV. 1. Introduction

Dissolved organic matter (DOM) is one of the Earth's major carbon reservoirs and the largest ocean pool of reduced carbon (662 Pg C)[1]. The fraction of DOM that absorbs light, referred to as chromophoric DOM (CDOM), and its fluorescent sub-fraction (FDOM) are ubiquitous constituents of the ocean DOM pool, affecting the optical properties of the water column[2,3]. The major sources of marine DOM are photosynthesis

from the ocean surface and terrestrial inputs, however, marine sediments are also considered to be an important source of DOM to the overlying seawater (~350 Tg C y^{-1})[4], comparable to that estimated for rivers (~250 Tg C y^{-1})[5]. Marine sediments are also a source of CDOM, but there is comparatively little information about the benthic flux of CDOM and the nature of these compounds[6]. Recent studies suggest that seafloor features related to large emissions of different fluids can act as sources of DOM and CDOM into the oceans[7–9] therefore, having a significant influence on the chemistry of the oceans[10].

Seafloor fluids can derive from microbiological and geological processes and they are classified in hydrothermal (40°C up to 400°C) and cold seeps (< 60°C). Hydrothermal vents have been described as sinks of DOC, removing 1.4 ± 0.7 × 10^4 tons C yr^{-1} from the deep-ocean[11,12]. However, they have been also found to act as a source of CDOM to the seawater[9]. Cold seeps comprise brines, methane and other hydrocarbons and are mainly controlled by tectonics[13], but there is little information regarding the behavior of DOM from these fluids. Submarine cold seepage could result in a variety of seafloor structures such as mud volcanoes (MVs).

Submarine MVs are broadly distributed on Earth continental shelves, insular slopes and abyssal parts of inland seas (10^3 ~10^5)[14]. MVs are cone-shaped structures built up by mud breccia containing gases (mainly methane), saline water, mud, and, occasionally, oil rising from deep pressurized sources through controlled conduits[15,16]. They can be associated with the presence of chemosynthetic biological communities[17,18]. A recent study in the South China Sea suggests that MVs are an important source of DOC to the deep waters through benthic fluxes, and these could represent up to 24% of the total annual flux from the largest river that drains into this

sea[19]. Moreover, Retelleti et al.[20] also measured a high concentration of DOC and FDOM in pore water from MVs (1- 6 mM and 0.01- 0.06 RU, respectively). The authors found that fluid migrating from deep sediments through MVs could be an important source of altered FDOM to the overlying water column, with a total fluorescence of up to eight times higher than sediments without MVs. They suggest that these structures may play a significant role in providing FDOM to the ocean. However, as far as we know, no studies have estimated benthic fluxes of CDOM and FDOM from MVs yet, and their role in the deep ocean is poorly understood.

The Gulf of Cádiz is a tectonically active area where large fields of submarine MVs, associated with tectonic compression due to the convergence of the African and the Eurasian plates[21], have been recently discovered[17,22,23]. Its geological features, the geochemistry and emission of fluids, and the benthic fauna associated with these fluids have been widely studied[16,17,24,25]. However, no studies have focused on the dynamic and diffusive benthic flux of DOM from these MVs.

This work aims to quantify and characterize DOM in the pore water of three MVs located in the Gulf of Cádiz (Fig. 1), and to determine the possible sources of the different fractions of DOM. To do so, we measured DOC concentration and DOM optical properties (absorbance and fluorescence). We also estimated diffusive benthic fluxes of DOC, CDOM, and FDOM across the sediment-water interface at these MVs to better understand their effect on the concentration and distribution of DOM into the deep water of the Gulf of Cádiz.

IV. 2. Methods

Site description. The Gulf of Cádiz is located between the SW continental margin of the Iberian Peninsula and the NW margin of Africa (Fig. 1). It is strongly influenced by the exchange of Atlantic and Mediterranean water masses through the Strait of Gibraltar and it is characterized by the presence of several areas of hydrocarbon-rich fluid venting structures (e.g., MVs, pockmarks, carbonate chimneys and crusts, mud mounds and diapiric ridges)[17,22,48,49].

The study was carried out in three MVs: Anastasya (AN) and Pipoca (PI), situated in the Guadalquivir Diapiric Ridge Field, and St. Petersburg (PT), in the deeper Tasyo field, located between 457 and 860 m depth (Table S1). Recent work found that bottom waters at these MVs exhibit high methane concentrations, especially in AN[31]. Based on cold seep fauna at the summit of these MVs and the characteristic of the mud breccia sediments (e.g., gas bubbles, smell of H_2S), AN seems to be the more active one among the three MVs studied here[17].

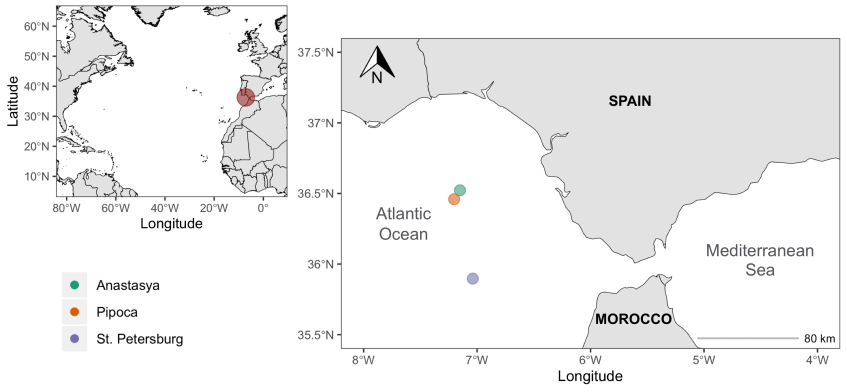

Fig. 1. Map of the Gulf of Cádiz showing the location of the mud volcanoes.

Sampling and analytical methods. Two cruises were carried out onboard R/V Angeles Alvariño and Ramón Margalef during June and December 2016. Seawater samples from the water column were collected from 5 m to the summit of each MV (n = 44), and pore water samples were collected from gravity cores inside each MV. The 44 seawater samples were taken using Niskin bottles (10 L) mounted on a rosette-sampler coupled to a Seabird CTD 911+ to measure temperature and salinity. Details regarding the measurements of physicochemical variables are described elsewhere[27]. For measuring DOC concentration, absorbance and fluorescence, seawater was filtered using precombusted filters (Whatman GF/F, nominal pore size 0.7 µm, 450°C, 4 h). Both optical analyses were performed on board with the same settings described below. Samples for DOC concentration were frozen in acid-clean HDPE bottles until analysis.

Two 1 m long gravity cores of 9.5 cm inner diameter were collected from inside each mud volcano. Subsamples from each core were taken onboard. Sections of 1 cm thickness were carefully sliced at different depths (~ 0.5 to 45 cm below the seafloor) and stored frozen until analysis. Sediments and pore water samples were treated in an inert atmosphere using N_2 to minimize exposure to oxygen. Pore water samples were collected by centrifugation (~ 100 g of sediment, 30 minutes, 10.000 G and 10 ºC, SIGMA-18KS, n = 60) and then filtered (Millipore HPF 0.45 µm). Combusted GF/F filters significantly increase their retention capacity due to compaction of the borosilicate microfibers[50], hence no significant differences associated with using different filters for pore water and seawater samples are expected in this work. Even though centrifugation could have an effect on DOM composition, it would be minimal compared to other techniques when analyzing FDOM[51,52]. It does not require pretreatment and it is

currently the most widely used method for collecting pore water from sediments for DOC and FDOM analyses (see references Table 2). Magnesium (Mg), chloride (Cl) and sulphate concentrations were measured in pore water samples by ionic chromatograph (Metrohm 881/882, Compact IC pro, plus, CV = 1.78 ± 0.26 %), and ammonium was measured using a segmented flow auto-analyser (Skalar, San Plus) (Jiménez-López et al. submitted). For DOC analysis, pore water was diluted in MilliQ and stored frozen until analysis using a Multi N/C 3100 Analytik Jena analyzer (instrument variability = 43 ± 1.8 mM, Hansell CRM Program). UV-visible absorption spectra were immediately scanned from 250 to 800 nm using a spectrometer (JASCO-V750) using a 1 cm path length quartz cuvette. The estimated detection limit of the spectrophotometer for quantifying CDOM absorption is 0.0015 absorbance units or 0.03 m^1 (1 cm cuvette), and the noise is 0.00004 absorbance units (specifications JASCO-750). A blank was measured every six samples to detect and correct instrument drift. We calculated the absorption coefficient at 254 and 350 nm and the spectral slope $S_{275\text{-}295}$[53,54]. Excitation-emission matrixes (EEMs) at 250–450/300–560 nm were immediately obtained using a spectrofluorometer with an accessory for temperature control (JASCO FP-8300, EHC-813). Prior to PARAFAC modeling, EEMs from seawater and pore water samples were standardized (e.g. blank subtraction, instrument correction factor, Raman and Rayleigh scatter band were trimmed, and inner filter effect was corrected), and normalized to Raman Unit (RU) using the drEEM 0.2 toolbox for Matlab[55]. Fluorescent components were validated using split-half validation and random-initialization analysis[55]. We also calculated the humification (HIX) and freshness index (BIX) following Huguet et al.[40]. Further details for the

calculation of spectral indexes, EEMs standardization, and PARAFAC analysis are described in a previous work[27].

Assuming diffusive transport across the sediment-water interface, we estimated the benthic fluxes of DOC, CDOM (as a_{254} and a_{350}), and FDOM components from the MVs using Fick's first law of diffusion following Burdige et al.[35] and Hung et al. [19].

$$J = \varphi Ds\, dC/dz$$

Where φ is porosity, Ds is the bulk sediment diffusion coefficient corrected for sediment tortuosity (θ^2) according to D_0/θ^2, where D_0 is the free solution coefficient (1.585×10^{-6} cm^2 s^{-1})[56] and θ^2 was estimated using the modified Weissberg relationship (Boudreau, 1997, $\theta^2 = [1 - 2 \text{ Ln } (\varphi)]$). Finally, dC/dz was calculated as the difference between the bottom water and pore water concentration at 0.5 cm. It should be noted that bottom water collected at ~ 5 m above MVs was used, thus benthic flux estimation should be treated with a degree of caution, since, in general, water overlying the sediments (~ 30 cm) should be used [36]. To apply the same method, for FDOM we used the values obtained by pick picking techniques of the four PARAFAC components in both bottom and pore water samples.

Statistical analysis. Two ways ANOVA and the post hoc Tukey test were performed to assess differences in DOM (factor 1: MVs and factor 2: cruises). A significance level of 0.05 was selected. Linear regression models were used to determine the relationship between DOM variables and were considered statistically significant when $p < 0.01$. All analyses were performed with R 1.3.1073 software[57].

IV. 3. Results

Sediment pore water profiles of DOM and proxy of MVs fluids. Differences between cruises in pore water samples were considered to be due to spatial heterogeneity previously described in MVs[16]. During December 2016, it was not possible to sample PT due to weather conditions. Overall, similar values between cruises were observed in PI and AN ($p > 0.05$). Only DOC concentration and BIX values were higher in AN during June ($p < 0.05$). Thus, for simplicity, only the pore water profiles of June will be presented, and those from December can be found in the Supplementary material (Fig. S1 and S2).

DOC concentration in pore water ranged from 0.63 to 4.08 mmol L^{-1}, with higher values in PT (Table 1, $p < 0.001$) and increasing with depth in the three MVs (Fig. 2A). The absorption coefficient a_{254} ranged between 9.58 and 36.25 m^{-1}, with higher values in AN (Fig. 2B, $p < 0.001$) while a_{350} showed similar variations between MVs (Fig. 2C, 0.48-3.91 m^{-1}, $p > 0.05$). Although the spectral slope $S_{275-295}$ showed similar values between MVs (Fig. 2D, $p > 0.05$), ranging from 0.020 to 0.062 nm^{-1}, AN and PI exhibited an opposite trend when compared to PT. Thus, $S_{275-295}$ decreased with depth in AN and PI while in PT, it increased. Average values of $S_{275-295}$ showed that most of the DOM in the MVs was of relatively low molecular weight (Table 1).

Table 1. Pore water average ± standard deviation values of dissolved organic carbon (DOC, mmol L^{-1}), absorption coefficient a_{254} and a_{350} (m^{-1}), the spectral slope $S_{275-295}$ (nm^{-1}), fluorescent components (C1 to C4, RU), humification (HIX) and freshness (BIX) indexes during June and December 2016 in Anastasya and Pipoca and during June 2016 in St. Petersburg. Interval variations are shown in brackets.

	Anastasya	Pipoca	St. Petersburg
DOC	1.44 ± 0.67 (0.63-3.59)	1.50 ± 0.43 (0.74-2.43)	2.85 ± 0.56 (1.83-4.08)
a_{254}	24.36 ± 5.02 (15.71-36.25)	14.17 ± 3.59 (9.59-23.59)	16.63 ± 5.79 (9.58-27.10)
a_{350}	1.93 ± 0.63 (1.06-3.91)	1.67 ± 0.66 (0.91-3.49)	1.59 ± 0.67 (0.48-3.25)
$S_{275-295}$	0.045 ± 0.012 (0.021-0.061)	0.038 ± 0.009 (0.020-0.061)	0.045 ± 0.010 (0.030-0.062)
C1	0.25 ± 0.17 (0.09-0.82)	0.18 ± 0.08 (0.09-0.40)	0.37 ± 0.016 (0.17-0.66)
C2	0.36 ± 0.24 (0.10-0.93)	0.14 ± 0.02 (0.10-0.18)	0.13 ± 0.06 (0.08-0.31)
C3	0.55 ± 0.31 (0.32-1.70)	0.21 ± 0.14 (0.09- 0.70)	0.29 ± 0.16 (0.10-0.58)
C4	1.58 ± 1.03 (0.51-4.07)	0.39 ± 0.25 (0.18-1.25)	0.62 ± 0.41 (0.23-1.36)
HIX	0.59 ± 0.12 (0.35-0.75)	0.74 ± 0.04 (0.61-0.80)	0.78 ± 0.07 (0.70-0.80)
BIX	1.19 ± 0.59 (0.75-3.42)	0.80 ± 0.07 (0.65-0.90)	0.80 ± 0.11 (0.57-0.98)

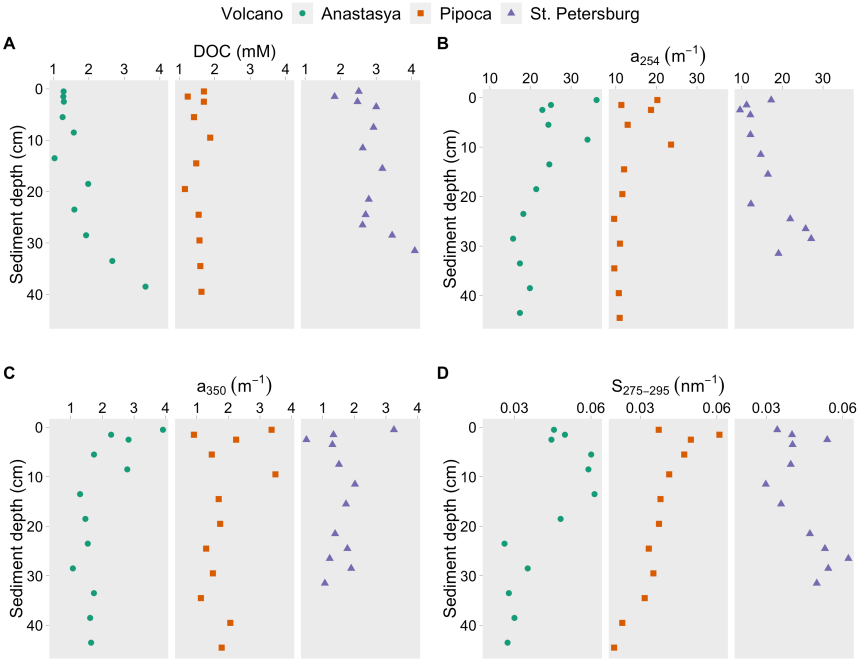

Fig. 2. Pore water profiles of dissolved organic carbon (A: DOC), absorption coefficients at 254 nm (B) and 350 nm (C) and the spectral slope $S_{275-295}$ (D) in the three mud volcanoes.

Parallel factor analysis (PARAFAC) of pore water samples from the three MV resulted in a four-fluorescent-components model (Fig. S3). The components were compared with previous studies in the OpenFluor database with a Tucker Congruence Coefficient (TCC) > 0.97 (Table S2)[26]. Component 1 (C1) and 2 (C2) were previously described as humic-like components of terrestrial and marine/microbial origin, respectively. Component 3 (C3) and component 4 (C4) were referred to as protein-like components, accounting for 68% ± 17% of the total FDOM. C4 resembles the amino acid tyrosine, and C3 is less common than other components. Amaral et al.[27] found a similar component to our C3 in the water column of the Gulf of Cádiz (labeled as C5) and they suggested it could be a mixture of polycyclic aromatic hydrocarbon (PAH) and protein-like substances.

Humic-like C1 showed similar values between MVs (Table 1, Fig. 3A, $p > 0.05$). The rest of the fluorescent components showed the highest intensities and variability in AN, with average values two and three-fold times higher than in the other MVs ($p < 0.001$). In PI and PT, C2 and C3 had similar constant vertical distribution with a slightly increase of C2 below 30 cm in PT (Fig. 3B and 3C). C4 also increased downward in PT while in PI, it remained relatively constant with depth (Fig. 3D). In AN, maximum values of C2, C3, and C4 were found in the first 0.5 cm, which sharply decreased until 2.5 cm, and below 13 cm C2 and C4 increased again downward while C3 remained relatively constant.

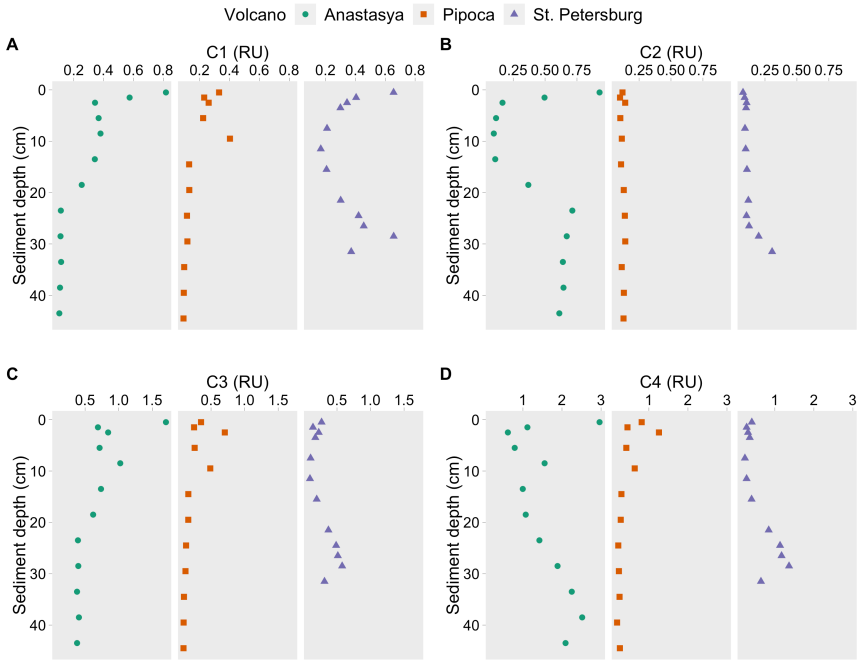

Fig. 3. Pore water profiles of the PARAFAC fluorescent components (A: C1, B: C2, C: C3 and D: C4) in the three mud volcanoes.

Only AN exhibited a linear relationship between total fluorescence (C1+C2+C3+C4) and DOC, with a y-intercept of 0.49 mmol L^{-1} ($p < 0.01$, $n = 22$), which is the colorless fraction of DOM. Since the average DOC

concentration in AN was 1.44 mmol L^{-1}, we estimated that 66 % of the DOC pool in the pore water of these mud volcano is composed of fluorescent material.

The humification and freshness indexes (HIX and BIX) showed an opposite pattern (Fig. 6S) with the lowest HIX values and highest BIX values in AN (Table 1, $p < 0.001$). In PI and PT, BIX values were lower than 1, while in AN, the average value was > 1.

Linear relationships between C1 with C2 and C4 revealed differences in their dynamics depending on the mud volcano (Table S3). C1 was negatively related with C2 and C4 in AN ($R^2 = 0.71$ and 0.53, $p < 0.01$), but positively in PI ($R^2 = 0.71$ and 0.82, $p < 0.01$) and PT ($R^2 = 0.60$ and 0.62, $p < 0.01$), while it was positively related with C3 in the three MV ($R^2 = 0.71$ and 0.53, $p < 0.01$). The other fluorescent components only exhibited significant linear relationships in PI and PT. Thus, the protein-like C3 and C4 showed a strong positive relationship between them and to a lesser exert with C2. a_{254} showed a positive relationship with all fluorescent components in PI and PT, but only with C1 and C3 in AN ($R^2 > 0.21$, $p < 0.01$). No significant relationships were observed with a_{350} ($p > 0.01$).

Chloride (Cl) and magnesium (Mg) were measured in pore water samples and are described elsewhere (Jiménez-López et al. submitted). Here, the Mg:Cl ratio was considered as a mixing indicator of seawater and MVs fluids (Fig. 4). The smaller the ratio, the higher it will be the fraction of MVs fluid in the pore water samples[22]. Similar values were observed in the uppermost samples from the three MVs (0.5 cm, 0.11 ± 0.01), which mainly correspond to the hemipelagic sediments. The Mg:Cl ratio decreased with depth in AN, reaching values of 0.03, even smaller than those observed in other active MVs[22]. Conversely, in PI and PT, the ratio remains relatively

constant, except for the last depth in PT where it decreases to 0.07 (31 cm). Similar trends and values were observed between sampling periods ($p > 0.05$).

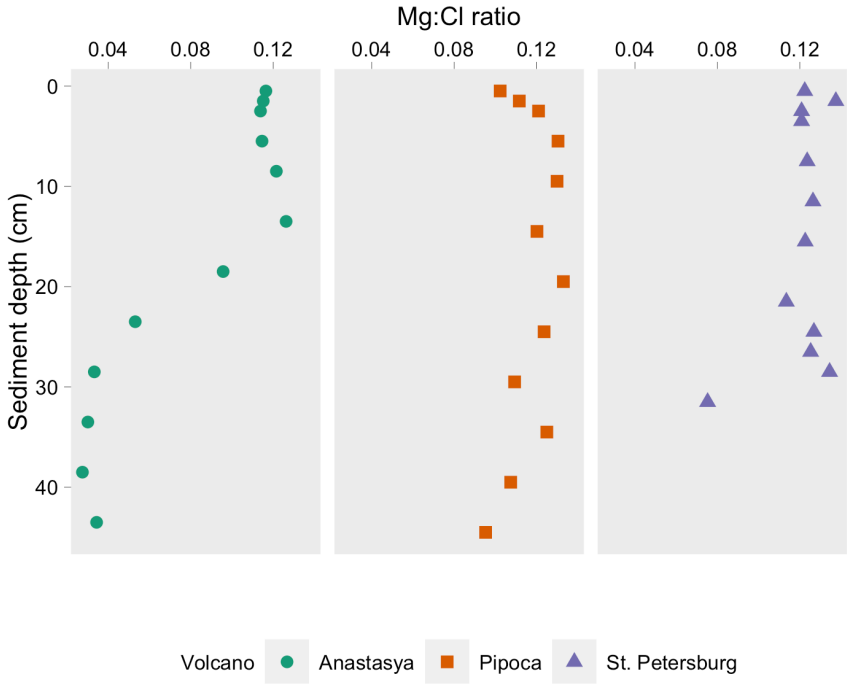

Fig. 4. Pore water profiles of the Mg:Cl ratio in the three mud volcanoes.

Seawater profiles of DOM in the water column above the MVs. The concentration of DOC, a_{254}, and a_{350} were one and two orders of magnitude lower than those observed in pore water, ranging between 0.04 to 0.14 mmol L^{-1}, 0.88 to 2.03 m^{-1}, and 0.01 to 0.4 m^{-1}, respectively (Fig. S4, $p < 0.05$). The spectral index $S_{275\text{-}295}$ ranged between 0.018 and 0.045 nm^{-1}, with an average value of 0.028 ± 0.007 nm^{-1}, lower than those observed in pore water samples (0.043 ± 0.01 nm^{-1}).

For the water column samples, the PARAFAC model validated three largely described components in aquatic systems, a humic-like and two protein-like components. The TCC between the fluorescent components in

the water column and pore water was < 0.95, implying that the components compared cannot be considered equal[28]. Therefore, to compare the FDOM between both datasets, we applied the pick picking technique in the EEMs from the water column[29] using the same Ex/Em wavelengths of the PARAFAC components identified in the pore water samples. Fluorescence intensity was tenfold higher in pore water than in the water column. C1 followed the same trends in the three sites ($p > 0.05$), increasing with depth (Fig. S5) with a strong relationship with T and S ($R^2 = 0.87$, $p < 0.01$). In the water column, C2 and C3 were higher in AN than the other sites ($p < 0.05$), increasing sharply with depth, associated with the thermocline and the peak of Chl *a* [27], while in PI and PT, they remained relatively constants. C4 exhibited an irregular profile in the three sites ($p > 0.05$), and an increase of C2, C3, and C4 was observed in the summit of AN and PT (Fig. S5).

Estimated diffusive benthic fluxes of DOC, CDOM, and FDOM. All variables showed positive benthic flux toward the water column (Table 2). The estimated benthic fluxes of DOC varied between 0.07-0.18 mmol $m^{-2}\,d^{-1}$, being highest in PT. The estimated benthic fluxes of CDOM, as a_{254} and a_{350}, ranged from 1.15 to 2.86 and from 0.11 to 0.31 ($m^{-1}\,L\,m^{-2}\,d^{-1}$), respectively, with higher values in AN. The humic-like C1 showed similar fluxes between MVs ranging from 0.02 to 0.05 (RU L $m^{-2}\,d^{-1}$), while C2 ranged between 0.008 and 0.070 (RU L $m^{-2}\,d^{-1}$) with the highest value in AN. Protein-like C4 showed the highest fluxes among the fluorescent components ranging from 0.02 to 0.240 RU L $m^{-2}\,d^{-1}$, with the highest value also in AN.

Table 2. Estimated diffusive benthic fluxes of DOC, CDOM, and FDOM in the three MVs. Fluxes from other regions are also displayed (WD: water column depth).

Variable	Studies	Range	WD (m)
DOC ($mM\ m^{-2}\ d^{-1}$)	Anastasya	0.07-0.1	457
	Pipoca	0.08-0.13	503
	San Petersburg	0.18	860
	MVs from China Sea[1]	0.03-0.52	367 - 668
	Weddell Sea[2]	0.1-0.54	316 - 494
	European margins[3]	0.05-0.16	180 - 4800
	N Atlantic Ocean[4]	0.08	300 - 1000
	Arabian Sea[5]	0.060-0.22	> 3000
	NE Atlantic Ocean[5]	0.05-0.12	> 4000
	Estuarine[6]	0.96-1.10	12-15
a_{254} ($m^{-1}\ L$)($m^{-2}\ d^{-1}$)	Anastasya	2.12-2.86	
	Pipoca	1.50-1.54	
	San Petersburg	1.15	
a_{350} ($m^{-1}\ L$)($m^{-2}\ d^{-1}$)	Anastasya	0.15-0.31	
	Pipoca	0.11-0.26	
	San Petersburg	0.22	
	Arctic Ocean[7]	-0.03-0.18	100-2240
C1 (RU L)($m^{-2}\ d^{-1}$)	Anastasya	0.03-0.05	
	Pipoca	0.02	
	San Petersburg	0.04	
	Arctic Ocean[7]	0-0.07	100-2240
	Estuarine[6]	0.08-3.41	12-15
C2 (RU L)($m^{-2}\ d^{-1}$)	Anastasya	0.02-0.07	
	Pipoca	0.01	
	San Petersburg	0.008	
	Arctic Ocean[7]	0.02-0.06	100-2240
	Estuarine[6]	0.08-3.97	12-15
C3 (RU L)($m^{-2}\ d^{-1}$)	Anastasya	0.02-0.13	
	Pipoca	0.003	
	San Petersburg	0.01	
	Estuarine[6]	0.19-6.09	12-15
C4	Anastasya	0.05-0.24	

(RU L)(m^{-2} d^{-1})	Pipoca	0.05-0.07	
	San Petersburg	0.03	
	Arctic Ocean[7]	-0.04-0.03	100-2240
	Estuarine[6]	0.19-6.09	12-15

[1]Hung et al. 2016, [2]Hulth et al. 1997, [3]Otto and Balzer, 1998, [4]Alperin et al. 1999, [5]Lhajnar et al. 2005, [6]Burdige et al. 2004*, [7]Chen et al. 2016. Positive fluxes are out of the MVs. *1 RU = 64 μg QS.

IV. 4. Discussion

The fluorescent components found in the pore water model have been described for several aquatic environments (Table S2). Our results support the hypothesis that similar components may have different sources[6,30]. In the water column above the MVs, C1 and C2 showed the usual positive relationship between humic-like components from similar sources (R^2 = 0.85, $p < 0.001$, n = 37), and mixing processes explained their distribution, in agreement with previous studies in this zone[27]. The same occurs with the protein-like components, where C3 and C4 were positively related (R^2 = 0.60, $p < 0.001$, n = 37), and probably associated with biological activity[27]. Conversely, different behaviors were observed in pore water samples from the MVs. In AN, humic-like C1 and C2 were negatively related (R^2 = 0.71, $p < 0.001$, n = 58), and no relationship was observed between protein-like C3 and C4, indicating differences in their sources and sinks. On the other hand, all fluorescent components in PI and PT, showed a positive relationship among them ($R^2 > 0.50$, $p < 0.001$, Table S3). Therefore, the processes that produce and remove FDOM also differ between MVs.

One possible source could be the production of thermogenic DOM together with the production of methane. More than 2.4% of DOM compounds in the ocean are thermogenic[7], and a previous work suggests that the FDOM coming from the deep sediments of MVs fluids was mainly

thermogenic[20]. According to the authors, the lower DOC-normalized fluorescence in the MVs, compared to those found in a reference site (without MVs), may be due to the thermal quenching of the fluorophores. Based on stable carbon isotope composition of dissolved methane in the column water above the MVs studied here, Sierra et al.[31] found that methane emissions in AN and PT are of thermogenic origin, while in PI, it seems to be of biogeochemical origin. Unfortunately, we did not measure DOM composition of other pore water sediments in the zone to use as a reference site, and similar values of DOC-normalized fluorescence were observed between AN, PT and PI. Thus, a thermogenic origin of FDOM in this work cannot be confirmed.

However, the differences in the DOM sources between MVs could be related to differences in their activity stage, hence, with the intensity of the fluids moving upward from the deeper sediments. MVs alternate between massive mudflow extrusion and dormant/sleeping periods[17]. According to Mazzini et al.[18], most of the MVs are currently in the latter, generally characterized by gas and water seepage of variable intensity only. The Mg:Cl ratio indicated a higher fraction of MVs fluid in AN than in the other MVs (Fig. 4) and Sierra et al.[31] found an increase of methane with depth in the water column above AN (100 – 125 nmol L^{-1}) and PT (10 – 15 nmol L^{-1}), whereas in PI this trend was not observed. This is in agreement with a previous work analyzing benthic fauna associated with seepage of MVs fluids, suggesting locally elevated gas fluxes that reach the seafloor surface, and higher activity in AN than PI[17]. Additionally, habitats with structures created by the escaping gas were also found in PT[32], and elevated methane fluxes have also been found in relatively active MVs in the Gulf of Cádiz[16,33]. The level of extrusion activity between the MVs studied here is

AN > PT > PI and it could be the reason for the existence of different sources of DOM in the MVs. For example, in AN, DOC, C2 and C4 exhibited a negative relationship with the Mg:Cl ratio (R^2 = 0.51, 0.79, 0.45, respectively, $p < 0.001$, n = 23, Fig. 5), indicating an increase with the increasing mud volcano fluids. In PT, DOC and C2 also showed an inverse relationship with this ratio, weaker than in AN, but significant (R^2 = 0.44 and 0.51, respectively, $p < 0.01$, n = 12, Fig. 5), while no relationships were observed in PI ($p > 0.01$). Our results indicate that cold seeps from MVs could be a source of DOC and FDOM to shallower sediments and, eventually, to the overlying water column.

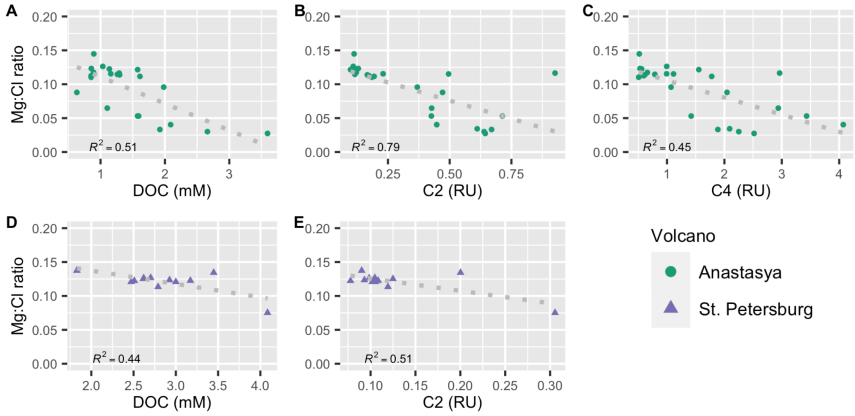

Fig. 5. Linear relationship between the Mg:Cl ration with dissolved organic carbon (DOC) and fluorescent components in Anastasya (A, B and C) and St. Petersburg (D and E). Only the relationships with $p < 0.01$ are shown.

We found a net production of DOC, CDOM, and FDOM to the overlying water column in all three MVs (Table 3). However, as previously discussed for PI, and given the R^2 of the relationship between DOM and the Mg:Cl ratio found in AN and PT, there might be other factors and sources implicated in the final distribution of DOM. In sediments, there is generally a net production of DOM as a result of organic matter degradation processes[4]. Sulfate is one of the main electron acceptors available for the

oxidation of organic matter in marine sediments; hence sulfate reduction is an important diagenetic process below the oxic zone[34]. Several studies in marine sediments found that FDOM could be produced via anaerobic degradation of particulate organic matter through sulfate reduction or oxidation of methane[35–37]. Luek et al.[30] found that the production of FDOM was directly related to sulfate-reducing bacteria in incubations of coastal sediments. The decomposition of organic matter by sulfate reduction consumes sulfate and releases ammonium[34]. Both sulfate and ammonium were measured in pore water samples from the three MVs and are described elsewhere (Jiménez-López et al. submitted). Accordingly, in AN, the increase of DOC concentration, C2 and C4 was accompanied by the increase in ammonium (Fig. 6A, B and C, R^2 = 0.28, 0.75 and 0.79, respectively, $p < 0.01$, n = 23) concurrent with the decrease of sulfate (Fig 6D, E and F, R^2 =0.39, 0.89 and 0.59, respectively, $p < 0.01$, n = 23). Moreover, in AN, these fluorescent components were related to a decrease in DOM humification and with an increase of freshly released DOM (Table S3). In PT, only C2 exhibited a strong relationship with ammonium and sulfate, with the same trends as in AN (Fig. 6G and H, R^2 = 0.91 and 0.87, respectively, $p < 0.01$, n =12), whereas no relationship was observed in PI ($p > 0.01$). These results suggest that DOC concentration, C2 and C4 could also be related to the activity of sulfate-reducing bacteria in MVs sediments.

Table 3. Production of dissolved organic carbon (DOC, mM), chromophoric DOM (as a_{254} and a_{350}, m^{-1}) and fluorescent components (C1 to C4, RU) in the pore water sediments of Anastasya (AN), Pipoca (PI) and St. Petersburg (PT) during June and December 2016. The net increase is indicated (= value bottom depth pore water – value bottom water).

MV Cruise	DOC	a_{254}	a_{350}	C1	C2	C3	C4
AN June	3.5	16.0	1.5	0.1	0.6	0.3	2.0
AN Dec.	2.0	30.9	1.8	0.1	0.4	0.4	4.0
PI June	1.6	9.6	1.6	0.1	0.1	0.1	0.2
PI Dec.	2.1	12.2	1.1	0.1	0.1	0.1	0.2
PT June	4.0	17.8	0.9	0.4	0.3	0.3	0.6

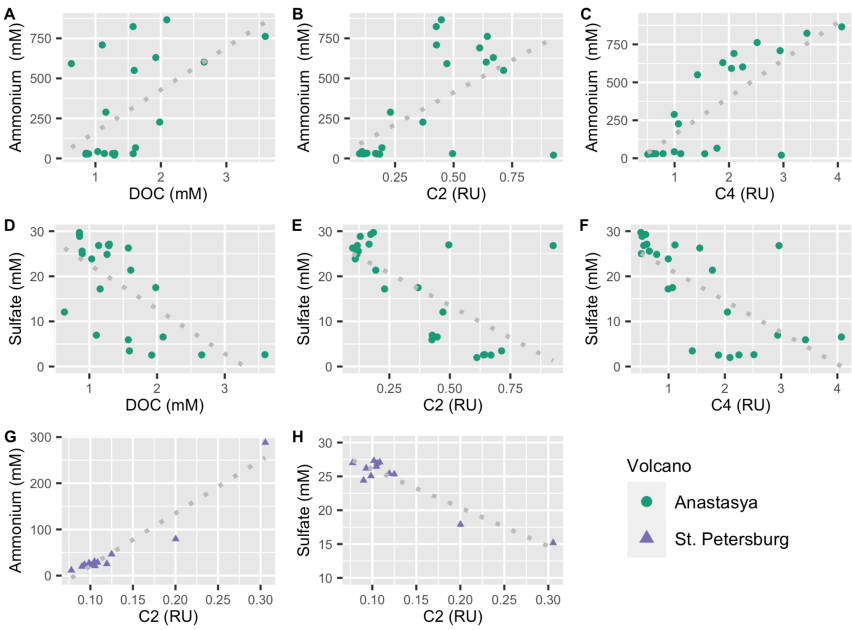

Fig. 6. Linear relationship between ammonium and sulfate with dissolved organic carbon (DOC) and fluorescent components C2 and C4 in Anastasya (A-F) and St. Petersburg (G and H). Only the relationships with $p < 0.01$ are shown.

Additionally, AN is characterized by the presence of large microbial mats in its summit, associated with cold seep and extremophiles conditions in its anoxic sediments, while chemosynthetic-based communities have also been found in PT[17,38]. The biological release of DOC has been previously reported in seep environment characterized by the presence of microbial

mats in the Hydrate Ridge[39]. The deep DOC in fluid seepage may stimulate the microbial community to release autochthonous organic matter and enhance heterotrophy in seep environments[39]. Based on BIX values, Retelleti et al.[20] suggested that MVs have more abundance of DOC from biological sources than sediments without MVs, which has been attributed to the direct release of DOC from microorganisms. This could explain the highest BIX values observed in AN (> 1 up to 3), which corresponds to the presence of DOM recently released[40]. Anaerobic production of DOM via sulfate-reducing bacteria might also be a source of DOM in AN and, to a lesser extent, in PT, providing energy to the microbial communities living there. These processes were also suggested as one of the responsible of FDOM composition in other MVs[20].

On the other hand, deep cold seep fluids and biological activity appear to be a minor source of DOM in PI, probably linked to the lower seepage activity of this mud volcano, as previously mentioned. Although PI is located in the same MVs field than AN (Table 1S), it is strongly influenced by bottom currents from Mediterranean waters[32] and organisms not associated with fluid emissions, but typical in these waters, such as dense crinoid beds, had been observed in its summits[17]. We hypothesized that the net increase of DOM observed in PI (Table 3) could be due to abiotic processes such as condensation, fragmentation, or physical dissolution of POM to DOM[3,42]. For example, abiotic condensation of FDOM could be responsible of refractory organic matter[3]. This could explain the negative relationship between FDOM components with the BIX observed in PI, but not observed in the other MVs (Table 3S), as well as the relatively less variable DOM profiles in pore water (Table 1, Fig. 2 and 3).

Our results agree with previous works that suggest that similar

fluorescent components may have different sources[6,30]. Humic-like C2 was first proposed as a component of marine origin[29], but further studies indicate that this component is observed in almost all aquatic environments (Table 2S), and its signal was then attributed to microbial humic-like fluorescence[3]. In the water column of the Gulf of Cádiz, C2 was described from both autochthonous and allochthonous sources[27], while in this work it was related to cold seeps from MVs and bacterial sulfate-reduction. Several works indicate that 'humic-like' DOM is also produced in the absence of terrestrial sources or humification processes[3,30,43]. Our results support the hypothesis that spectral regions originally defined as "humic-like" can have many diverse sources not considered by the traditional classification[29]. On the other hand, the distribution of C1 might be explained by deposition from the water column and/or solubilization, given the similar distribution observed between MVs ($p > 0.05$), while the net increase observed might be due to abiotic processes. Another possibility could be C1 production by solubilization of the terrestrial organic matter that has settled.

Finally, C3 was described as a mixture of PAH and protein-like components related to anthropogenic pollution in the water column of the Gulf of Cádiz[27]. Although MVs could also be a source of PAH[18], a unique source cannot be distinguished using PARAFAC. Spectral fluorescence overlapping between fluorophores with low excitation wavelength such as PAH[44] and signals from proteins[45] might result in a mixture of fluorophores. Moreover, Sharma et al.[46] found a similar component to our C3 in soil organic matter and described it as a mixture of terrestrial humic-like and tryptophan fluorescence (peak-T)[29] with almost no biological production, degradation or absorption. Accordingly, C3 was positively related to the terrestrial C1 in the three MVs (Table 3S) and also with the peak-T (R^2 =

0.63, $p < 0.01$, $n = 60$) suggesting that C3 could be a mixture of fluorophores with different sources.

Continental margin sediments may be responsible for a significant fraction of DOM delivered to the marine environment[6,35,47]. The benthic fluxes of DOC were in the range of those estimated in other MVs and most continental slopes, and lower than those from estuarine sediments (Table 2). The highest estimated benthic flux of DOC was observed in PT, which could be due to the higher DOC concentrations observed (Table 1). We can conclude that cold seep from MVs acts as a source of DOC to the deep waters, probably minimal compared to other oceanic sources (e.g. 250×10^6 tons y^{-1} from rivers).

Although no information of diffusive benthic flux of CDOM and FDOM from MVs was found, our data was compared with those from marine sediments and hydrothermal vents. Benthic flux of CDOM (as a_{254} and a_{350}) showed higher values than those reported for marine sediments, whereas the fluxes from the humic-like components were in the same range (Table 2). Among the fluorescent components, protein-like estimated benthic fluxes from AN were one order of magnitude higher than those in PI and PT and also in marine sediments. Our results suggest that the MVs could act as a source of CDOM and FDOM to the deep waters of the Gulf of Cádiz. Noteworthy, benthic fluxes from a reference site without mud volcanoes in this zone will improve our findings.

IV. 5. Conclusions

Cold seeps from MVs and biological activity via anaerobic sulfate-reducing bacteria represent a source of DOC, CDOM, and FDOM to the deep waters of the Gulf of Cádiz, providing energy and resources to the deep heterotrophic microbial communities. However, further studies are needed

to better understand the role of mud volcanoes in DOM cycling in the deep water of the Gulf of Cádiz (e.g. stable isotopes, FT-ICR-MS, amino acid analysis).

References

1. Hansell, D. A., Carlson, C. A. ., Repeta, D. J. . R. & Schlitzer, R. Dissolved Organic Matter in the Ocean. *Oceanography* **22**, (2009).
2. Nelson, N. B. & Siegel, D. A. The Global Distribution and Dynamics of Chromophoric Dissolved Organic Matter. *Ann. Rev. Mar. Sci.* **5**, 447–476 (2013).
3. Coble, P. G., Lead, J., Baker, A., Reynolds, D. M. & Spencer, R. G. M. *Aquatic Organic Matter Fluorescence*. (2014).
4. Burdige, D. J. & Komada, T. *Sediment Pore Waters*. *Biogeochemistry of Marine Dissolved Organic Matter: Second Edition* (Elsevier Inc., 2015). doi:10.1016/B978-0-12-405940-5.00012-1
5. Raymond, P. A. & Spencer, R. G. M. Riverine DOM. *Biogeochem. Mar. Dissolved Org. Matter Second Ed.* 509–533 (2015). doi:10.1016/B978-0-12-405940-5.00011-X
6. Stedmon, C. A. & Nelson, N. B. The Optical Properties of DOM in the Ocean. *Biogeochem. Mar. Dissolved Org. Matter Second Ed.* 481–508 (2015). doi:10.1016/B978-0-12-405940-5.00010-8
7. Dittmar, T. & Koch, B. P. Thermogenic organic matter dissolved in the abyssal ocean. *Mar. Chem.* **102**, 208–217 (2006).
8. Pohlman, J. W., Bauer, J. E., Waite, W. F., Osburn, C. L. & Chapman, N. R. Methane hydrate-bearing seeps as a source of aged dissolved organic carbon to the oceans. *Nat. Geosci.* **4**, 37–41 (2011).
9. Yang, L. *et al.* Absorption and fluorescence of dissolved organic matter in submarine hydrothermal vents off NE Taiwan. *Mar. Chem.* **128–129**, 64–71 (2012).
10. Tryon, M., Brown, K., Dorman, L. R. & Sauter, A. A new benthic aqueous flux meter for very low to moderate discharge rates. *Deep. Res. Part I Oceanogr. Res. Pap.* **48**, 2121–2146 (2001).
11. Lang, S. Q., Butterfield, D. A., Lilley, M. D., Paul Johnson, H. & Hedges, J. I. Dissolved organic carbon in ridge-axis and ridge-flank hydrothermal systems. *Geochim. Cosmochim. Acta* **70**, 3830–3842 (2006).
12. Hawkes, J. A. *et al.* Efficient removal of recalcitrant deep-ocean dissolved organic matter during hydrothermal circulation. *Nat. Geosci.* **8**, 856–860 (2015).
13. Ceramicola, S., Dupré, S., Somoza, L. & Woodside, J. *Cold seep systems*. *Submarine Geomorphology* (2018). doi:10.1007/978-3-319-57852-1
14. Milkov, A. V. Worldwide distribution of submarine mud volcanoes and associated gas hydrates. *Mar. Geol.* **167**, 29–42 (2000).
15. Dimitrov, L. I. Mud volcanoes - A significant source of atmospheric methane. *Geo-Marine Lett.* **23**, 155–161 (2003).
16. Vanneste, H. *et al.* Spatial variation in fluid flow and geochemical fluxes across the sediment-seawater interface at the Carlos Ribeiro mud volcano (Gulf of Cadiz). *Geochim. Cosmochim. Acta* **75**, 1124–1144 (2011).

17. Palomino, D. *et al.* Multidisciplinary study of mud volcanoes and diapirs and their relationship to seepages and bottom currents in the Gulf of Cádiz continental slope (northeastern sector). *Mar. Geol.* **378**, 196–212 (2016).
18. Mazzini, A. & Etiope, G. Mud volcanism: An updated review. *Earth-Science Rev.* **168**, 81–112 (2017).
19. Hung, C. W. *et al.* Benthic fluxes of dissolved organic carbon from gas hydrate sediments in the northern South China Sea. *Sci. Rep.* **6**, 1–8 (2016).
20. Retelletti Brogi, S. *et al.* Exploring sediment porewater dissolved organic matter (DOM) in a mud volcano: Clues of a thermogenic DOM source from fluorescence spectroscopy. *Mar. Chem.* **211**, 15–24 (2019).
21. Maldonado, A., Somoza, L. & Pallarés, L. The Betic orogen and the Iberian-African boundary in the Gulf of Cadiz: Geological evolution (central North Atlantic). *Mar. Geol.* **155**, 9–43 (1999).
22. Mazurenko, L. L., Soloviev, V. A., Belenkaya, I., Ivanov, M. K. & Pinheiro, L. M. Mud volcano gas hydrates in the Gulf of Cadiz. *Terra Nov.* **14**, 321–329 (2002).
23. Pinheiro, L. M. *et al.* Mud volcanism in the Gulf of Cadiz: Results from the TTR-10 cruise. *Mar. Geol.* **195**, 131–151 (2003).
24. Rueda, J. L. *et al.* New records of recently described chemosymbiotic bivalves for mud volcanoes within the European waters (Gulf of Cádiz). *Mediterr. Mar. Sci.* **13**, 262–267 (2012).
25. Sánchez-Guillamón, O. Deep Submarine volcanoes in two geodynamic settings (Canary Basin and Gulf of Cádiz): Morphology and shallow structure. (2019).
26. Murphy, K. R., Stedmon, C. A., Wenig, P. & Bro, R. OpenFluor- An online spectral library of auto-fluorescence by organic compounds in the environment. *Anal. Methods* **6**, 658–661 (2014).
27. Amaral, V., Romera-Castillo, C. & Forja, J. Dissolved Organic Matter in the Gulf of Cádiz: Distribution and Drivers of Chromophoric and Fluorescent Properties. *Front. Mar. Sci.* **7**, 1–15 (2020).
28. Lorenzo-Seva, U. & ten Berge, J. M. F. Tucker's congruence coefficient as a meaningful index of factor similarity. *Methodology* **2**, 57–64 (2006).
29. Coble, P. Characterization of marine and terrestrial DOM in seawater using excitation-emission matrix spectroscopy. *Mar. Chem.* **51**, 325–346 (1996).
30. Luek, J. L., Thompson, K. E., Larsen, R. K., Heyes, A. & Gonsior, M. Sulfate Reduction in Sediments Produces High Levels of Chromophoric Dissolved Organic Matter. *Sci. Rep.* **7**, (2017).
31. Sierra, A. *et al.* Methane dynamics in the coastal – Continental shelf transition zone of the Gulf of Cadiz. *Estuar. Coast. Shelf Sci.* **236**, (2020).
32. Díaz del Río, V. *et al.* Volcanes de Fango del Golfo de Cádiz. 132 (2014).
33. Sommer, S. *et al.* Seabed methane emissions and the habitat of frenulate tubeworms on the Captain Arutyunov mud volcano (Gulf of Cadiz). *Mar. Ecol. Prog. Ser.* **382**, 69–86 (2009).
34. Malcolm, S. J., Battersby, N. S., Stanley, S. O. & Brown, C. M. Organic degradation, sulphate reduction and ammonia production in the sediments of Loch Eil, Scotland. *Estuar. Coast. Shelf Sci.* **23**, 689–704 (1986).
35. Burdige, D. J., Kline, S. W. & Chen, W. Fluorescent dissolved organic matter in marine sediment pore waters. *Mar. Chem.* **89**, 289–311 (2004).
36. Chen, M. *et al.* Production of fluorescent dissolved organic matter in Arctic Ocean sediments. *Sci. Rep.* **6**, 1–10 (2016).
37. Chen, M., Kim, J. H., Choi, J., Lee, Y. K. & Hur, J. Biological early diagenesis and

insolation-paced paleoproductivity signified in deep core sediment organic matter. *Sci. Rep.* **7**, 1–11 (2017).
38. Rueda, J. L. *et al.* From chemosynthesis-based communities to cold-water corals: Vulnerable deep-sea habitats of the Gulf of Cádiz. *Mar. Biodivers.* **46**, 473–482 (2016).
39. Valentine, D. L. *et al.* Biogeochemical investigations of marine methane seeps, Hydrate Ridge, Oregon. *J. Geophys. Res. Biogeosciences* **110**, n/a-n/a (2005).
40. Huguet, A. *et al.* Properties of fluorescent dissolved organic matter in the Gironde Estuary. *Org. Geochem.* **40**, 706–719 (2009).
41. Krom, M. D. & Sholkovitz, E. R. Nature and reactions of dissolved organic matter in the interstitial waters of marine sediments. *Geochim. Cosmochim. Acta* **41**, 1565–1574 (1977).
42. Liu, Z. & Lee, C. The role of organic matter in the sorption capacity of marine sediments. *Mar. Chem.* **105**, 240–257 (2007).
43. Murphy, K. R. *et al.* Photochemistry Illuminates Ubiquitous Organic Matter Fluorescence Spectra. *Environ. Sci. Technol.* **52**, 11243–11250 (2018).
44. Ferretto, N. *et al.* Identification and quantification of known polycyclic aromatic hydrocarbons and pesticides in complex mixtures using fluorescence excitation-emission matrices and parallel factor analysis. *Chemosphere* **107**, 344–353 (2014).
45. Mayer, L. M., Schick, L. L. & Loder, T. C. Dissolved protein fluorescence in two maine estuaries. *Mar. Chem.* **64**, 171–179 (1999).
46. Sharma, P. *et al.* Green manure as part of organic management cycle: Effects on changes in organic matter characteristics across the soil profile. *Geoderma* **305**, 197–207 (2017).
47. Burdige, D. J., Berelson, W. M., Coale, K. H., McManus, J. & Johnson, K. S. Fluxes of dissolved organic carbon from California continental margin sediments. *Geochim. Cosmochim. Acta* **63**, 1507–1515 (1999).
48. Somoza, L. *et al.* Seabed morphology and hydrocarbon seepage in the Gulf of Cádiz mud volcano area: Acoustic imagery, multibeam and ultra-high resolution seismic data. *Mar. Geol.* **195**, 153–176 (2003).
49. Kenyon, N. H. . et al. Multidisciplinary Study of Geological Processes on the North East Atlantic and Western Mediterranean Margins. *Intergov. Oceanogr. Comm. Tech. Ser. - UNESCO* **56**, 136 (2000).
50. Nayar, S. & Chou, L. M. Relative efficiencies of different filters in retaining phytoplankton for pigment and productivity studies. *Estuar. Coast. Shelf Sci.* **58**, 241–248 (2003).
51. Akkanen, J., Lyytikäinen, M., Tuikka, A. & Kukkonen, J. V. K. Dissolved organic matter in pore water of freshwater sediments: Effects of separation procedure on quantity, quality and functionality. *Chemosphere* **60**, 1608–1615 (2005).
52. Chen, M., Lee, J. H. & Hur, J. Effects of sampling methods on the quantity and quality of dissolved organic matter in sediment pore waters as revealed by absorption and fluorescence spectroscopy. *Environ. Sci. Pollut. Res.* **22**, 14841–14851 (2015).
53. Blough, N. V. & Del Vecchio, R. Chromophoric DOM in the Coastal Environment. *Biogeochem. Mar. Dissolved Org. Matter* 509–546 (2002). doi:10.1016/b978-012323841-2/50012-9
54. Helms, J. R. *et al.* Absorption spectral slopes and slope ratios as indicators of molecular weight, source, and photobleaching of chromophoric dissolved organic matter. *Limnol. Oceanogr.* **53**, 955–969 (2008).

55. Murphy, K. R., Stedmon, C. A., Graeber, D. & Bro, R. Fluorescence spectroscopy and multi-way techniques. PARAFAC. *Anal. Methods* **5**, 6557–6566 (2013).
56. Komada, T. *et al.* Dissolved organic carbon dynamics in anaerobic sediments of the Santa Monica Basin. *Geochim. Cosmochim. Acta* **110**, 253–273 (2013).
57. R Core Team (2020). R: A language and environment for statistical computing. R Foundation for Statistical Computing, Vienna, Austria. URL https://www.R-project.org/.

Acknowledgements

This work was funded by the Spanish CICYT (Spanish Program for Science Technology) under the contract CTM2014-59244- C3-1-R and RTI2018-100865-B-C21. VA was financed by the National Research and Innovation Agency of Uruguay (ANII) with a Ph.D. fellowship (POS_EXT_2015_1_122780). CR-C was funded by a Postdoctoral Fellowship from the Spanish "Ministerio de Economía y Competitividad, Juan de la Cierva-Incorporación". The authors would like to thanks the crews of the R/V's Angeles Alvariño and Ramón Margalef for their assistance during fieldwork. Teodora Ortega and Dolores Jiménez-López for their assistance in field sampling and processing. We acknowledge the help of Jose Sanabria with Figure 1. Gastón Pereyra performed the final language revision.

Supplementary Material

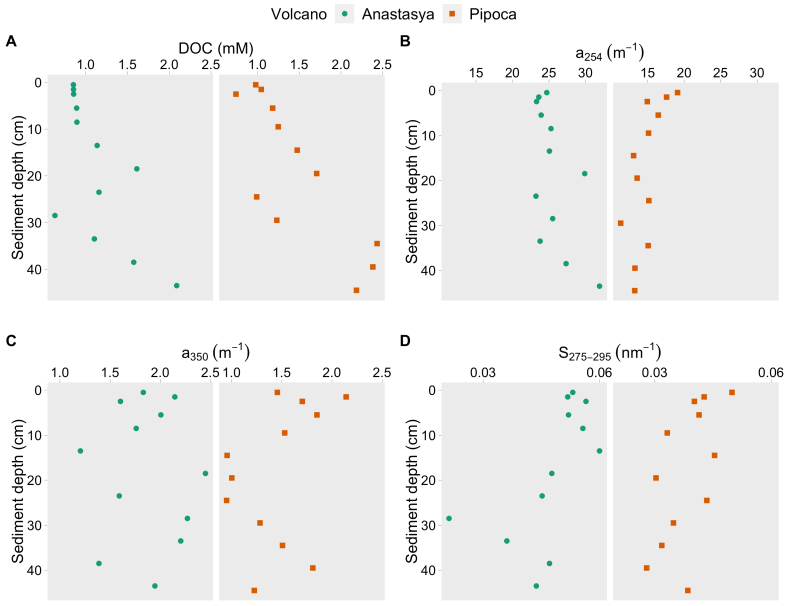

Fig. S1. Pore water profiles of dissolved organic carbon (DOC), absorption coefficients (a_{254} and a_{350}) and the spectral slope ($S_{275-295}$) in Anastasya and Pipoca during December 2016.

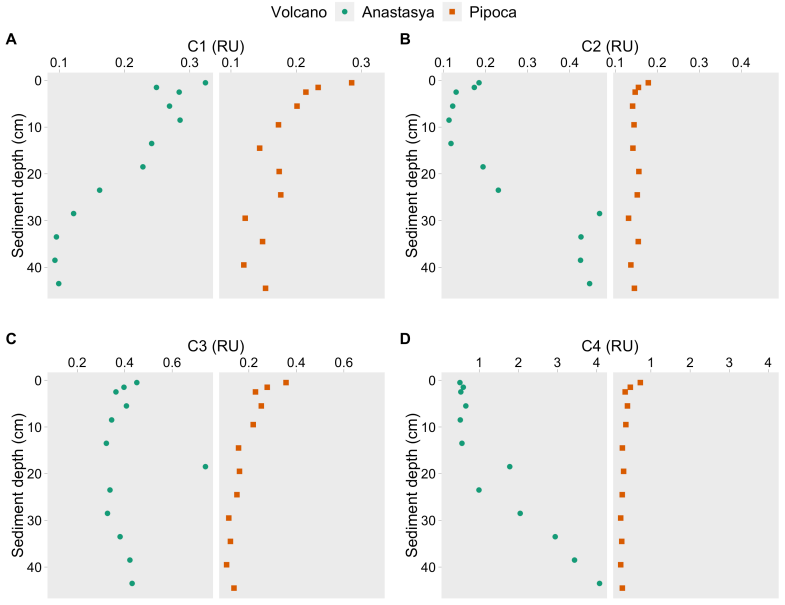

Fig. S2. Pore water profiles of the four fluorescent components (C1 to C4) in Anastasya and Pipoca during December 2016.

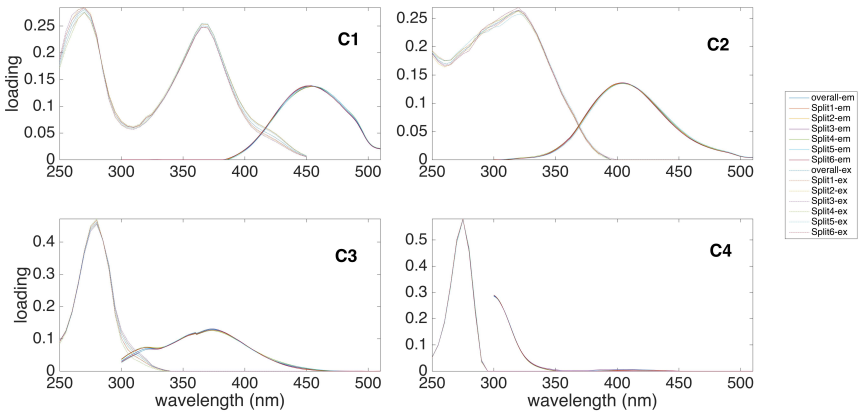

Fig. S3. Split-half validation of the four PARAFAC components validated in the pore water model.

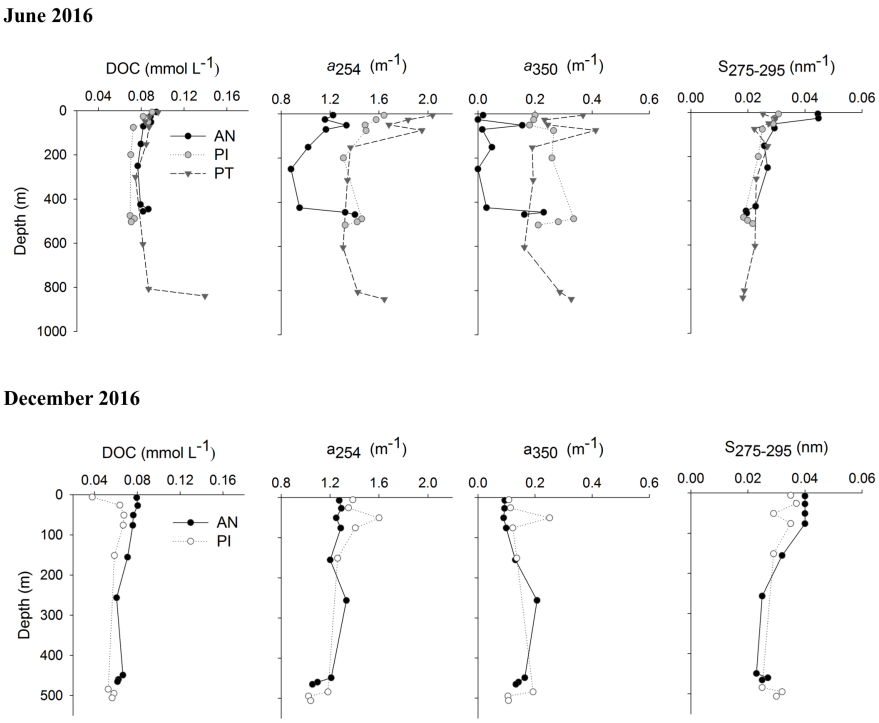

Fig. S4. Seawater vertical profiles of dissolved organic carbon (DOC), absorption coefficients (a_{254} and a_{350}) and the spectral slope ($S_{275\text{-}295}$) above AN: Anastasya, PI: Pipoca and PT: St. Petersburg during June and December 2016.

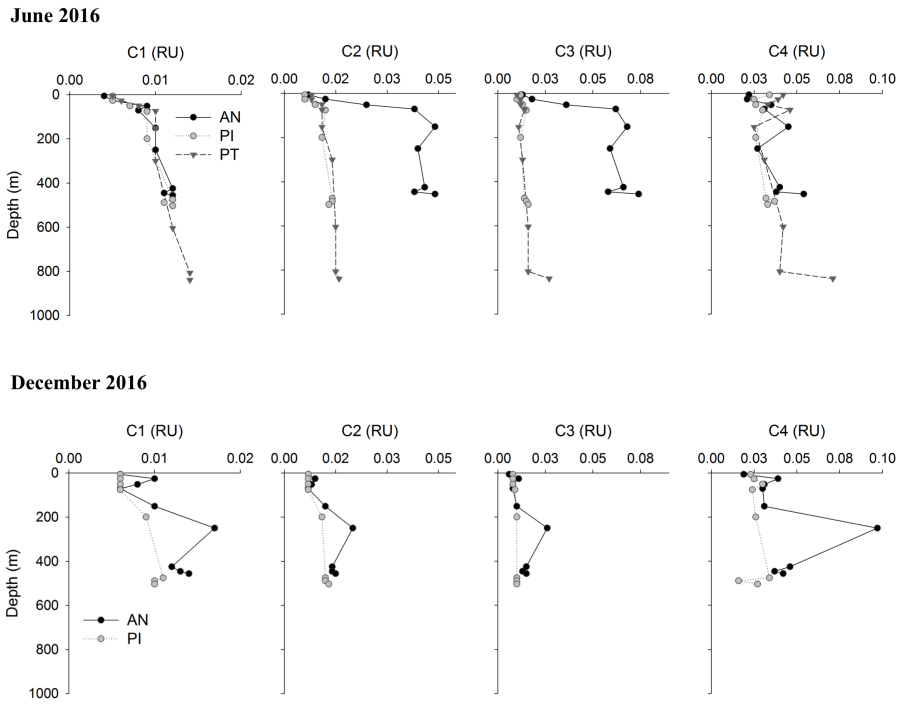

Fig. S5. Seawater vertical profiles of fluorescent components (C1 to C4) above AN: Anastasya, PI: Pipoca and PT: St. Petersburg during June and December 2016.

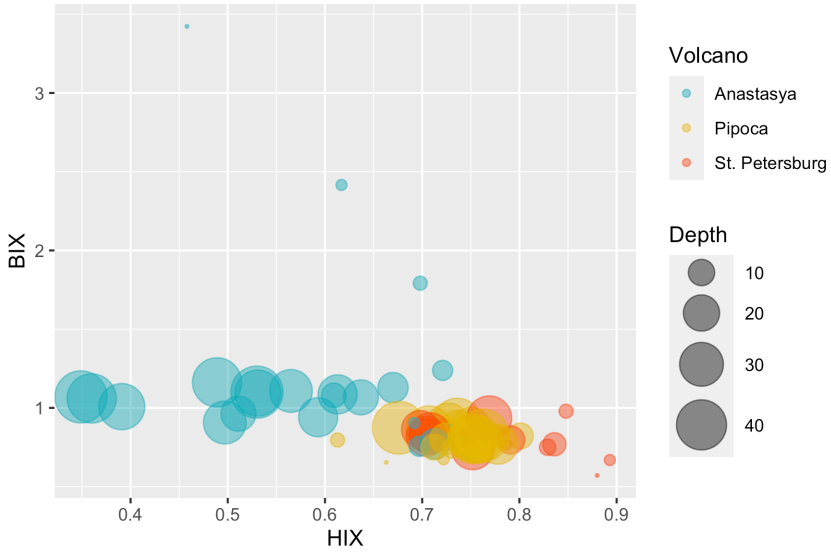

Fig. S6. Biplot of HIX versus BIX for each mud volcano during the study period. Size of circles represents depth.

Table S1. Location and morphological parameters of the three mud volcanoes in the study area. Data from Palomino et al.[1] 2016 and Sánchez-Guillamón,[2] 2019.

Name	Coordinates	Max/min depth (m)	Height (m)	Area (km^2)	Cone shape
Anastasya	7.15 ºW, 36.52 ºN	555/457	98	3.26	symmetric
Pipoca	7.20 ºW, 36.46 ºN	762/503	115	4.54	asymmetric
San Petersburg	7.03 ºW,35.89 ºN	935/1000	110	2.98	asymmetric

Table S2. Excitation (Ex.) and Emission (Em.) maxima of the four PARAFAC components in the pore water model (n = 58). Matching with Openfluor database with a TCC > 0.97 are shown (* TCC = 0.95).

	Ex/Em	Openfluor matching	Description	Zone
C1	270	C3, Chen et al.[3] 2016	Terrestrial, humic	Arctic sediments
	(365)/454	C3, Cawley et al.[4] 2012	Humic-like	Shark Bay
		C3, Graeber et al.[5] 2012	Humic-like	Agricultural
		C3, Osburn & Stedmon[6] 2011	Terrestrial, humic	Baltic Sea
		C3, Murphy et al.[7] 2013	-	-
		C3, Amaral et al. 2020[8]	Terrestrial, humic	Gulf of Cádiz
C2	320/405	C1, Amaral et al. 2020[8]	Ubiquitous humic-like	Gulf of Cádiz
		C2, Schittich et al. 2018[9]	Humic-like	Groundwater
		C2, Catalá et al.[10] 2015	Marine	Global ocean
		C3, Kowalczuk et al. [11]2009	Marine/microbial	Atlantic Bight
		C6, Stedmon et al.[12] 2011	Marine	Antarctic sea ice
		C2, Kothawala et al.[13] 2012	Marine	Lakes, incubations
		C2 Kulkarni et al.[14] 2016	Terrestrial	Groundwater
		C1, Wünsch et al.[15] 2018	-	Arctic Fjords

		C2, Asmala et al.[16] 2018	-	Coastal zone
		C2, Hambly et al.[17] 2015	Ubiquitous	Aquaculture
		C2, Chen et al.[18] 2018	Marine	Arctic waters
		C2, Chen et al.[3] 2016	Microbial/Marine	Arctic pore water
		C2, Osburn et al.[19] 2016	Microbial humic-like	Estuarine and Coastal
		C6, Yamashita et al.[20] 2010	Ubiquitous humic-like	Subtropical wetlands
		C2, Dalmagro et al.[21] 2019	Ubiquitous humic-like	Streams riparian forest
		C4, Podgorski et al.[22] 2019	Microbial/Marine	Groundwater oil derived
C3	280/375	C3, Sharma et al.[23] 2017	Complex nature	Soil organic matter
		C5, Amaral et al.[8] 2020*	PAH-protein like	Gulf of Cádiz
C4	275/303	C1, Murphy et al. [24]2006	Tyrosine	Ocean
		C4 Kowalczuk et al.[25] 2013	Tyrosine	Coastal
		C5, Osburn et al. 2016[19]	Tyrosine	Coastal
		C6, Amaral et al.[8] 2020*	Tyrosine	Gulf of Cádiz

Table S3. Linear relationships between FDOM components and with DOM variables in the three MVs (AN: Anastasya, PI: Pipoca, n = 24 and PT: St. Petersburg, n = 12). The coefficient of determination R^2 is indicated when $p < 0.01$ and ns is $p > 0.01$. A negative R^2 is indicative of an inverse relationship between variables.

	AN	PI	PT
C1-C2	-0.71	0.71	0.60
C1-C3	ns	0.95	0.65
C1-C4	-0.53	0.82	0.62
C2-C4	ns	0.53	0.56
C2-C3	ns	0.52	0.50
C3-C4	ns	0.92	0.96
a_{254}-C1	0.31	0.81	0.35
a_{254}-C2	ns	0.38	0.36
a_{254}-C3	0.31	0.60	0.65
a_{254}-C4	ns	0.52	0.73
$S_{275\text{-}295}$-C1	0.56	ns	ns
$S_{275\text{-}295}$-C2	-0.75	ns	ns
$S_{275\text{-}295}$-C4	-0.53	ns	ns
HIX-C1	0.59	ns	ns
HIX-C2	-0.36	ns	ns
HIX-C4	-0.94	ns	ns
BIX-C1	ns	-0.57	ns
BIX-C2	0.41	-0.37	ns
BIX-C3	ns	-0.60	ns
BIX-C4	0.33	-0.58	ns

References

1. Palomino, D. *et al.* Multidisciplinary study of mud volcanoes and diapirs and their relationship to seepages and bottom currents in the Gulf of Cádiz continental slope (northeastern sector). *Mar. Geol.* **378**, 196–212 (2016).
2. Sánchez-Guillamón, O. Deep Submarine volcanoes in two geodynamic settings (Canary Basin and Gulf of Cádiz): Morphology and shallow structure. (2019).
3. Chen, M. *et al.* Production of fluorescent dissolved organic matter in Arctic Ocean sediments. *Sci. Rep.* **6**, 1–10 (2016).
4. Cawley, K. M., Ding, Y., Fourqurean, J. W. & Jaffé, R. Characterising the sources and fate of dissolved organic matter in Shark Bay , Australia : A preliminary study using a preliminary study using optical properties and stable carbon isotopes. **63**, 1098–1107 (2012).
5. Graeber, D., Gelbrecht, J., Pusch, M. T., Anlanger, C. & von Schiller, D. Agriculture has changed the amount and composition of dissolved organic matter in Central European headwater streams. *Sci. Total Environ.* **438**, 435–446 (2012).
6. Osburn, C. L. & Stedmon, C. A. Linking the chemical and optical properties of dissolved organic matter in the Baltic-North Sea transition zone to differentiate three allochthonous inputs. *Mar. Chem.* **126**, 281–294 (2011).
7. Murphy, K. R., Stedmon, C. A., Graeber, D. & Bro, R. Fluorescence spectroscopy and multi-way techniques. PARAFAC. *Anal. Methods* **5**, 6557–6566 (2013).
8. Amaral, V., Romera-Castillo, C. & Forja, J. Dissolved Organic Matter in the Gulf of Cádiz: Distribution and Drivers of Chromophoric and Fluorescent Properties. *Front. Mar. Sci.* **7**, 1–15 (2020).
9. Schittich, A. R. *et al.* Investigating Fluorescent Organic-Matter Composition as a Key Predictor for Arsenic Mobility in Groundwater Aquifers. *Environ. Sci. Technol.* **52**, 13027–13036 (2018).
10. Catalá, T. S. *et al.* Turnover time of fluorescent dissolved organic matter in the dark global ocean. *Nat. Commun.* **6**, (2015).
11. Kowalczuk, P. *et al.* Characterization of dissolved organic matter fluorescence in the South Atlantic Bight with use of PARAFAC model: Interannual variability. *Mar. Chem.* **113**, 182–196 (2009).
12. Stedmon, C. A., Thomas, D. N., Papadimitriou, S., Granskog, M. A. & Dieckmann, G. S. Using fluorescence to characterize dissolved organic matter in Antarctic sea ice brines. *J. Geophys. Res. Biogeosciences* **116**, 1–9 (2011).
13. Kothawala, D. N., von Wachenfeldt, E., Koehler, B. & Tranvik, L. J. Selective loss and preservation of lake water dissolved organic matter fluorescence during long-term dark incubations. *Sci. Total Environ.* **433**, 238–246 (2012).
14. Kulkarni, H. V., Mladenov, N., Johannesson, K. H. & Datta, S. Contrasting dissolved organic matter quality in groundwater in Holocene and Pleistocene aquifers and implications for influencing arsenic mobility.

Appl. Geochemistry **77**, 194–205 (2017).
15. Wünsch, U. J. *et al.* Quantifying the impact of solid-phase extraction on chromophoric dissolved organic matter composition. *Mar. Chem.* **207**, 33–41 (2018).
16. Asmala, E. *et al.* Eutrophication Leads to Accumulation of Recalcitrant Autochthonous Organic Matter in Coastal Environment. *Global Biogeochem. Cycles* **32**, 1673–1687 (2018).
17. Hambly, A. C. *et al.* Characterising organic matter in recirculating aquaculture systems with fluorescence EEM spectroscopy. *Water Res.* **83**, 112–120 (2015).
18. Chen, M., Jung, J., Lee, Y. K. & Hur, J. Surface accumulation of low molecular weight dissolved organic matter in surface waters and horizontal off-shelf spreading of nutrients and humic-like fluorescence in the Chukchi Sea of the Arctic Ocean. *Sci. Total Environ.* **639**, 624–632 (2018).
19. Osburn, C. L. *et al.* Optical proxies for terrestrial dissolved organic matter in estuaries and coastal waters. *Front. Mar. Sci.* **2**, (2016).
20. Yamashita, Y., Scinto, L. J., Maie, N. & Jaffé, R. Dissolved Organic Matter Characteristics Across a Subtropical Wetland's Landscape: Application of Optical Properties in the Assessment of Environmental Dynamics. *Ecosystems* **13**, 1006–1019 (2010).
21. Dalmagro, H. J. *et al.* Streams with riparian forest buffers versus impoundments differ in discharge and DOM characteristics for pasture catchments in Southern Amazonia. *Water (Switzerland)* **11**, 1–20 (2019).
22. Podgorski, D. C. *et al.* Examining Natural Attenuation and Acute Toxicity of Petroleum-Derived Dissolved Organic Matter with Optical Spectroscopy. *Environ. Sci. Technol.* **52**, 6157–6166 (2018).
23. Sharma, P. *et al.* Green manure as part of organic management cycle: Effects on changes in organic matter characteristics across the soil profile. *Geoderma* **305**, 197–207 (2017).
24. Murphy, K. R., Ruiz, G. M., Dunsmuir, W. T. M. & Waite, T. D. Optimized parameters for fluorescence-based verification of ballast water exchange by ships. *Environ. Sci. Technol.* **40**, 2357–2362 (2006).
25. Kowalczuk, P., Tilstone, G. H., Zabłocka, M., Röttgers, R. & Thomas, R. Composition of dissolved organic matter along an Atlantic Meridional Transect from fluorescence spectroscopy and Parallel Factor Analysis. *Mar. Chem.* **157**, 170–184 (2013).
26. Sierra, A. *et al.* Methane dynamics in the coastal – Continental shelf transition zone of the Gulf of Cadiz. *Estuar. Coast. Shelf Sci.* **236**, (2020).

Capítulo 3

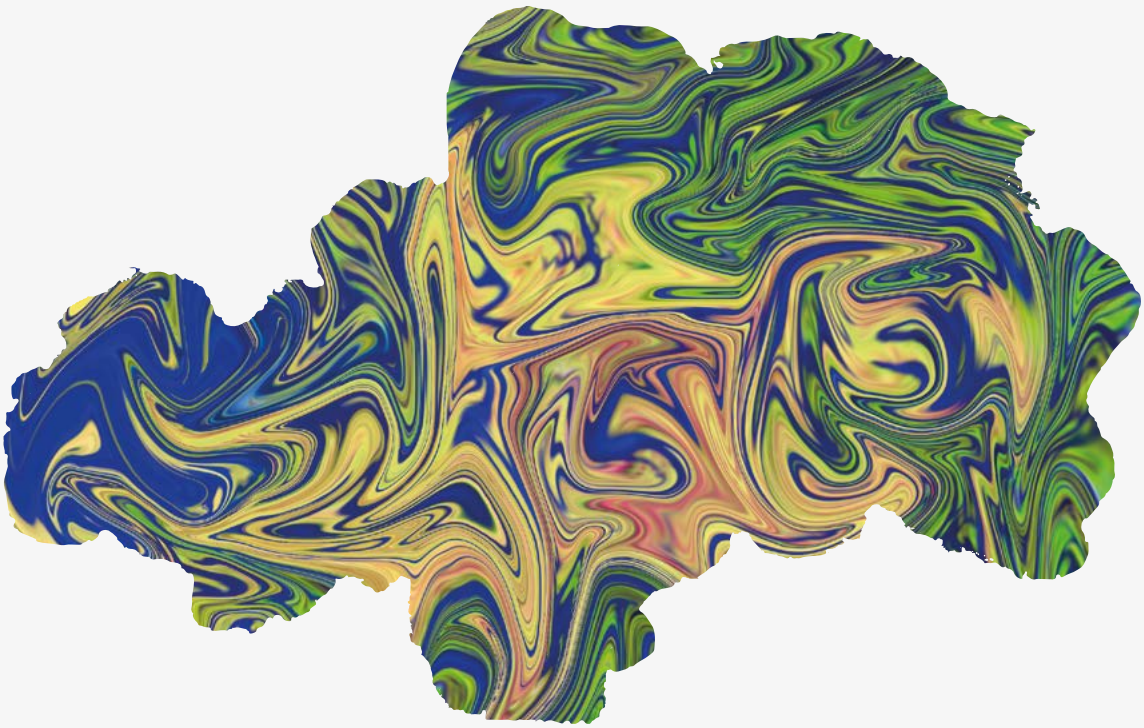

"Thousands have lived without love, not one without water".
'First Things First', 1957.

Distribution of dissolved organic matter in estuaries of the Southern Iberian Atlantic Basin: sources, behavior and export to the coastal zone*

Amaral, V.[1,2*], Romera-Castillo, C.[3], García-Delgado, M.[1], Gómez-Parra, A.[1], Forja, J.[1]

[1]Departamento de Química-Física, INMAR, Universidad de Cádiz, Puerto Real, España.
[2]Ecología Funcional de Sistemas Acuáticos, Centro Universitario Regional Este, Universidad de la República, Rocha, Uruguay.
[3]Instituto de Ciencias del Mar-CSIC, Barcelona, España.

Publicado en *Marine Chemistry

Abstract

The Gulf of Cádiz, located in the Southern Iberian Atlantic Basin, connects the North Atlantic Ocean and the Mediterranean Sea and receives freshwater input from three main estuaries: Guadalquivir, Guadiana, and Tinto-Odiel. These estuaries differ in their hydrology, basin characteristic, and land use. One of them, Tinto-Odiel, is one of the most polluted estuaries in the world. However, little is known about the export of DOM from these estuaries to the Gulf of Cádiz. In this work, the estuaries were sampled during the dry season. Dissolved organic matter (DOM) was chemically characterized along a longitudinal gradient to better understand the reactivity and fate of carbon exported to the Gulf of Cádiz. We also performed a tidal study at the mouth of each estuary to understand how the tide affects the composition of DOM and its export to the coastal zone. Fluorescent DOM (FDOM) modeling employing multivariate parallel factor analysis and analytical pyrolysis were used to characterize DOM. DOM from Guadalquivir and Guadiana estuaries presented a predominant allochthonous origin with humic-like compounds making up to ~80 % of the total fluorescent DOM. These estuaries receive lateral inputs from surrounding watersheds and agricultural practices. Instead, in Tinto-Odiel estuary, DOM was predominantly autochthonous with a higher content of protein-like material associated with the prevalence of the marine influence over the low water discharges and anthropogenic pollution from industrial activities. Tidal cycles affected the distribution of DOM and its quality with higher humic-like material during low tide and protein-like substances predominating during high tide. During the dry season, the three estuaries represented a source of DOM to the Gulf of Cádiz. Guadalquivir was the main contributor with 1.25 Kg C s^{-1} and 0.22 x 10^3 m^2 s^{-1}, for DOC and

CDOM, respectively. Around 70 % of the FDOM exported from the three estuaries was of humic nature. The results obtained in this work highlight the importance of local conditions, such as the basin characteristic and estuarine biogeochemical reactivity in the composition of the DOM exported to the coastal ocean. Moreover, Py-GC–MS analysis was a useful technique, complementary to fluorescence spectroscopy, which improves DOM characterization in estuarine systems.

IV. 1. Introduction

The input of dissolved organic matter (DOM) by rivers to the oceans occurs primarily via estuaries, being a significant fraction in the global carbon budget (Raymond and Spencer, 2015). Annually, rivers transport ~ 0.25 Gt of dissolved organic carbon (DOC) from continents to the ocean (Hedges et al., 1997), yet the processes which control its distribution and fate are not completely understood (Bauer and Bianchi, 2012). Riverine DOM is considered to be recalcitrant and conservatively transported to the ocean; that is, an inverse linear relationship with salinity is often observed. However, the biogeochemical complexity of estuaries, which comprises both allochthonous and autochthonous sources of DOM (Cauwet, 2002), can contribute to a non-conservative behavior. Diverse factors (physical, chemical, biological), such as anthropogenic pollution, land use, and microbial metabolism, as well as the presence of wetlands and salt marshes, can significantly alter the composition, reactivity and optical properties of DOM before it reaches the coastal zone (e.g., Benner and Opsahl, 2001, Abril et al., 2002, Jaffé et al., 2004). These factors regulate the net efflux of DOM from land to the global ocean. Therefore, it is important to better understand the composition and biogeochemical reactivity of DOM in these land-ocean transitional systems.

The colored fraction of DOM (CDOM), and the sub-fraction that emits light as fluorescent radiation, named fluorescent DOM (FDOM), have been widely used to assess the sources and behavior of different fractions of DOM in estuaries (e.g., Rochelle-Newall and Fisher, 2002, Jaffé et al., 2004, Guo et al., 2007). FDOM can be divided into two major groups, humic-like and protein-like components, which presence and relative intensities vary according to the type, origin, and concentration of DOM (Coble, 1996). River discharge is generally the main source of humic-like components into coastal waters, whereas protein-like FDOM is associated with amino acids occurring in proteins (tryptophan, tyrosine, and phenylalanine, Determann et al., 1998) associated with biological production (Coble et al., 2014). Additionally, protein-like signals have also been interpreted as an indication of anthropogenic DOM (Hong et al., 2005). Furthermore, many other natural and anthropogenic aromatic compounds exhibit fluorescence in the protein region (Maie et al., 2007, Hammas et al., 2013). The use of excitation-emission matrixes (EEMs) coupled with the multivariate statistical method, parallel factor analysis (PARAFAC), allows for the differentiation of a wider range of underlying FDOM components (Stedmon and Bro, 2008).

Although in estuarine systems the supply of terrestrial CDOM often dominates (Stedmon and Nelson, 2015), autochthonous sources and anthropogenic inputs from the watershed (industrial or agriculture) have also been shown to be important contributors to estuarine CDOM pools (e.g., Hong et al., 2005, Coble, 2007). Furthermore, microbial transformation (Moran et al., 2000) and photochemical removal of DOM (Vodacek et al., 1997) play an important role in altering the physicochemical characteristics of these materials. Thereby, estuaries discharging into the same coastal region may contribute with different quantity and quality of DOM (Coble,

1996).

The Gulf of Cádiz, located in the southern Iberian Atlantic Basin, is the only connection between the North Atlantic Ocean and the Mediterranean Sea, and receives freshwater input from three main estuaries: Guadalquivir, Guadiana, and Tinto-Odiel. These estuaries differ in terms of their morphology and hydrology, as well as their basin vegetation and land use. Guadalquivir estuary has been identified as a net source of DOC to the adjacent coast (Ribas-Ribas et al., 2011). However, the origin of this DOC is barely known. González-Ortegón et al., (2018) suggest that these three rivers discharge large amounts of humic-like FDOM to the Gulf of Cádiz, mainly through Guadalquivir and Guadiana rivers and much less through Tinto-Odiel. However, their work was performed in the coastal zone with only one station sampled at the mouth of each estuary using an EXO FDOM sensor limited to humic substances from terrestrial sources. On the other hand, a recent study found that protein-like was the most abundant fraction of FDOM in the coastal-ocean zone of the Gulf of Cádiz. The distribution of both DOC and protein-like FDOM was related to biological activity. In contrast, the distribution of humic-like FDOM was mainly explained by water mass mixing (Amaral et al., 2020). To the best of our knowledge, there is no information about the dynamic of DOM in these three estuaries, as well as the quality and quantity of the DOM that they export to the Gulf of Cádiz. Furthermore, it is largely unknown how the basin characteristics of these rivers influence the export of DOM and whether the processes occurring during its transport change the chemical composition and biogeochemical reactivity of DOM in the estuaries.

The objective of this study was to determine the composition and behavior of DOM in Guadalquivir, Guadiana, and Tinto – Odiel estuaries.

This study presents the concentration of DOC and the optical characteristics of DOM for longitudinal salinity transects and a tidal cycle study in each system. It also estimated the fluxes of DOC, CDOM, and different fractions of FDOM from these estuaries to the Gulf of Cádiz. We applied spectroscopic techniques coupled with PARAFAC (Murphy et al., 2013) and pyrolysis-gas chromatography-mass spectroscopy analysis (Py-GC-MS, Kaal, 2019) to assess DOM composition. Despite the quantitative limitations of Py-GC–MS since only estimations of relative proportions of pyrolysis products can be obtained, it has been proved to provide valuable information about DOM sources (Kaal, 2019). Additionally, few studies have applied this technique to assist in the interpretation of fluorescence spectroscopy characterization (Jiang et al., 2017).

We hypothesized that the different river basin characteristics, freshwater discharge, tidal cycles, and each basin singularities might lead to different DOM composition and behavior between estuaries.

IV. 2. Methods and Materials

IV. 2.1. Study Area

The study was carried out in three estuaries located on the Southwest coast of the Iberian Peninsula: Guadalquivir, Guadiana, and Tinto-Odiel (Fig. 1). These rivers basins are located within the Mediterranean-climate region, a semiarid environment, and regulated by dams.

The three estuaries are affected by a tidal cycle showing a semidiurnal period and a mesotidal regime with a maximum range of ~3.3 m (spring tides) and an average of 2 m (Carro et al., 2019; Morales and Garel, 2019; Rodríguez-Ramírez et al., 2019). Guadalquivir and Guadiana rivers have similar length and dams regulate their freshwater discharge into the estuary.

Guadalquivir river discharge is the highest with an annual mean of 164 m^3 s^{-1}(Rodríguez-Ramírez et al., 2019). Although Guadiana river annual discharge is generally low (< 50 m^3 s^{-1}) (Garel and Cai, 2018), it is highly variable along the year with severe droughts and episodic flood events in the lower part of the estuary (Garel et al., 2009). The Guadalquivir river basin covers an area of 57527 Km^2. An extensive wetland area surrounds the Guadalquivir estuary and its middle zone is dominated by intertidal salt marshes (Rodríguez-Ramírez et al., 2019). However, this river is subjected to elevated anthropogenic pressure due to densely populated areas on its margins (4.2 million people), as well as the development of agriculture and aquaculture industries, and a high demand of freshwater for irrigation. Irrigated crops occupy ~ 8100 Km^2 (Carrasco et al., 2010) that used ~ 85 % of the withdrawal water from this river (www.chguadalquivir.es). Guadiana is a rock-bound estuary, which consists of a single narrow channel (50 – 700 m wide) (Morales and Garel, 2019). Although salt marshes are highly reduced due to the strong anthropogenic pressure, an extensive wetland area (~ 1000 ha) surrounds its mouth (Ménanteau et al., 2005). The Tinto-Odiel estuary extends 35 km from its mouth towards the upstream tidal limit (Carro et al., 2019). This estuary is composed by two rivers, Tinto and Odiel that converge in a common marine area called Padre Santo channel, which flows to the Gulf of Cádiz. Tinto and Odiel rivers have a short length of 100 and 140 km and a discharge of 5 m^3 s^{-1} and 14 m^3 s^{-1}, respectively. The fluvial basin of both rivers mainly lies on top of a volcano-sedimentary area. It flows through materials of the Iberian Pyrite Belt complex, which contains the largest polymetallic sulfide deposits in the world (Leblanc et al., 2000). Mining activity led to great pollution of its waters, which now contain high concentrations of heavy metals and extremely low pH values (<

3, Grande et al., 2000). Consequently, the mixing of acidic waters from mines, industrial effluents, and seawater leads to significant changes in the chemical composition of the water (Carro et al., 2019).

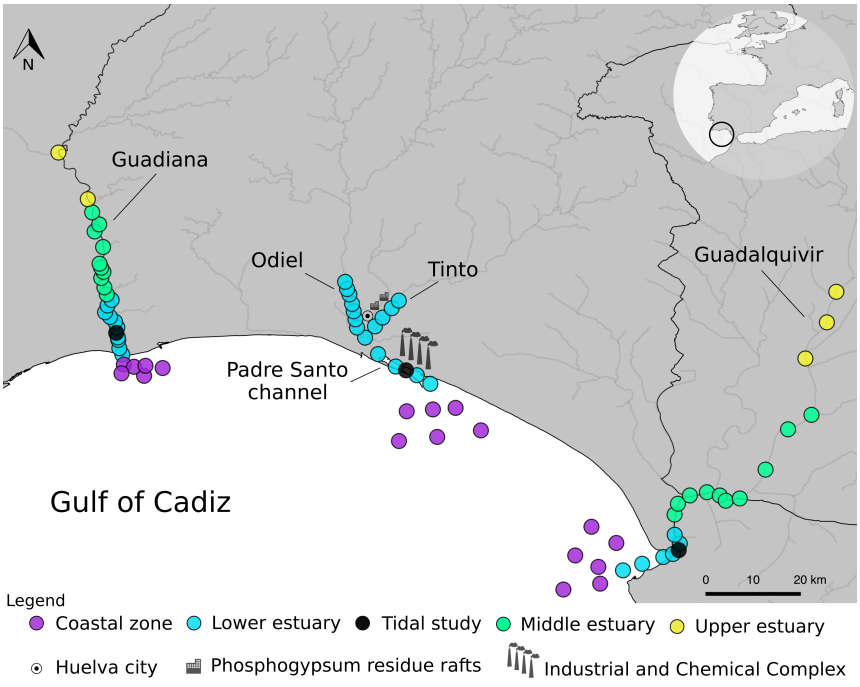

Figure 1. Map with the samples stations in the Guadalquivir, Guadiana and Tinto-Odiel transect. Tinto-Odiel estuary comprises three parts: Tinto river, Odiel river and the common marine part named Padre Santo channel.

IV. 2.2. Field Sampling

Surface water samples were collected in July 2017 onboard the R/V UCADIZ, using an auxiliary boat in the inner part of the Tinto-Odiel estuary. Since the objective of the study was to determine DOM dynamics along these estuaries and the effect of tidal cycles, two different types of sampling were carried out. A longitudinal transect along a salinity gradient including external stations in the coastal zone and a tidal study. We divided the different samples as coastal (external stations) and estuarine samples, where we differentiated three zones within each estuary: upper estuary ($S < 2$), middle estuary ($2 < S < 30$) and lower estuary ($S > 30$) (Fig. 1). Samples

for the tidal study were collected during two tidal cycles at a fixed station at the mouth of each estuary (black dots, Figure 1).

Surface water samples were taken with Niskin bottles (10 L) mounted on a rosette-sampler coupled to a CTD Seabird 25, which was able to measure temperature and salinity. During the tidal study, the water current and tidal height were measured every 5 minutes with a Nortek Aquapro Current Meter. The current velocity was measured every one meter from the bottom to the surface. Estuaries sections were calculated during low tide using small boats equipped with depth probe (Guadalquivir estuary) or nautical charts (Guadiana and Tinto-Odiel, https://www.navionics.com). In this latter case, the tidal height during low tide was corrected taking into account the tidal intensity during the days the study was conducted. Salinity and temperature in superficial water were continuously measured with a Seabird SBE - 45 thermosalinograph.

IV. 2.3. Analysis of DOC and optical properties, and estimation of dissolved lignin concentration

Following the sampling, all water samples (n = 150) were filtered through pre-combusted Whatman GF/F glass-fiber filters (450 °C, 4 h, nominal pore size 0.7 µm) using acid-cleaned glass filtration systems, previously rinsed with the sample. Although fine particles released by phytoplankton (0.2-0.7 µm) could have a significant impact in CDOM absorption in productive environments (Massicotte et al., 2017), in aquatic ecosystem influenced by terrestrial DOM, this fraction has not a significant effect on CDOM composition (Nimptsch et al., 2014, Massicotte et al., 2017). Moreover, unlike 0.2 µm polycarbonate filters, GF/F filters can be cleaned by combustion at high temperatures and it is possible to filter an adequate volume and number of samples without clogging. It should be

noted that pre-combustion might reduce the effective pore size to 0.3 µm for GF/F (Nayar and Chou, 2003). Therefore, we opted for the use of the GF/F filters.

DOC concentrations were measured using the high-temperature catalytic combustion method with a Multi N/C 3100 Analytik Jena analyzer, and potassium hydrogen phthalate was used to calibrate the system daily. Deep seawater and low carbon reference waters (Hansell CRM Program, 42-45 µM) were measured to assess instrument variability (n = 5, 43 ± 1.8 µM). UV-visible absorption spectra were obtained immediately on board, from 250 nm to 800 nm using a 1 cm path length quartz cuvette in a JASCO-V750 spectrometer connected to a programmable temperature control system set at 20 °C. The absorbance values were then converted to Napierian absorption coefficients (a_λ) in m^{-1} (Green and Blough, 1994). We focused on the absorption coefficients at 254 (a_{254}), proportional to the abundance of conjugated carbon double bonds, and 350 (a_{350}), used as a quantitative indicator of CDOM (Coble, 2007). The C-specific ultraviolet absorption coefficient at 254 nm ($SUVA_{254}$) strongly correlated with the aromaticity percentage and was calculated by dividing the decadic absorption coefficient at 254 (in m^{-1}) by the concentration of DOC (in mg L^{-1}) (Weishaar et al., 2003). Concentrations of total dissolved lignin phenol (TDLP9, nmol L^{-1}), a proxy for terrigenous and plant-derived DOM, were estimated from CDOM absorption coefficient using the equation proposed by Fichot et al. (2016). When a_{250} values were lower than 4 m^{-1}: ln (TDLP9) = 0.7672 × a_{263} – 0.3987 and when a_{250} values were higher than 4 m^{-1}: ln (TDLP9) = –2.282 × ln(a_{350}) – 8.209 × ln(a_{275}) +11.365 × ln(a_{295}) + 2.909. These equations were established with samples from a wide variety of rivers, estuaries, and coastal waters across the northern hemisphere (subtropical and temperate) and are

expected to be widely applicable in terrestrially influenced coastal systems (Fichot et al., 2016).

Excitation-emission matrixes were obtained immediately onboard using a spectrofluorometer (JASCO FP-8300) connected to a Peltier Thermostatted Cell Holder with stirrer accessory (EHC-813) for temperature control (20 °C) using a 1-cm quartz cuvette. The excitation wavelength ranged from 250 nm to 450 nm (5 nm steps) and emissions wavelength from 300 nm to 560 nm (1 nm steps), with a bandwidth of 5 nm, and the integration time was 0.2 s. The drEEM 0.2.0 toolbox was used to standardize the EEMs (Murphy et al., 2013). Spectra were improved by the instrument correction factors and the inner filter effect was addressed by correcting EEMs using the absorbance-based approach (Kothawala et al., 2013). Data was standardized and normalized to Raman Units (RU) based on measurements of Raman peak at 350 nm (Lawaetz and Stedmon, 2009). We used PARAFAC to identify the different fluorescent components that comprise the estuaries DOM and trace their distribution and changes in the systems. PARAFAC was performed using drEEMs toolbox (version 0.2.0; Murphy et al., 2013) for Matlab (R2015b).

Two indexes were further derived from the EEMs: 1) the humification index (HIX), calculated as the area under the emission spectra 435–480 nm divided by the peak area 300–345 nm + 435–480 nm, at excitation 254 nm. HIX values ranges from 0 to 1, with higher values indicating a higher degree of humification (Ohno, 2002); 2) the index of recent autochthonous contribution (BIX), calculated as the ratio of emission intensity at 380 nm divided by the emission intensity at 430 nm, obtained at excitation 310 nm (Huguet et al., 2009). BIX values > 1 correspond to freshly released DOM, while values < 0.6–0.7 correspond to a lower DOM

production in the system.

IV. 2.4. Molecular characterization

A representative sample of each estuary (black dot, Figure 1) was extracted by solid phase extraction using PPL cartridges following Dittmar et al. (2008). Briefly, 2 L of each sample were immediately filtered through pre-combusted GF/F filter, acidified to pH 2 and passed through the PPL cartridges. DOM was eluted with methanol and stored at – 20°C in glass ampoules until analysis. Py-GC-MS was performed using a Pyroprobe 5000 coupled to an Agilent 5975 MSD system. The samples were put into quartz tubes either by cutting and homogenizing solid particles that were added to quartz wool contained in quartz tubes or by sweeping liquid into quartz wool, which was then inserted into the tube. The pyrolysis was performed at 650 °C for 20 seconds (heating rate 10 °C ms^{-1}) and the GC-MS with a temperature program of 10 °C min^{-1} and operating in 1:50 split mode. The GC was equipped with an HP5-MS non-polar column and the MS was scanning in the m/z range 50-500. For additional details, refer to Kaal et al. (2017). Relative proportions were calculated for a series of products that reflect the macromolecular DOM fraction of interest, based on the peak area integration and expressed as the % of total quantified peak area.

IV. 2.5. Transport estimations

The amount of different DOM components that are exchanged with the tides at the mouth of the estuaries was estimated from simple mass balance. Applying mass balance for the evaluation of estuarine cross-sectional fluxes has been widely used by other authors (Gardner and Kjerfve, 2006; Chen et al., 2012).

The instantaneous water flow (Q_i) was calculated from the average current velocity in the water column (v_i) and the section area (A_i):

$$Q_i = A_i\, v_i = (A_0 + (h_i - h_0)\, L_0)\, v_i$$

(1)

where h_i is the depth at a given instant and A_0, h_0, L_0 are the section area, depth and length of the section in low tide, respectively. In Guadalquivir and Guadiana estuaries, the increase of the section in high tide was included due to the existence of small intertidal zones on its margins that flooded during high tides and represents < 0.5 % and 2 % of the estuary, respectively. Q_i and v_i were attributed to a positive sign for ebb conditions and negative for flood conditions.

The approach that was used assumes that the estuary is vertically homogenous and that there are no changes in concentration along the sections considered. Moreover, the tidal cycle is considered to be in steady state and only horizontal advection transport is considered. Under these conditions, river flow rates (Q_R) were calculated using the following equation:

$$\int_{t_0}^{t_F} Q_i\, dt = Q_R\, (t_F - t_0)$$

(2)

where $t_F - t_0$ includes two consecutive tidal cycles (25 h).

Net transport with tides has also been estimated using a simple mass balance:

$$Tidal\ transport = \int_{t_0}^{t_F} Q_i\ C_i\ dt$$

(3)

$$River\ transport = Q_R\ C_R\ (t_F - t_0)$$

(4)

where C_i and C_R are the concentrations during the tidal cycle and in the river, respectively. Positive transport is associated with an output of the studied component from the estuary to the coastal area.

IV. 2.6 Statistical Analysis

We performed two ways ANOVA and post hoc Tukey multiple comparisons of means 95 % family-wise confidence level to assess spatial differences within the estuaries and between them in DOM characteristics. Linear regression analysis between DOC and DOM properties and with salinity were fitted and considered statistically significant when $p < 0.01$. All analyses were performed in R 3.5 software (R Development Core Team, 2018).

IV. 3. Results

IV. 3.1. Hydrological characteristics

In the coastal zone next to the three estuaries, salinity varied between 36.2 and 36.5 and temperature between 21.6 and 23.8 °C ($p > 0.05$). In the estuaries, salinity ranged between 0.3 and 36.4 in both Guadalquivir and Guadiana estuaries, increasing downstream (Fig. 2A and 2B, respectively). In Tinto-Odiel estuary, salinity was higher than in the other two estuaries ($p <$

0.05), and an opposite pattern was observed. Thus, salinity decreased from 38.8 to 36.4, with higher values upstream (Fig. 2C). This inverse behavior is due to the strong evaporation and low flow rate of freshwater during summer that makes this system to be regarded as a sea arm. Temperature ranged between 21.6 and 28.0 ºC, increasing upstream in the three estuaries ($p > 0.05$).

The highest Q_R measured in this work (Eq. 2) was in Guadalquivir followed by Guadiana (47.1 and 5.85 $m^3\ s^{-1}$, respectively). A negative value was obtained for Tinto-Odiel (-0.13 $m^3\ s^{-1}$) since, in summer, evaporation exceeds freshwater discharge in this system. Similar values have been reported for Guadalquivir (46.04 $m^3\ s^{-1}$) and Guadiana (5.04 $m^3\ s^{-1}$) by their respective Hydrographic Confederation (www.chguadalquivir.es and www.chguadiana.es), and no data was available for Tinto-Odiel estuary.

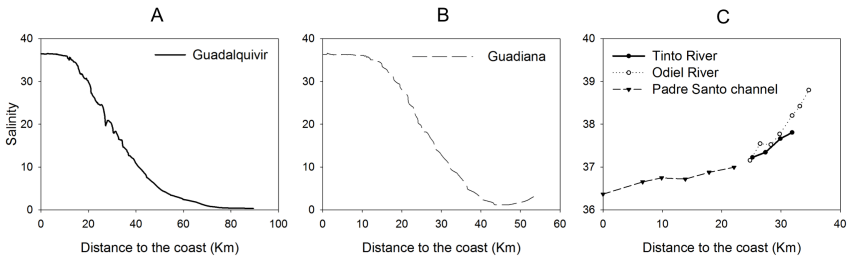

Figure 2. Salinity gradient along the three estuaries. A: Guadalquivir, B: Guadiana and C: Tinto-Odiel.

A clear tidal effect was observed (Fig. 3) with maximum tidal flow rates in Guadalquivir followed by Tinto-Odiel and Guadiana (5084, 4651, and 1493 $m^3\ s^{-1}$, respectively). This may be due to the bigger estuary sections where the tidal study was performed in Tinto-Odiel (7682 ± 707 m^2) and Guadalquivir (5936 ± 448 m^2) compared to Guadiana (2461 ± 229 m^2). Throughout the tidal cycles study, salinity values fluctuated between 25.5 and 36.2 in both Guadalquivir and Guadiana estuaries, with the lowest

values at low tide and the highest ones during high tide. Conversely, in Tinto-Odiel estuary, salinity barely varied 0.3 units (36.3- 36.6) with the highest values during low tide. No stratification of the water column was observed in the salinity profiles and current velocities showed typical parabolic vertical profiles (Uncles et al., 1985), decreasing towards the surface and close to the bottom (Fig S1).

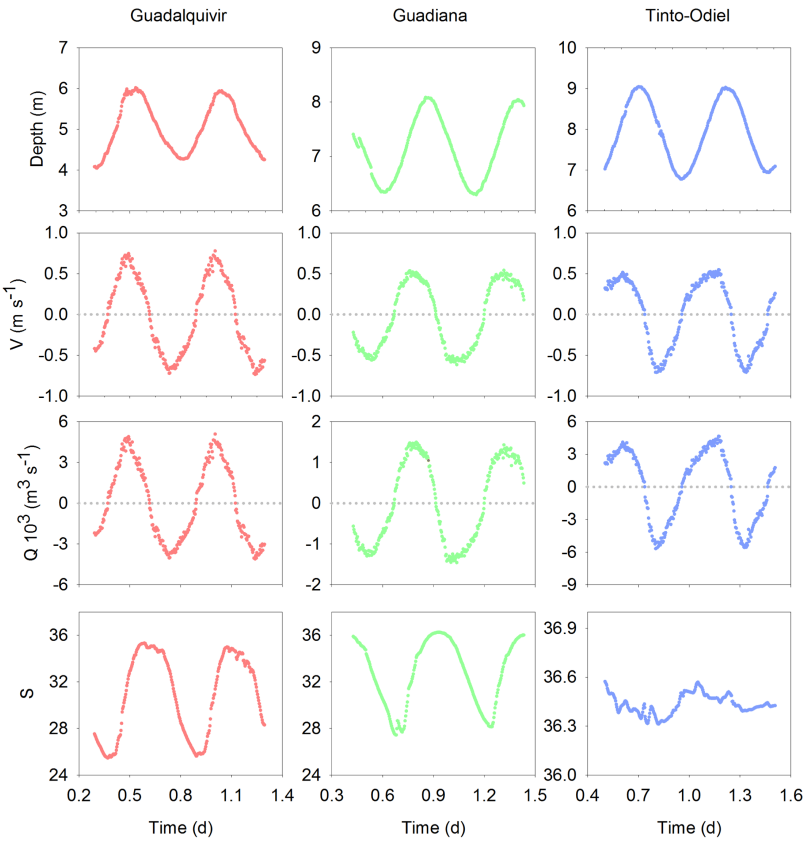

Figure 3. Depth, current velocity (V), tidal flow rate (Q) and salinity (S) during the two tidal cycles at the mouth of Guadalquivir, Guadiana and Tinto-Odiel estuaries. Q was calculated during low tide (depth (h_0) = 4.05, 6.30 and 6.78 m, respectively; section (A_0) = 5197, 2135 and 6598 m^2, respectively; length of the section (L_0) = 722, 387 and 927 m, respectively).

IV. 3.2. Longitudinal variation in DOM composition

DOC concentrations and the optical properties of DOM are presented in Table 1. The lowest average values of DOC, CDOM (a_{254} and a_{350}), and FDOM components were observed in the coastal zone of the three transects ($p > 0.05$). Tinto-Odiel estuary did not show significant differences in DOC and CDOM between coastal and estuarine stations ($p > 0.05$).

In the estuaries, the highest DOC values were observed in the Guadalquivir ($p < 0.05$) and the lowest ones in the Tinto-Odiel. In the Guadalquivir estuary, DOC showed higher values upstream (321.0 µM) than in the lower zone (108.8 µM). However, its maximum values were observed in its middle part (Fig. 4A, max. 541.5 µM). For Guadiana estuary, instead, DOC showed a continuous decrease with increasing salinity, with values ranging from 103.3 to 404.2 µM (Fig. 4B). Lastly, in Tinto-Odiel, an increase in DOC concentrations upstream was also observed with values ranging from 97.6 to 340.6 µM (Fig. 4C). CDOM ($a254$ and $a350$) followed the same trend as DOC in the three estuaries, decreasing with salinity in Guadalquivir and Guadiana and increasing in Tinto-Odiel. The highest a_{254} values were observed in the Guadalquivir estuary ($p < 0.05$), with maximum values in the middle zone (34.62 m^{-1}, Fig. 4A). Overall, lower values were found in Guadiana and Tinto-Odiel estuaries with maximum values upstream (21.25 m^{-1}, Fig. 4B and 14.72 m^{-1}, Fig. 4C). Absorption coefficient a_{350} and $SUVA_{254}$ index showed similar values between estuaries ($p > 0.05$) ranging from 0.30 to 6.31 m^{-1} and 0.26 to 2.83 mg^{-1} L m^{-1}, respectively. Both a_{350} and $SUVA_{254}$ showed the same pattern as a_{254} and DOC in each estuary.

Fluorescence indexes HIX and BIX showed similar values and trends in both Guadalquivir and Guadiana estuaries ($p > 0.05$), with HIX

increasing upstream while BIX decreased. In Tinto-Odiel estuary, maximum values of BIX (4.27) and minimum of HIX (0.21) were observed in the confluence of both Tinto and Odiel rivers.

Similar to DOC and CDOM concentration, the highest TDLP9 were found in Guadalquivir estuary ($p < 0.05$), ranging between 0.98 and 536 nmol L^{-1}, and one order of magnitude higher than in Guadiana and Tinto-Odiel (0.02-68.95 nmol L^{-1}). These values were within the range of those found in Fichot et al. (2016).

Table 1. Variation ranges of physical conditions and DOM optical properties in the coastal and estuarine zone of each transect. Salinity (S), temperature (T, °C) dissolved organic carbon (DOC, µM), CDOM absorption coefficients at 254 nm (a_{254}, m^{-1}) and 350 nm (a_{350}, m^{-1}), $SUVA_{254}$ index (mg^{-1} L m^{-1}), PARAFAC fluorescent components (C1 to C4, RU), humification index (HIX) and freshness index (BIX).

	Guadalquivir		Guadiana		Tinto-Odiel	
	Coastal	Estuarine	Coastal	Estuarine	Coastal	Estuarine
S	36.19-36.49	0.33-36.43	36.25-36.45	0.27-36.61	36.37-36.47	36.65-38.80
T	21.62-22.68	21.95-27.12	22.72-23.83	22.71-28.02	22.12-23.56	21.56-27.58
DOC	98.0-114.7	108.8-541.5	100.7-121.3	103.8-404.2	104.8-164.1	97.6-340.6
a_{254}	1.64-3.46	1.21-34.62	0.79-3.35	1.68-21.25	1.59-8.21	2.43-14.71
a_{350}	0.03-0.56	0.30-6.31	0.04-1.23	0.39-3.38	0.12-3.53	0.40-3.95
$SUVA_{254}$	0.59-1.21	0.32-2.81	0.26-1.15	0.57-2.56	0.35-2.83	0.82-2.14
C1	0.009-0.021	0.022-1.07	0.010-0.018	0.016-0.49	0.005-0.016	0.011-0.25
C2	0.006-0.012	0.014-0.46	0.006-0.010	0.010-0.22	0.002-0.009	0.005-0.11
C3	0.002-0.024	0.011-0.15	0.002-0.056	0.009-0.069	0.005-0.022	0.007-1.19
C4	0.008-0.016	0.011-0.11	0.006-0.022	0.008-0.054	0.006-0.019	0.007-0.79
HIX	0.73-0.87	0.71-0.95	0.45-0.82	0.71-0.95	0.53-0.80	0.21-0.92
BIX	0.54-1.34	0.57-1.31	0.50-2.12	0.56-1.38	0.76-1.97	0.57-4.27

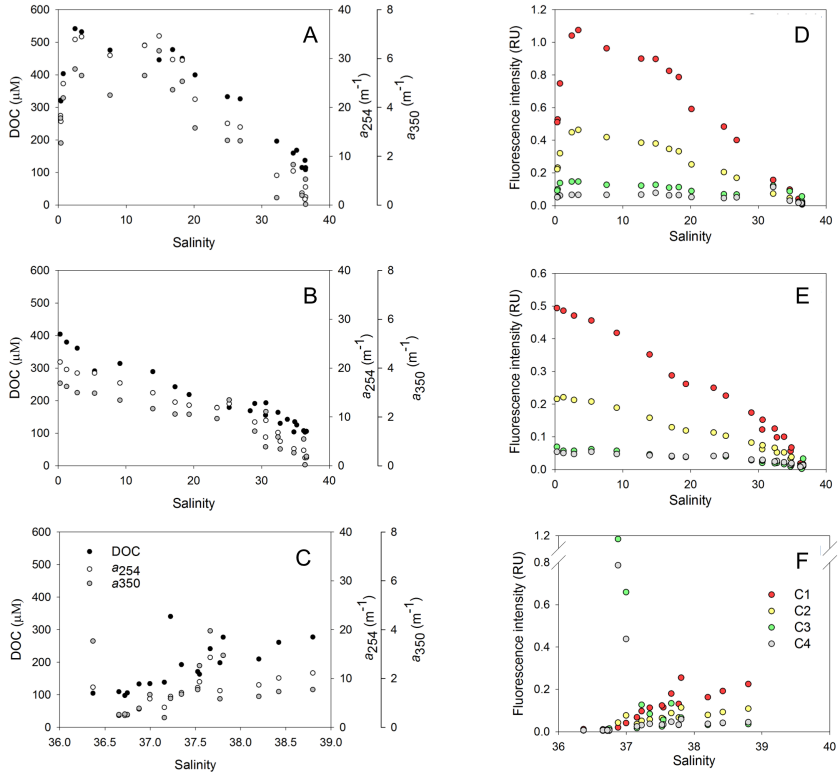

Figure 4. Longitudinal distribution of dissolved organic carbon (DOC), CDOM absorption coefficient (a_{254} and a_{350}) and fluorescent components (C1 to C4) along the three estuaries: Guadalquivir (A and D), Guadiana (B and E) and Tinto-Odiel (C and F). Confluence of Tinto and Odiel rivers at salinity = 36.9.

IV. 3.3. Assignments and distribution of FDOM components

Four fluorescent components were validated, and their characteristics are reported in Table S1 and Fig. S2. The components were distinguished by their excitation-emission spectra and compared with previously published data on the open-access spectral database OpenFluor by Murphy et al. (2014) (Table S1). The four fluorescent components were found in the coastal zone of the Gulf of Cádiz (Amaral et al., 2020). Component 1 (C1) and component 2 (C2) were identified as humic-like components. C1 has been reported as ubiquitous, found in almost all environments and derived

from both allochthonous and autochthonous sources. C2 was referred to as terrestrial origin observed in freshwater impacted by agriculture. Component 3 (C3) and component 4 (C4) represent protein-like fluorescence containing fractions of autochthonous DOM, and they resembled the amino acids tryptophan and tyrosine, respectively (Coble, 1996). Humic-like components C1 and C2 were strongly correlated as well as the protein-like components C3 and C4 among them (R^2 = 0.98 and 0.69, respectively, n = 150, $p < 0.01$).

Similar to the concentration of DOC and CDOM, humic-like C1 and C2 showed the highest values in Guadalquivir estuary (Fig. 4D and Table 1), followed by Guadiana (Fig. 4E) and Tinto-Odiel estuary (Fig. 4F) ($p < 0.05$). No significant differences were observed in protein-like C3 and C4 between estuaries ($p > 0.05$). Regarding the longitudinal transects, FDOM components also followed the same pattern as DOC and CDOM. Thus, in Guadalquivir estuary, the highest values were observed in the middle zone, while in Guadiana and Tinto-Odiel increased upstream; however, Tinto-Odiel estuary showed the maximum values of protein-like C3 and C4 in the confluence of both rivers and in the Pedro Santo channel.

IV. 3.4. Molecular characterization: Py-GC-MS analysis

Table S2 shows the list of products that were considered of interest and their relative contributions to the pyrolyzed sample. The identified products were grouped based on structural features and prevailing sources (Table 2). The pyrolysis chromatograms for each estuarine are presented in Fig. S2.

All samples produced a peak that corresponds to elemental sulfur or sulfur dioxide (m/z 64), which is probably indicative of inorganic sulfur

from mineral particles (e.g., pyrite). The samples produced isooctylphthalate, which is probably indicative of plastic contamination (Roy, 2004), and N-butylbenzenesulfonamide, that is not related with DOM from natural environments and could also be from contamination, i.e., from the sample itself (industrial activities), sample preparation or from the interaction of compounds with instrument parts. Another relatively abundant product in Tinto-Odiel, was dichlorobenzoic acid, which may originate from pharmaceutical and agrochemical sources (Rappe, 1979) but also could be released by marine organisms (Repeta et al., 2004).

Lignin products (guaiacol and 4-vinyl guaiacol), which represent a DOM fraction that originates from terrestrial or subaquatic vegetation (vascular plants), were most abundant in Guadalquivir, followed by Guadiana and Tinto-Odiel estuaries. Products with nitrogen (N-compounds), such as pyrrole, pyridine, acetamide, indole, and diketodipyrrole, were enriched in the sample from Guadiana estuary. The balance between lignin from vascular plants, and N-compounds from protein, peptidoglycan and chitin from marine primary producers, was also highest in Guadalquivir (0.38) and lowest in Tinto-Odiel (0.2) and Guadiana (0.14), indicative of a larger proportion of plant-derived DOM in the former. Monocyclic aromatic hydrocarbon compounds (MAH), indicative of degraded polyphenolic material from higher plants, were higher in Guadiana and lower in Tinto-Odiel estuary. Phenols are considered to be indicative of degradation of lignin-derived DOM (van Heemst et al., 1999) and from microbial material (Martin, 1979) and were also higher in Guadalquivir, followed by Guadiana. The compounds that represent methylene chain compounds (MCC) were, by far, most abundant in Tinto-Odiel estuary and may originate from anthropogenic or natural sources

(Peulvé et al., 1996). Polycyclic aromatic hydrocarbons that may represent pyrogenic organic matter (fire residues) showed the lowest proportion in Tinto-Odiel, but additional caution is required here as matrix effects can cause aromatization and perhaps contamination contributes to these compounds.

Table 2. Pyrolysis product groups and relative proportions (%) of the DOM sample analyzed in each estuary. MAHs (monocyclic aromatic hydrocarbons); MCCs (methylene chain compounds); PAHs = polycyclic aromatic hydrocarbons.

Class group	Guadalquivir	Guadiana	Tinto-Odiel
Carbohydrate	6.77	8.31	4.47
Lignin	2.07	1.39	0.85
MAHs	34.75	44.86	23.54
MCCs	1.06	3.20	24.79
N-Compounds	5.41	9.60	4.24
Phenols	20.44	19.00	10.95
Plasticizers	19.53	5.55	17.34
PAHs	6.92	7.04	4.71
Others	3.04	1.06	9.09

IV. 3.5. Tidal Cycles

Similar to the longitudinal transects, DOC, CDOM (a_{254} and a_{350}), $SUVA_{254}$ and HIX values were higher in Guadalquivir estuary, followed by Guadiana and Tinto-Odiel estuaries, while BIX values were higher in Tinto-Odiel estuary (Fig. 5, $p < 0.05$).

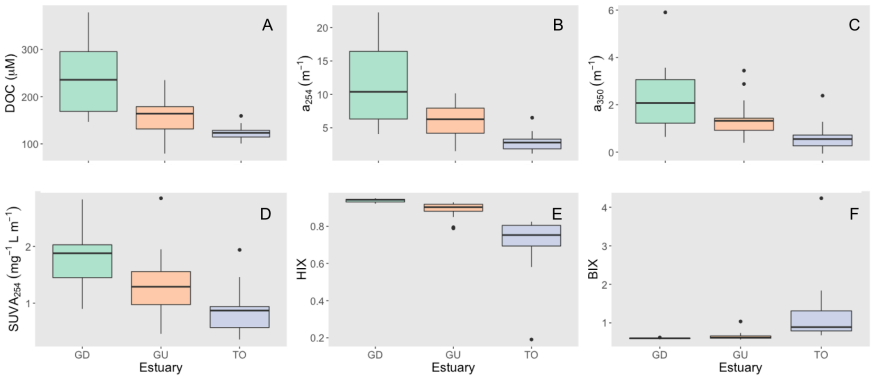

Figure. 5. Boxplots showing dissolved organic carbon (A: DOC), CDOM absorption coefficient (B: a_{254} and C: a_{350}), $SUVA_{254}$ index (D), humification index (E: HIX) and the index of recent autochthonous contribution (F: BIX) for Guadalquivir (GD), Guadiana (GU) and Tinto-Odiel (TO) during the tidal study.

In Guadalquivir and Guadiana estuaries, DOC and CDOM (a_{254} and a_{350}), followed the typical sinusoidal shape along time, associated with tidal cycles with maximum values during low tide and minimum at high tide (Fig. 6A and 6B, respectively). In Guadalquivir estuary, DOC concentration was between 146.6 and 378. 5 µM, while in Guadiana, it ranged between 79.4 and 235.1 µM. Absorption coefficients a_{254} and a_{350} fluctuated from 4.06 to 22.28 m^{-1} and from 0.64 to 5.90 m^{-1} in Guadalquivir, respectively. In Guadiana they ranged from 1.50 to 10.16 m^{-1} and from 0.39 to 3.44 m^{-1}, respectively. For Tinto-Odiel, no clear tidal variations were observed (Fig. 6C), with DOC values ranging between 100.8 and 159.2 µM, a_{254} ranged from 1.13 to 6.51 m^{-1} and a_{350} from 0.05 to 2.39 m^{-1}.

The concentration of DOC, a_{254} and a_{350} showed an inverse relationship with salinity during the tidal study in both Guadalquivir (R^2 = 0.89, 0.90 and 0.64, respectively, $p < 0.01$) and Guadiana (R^2 = 0.52, 0.73 and 0.40, respectively, $p < 0.01$) estuaries, as seen for the longitudinal transects. Although in Tinto-Odiel estuary, a smaller variability in salinity was observed (Fig. 3), a_{254} and a_{350} followed a similar behavior than salinity

(R^2 = 0.31 ad 0.28, respectively, $p < 0.01$), while DOC remains relatively constant.

Similar to DOC and CDOM, the fluorescence intensity of the four components also show a clear distribution depending on salinity during the tidal cycles in both Guadalquivir ($R^2 > 0.91$, $p < 0.01$) and Guadiana estuaries ($R^2 > 0.74$, except for C3 where $R^2 = 0.32$, $p < 0.01$) with higher concentrations of humic-like components during low tide (Fig 6D and 6E). This trend was not observed in Tinto-Odiel estuary (Fig. 6F), although a slight dependence with salinity was observed, especially in the humic-like fraction (R^2 C1 = 0.18 and C2 = 0.31, $p < 0.01$). Fluorescent indexes, HIX and BIX, showed the lowest variation in Guadalquivir and Guadiana estuary (Fig. 6G and 6H) and the highest in Tinto-Odiel (Fig. 6I). The indexes showed opposite trends, thus, HIX decreased during high tide while BIX increased.

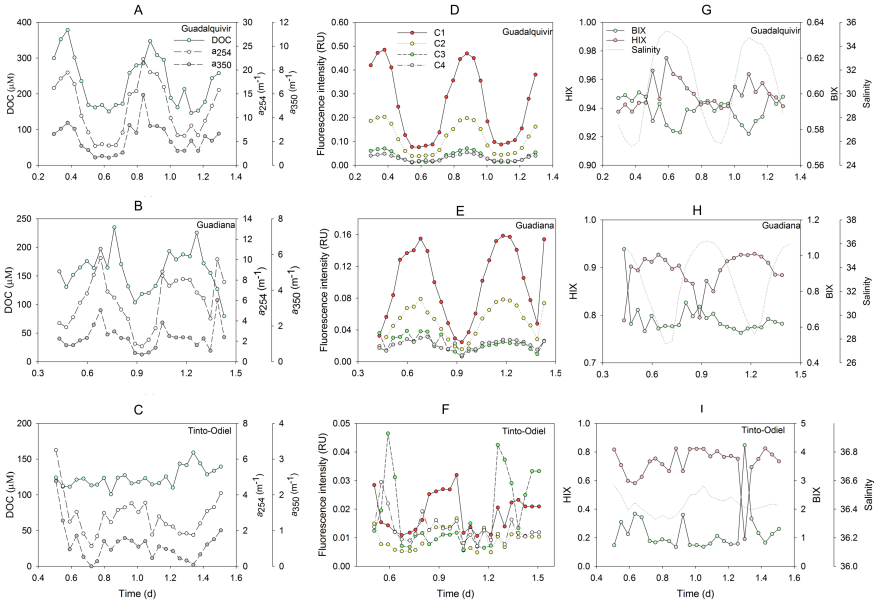

Figure. 6. Distribution of dissolved organic carbon (DOC), CDOM absorption coefficient (a_{254} and a_{350}) and fluorescent components (C1 to C4), and fluorescent indexes in the three estuaries during the tidal study: Guadalquivir (A, D and G), Guadiana (B, E and H) and Tinto-Odiel (C, F and I).

IV. 4. Discussion

IV. 4.1. Distribution of DOM in the estuaries

Four fluorescent components widely distributed in aquatics systems and found in the online repository OpenFluor database (Murphy et al., 2014) were validated using PARAFAC. The components explained 93 % of FDOM variability observed in the estuaries.

DOC concentrations and CDOM absorption coefficients (a_{254} and a_{350}) obtained in this study were similar to those values found in other estuarine systems (e.g., Rochelle-Newall and Fisher, 2002, Guo et al., 2007). Our results indicate that the Guadalquivir estuary has the highest concentrations of DOC, CDOM, and humic-like material, followed by Guadiana and Tinto-Odiel. The Guadalquivir river is the major river flowing into the continental shelf of the Gulf of Cádiz with the largest freshwater discharges. In contrast, Tinto-Odiel estuary has a predominantly marine influence, and the lower freshwater discharge could explain this trend during the dry season. Regarding the DOM sources, protein-like fluorescence is known to dominate in estuarine systems where autochthonous production overwhelms the diluted terrestrial signal (Osburn and Stedmon, 2011), and in systems under the influence of urban and industrial activities (Hong et al., 2005, Coble et al., 2014). During the whole study, maximum intensities of protein-like C3 and C4 were recorded in the confluence of Tinto and Odiel rivers. The contribution of protein-like components (% C3 + % C4) to the total FDOM pool in this estuary was 53 %. Also, BIX values > 1, observed in Tinto-Odiel estuary, indicated the presence of autochthonous DOM and organic matter freshly released into the water (Huguet et al., 2009). In Guadalquivir and Guadiana estuaries, protein-like components only accounted for 28 %, being the humic fraction

the dominant one with ~ 82 % of the total FDOM pool.

IV. 4.2. Behavior of DOM during estuarine mixing

DOM can undergo a variety of biogeochemical reactions within estuaries that determine the concentration and composition of DOM reaching the ocean. The behavior of terrestrial DOM during estuarine mixing is highly variable.

Mixing diagrams of DOM concentration along the salinity gradient were used to characterize the estuarine behavior of DOM and identify changes in its properties within estuaries. A linear behavior may reflect fewer changes in DOM properties along the estuary. In contrast, points falling below the theoretical dilution line could be associated with removal of DOM (photochemical or microbial removal) while points falling above the line indicate that *in situ* production and/or inputs from lateral sources are occurring (e.g., anthropogenic pollution, autochthonous production, inputs from tributaries) (Guo et al., 2007, Raymond and Spencer, 2015). Concentrations of DOC, CDOM (as absorption coefficients), and fluorescent components of each estuary were plotted as a function of salinity and non-linearity was examined (Table 3). Differences in the mixing behavior of DOM between estuaries were observed. In Guadiana, DOM showed linear trends with salinity, indicating a major terrestrial origin of DOM (Fig. 4B and 4E). Dilution and physical mixing explain the majority of the spatial variability observed as fresh and coastal waters mix along the Guadiana estuary. Similar behavior during estuarine mixing has been reported in other coastal systems (Rochelle-Newall and Fisher, 2002, Jaffe et al., 2004, Guo et al., 2007, Yamashita et al., 2008). However, positive deviations from the linear mixing were observed in most variables of DOM. To quantify those deviations from the theoretical dilution line we calculated

the anomalies/residuals. We found an average DOC excess of 29.9 ± 9.9 µM in stations with S > 29, that is mainly in the lower zone of the estuary. The average excess of CDOM, as both a_{254} and a_{350}, and humic-like components (C1+C2) in those stations was 3.5 ± 0.8 m^{-1}, 0.7 ± 0.5 m^{-1} and 0.04 ± 0.01 RU, respectively. These deviations could be due to DOM inputs from the ~ 16 km^2 salt marshes near Guadiana mouth, in the lower zone of the estuary, where the Natural Park "Marismas de Castro Marim y Vila Real de Santo Antonio" are located (www.chguadiana.es).

Table 3. Summary of distributions of dissolved organic carbon (DOC), CDOM absorption coefficients at 254 and 350 nm and fluorescent components (C1 to C4) along the salinity gradient in each estuary. The R^2 values are from the lineal regression and distributions are interpreted as linear or non-linear with a $p < 0.01$. *indicate a positive slope.

Estuary	Type	DOC	a_{254}	a_{350}	C1	C2	C3	C4
Guadalquivir	Non-linear	0.65	0.61	0.60	0.68	0.69	0.57	0.24
Guadiana	Linear	0.96	0.95	0.82	0.98	0.98	0.88	0.86
Tinto-Odiel								
Padre Santo	Linear*	0.75	0.91	0.87	0.87	0.94	0.78	0.57
Tinto	Linear*	0.98	0.95	0.73	0.95	0.97	-	0.97
Odiel	Linear*	0.96	0.69	0.49	0.98	0.96	0.76	0.93

In Guadalquivir estuary, a non-linear relationship between DOM variables and salinity was observed (Table 3, Fig. 4A and 4D), with the highest values (positive deviations) in the upper and middle zone coinciding with the maximum turbidity zone. This implies a possible contribution of organic matter to the dissolved phase that may be derived from different

sources. In the upper zone, Guadalquivir received the freshwater inputs of a tributary (Guadaira river), however its discharge is less than 5 % of the one measured in Guadalquivir, thus a minor effect in DOM properties is expected. On the other hand, 36000 ha of rice crops are situated in the margins of Guadalquivir estuary (www.chguadalquivir.es), between 45 and 80 km from the mouth, where these maximum values were found. Noteworthy, ~ 15 % of the water withdrawal for irrigation is used in these crops (Carrasco et al., 2010). Given the shape of the curve with a progressive increase of DOM through the area where the rice fields end and an almost linear behavior towards the mouth (R^2 = 0.98), we can conclude that this could be the main explanation for the positive deviation observed here. Furthermore, the strong relation observed between TDLP9 with DOC (R^2 > 0.94), humic-like components (R^2 > 0.98), and protein-like components (R^2 > 0.90), indicated that terrestrial DOM dominates the bulk of DOM pool. This was also evident in the Py-GC-MS analysis, where DOM fractions from terrestrial sources were more abundant in Guadalquivir (e.g., lignin, phenols, Table 2), as observed in headwater streams (Kaal et al., 2016, 2017). Additionally, wetlands have been considered an important factor in the transport of large amounts of organic matter into inland waters (Wetzel, 1992), and Guadalquivir is located in one of the largest wetlands of Europe (Doñana Natural Park), where salt marshes occupy ~ 27000 ha (www.juntadeandalucia.es). *Spartina* salt marshes, found in this estuary, have shown to be a major source of CDOM in other estuarine systems (Gardner et al., 2005, Tzortziou et al., 2008). Therefore, our results suggest the existence of two main allochthonous sources of DOM located on the banks of this estuary, rice crops and wetlands.

It should be noted that the salinity gradient in Tinto-Odiel barely

exceeds two units and that this system comprises different parts (Tinto River, Odiel River, and the common marine area Padre Santo channel, Fig. 1). Therefore, we examined DOM mixing behavior independently in each part of the estuary. In general, positive linear relationships with salinity were found (Table 3) when removing maximum values of DOC in Tinto river (340 µM) and protein-like components in the confluence of both rivers and the Pedro Santo channel (> 0.4 RU, Fig. 4F). These stations are located near the Industrial and Chemical Complex of Huelva which comprises a marine loading dock and embraces fertilizer, metal, oil, and paint factories that could have an influence in the composition of DOM in this system (Fig. 1). There is also the water treatment plant from Huelva city (150000 pop.) and 1200 ha of phosphogypsum (PG) residue rafts from the fertilizer industry that were stockpiled on the salt marshes of the Tinto river (Pérez-López et al., 2011). PG shows emission peaks at 300 nm and 342 nm after excitation in the UV (Hammas et al., 2013) but identifying its characteristic peak using PARAFAC was not possible here since it fluoresces in the same region than the protein-like components (Table 1S). However, we found that fluorescence intensity at Ex/Em 260 nm/342 nm ("peak picking" technique, Coble, 1996) was one and two order of magnitude higher in the samples located downstream the PG deposit (0.14 and 0.25 RU) than in the rest of the samples (< 0.06 RU). Nevertheless, further analysis will be necessary to confirm the origin of this elevated fluorescent signal. Tinto-Odiel estuary is one of the most polluted estuaries in the world due to the mining of the massive sulfide deposits in its basin and the industrial activities occurring in its margins (Davis et al., 2000). This could explain the presence of relatively elevated chemical pollutants in pyrolyzates of DOM in this estuary (Table 2).

On the other hand, the positive trend observed between DOM variables and salinity in Tinto-Odiel estuary is because evaporation exceeds riverine inputs during the dry season and makes this system to behave as an inverse estuary. This is often the case in Mediterranean estuaries during the dry season (Catalá et al., 2013). In addition to its inverse nature and low freshwater discharge, there is an autochthonous production of DOM, as well as anthropogenic sources of pollution. Unlike Guadalquivir and Guadiana estuaries, DOC and protein-like components showed a low correlation with TDLP9 in Tinto-Odiel ($R^2 < 0.3$, $p < 0.01$). Hence, the main sources of these components were probably not from terrestrial origin. The microbial production of protein-like components has been reported in other coastal environments (Yamashita et al., 2011, Amaral et al., 2016) as well as in phytoplankton and bacterial experiments (Romera-Castillo et al., 2010, Fox et al., 2017). Usually, lower freshwater discharge, as it is the case in this estuary, results in greater potential for microbial mineralization, prevailing its byproducts over the terrestrial sources of DOM (Raymond and Spencer, 2015). Results from Py-GC-MS analysis support this statement since DOM fractions from vascular plants were lower in Tinto-Odiel while the structures likely derived from *in situ* production and anthropogenic pollutants were the most abundant (Table 2). For example, the higher proportion of MCC in Tinto-Odiel estuary (~ 25 %) than Guadalquivir and Guadiana (< 3 %) could be indicative of larger proportions of planktonic and aliphatic-rich materials (Peulvé et al., 1996, Jiang et al., 2017). We can conclude that estuarine biological activity, together with anthropogenic contamination, might be the dominant sources of DOM in Tinto-Odiel estuary.

CDOM removal associated with photodegradation has been observed along the salinity gradient in other estuarine systems (Vodacek et

al., 1997, Li et al., 2015). However, this was not the case for the estuaries studied here, in agreement with other estuarine systems (Rochelle-Newell and Fisher 2002, Guo et al., 2007), possibly due to the low transparency and a relatively short water residence time (Guo et al., 2007). Guadalquivir and Guadiana showed a high turbidity nature reaching values of 1000 and 600 FTU, respectively (data not shown), which could affect the photochemical processes (Hansell and Carlson, 2014). Also, photochemical alteration could be smaller than the terrestrial DOM inputs (Rochelle-Newell and Fisher 2002). On the other hand, the minor effect of photodegradation observed in plankton-derived material (Obernosterer and Benner, 2004) could explain the case of Tinto-Odiel estuary.

IV. 4.3. The effect of tidal cycles in DOM properties

Tidal cycles were clearly observed in DOC and CDOM distribution in both Guadalquivir and Guadiana estuaries, with higher values during low tide and lower during high tide (Fig. 6). Tidal cycles also affected DOM composition in these estuaries, indicating that a discharge increase provokes a terrigenous DOM enrichment of the estuarine water, as it has been previously observed in other tidal-influenced systems (Tzortziou et al., 2008, Zhou et al., 2019). In contrast, in Tinto-Odiel estuary, only a slight dependence with salinity was found (Fig. 6), indicating, again, the minor contribution of terrestrial DOM to this system.

The relative contribution (%) of each fluorophore was calculated to evaluate the influence of tidal cycles in FDOM variability. During the two tidal cycles, in Guadalquivir and Guadiana, humic-like components account for an average of 83 % ± 1.7 % and 75 % ± 2.7 % of the FDOM pool, respectively. The higher values observed during the low tides were due to a larger contribution of these compounds from the rivers. On the other hand,

protein-like components increased almost twofold their contribution at high tide, since they are associated with the production of organic matter in the lower zone of the estuaries. In Tinto-Odiel estuary, humic-like components contribution (47 % ± 1.7 %) was smaller than in the other two estuaries but similar to the protein-like fraction (53 % ± 5.2 %). These results reinforced the hypothesis that DOM in Guadalquivir and Guadiana is mainly from terrestrial origin, while in Tinto-Odiel DOM has a major autochthonous character. Although, this elevated protein-like fluorescence could also be due to anthropogenic inputs from the industrial activities occurring in its margins. Thus, both biological production and anthropogenic pollutants could explain the highest contribution of the protein-like fraction observed in this system.

IV. 4.4. Flux of DOC, CDOM, and FDOM

Figure 7 shows the evolution of instantaneous fluxes of DOC, a_{254}, a_{350}, and the different components of FDOM during the tidal cycles. Maximum and minimum values are produced during the ebb and flood tides, respectively. The asymmetries observed in its variation are related to the evolution of each variable during the tidal cycle.

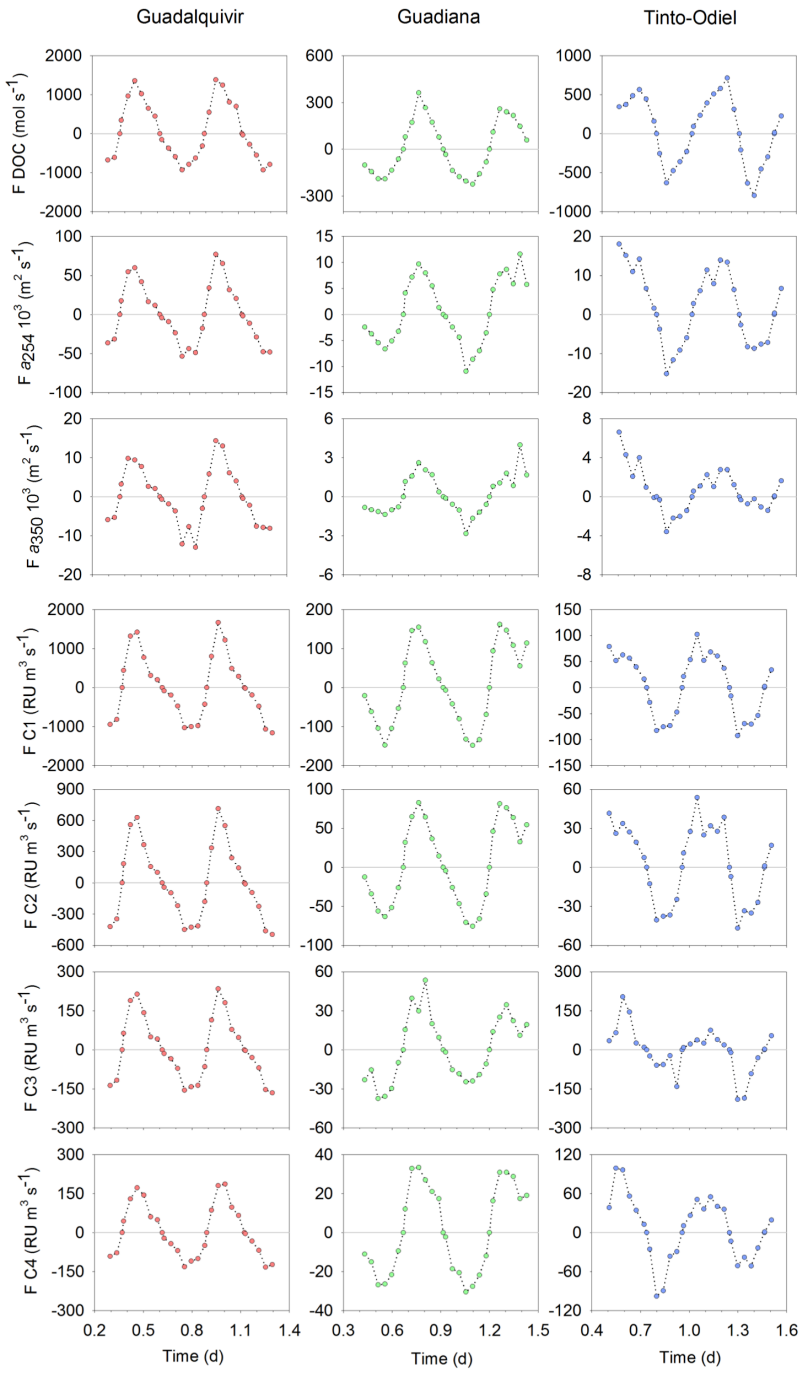

Figure 7. Tidal fluxes of dissolved organic carbon (DOC), CDOM absorption coefficient (a_{254} and a_{350}) and fluorescent components (C1 to C4) in each estuary.

Table 4 shows the flux values estimated for both tidal (Eq. 3) and river transport (Eq. 4) in Guadalquivir and Guadiana, but only tidal transport in Tinto-Odiel since Q_R here was negligible (Eq. 2). Guadalquivir estuary showed the highest DOC, CDOM and FDOM flux estimates in both cases, even one order of magnitude higher than the other two estuaries. Besides, the highest concentration of DOM and discharge were observed in Guadalquivir, and it is generally accepted that rivers with higher discharges have greater DOM export (Raymond and Spencer, 2015). Additionally, lateral inputs of DOM in the upper and middle zone of the estuary from the rice crops and the extensive wetland coverage in Guadalquivir watershed may also contribute to explain these results, as it has been observed in other systems (Spencer et al., 2013). In Guadiana estuary, the tidal net transport of DOM was considerably higher than river transport. Salt marshes could be a source of DOC and CDOM to adjacent estuarine ecosystems (Tzortziou et al., 2008). Thus, the existence of salt marshes in the lower zone of this estuary, could explain this trend since DOC, CDOM and humic-like FDOM showed positive deviation from the linear mixing behavior in the lower zone of the estuary. Unexpectedly, Tinto-Odiel estuary showed a substantial transport of DOC, CDOM and FDOM to the coastal zone (except for C3 that is imported), even higher than Guadiana estuary. This could be due to the higher discharge observed where the tidal study was performed in Tinto-Odiel (± 5000 m^3 s^{-1}) in comparison with Guadiana estuary (± 1500 m^3 s^{-1}).

Among fluorescent components, there was a relatively higher net export of humic-like components (C1+C2) than protein-like components (C3+C4). Thus, between 68 % and 77 % of the FDOM exported from the three estuaries was of humic nature with a low contribution of

autochthonous DOM, as it has been observed in riverine DOM fluxes (Stepanauskas et al., 2005). According to Sickman et al. (2010), land use and disturbance result in the export of aged components that could also explain these results, mainly in Guadalquivir and Guadiana. Noteworthy, in Tinto-Odiel, the protein-like C4 accounts for almost 50 % of the total FDOM that this system exports to the coastal zone. This may be associated with anthropogenic sources, such as the PG residue rafts from the above-mentioned fertilizer industry.

Table 4. Tidal and river net flux during dry season of dissolved organic carbon (DOC, mol s^{-1}), CDOM (a_{254} and a_{350}, 10^3 m^2 s^{-1}) and fluorescent components C1 to C4 (RU m^3 s^{-1}) in each estuary.

	Guadalquivir		Guadiana		Tinto-Odiel
	Tidal	River	Tidal	River	Tidal
DOC	104.04	15.14	13.54	2.36	39.33
a_{254}	2.60	0.86	0.56	0.12	1.84
a_{350}	0.22	0.17	0.20	0.02	0.13
C1	43.33	24.04	3.10	2.89	3.26
C2	22.23	10.50	2.10	1.27	2.38
C3	8.49	4.32	1.05	0.40	-2.90
C4	10.87	2.40	1.37	0.32	5.57

Sampling only one season is not enough to capture the full variability range over one year, and recent studies have demonstrated large seasonal variations in DOC export from rivers to the ocean (Lee and Kim, 2018, Li et al., 2019). If these data were extrapolated to an annual export, the contribution of the freshwater discharge from Guadalquivir and Guadiana (1.67 Km^3 yr^{-1}) would account for < 0.004 % to the total rivers discharge in the world (37400 Km^3 yr^{-1}, Cauwet, 2002). The total DOC load from these three rivers would be 0.06 Tg yr^{-1}, equivalent to 0.024 % of the global

annual riverine load of DOC (250 Tg yr^{-1}) transported to the oceans (Hedges et al., 1997), and CDOM export (derived from a_{350}) would be 1.73 x 10^{10} m^2 yr^{-1}. These values are lower than those observed for other rivers (Spencer et al., 2013, Raymond and Spencer 2015, Li et al., 2019). Noteworthy, the fluxes estimated in our work were during the dry season, in the absence of precipitations, when the lower discharge occurs. For example, during the rainy season (January-February), discharges in Guadalquivir river can reach values of 5000 m^3 s^{-1} (Vanney, 1970). Thus, sampling during the rainy season will be necessary to obtain sufficient temporal data required for accurate estimates of DOC and CDOM annual fluxes. However, our results could be a baseline for these three systems in dry conditions, where, as far as we know, no DOM composition studies and flux estimations have been done until now. Seasonal studies of DOM fluxes will be also necessary to understand its potential impact on the coastal ocean under a climate change scenario, where rainfall increase has been predicted (IPCC, 2012).

IV. 4.5. Relation between DOM properties

Several studies have found strong correlations between DOC, CDOM, and FDOM in a variety of aquatic systems (Rochelle-Newel and Fisher, 2002, Spencer et al., 2013, Rochelle-Newel et al., 2014, Osburn et al., 2016). In this work, when all water samples are combined (n = 150), a positive linear relationship was also observed between DOC concentrations, CDOM absorption coefficients and FDOM components (Fig. 8). Humic-like components and a_{254} showed the strongest relationship with DOC (R^2 > 0.91) indicating that allochthonous materials dominated the DOC pool since CDOM is generally terrestrial in estuaries (Osburn et al., 2016). On the other hand, protein-like components and a_{350} had lower relationships with DOC (R^2 = 0.68-0.81). A higher contribution of protein-like

components in Tinto-Odiel estuary may affect the lower relationship compared to humic-like components. Rochelle-Newel et al. (2014) suggest that variations in the ratio of terrestrially / microbial-derived DOC and CDOM will result in alterations in the relationship between CDOM and DOC. Although CDOM and FDOM are often proposed as a rapid method for the estimation of DOC, a high seasonal variability has been observed in DOC-CDOM and DOC-FDOM relationships (Rochelle-Newel et al., 2014) in estuaries mostly associated to river discharge (Osburn et al., 2016). Thereby, the strong relationship found in this work may only be useful during the dry season when the lowest river discharge occurs.

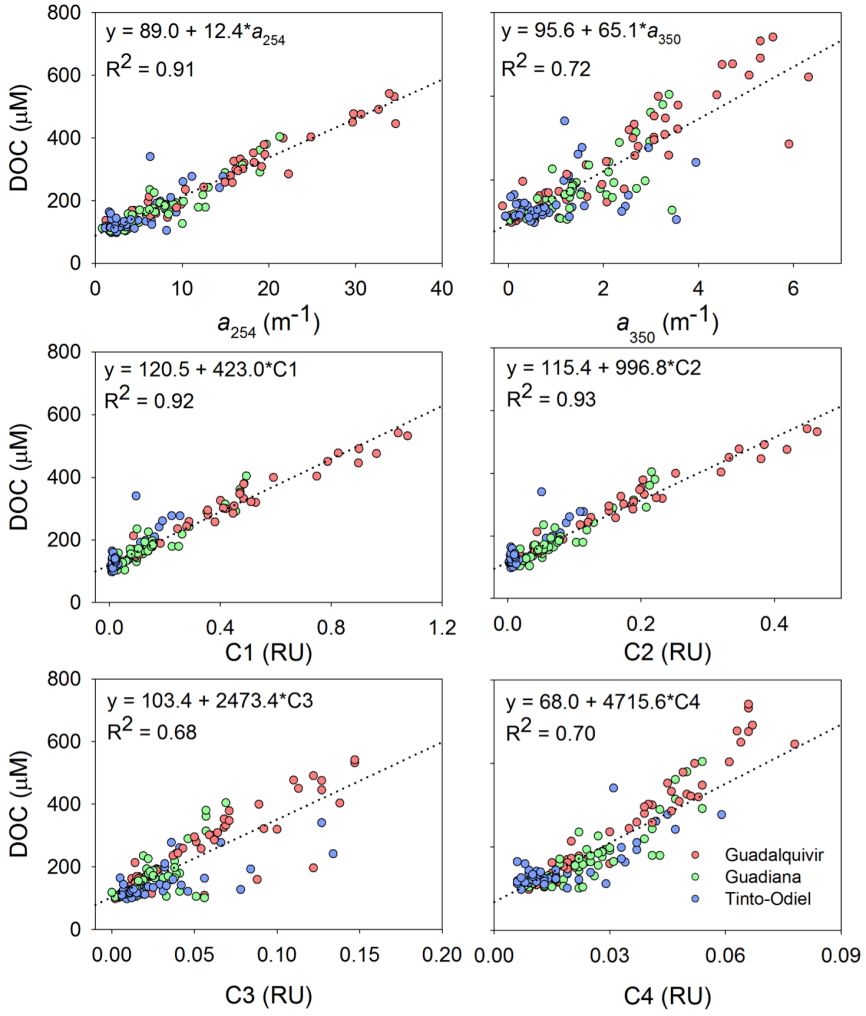

Figure 8. Linear relationship between dissolved organic carbon (DOC) with CDOM absorption coefficient (a_{254} and a_{350}) and fluorescent components (C1 to C2) with a $p < 0.01$ and n = 150.

IV. 5. Conclusions

The application of EEM-PARAFAC, together with Py-GC-MS analysis in the assessment of DOM dynamics in the estuaries of the Southern Iberian Atlantic Basin, showed to improve the understanding of the biogeochemical processes controlling DOM. As such, while in Guadiana DOC and FDOM components decreased linearly with increasing salinity, it was not the case for Guadalquivir estuary. This result was attributed to

lateral inputs in the upper and middle zone of the estuary, where a large extension of rice crops and wetlands exists. Both Guadiana and Guadalquivir estuaries showed that DOM was predominantly from allochthonous origin with a contribution of 83 % of humic-like components to the total FDOM pool. Conversely, DOM in Tinto-Odiel estuary showed that biological activity and anthropogenic pollution from industrial activities were the main sources of DOM. Py-GC-MS analysis supported these results with the highest relative proportions of products from terrestrial/coastal vegetation in Guadalquivir and Guadiana, and products from marine organisms and potential anthropogenic contaminants in Tinto-Odiel estuary. Moreover, results from TDLP9 were consistent with our data, with the highest values in Guadalquivir estuary, and strongly related with the concentration of DOC in this system where terrestrial DOM predominates ($R^2 = 0.95$, $p < 0.01$). Instead, in Tinto-Odiel estuary, where terrestrial DOM is not the main source, a weaker relation was observed ($R^2 < 0.34$, $p < 0.01$). Therefore, we trust that TDLP9 equations may be valid for our systems. The results of the tidal study indicated that these systems are a net source of DOC and CDOM, mainly of humic nature, to the Gulf of Cádiz. Guadalquivir exhibited the highest estimated DOC, CDOM, and FDOM values, followed by Tinto-Odiel and Guadiana, which together export 1.88 Kg s^{-1} of DOC, 0.55 m^2 s^{-1} of CDOM and 76.4 RU m^3 s^{-1} of humic-like substances and 24.4 RU m^3 s^{-1} of protein-like material to the Gulf of Cádiz. DOC and CDOM exports are among the lowest of the major world rivers; however, this work was performed during the dry season, in the absence of precipitation. Climate change is expected to increase riverine freshwater, hence DOM supply. Therefore, this work could be a baseline for the export of terrestrial DOM to the Gulf of Cadiz. Overall, a robust positive linear

relationship between DOC, CDOM and FDOM was found, with R^2 higher than 0.91 for a_{254} and humic-like components, which could be used for a rapid estimation of DOC in these estuaries during the dry season. Thus, spectroscopic techniques have potential to improve the estimations of DOC fluxes to the ocean either through CDOM measurements or via remote sensing techniques.

Acknowledgments

Valentina Amaral was financed by the Uruguayan Agency for Research and Innovation (ANII) with a Ph.D. fellowship (POS_EXT_2015_1_122780). Cristina Romera-Castillo was funded by a Juan de la Cierva-Incorporación Postdoctoral Fellowship from the Spanish "Ministerio de Economía y Competitividad". We thank the crews of the R/V UCádiz for their assistance during field works. We acknowledge the help of José Sanabria with QGIS application (Figure 1), Joeri Kaal with the interpretation of Py-GC-MS data and the anonymous reviewers for their helpful comments that greatly contributed to improves this manuscript. Gastón Pereyra performed the final language revision. This study was financed by the Spanish CICYT (Spanish Program for Science and Technology) under contracts CTM2014-59244-C3-1-R and RTI2018-100865-B-C21.

References

Abril, G., Nogueira, M., Etcheber, H., Cabeçadas, G., Lemaire, E., and Brogueira, M. J. (2002). Behaviour of organic carbon in nine contrasting European estuaries. *Estuar. Coast. Shelf Sci.* 54, 241–262.

Amaral, V., Graeber, D., Calliari, D., and Alonso, C. (2016). Strong linkages between DOM optical properties and main clades of aquatic bacteria. *Limnol. Oceanogr.* 61, 906–918.

Amaral, V., Romera-Castillo, C., and Forja, J. (2020). Dissolved Organic Matter in the Gulf of Cádiz: Distribution and Drivers of Chromophoric and Fluorescent Properties. *Front. Mar. Sci. 7*, 126.

Bauer, J. E., and Bianchi, T. S. (2012). *Dissolved Organic Carbon Cycling and Transformation*. Elsevier Inc.

Benner, R., and Opsahl, S. (2001). Molecular indicators of the sources and transformations of dissolved organic matter in the Mississippi river plume. *Org. Geochem.* 32, 597–611.

Carrasco, J. M., Piston, J. M., and Berbel, J. (2010). Evolución de la productividad del agua en la Cuenca del Guadalquivir 1989-2005. *Agricultural and Economic Resources*, *10*(1380-2016-115403),59-69.

Carro, B., Borrego, J., and Morales, J. A. (2019). Estuaries of the Huelva Coast: Odiel and Tinto Estuaries (SW Spain). In *The Spanish Coastal Systems* (pp. 543-564). Springer, Cham.

Catalá, T. S., Mladenov, N., Echevarría, F., and Reche, I. (2013). Positive trends between salinity and chromophoric and fluorescent dissolved organic matter in a seasonally inverse estuary. *Estuar. Coast. Shelf Sci.* 133, 206–216.

Cauwet, G., 2002. DOM in the coastal zone. In: Hansell, D.A., Carlson, C.A. (Eds.), *Biogeochem. Mar. Dissolved Org. Matter*. Academic Press/Elsevier Science, New York, NY, pp. 579–602.

Chen, S. N., Geyer, W. R., Ralston, D. K., and Lerczak, J. A. (2012). Estuarine Exchange Flow Quantified with Isohaline Coordinates: Contrasting Long and Short Estuaries. *J. Phys. Oceanogr.* 42, 748–763.

Coble, P. (1996). Characterization of marine and terrestrial DOM in seawater using excitation-emission matrix spectroscopy. *Mar. Chem.* 51, 325–346.

Coble, P. G. (2007). Marine Optical Biogeochemistry: The Chemistry of Ocean Color. *Chem. Rev.* 107, 402–418.

Coble, P. G., Lead, J., Baker, A., Reynolds, D. M., and Spencer, R. G. M. (2014). *Aquatic Organic Matter Fluorescence*. , eds. P. G. Coble, J. Lead, A. Baker, D. M. Reynolds, and R. G. M. Spencer.

Davis Jr, R. A., Welty, A. T., Borrego, J., Morales, J. A., Pendon, J. G., and Ryan, J. G. (2000). Rio Tinto estuary (Spain): 5000 years of pollution. *Environ. Geol. 39*(10), 1107-1116.

Determann, S., Lobbes, J. örg M., Reuter, R., and Rullkötter, J. ürgen (1998). Ultraviolet fluorescence excitation and emission spectroscopy of marine algae and bacteria. *Mar. Chem.* 62, 137–156.

Dittmar, T., Koch, B., Hertkorn, N., and Kattner, G. (2008). A simple and efficient method for the solid-phase extraction of dissolved organic matter (SPE-DOM) from seawater. *Limnol. Oceanogr. Methods* 6, 230–235.

Fichot, C. G., Benner, R., Kaiser, K., Shen, Y., Amon, R. M. W., Ogawa, H., et al. (2016). Predicting dissolved lignin phenol concentrations in the coastal ocean from

chromophoric dissolved organic matter (CDOM) absorption coefficients. *Front. Mar. Sci.* 3, 1–15.

Fox, B. G., Thorn, R. M. S., Anesio, A. M., and Reynolds, D. M. (2017). The in situ bacterial production of fluorescent organic matter; an investigation at a species level. *Water Res.* 125, 350–359.

Gardner, G. B., Chen, R. F., and Berry, A. (2005). High-resolution measurements of chromophoric dissolved organic matter (CDOM) in the Neponset River Estuary, Boston Harbor, MA. *Mar. Chem.* 96, 137–154.

Gardner, L. R., and Kjerfve, B. (2006). Tidal fluxes of nutrients and suspended sediments at the North Inlet-Winyah Bay National Estuarine Research Reserve. *Estuar. Coast. Shelf Sci.* 70, 682–692.

Garel, E., and Cai, H. (2018). Effects of Tidal-Forcing Variations on Tidal Properties Along a Narrow Convergent Estuary. *Estuaries and Coasts* 41, 1924–1942.

Garel, E., Pinto, L., Santos, A., and Ferreira, Ó. (2009). Tidal and river discharge forcing upon water and sediment circulation at a rock-bound estuary (Guadiana estuary, Portugal). *Estuar. Coast. Shelf Sci.* 84, 269–281.

González-Ortegón, E., Amaral, V., Baldó, F., Sánchez-Leal, R. F., Bellanco, M. J., Jiménez, M. P., et al. (2018). Sources and coastal distribution of dissolved organic matter in the Gulf of Cadiz. *Sci. Total Environ.* 630, 1583–1595.

Grande, J. A., Borrego, J., and Morales, J. A. (2000). A study of heavy metal pollution in the Tinto-Odiel estuary in southwestern Spain using factor analysis. *Environ. Geol. 39*(10), 1095-1101.

Green, S. A., and Blough, N. V (1994). Optical absorption and fluorescence of chromophoric properties dissolved organic matter in natural waters. *Limnology* 39, 1903–1916.

Guo, W., Stedmon, C. A., Han, Y., Wu, F., Yu, X., and Hu, M. (2007). The conservative and non-conservative behavior of chromophoric dissolved organic matter in Chinese estuarine waters. *Mar. Chem.* 107, 357–366.

Hammas, I., Horchani-Naifer, K., and Férid, M. (2013). Characterization and Optical Study of Phosphogypsum Industrial Waste. *Stud. Chem. Process Technol.* 1, 30–36.

Hansell, D. A., and Carlson, C. A. (Eds.). (2014). *Biogeochemistry of marine dissolved organic matter*. Academic Press.

Hedges, J. I., Keil, R. G., and Benner, R. (1997). What happens to terrestrial organic matter in the ocean? *Org. Geochem.* 27, 195–212.

Hong, H., Wu, J., Shang, S., and Hu, C. (2005). Absorption and fluorescence of chromophoric dissolved organic matter in the Pearl River Estuary, South China. *Mar. Chem. 97*(1-2), 78-89.

Huguet, A., Vacher, L., Relexans, S., Saubusse, S., Froidefond, J. M., and Parlanti, E. (2009). Properties of fluorescent dissolved organic matter in the Gironde Estuary. *Org. Geochem.* 40, 706–719.

Jaffé, R., Boyer, J. N., Lu, X., Maie, N., Yang, C., Scully, N. M., et al. (2004). Source characterization of dissolved organic matter in a subtropical mangrove-dominated estuary by fluorescence analysis. *Mar. Chem.* 84, 195–210.

Jiang, T., Kaal, J., Liang, J., Zhang, Y., Wei, S., Wang, D., and Green, N. W. (2017). Composition of dissolved organic matter (DOM) from periodically submerged soils in the Three Gorges Reservoir areas as determined by elemental and optical analysis, infrared spectroscopy, pyrolysis-GC–MS and thermally assisted hydrolysis and methylation. *Sci. Total Environ. 603*, 461-471.

Kaal, J. (2019). Analytical pyrolysis in marine environments revisited. *Anal. Pyrolysis Lett.*,

1–16.

Kaal, J., Cortizas, A. M., and Biester, H. (2017). Downstream changes in molecular composition of DOM along a headwater stream in the Harz mountains (Central Germany) as determined by FTIR, Pyrolysis-GC–MS and THM-GC–MS. *J. Anal. Appl. Pyrolysis* 126, 50–61.

Kaal, J., Wagner, S., and Jaffé, R. (2016). Molecular properties of ultrafiltered dissolved organic matter and dissolved black carbon in headwater streams as determined by pyrolysis-GC-MS. *J. Anal. Appl. Pyrolysis* 118, 181–191.

Kothawala, D. N., Murphy, K. R., Stedmon, C. A., Weyhenmeyer, G. A., and Tranvik, L. J. (2013). Inner filter correction of dissolved organic matter fluorescence. *Limnol. Oceanogr. Methods* 11, 616–630.

Lawaetz, A. J., and Stedmon, C. A. (2009). Fluorescence intensity calibration using the Raman scatter peak of water. *Appl. Spectrosc.* 63, 936–940.

Leblanc, M., Morales, J. A., Borrego, J., and Elbaz-Poulichet, F. (2000). 4,500-year-old mining pollution in southwestern Spain: Long-term implications for modern mining pollution. *Econ. Geol.* 95, 655–661.

Lee, S. A., and Kim, G. (2018). Sources, fluxes, and behaviors of fluorescent dissolved organic matter (FDOM) in the Nakdong River Estuary, Korea. *Biogeosciences* 15, 1115–1122.

Li, P., Chen, L., Zhang, W., and Huang, Q. (2015). Spatiotemporal distribution, sources, and photobleaching imprint of dissolved organic matter in the Yangtze Estuary and its adjacent sea using fluorescence and parallel factor analysis. *PLoS One* 10, 1–18.

Li, Y., Song, G., Massicotte, P., Yang, F., Li, R., and Xie, H. (2019). Distribution, seasonality, and fluxes of dissolved organic matter in the Pearl River (Zhujiang) estuary, China. *Biogeosciences* 16, 2751–2770.

Maie, N., Scully, N. M., Pisani, O., and Jaffé, R. (2007). Composition of a protein-like fluorophore of dissolved organic matter in coastal wetland and estuarine ecosystems. *Water Res.* 41, 563–570.

Martin, B. F. (1979). Pyrolysis — Gas Chromatography — Mass Spectrometry of Lignins. 33, 210–212.

Massicotte, P., Stedmon, C., and Markager, S. (2017). Spectral signature of suspended fine particulate material on light absorption properties of CDOM. *Mar. Chem. 196*, 98-106.

Ménanteau, L., Céline, C., and Choblet, C. (2005). Les marais du Bas-Guadiana (Algarve, Andalousie): emprise, déprise et reprise humaines. Aestuaria 9, 309-331.

Morales, J.A., Garel, E., 2019. The Guadiana River Delta, in: The Spanish Coastal Systems. Springer International Publishing, pp. 565–581.

Moran, M. A., Sheldon Jr, W. M., and Zepp, R. G. (2000). Carbon loss and optical property changes during long-term photochemical and biological degradation of estuarine dissolved organic matter. *Limnol. Oceanogr. 45*(6), 1254-1264.

Murphy, K. R., Stedmon, C. A., Graeber, D., and Bro, R. (2013). Fluorescence spectroscopy and multi-way techniques. PARAFAC. *Anal. Methods* 5, 6557–6566.

Murphy, K. R., Stedmon, C. A., Wenig, P., and Bro, R. (2014). OpenFluor- An online spectral library of auto-fluorescence by organic compounds in the environment. *Anal. Methods* 6, 658–661.

Nayar, S. and Chou, L., 2003. Relative efficiencies of different filters in retaining phytoplankton for pigment and productivity studies. *Estuar. Coast. Shelf Sci.* 58 (2), 241–248.

Nimptsch, J., Woelfl, S., Kronvang, B., Giesecke, R., González, H.E., Caputo, L.,

Gelbrecht, J., von Tuempling, W., Graeber, D., 2014. Does filter type and pore size influence spectroscopic analysis of freshwater chromophoric DOM composition? *Limnologica* 48, 57–64.

Obernosterer, I., and Benner, R. (2004). Competition between biological and photochemical processes in the mineralization of dissolved organic carbon. *Limnol. Oceanogr. 49*(1), 117-124.

Ohno, T. (2002). Fluorescence inner-filtering correction for determining the humification index of dissolved organic matter. *Environ. Sci. Technol. 36*(4), 742-746.

Osburn, C. L., Boyd, T. J., Montgomery, M. T., Bianchi, T. S., Coffin, R. B., and Paerl, H. W. (2016). Optical proxies for terrestrial dissolved organic matter in estuaries and coastal waters. *Front. Mar. Sci.* 2,127.

Osburn, C. L., and Stedmon, C. A. (2011). Linking the chemical and optical properties of dissolved organic matter in the Baltic-North Sea transition zone to differentiate three allochthonous inputs. *Mar. Chem.* 126, 281–294.

Pérez-López, R., Castillo, J., Sarmiento, A. M., and Nieto, J. M. (2011). Assessment of phosphogypsum impact on the salt-marshes of the Tinto river (SW Spain): Role of natural attenuation processes. *Mar. Pollut. Bull.* 62, 2787–2796.

Peulvé, S., Sicre, M.-A., Saliot, A., De Leeuw, J.W., Baas, M., (1996). Molecular characterization of suspended and sedimentary organic matter in an Arctic delta. *Limnol. Oceanogr.* 41 (3), 488–497.

Rappe, C., Buser, H. R., and Bosshardt, H. P. (1979). Dioxins, dibenzofurans and other polyhalogenated aromatics: Production, use, formation, and destruction. *Annals of the New York Academy of Sciences*, *320*(1), 1-18.

Raymond, P. A., and Spencer, R. G. M. (2015). Riverine DOM. *Biogeochem. Mar. Dissolved Org. Matter Second Ed.*, 509–533.

Repeta, D. J., Hartman, N. T., John, S., Jones, A. D., and Goericke, R. (2004). Structure elucidation and characterization of polychlorinated biphenyl carboxylic acids as major constituents of chromophoric dissolved organic matter in seawater. *Environ. Sci. Technol. 38*(20), 5373-5378.

Ribas-Ribas, M., Gómez-Parra, A., and Forja, J. M. (2011). Spatio-temporal variability of the dissolved organic carbon and nitrogen in a coastal area affected by river input: The north eastern shelf of the Gulf of Cádiz (SW Iberian Peninsula). *Mar. Chem.* 126, 295–308.

Rochelle-Newall, E., Hulot, F. D., Janeau, J. L., and Merroune, A. (2014). CDOM fluorescence as a proxy of DOC concentration in natural waters: A comparison of four contrasting tropical systems. *Environ. Monit. Assess.* 186, 589–596.

Rochelle-Newall, E. J., and Fisher, T. R. (2002). Chromophoric dissolved organic matter and dissolved organic carbon in Chesapeake Bay. *Mar. Chem.* 77, 23–41.

Rodríguez-Ramírez, A., Villarías-Robles, J.J.R., Pérez-Asensio, J.N., Celestino-Pérez, S., 2019. The Guadalquivir Estuary: Spits and Marshes, in: *The Spanish Coastal Systems*. pp. 517–541.

Romera-Castillo, C., Sarmento, H., Álvarez-Salgado, X. A., Gasol, J. M., and Marrasé, C. (2010). Production of chromophoric dissolved organic matter by marine phytoplankton. *Limnol. Oceanogr.* 55, 1466–1466.

Roy, W. R. (2004). The environmental fate of plasticizers. *Handbook of Plasticizers. Ontario, ChemTec Publishing, 2004.*, 591-613.

Sickman, J. O., DiGiorgio, C. L., Davisson, M. L., Lucero, D. M., and Bergamaschi, B. (2010). Identifying sources of dissolved organic carbon in agriculturally dominated rivers using radiocarbon age dating: Sacramento-San Joaquin River Basin, California.

Biogeochemistry 99, 79–96.

Spencer, R. G. M., Aiken, G. R., Dornblaser, M. M., Butler, K. D., Holmes, R. M., Fiske, G., et al. (2013). Chromophoric dissolved organic matter export from U.S. rivers. *Geophys. Res. Lett.* 40, 1575–1579.

Stedmon, C., and Bro, R. (2008). Characterizing dissolved organic matter fluorescence with parallel factor analysis: a tutorial. *Limnol. Oceanogr. Methods* 6, 572–579.

Stepanauskas, R., Moran, M. A., Bergamaschi, B. A., and Hollibaugh, J. T. (2005). Sources, bioavailability, and photoreactivity of dissolved organic carbon in the Sacramento-San Joaquin River Delta. *Biogeochemistry* 74, 131–149.

Tzortziou, M., Neale, P. J., Osburn, C. L., Megonigal, J. P., Maie, N., and Jaffé, R. (2008). Tidal marshes as a source of optically and chemically distinctive colored dissolved organic matter in the Chesapeake Bay. *Limnol. Oceanogr.* 53, 148–159.

Uncles, R.J., Elliott, R.C.A, Weston., S.A., 1985. Observed fluxes of water, salt and suspended sediment in a partly mixed estuary. *Estuar. Coast. Shelf Sci.* 20(2): 147-167

Van Heemst, J. D. H., Van Bergen, P. F., Stankiewicz, B. A., and De Leeuw, J. W. (1999). Multiple sources of alkylphenols produced upon pyrolysis of DOM, POM and recent sediments. *J. Anal. Appl. Pyrolysis* 52, 239–256.

Vanney, J. R. (1970). L'hydrologie du Bas Guadalquivir (p. 176). Madrid: Editorial CSIC.

Vodacek, A., Blough, N. V, Degrandpre, M. D., Peltzer, E. T., Robert, K., Jun, N., et al. (1997). Seasonal variation of CDOM and DOC in the Middle Atlantic Bight: Terrestrial inputs and photooxidation. *Limnol. Oceanogr.* 42, 674–686.

Weishaar, J., Aiken, G., Bergamaschi, B., Fram, M., Fujii, R., and Mopper, K. (2003). Evaluation of specific ultra-violet absorbance as an indicator of the chemical content of dissolved organic carbon. *Environ. Chem.* 41, 843–845.

Wetzel, R. G. (1992). Gradient-dominated ecosystems: sources and regulatory functions of dissolved organic matter in freshwater ecosystems. *Hydrobiologia* 229, 181–198.

Yamashita, Y., Jaffe, R., Maie, N., and Tanoue, E. (2008). Assessing the dynamics of dissolved organic matter (DOM) in coastal environments by excitation emission matrix fluorescence and parallel factor analysis (EEM-PARAFAC). *Limnol. Oceanogr.* 53, 1900–1908.

Yamashita, Y., Panton, A., Mahaffey, C., and Jaffé, R. (2011). Assessing the spatial and temporal variability of dissolved organic matter in Liverpool Bay using excitation-emission matrix fluorescence and parallel factor analysis. *Ocean Dyn.* 61, 569–579.

Zhou, Y., Li, Y., Yao, X., Ding, W., Zhang, Y., Jeppesen, E., et al. (2019). Response of chromophoric dissolved organic matter dynamics to tidal oscillations and anthropogenic disturbances in a large subtropical estuary. *Sci. Total Environ.* 662, 769–778.

Supplementary Material

Supplementary Figures

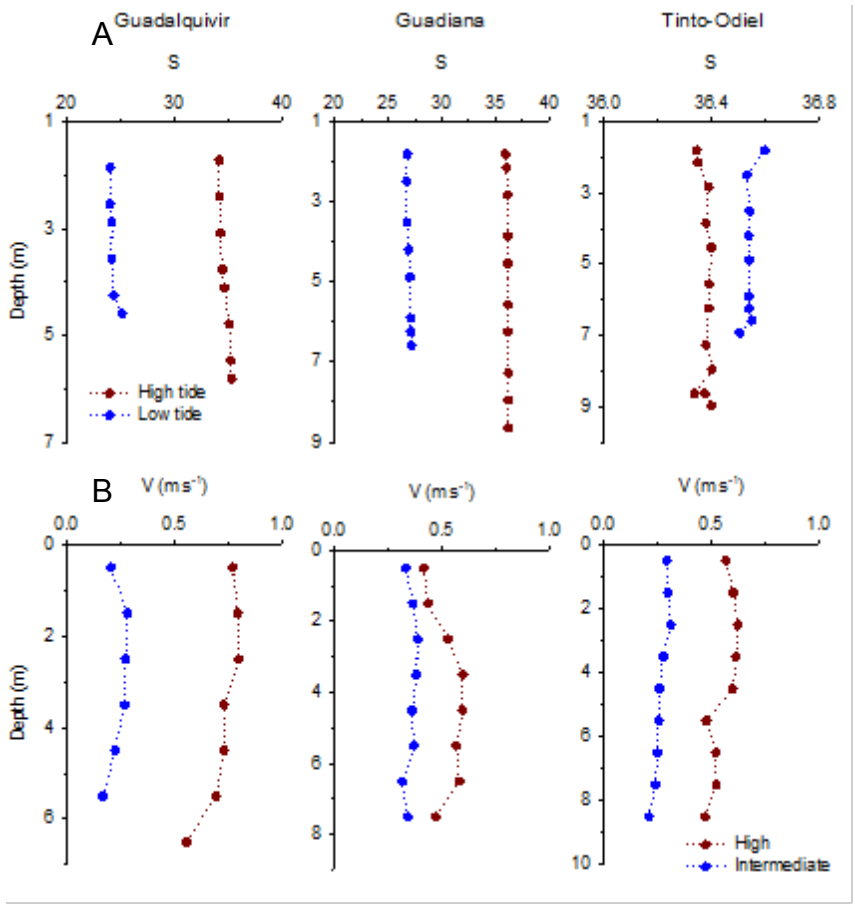

Figure S1. Vertical profiles of salinity (A) and current velocity (B) during the tidal study for each estuary.

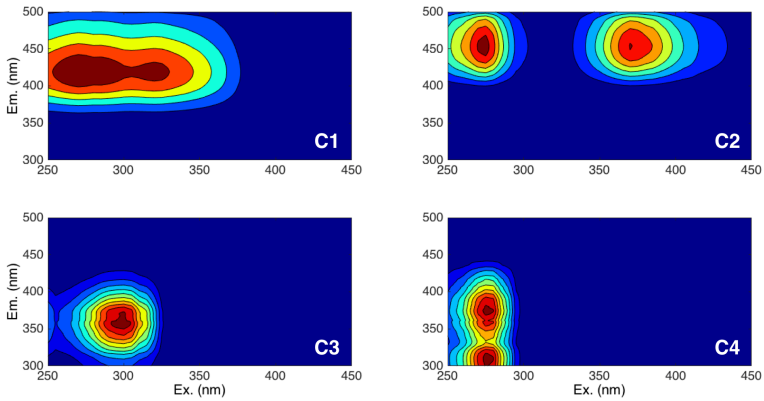

Figure S2. Fluorescent components identified using PARAFAC. C1 and C2: humic-like, C3 and C4: protein-like.

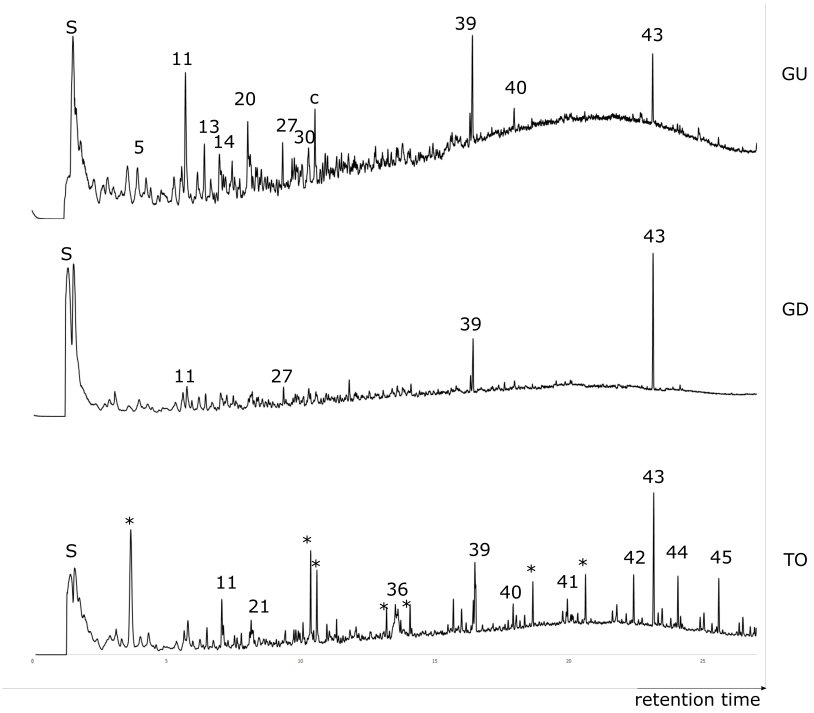

Figure S3. Py-MS-GC chromatograms for Guadiana (GU), Guadalquivir (GD) and Tinto-Odiel (TO). Peak labels correspond to pyrolysis products numbers in Table S2. S=inorganic sulfur, c=system contamination, *=other alkyl compounds not listed in Table S2.

Table S1. Spectral characteristics of excitation (Ex.) and emission (Em.) maxima of the four components validated by PARAFAC modeling (n = 150). Matching with Openfluor database with a Tucker congruence coefficient higher than 0.96 are shown (*TCC = 0.95).

	Ex/Em	OpenFluor	Ex/Em	Description	Environment
C1	270-320/419	C2, Chen et al. 2018	260 (305)/404	Marine humic-like	Artic Sea water
		C2, Murphy et al. 2006	320/414	Marine humic-like	Atlantic and Pacific Ocean
		C3, Yamashita et al. 2010	> 260 (> 315)/421	Microbial humic-like	Tropical rivers
			260 (320)/ 425	Humic-like, fulvic acids	Watersheds
		C1, Yamashita et al. 2011	-	Ubiquitous, autochthonous and allochthonous	Antarctic lakes
		C415, Kida et al. 2019	240 (310)/429	Peak A+M, terrestrial	Mountain streams
			-	Terrestrial	Lakes
		C1, Garcia et al. 2015	260 (305)/ 416	Terrestrial (humic and fulvic)	Everglades
		C2, Li et al. 2016	260 (311)/411	Ubiquitous	Pantanal
		C3, Yamashita et al. 2011	-	Humic-like	Lena River
		C1, Murphy et al. 2018	(>260) 310/414	Marine and terrestrial, peak M.	Pacific and Atlantic Ocean
		C1, Gonçalves-Araujo et	240 (329)/400	Humic-like, terrestrial	Groundwater

al. 2015	< 260 (305)/416	Humic and fulvic-like	Wetlands
P1, Murphy et al. 2008	< 250 (310)/432	Terrestrial	Artic Rivers
C2, Kulkarni et al. 2017	-	Microbial humic-like	Patagonian aquatic systems
C3, Yamashita et al.	< 250 (320)/422	Terrestrial humic-like	River
2010	< 240 (315)/420	Terrestrial humic-like	Streams
C1, Walker et al. 2014	315/436	Humic-like	Estuary
C1, Garcia et al. 2019	< 250 (310)/414	Humic and fulvic-like	Subtropical coastal lagoon
C430, Wünsch et al.	< 240 (310)/425	Terrestrial, fulvic acid type	Coastal system
2018	< 250 (320)/428	Terrestrial, ubiquitous	Artic Ocean
C1, Graeber et al. 2012	< 290/400-500	Terrestrial, humic-like	Water treatments
C1, Bittar et al. 2016	< 260 (305)/412	Marine humic-like	Coastal system
C1, Amaral et al. 2016	< 240 (305)/412	Peak A+M	Temperate lakes
C3, Brym et al. 2014	-	Terrestrial, humic-like	Water treatments
C1, Walker et al. 2009	270 (320)/411	Ubiquitous, autochthonous	Gulf of Cádiz
C1, Shutova et al. 2014		and allochthonous	
C1, Yamashita et al.			
2013			

		C1, Cardenas et al. 2017 C1, Peleato et al. 2016 C1, Amaral et al. 2020			
C2	275 (370)/454	C3, Chen et al. 2016 C2, Stedmon et al. 2011 C2, Bittar et al. 2016 C3, Amaral et al. 2020	275 (370)/ 452 315/384 270 (380)/ 476 275-370/446	Terrestrial humic-like Freshwater impact by agriculture Humic and fulvic-like Terrestrial humic-like	Artic ocean sediments Groundwater Estuary Gulf of Cádiz
C3	300/358	C4, Schittich et al. 2018 C3, Catalá et al. 2015 C3, Amaral et al. 2016 C6, Murphy et al. 2011 C2, Amaral et al. 2020	300/350 298/343 300/340 290/352 300/359	Protein-like Tryptophan-like Tryptophan-like Protein-like, Tryptophan-like Protein-like, Tryptophan-like	Groundwater Global dark ocean Coastal subtropical lagoon Recycled wastewaters Gulf of Cádiz
C4	275/311	C3, Kowalczuk et al. 2013 C5, Amaral et al. 2020*	275/325 (349) 280/317 (378)	Bound to proteins Mixture of protein and PAH-like	Ocean Gulf of Cádiz

Table S2. Pyrolysis product list, with retention time (RT), ion fragments used for quantification (m/z) and compound classes (MAH/PAH = monocyclic/polycyclic aromatic hydrocarbon, MCC = methylene chain compounds). Label (Fig. S3)

Label	Pyrolysis product	RT (min)	m/z	Class
1	pyridine	2.713	79	N-compounds
2	pyrrole	2.780	67	N- compounds
3	toluene	2.895	91+92	MAH
4	acetamide	3.307	59	N- compounds
5	C2-benzene	4.015	91+106	MAH
6	propionamide/alkanoic acid	4.332	73	Other
7	C2-benzene	4.335	91+106	MAH
8	2-methyl-2-cyclopentenone	4.508	67 (96)	Carbohydrate
9	C3-benzene	5.232	105+120	MAH
10	phenol	5.634	94+66	Phenol
11	C3-benzene	5.790	105+120	MAH
12	C3-benzene	6.240	105+120	MAH
13	2,3-dimethyl-2-cyclopentenone	6.505	67 (110)	Carbohydrate
14	C1-phenol	6.739	107+108	Phenol
15	trimethylcyclopentenone	6.854	109+124	Carbohydrate
16	C1-phenol	7.066	107+108	Phenol
17	guaiacol (T)	7.279	124+109	Lignin
18	unidentified cyclopentenone	7.528	67 (X)	Carbohydrate
19	C2-phenol	8.166	107+122	Phenol
20	C1-indene	8.191	130+115	PAH
21	C4-benzene	8.234	119+134	MAH
22	C1-indene	8.291	130+115	PAH

23	C2-phenol	8.472	107+122	Phenol
24	C2-phenol	8.618	107+122	Phenol
25	naphthalene	8.747	128	PAH
26	C2-phenol	8.851	107+122	Phenol
27	C3-1H-pyrrole-2,5-dione	9.401	67 (139)	Carbohydrate
28	C1-naphthalene	10.330	142+115	PAH
29	indole	10.340	117+90	N- compounds
30	C1-naphthalene	10.584	142+115	PAH
31	C4-phenol (T)	11.202	135+150	Phenol
32	trimethylindene	11.404	143+158	PAH
33	trimethylindene	11.497	143+158	PAH
34	trimethylindene	11.715	143+158	PAH
35	4-vinylguaiacol (T)	12.110	135+150	Lignin
36	dichlorobenzoic acid	13.531	173+192	Other
37	diketodipyrrole	15.550	186+93	N-compounds
38	C14 fatty acid	15.984	60+73	MCC
39	N-butylbenzenesulfonamide	16.349	141+170	Plasticizer
40	C16 fatty acid	17.999	60+73	MCC
41	C18 fatty acid	19.867	60+73	MCC
42	alkyl compound	22.419	69+83	MCC
43	isooctylphthalate	23.146	149+167	Plasticizer
44	alkyl compound	24.069	69+83	MCC
45	alkyl compound	25.595	69+83	MCC
46	alkyl compound	27.011	69+83	MCC
47	alkyl compound	28.350	69+83	MCC
48	alkyl compound	29.882	69+83	MCC

Capítulo 4

"Somewhere, something incredible is waiting to be known.".
Carl Sagan

Dissolved free amino acids in estuarine systems: Sources, distribution and implication for DOM reactivity*

V. Amaral[1,2*], J. Forja[1], B. Mähnert[3], G.J. Herndl[3,4] and C. Romera-Castillo[5]

[1]Departamento de Química-Física, INMAR, Universidad de Cádiz, Puerto Real, España
[2]Ecología Funcional de Sistemas Acuáticos, Centro Universitario Regional Este, Universidad de la República, Rocha, Uruguay
[3]University of Vienna, Department of Functional and Evolutionary Ecology, Bio-Oceanography and Marine Biology Unit, Vienna, Austria
[4] Department of Marine Microbiology and Biogeochemistry, NIOZ, Royal Netherlands Institute for Sea Research, Utrecht University, The Netherlands
[5]Instituto de Ciencias del Mar-CSIC, Barcelona, España

Submitted to Organic Geochemistry

Abstract

Dissolved organic matter (DOM) is one of the largest reservoirs of reduced carbon on the Earth. The input of DOM by rivers to the oceans occurs primarily via estuaries. Dissolved amino acids represent the most labile fraction of DOM, and variations in their relative abundance offer a powerful tool for determining the composition and diagenetic state of DOM. We analyzed the distribution of dissolved free amino acids (DFAA) in three estuaries from the southern Iberian Atlantic basin: Guadalquivir, Guadiana, and Tinto- Odiel. DFAA concentrations were measured along the salinity gradients and during a complete tidal cycle. We found similar DFAA concentration between estuaries and zones (coast versus estuary interior) ranging from 176.6 nM to 1772.7 nM. However, we found differences in the relative abundance (mol %) of individual amino acids (AAs) between estuaries and zones indicating different degrees of DOM alteration. In the coastal zone, the predominant AAs (≥ 10 mol %) were the same: serine, glycine and the non-protein AAs (NPAAs) ornithine, indicative of an increasing extent of degradation. In the estuaries, acidic AAs were among the predominant AA and their contribution increased due to the terrestrial runoff, lateral input from the surrounding watersheds, agricultural and industrial activities at the estuaries' margins. Among the molecular proxies based on AAs, the degradation index and the relative abundance of NPAAs were not appropriate to differentiate the diagenetic state of DOM in our systems, probably due to the several sources of DOM and relatively high water renewal time. Our results further suggest that estuarine DOM is less diagenetically altered than coastal DOM, tidal cycles exert an influence on AA distribution and changes in DOM degradation are reflected in chromophoric and fluorescent DOM composition. The source of DOM and

microbial degradation are important processes in determining the distribution of AAs in coastal systems.

Keywords: Amino acids, DFAA, DOM, estuaries, Gulf of Cadiz

IV. 1. Introduction

Dissolved organic matter (DOM) in the ocean is one of the largest and most dynamic reservoirs of reduced carbon on the Earth (Hedges, 2002) with an estimated stock comparable to the amount of CO_2 in the atmosphere (662 Pg, Hansell et al., 2009). Rivers transport ~0.25 Pg y^{-1} of dissolved organic carbon (DOC) from continents to the ocean (Hedges et al., 1997) primarily via estuaries representing a significant fraction in the global carbon budget (Raymond and Spencer, 2015). Traditionally, riverine DOM is considered recalcitrant and conservatively transported to the ocean (Bauer and Bianchi, 2011). However, estuaries are complex ecosystems with allochthonous and autochthonous sources of DOM (Cauwet et al., 2002). Several factors such as anthropogenic pollution, land use, and microbial metabolism, as well as the presence of wetlands and salt marshes can significantly alter the composition and reactivity of DOM before it reaches the coastal zone (Abril et al., 2002; Benner and Opsahl, 2001; Jaffé et al., 2004). The sources and cycling of estuarine DOM is thus a key component of the global carbon cycle.

Heterotrophic microorganisms rapidly utilize freshly produced DOM thus, the reactive components are selectively removed, inorganic nutrients are regenerated and an enrichment of less reactive components occurs (Benner, 2003; Wakeham et al., 1997; Lee et al., 2004). Therefore, the extent of degradation of the DOM is a predictor of its further reactivity

(Dauwe et al., 1999). Amino acids (AAs) derived mainly from living organisms represent the most labile fraction of DOM and are tightly coupled to the metabolism of organisms. Therefore, variations in the concentration and the relative abundance of AAs offer a powerful tool for determining the composition and diagenetic state of organic matter (e.g. Jorgensen 1982, Coffin, 1989, Davis et al. 2009). For example, carbon-normalized yields of AAs are good indicators of DOM ‘‘freshness” and diagenetic state since they are preferentially utilized during biodegradation (Keil et al., 2000; Amon and Fitznar, 2001; Benner, 2002). In contrast, non-protein amino acids (NPAAs) such as β-alanine, γ-aminobutyric acid (GABA), and ornithine are thought to be largely diagenetic in origin since they are produced enzymatically during decay processes from other AA precursors such as aspartic acid, glutamic acid, and arginine, respectively (Cowie and Hedges, 1994). As a result, NPAAs have also been used as an index of organic matter degradation (Lee and Bada, 1977; Cowie and Hedges, 1994). Amino acids have been measured in marine and estuarine waters since the 1970s (e.g. (Coffin, 1989; Jørgensen, 1982; Lindroth and Mopper, 1979). Dissolved “free” amino acids (DFAA) are measured directly in filtered water and are thought to represent monomeric AAs present in a sample while “total hydrolysable” (THAA) and “total dissolved” amino acids (THAA and TDAA, respectively) are measured from filtered water treated with acid (Lee and Bada, 1977, 1975). The difference between THAA and DFAA represents dissolved combined amino acids (DCAA), the fraction of amino acids bound as proteins, peptides, and other amino acid polymers. Most DFAA are derived from the heterotrophic breakdown of peptides and proteins in particulate organic matter and DOM. Estuarine and coastal DOC is almost always dominated by DCAA with DFAA concentrations

being typically substantially lower, since microorganisms preferentially utilize DFAA (Bauer and Bianchi, 2011; Coffin, 1989). A large percentage of bacterial production can be supported by DFAA uptake in estuaries (Keil and Kirchman, 1991), with some AA being more labile than others (Dauwe et al., 1999). For example, aromatic AAs, such as tryptophan, tyrosine and phenylalanine, along with glutamic acid and arginine, decay more rapidly than some of the more refractory species such as glycine, serine, alanine, and lysine (Dauwe et al., 1999; Cowie and Hedges, 1992).

DFAA have been shown to be important sources of C and N to microbial communities in estuarine and coastal systems (e.g. Crawford et al., 1974; Keil and Kirchman, 1991). To date, the majority of studies of the dynamics of dissolved AAs has focused on THAA, probably due to their higher concentrations (e.g. Mai-Thi et al., 2017; Mannino and Harvey, 2000; Yamashita et al., 2015; Yamashita and Tanoue, 2003). Most studies were performed in the oceanic environments (e.g. Reinthaler et al., 2008; Sarmento et al., 2013) and fewer studies have analyzed DFAA in estuarine systems (e.g. Jørgensen, 1982, Coffin et al., 1989).

The aim of this study was to analyze the distribution of DFAA in three estuaries of the Gulf of Cadiz: Guadalquivir, Guadiana and Tinto-Odiel. These estuaries differ in terms of their morphology and hydrology, as well as in their dominant basin vegetation, land use and DOM composition (Amaral et al., 2020). This study presents the concentration of DFAA along three salinity gradients and a tidal cycle study in each estuary using some of the AA species as proxies of the diagenetic state of DOM. It also investigates the relationship between the dynamics in DFAA and the chemical characteristics of DOM present in these estuaries using optical properties (absorbance and fluorescence) (Amaral et al., 2020).

IV. 2. Material and Methods

IV. 2.1 Study site

The sampling was carried out in three estuaries located on the Gulf of Cadiz: Guadalquivir, Guadiana, and Tinto-Odiel (Fig. 1).

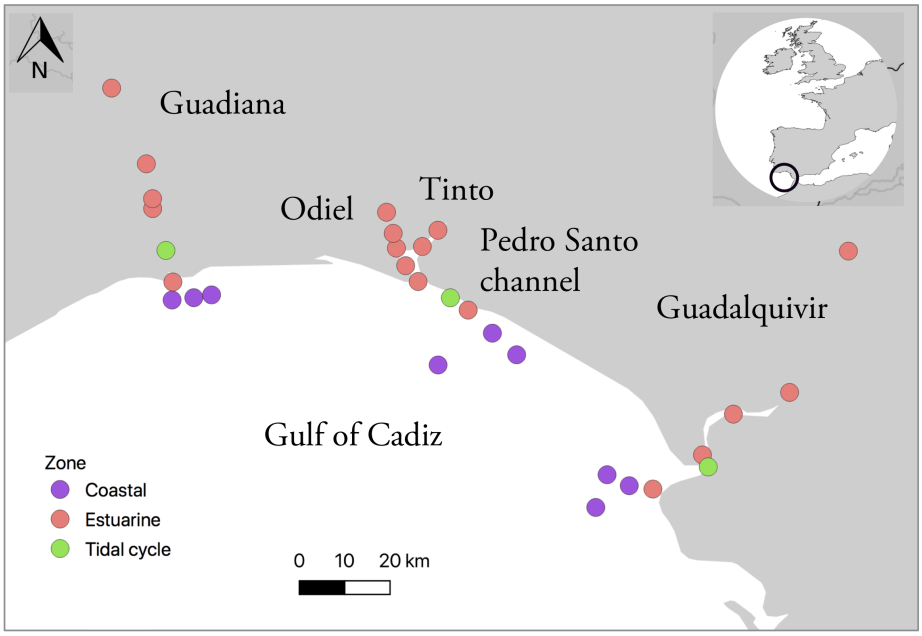

Fig. 1. Map with the samples stations in the Guadalquivir, Guadiana and Tinto-Odiel transect. Tinto-Odiel estuary comprises three parts: Tinto River, Odiel River and the common marine part named Padre Santo channel.

These river basins are located within the Mediterranean climate region, a semi-arid environment, and regulated by dams. The three estuaries are affected by a tidal cycle showing a semi-diurnal periodicity and a mesotidal regime with a maximum tidal range of ~3.3 m (spring tides) and an average of 2 m (Carro et al., 2018; Morales and Garel, 2018; Rodriguez-Ramirez et al., 2019). Guadalquivir river discharge is the highest among the investigated estuaries with an annual mean of 164 $m^3 s^{-1}$ (Rodriguez-Ramirez et al., 2019). The annual discharge of the Guadiana river is generally low (< 50 $m^3 s^{-1}$) (Garel and Cai, 2018) but highly variable with severe droughts and

episodic flood events in the lower part of the estuary (Garel et al., 2009). Guadalquivir estuary is surrounded by an extensive wetland area and its middle zone is dominated by intertidal salt marshes (Rodriguez-Ramirez et al., 2019). This river is subjected to elevated anthropogenic pressure due to densely populated areas on its margins (4.2 million people) as well due to agriculture and aquaculture industries and a high demand of freshwater for irrigation. Guadiana is a rock-bound estuary and consists in a single narrow channel (50–700 m wide) (Morales and Garel, 2018). Salt marshes are highly reduced due to the strong anthropogenic pressure, but an extensive wetland area (~ 1000 ha) surrounds its mouth (Ménanteau et al., 2005). The Tinto-Odiel estuary extends 35 km from its mouth towards the upstream tidal limit (Carro et al., 2018) and is composed by two rivers: Tinto and Odiel. These two rivers have a short length of 100 km and 140 km and the mean rivers discharge is normally < 10 m^3 s^{-1} (Carro et al., 2018). They converge in a common marine area called Padre Santo channel, which flows to the Gulf of Cadiz. The fluvial basin of both rivers mainly lies on top of a volcano-sedimentary area and flows through the Iberian Pyrite Belt complex that contains the largest polymetallic sulfide deposits in the world (Leblanc et al., 2000). The Tinto-Odiel estuary is one of the most polluted estuaries in the world due to mining activity that led to severe pollution of its water, which now contain high concentrations of heavy metals and extremely low pH values (< 3, Grande et al., 2000). Consequently, the mixing of acidic waters from mines, industrial effluents, and seawater leads to significant changes in the chemical composition of the water (Carro et al., 2018).

IV. 2.2 Field sampling

Surface water samples were collected in July 2017 onboard the R/V UCADIZ. In the inner part of the Tinto-Odiel estuary we used an auxiliary

boat. We performed a transect along a salinity gradient including stations in the coastal zone and a tidal study (Fig. 1). We divided the samples into coastal (external stations) and estuarine samples. Samples for the tidal study were collected during two tidal cycles at a fixed station at the mouth of each estuary during low and high tide (green dots, Fig. 1). Surface water samples were taken with Niskin bottles (10L) mounted on a rosette-sampler coupled to a CTD Seabird 25 measuring temperature and salinity.

IV. 2.3 Amino acid analysis

IV. 2.3.1 L-Amino acids

Samples were filtered using 0.2 µm polycarbonate filters and stored at -20°C until further analysis. We used high-pressure liquid chromatography (HPLC) and fluorescence detection after pre-column ortho-phthaldialdehyde (OPA) derivatization according to Taubner et al. (2019). This method is applied to samples where the ammonia concentration immensely exceeds the DFAA concentrations. All the measured AAs and their abbreviations are shown in Table 1. Analyses were conducted by duplicate on an Agilent 1260 Infinity Bioinert HPLC system consisting of an autosampler, a quaternary pump, a column oven and a fluorescence detector. For peak identification and quantification, a primary amino acid standard mix was prepared for each run (AAS18, Sigma Aldrich). β-alanine, asparagine, γ-aminobutyric acid, glutamic acid, ornithine, taurine and tryptophane (Sigma Aldrich) were added to the AAS18 standard mix in known concentrations. Borate buffer (75 µl, 0.4 N in water, pH = 10.2, Agilent Technologies) was added by the autosampler to 1 ml sample and mixed. Thereafter 5 µl of OPA reagent (10 mg mL^{-1} o-phthalaldehyde and 3-mercaptopropionic acid in 0.4 mol L^{-1} borate buffer; Agilent

Technologies) was added to the mixture. After 2 min derivatization time at 27°C, 500 µl of the mixture were injected to the HPLC system.

Table 1. Measured amino acids by groups and abbreviations used in this study.

Amino acid	Abbreviation
Neutral Aliphatic - R-groups	
Glycine	Gly
Alanine	Ala
Valine	Val
Leucine	Leu
Isoleucine	Ile
Neutral –Hydroxyl and Sulfur R-groups	
Serine	Ser
Threonine	Thr
Methionine	Met
Acidic Amino Acids and Their Amides	
Asparagine	Asn
Aspartic Acid	Asp
Glutamic Acid	Glu
Glutamine	Gln
Basic Amino Acids	
Lysine	Lys
Arginine	Arg
Histidine	His
Aromatic Amino Acids	
Phenylatanine	Phe
Tryptophan	Trp
Tyrosine	Tyr
Non-protein amino acids	
γ-aminoglutaric acid	GABA
β-alanine	β- Ala
Ornithine	Orn
Amino sulfonic acid	
Taurine	Tau

Amino acids were separated using the gradient of Taubner et al. (2019): NaH_2PO_4 buffer and methanol-trifluoroacetic acid-water mix (HPLC grade) within 90 min. Tetrahydrofuran was used to improve

separation of individual components, especially between methionine and valine. Trifluoroacetic acid was added as an ion-pairing agent to improve peak shape and thus, reduce the broadening. The fluorescence was measured at 340 nm excitation and 450 nm emission wavelengths at gain factor 12.

IV. 2.3.2 D-Amino acids

We applied the pre-column derivatization method of Reinthaler et al. (2008) combined with gradient and column types described in Taubner et al. (2019). Single D-AA standards (Carl Roth) were calculated and pooled together to one standard row for each sample batch. All other system settings were same as applied for L-AA described above.

IV. 2.4 Calculation of AA-based indices of DOM diagenesis

DFAA concentrations were calculated as the sum of the concentration of individual AAs (nM) measured in this work (Table 1). Amino acid comprises a major portion of freshly produced DOM (Davis et al., 2009). Since microorganisms readily utilize them, their relative contribution to the total DOM reservoir decreases during the early stages of decomposition (Davis et al., 2009). Thus, carbon-normalized yields of AAs (AA-C) have been used as qualitative indicators of DOM freshness (Benner, 2003; Davis et al., 2009; Yamashita and Tanoue, 2003). The AA-C yields were calculated as the AA carbon (in nM) divided by bulk of DOC concentration (in nM), which was taken from Amaral et al. (2020). The relative abundance (mol %) of individual AAs (AA concentration (nM)/sum of all DFAAs (nM) x 100) was used to identify diagenetic trends and also to calculate other degradation indices. We calculated the degradation index (DI) (Eq. 1) proposed by Dauwe and Middelburg (1998) in particulate and sediment studies which reflects progressing diagenesis. Later, DI was applied

to marine and groundwater DOM samples (Davis et al., 2009; Kaiser and Benner 2009; Peter et al., 2012).

$$DI = \sum_i \left(\frac{var\ (i) - AVGvar\ (i)}{STDvar\ (i)}\right) \times fact.coef\ (i) \quad (1)$$

where var, AVGvar and STDvar are the molar percentage of AA, the mean molar percentage and the standard deviation of the AA in the sample, respectively. The factor coefficient is the PCA AA score obtained from marine DOM samples (Davis et al., 2009; Kaiser and Benner, 2009). This index is a variance-based statistical model that uses the changes in AA composition to determine the overall degradation status of organic matter. The AAs used to calculated DI were Asp, Asn, Glu, Ser, His, Gly, Thr, Arg, Ala, Tyr, Val, Phe, Ile, Leu y Lys. We also used the mol % contribution of the NPAAs β-alanine and GABA, which are produced enzymatically during decay processes from the precursors aspartic and glutamic acid, respectively, and the ratio of D and L- AA (D/L) as a AA-based diagenetic indicator of DOM. The enrichment of NPAAs indicates the aging and advanced diagenesis status of the DOM (Cowie and Hedges, 1994). Therefore, elevated concentrations (e.g. > 1%) can be used to infer the diagenetic status (Cowie and Hedges, 1994, Davis et al., 2009). D-amino acids are major and specific components of bacterial cell wall complexes and thus are valuable biomarkers for bacterial-derived organic matter in the environment (Pérez et al., 2003, Kaiser and Benner, 2008). Table S1 summarizes the AA-based indicators of DOM degradation used in this work.

IV. 2.5 Statistical Analysis

We used the analysis of variance ANOVA (two way) to assess spatial differences between estuaries and zones in DFAA and AAs based molecular indicators. We performed simple linear regression to assess the relationship between AAs and salinity as well as other DOM variables described in previous work (Amaral et al., 2020). All analyses were performed in R 3.5 software (R Development Core Team, 2018).

IV. 3. Results and Discussion

IV. 3.1 Longitudinal distribution AAs: differences among estuaries

The concentration of individual DFAA ranged from 0.28 to 421.9 nM with similar values between estuaries and zones (Table S2A and S2B, $p > 0.05$) except for Tau, the acidic amino acids Glu and Gln exhibiting higher concentrations in the estuarine zone of Tinto-Odiel than the other estuaries (Fig. 2, $p < 0.05$). The concentration of DFAA was similar between estuaries and zones (Table 2, $p > 0.05$). The highest DFAA concentration was observed in the middle zone of Guadalquivir estuary (1772.7 nM) while the lowest occurred in the coastal zone of Guadiana (170.6 nM) (Fig. 3). The DFAA values were in the range of those observed in other estuaries (e.g. Coffin, 1989, Jørgensen, 1982) and higher than typical concentrations for open ocean and coastal systems (e.g. Hammer and Kattner, 1986; Sarmento et al., 2013). The concentration of DFAA was highly variable along the salinity gradient in the three estuaries, showing a non-linear relationship with salinity ($R^2 < 0.1$, $p > 0.01$, Fig. S1). This suggests several sources of DFFA as observed in other estuaries and coastal zones as well (e.g. Coffin 1989).

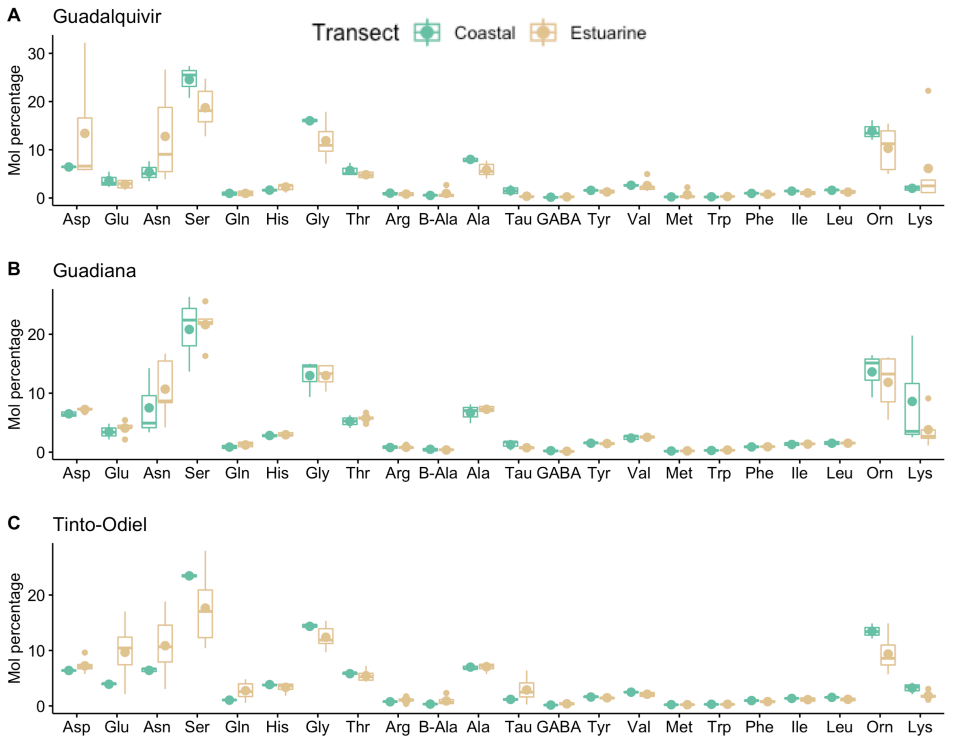

Fig. 3. Relative contribution (mol percentage) of amino acids to the total bulk of DFAA in the coastal and estuarine zone of Guadalquivir, Guadiana and Tinto-Odiel estuary.

IV. 3.1.1 Comparison of the relative contribution of AAs between estuaries

In the coastal zone of the three estuaries, the predominant AAs (present at ≥ 10 mol %) were the same: Ser, Gly and the NPAA Orn, together making up almost half of the total DFAA pool. These AAs together with Glu and Ala are generally reported to be among the most abundant AAs in seawater (e.g. Jorgensen, 1982; Hammer and Kattner 1986; Keil and Kirchman 1999). Ser and Gly have been shown to be concentrated in the silicious exoskeletons of diatom cell walls (Hecky et al., 1973) and are considered comparatively recalcitrant (Jorgensen, 1982; Cowie and Hedges, 1992). Protection by the silicious exoskeletons may render Ser and Gly less easily degraded by bacteria and it has been proposed as a mechanism for

their preservation (Siezen and Mague 1978; Nguyen and Harvey 1997). The relative enrichment of Gly is indicative of an increasing extent of biodegradation (Amon and Fitznar, 2001; Yamashita and Tanoue, 2003). Moreover, the NPAAs, such as Orn, are primarily alteration products of protein amino acids and tend to concentrate as diagenesis progresses (Cowie and Hedges, 1994). Orn is produced enzymatically during decay processes from the precursor Arg and it is relatively absent or at trace concentrations in organisms (Cowie and Hedges, 1994). Thus, elevated concentrations of Orn may also indicate diagenetic alteration of DOM. The dominance of Ser, Gly and Orn in the DFAA pool of the coastal zone in the three estuaries suggests that degradation might be the major factor controlling the concentration and composition of DFAA in the bulk DOM.

In the estuaries, the predominant DFAA species differed from those observed in the coastal zone (Fig. 3), suggesting a different degree of DOM alteration than the coastal zone. Despite Ser and Gly were the major contributors, the acidic AAs Asn, Asp and Glu increased in their contribution and appeared within the predominant AAs in the estuarine zone. The mol % of Asn increased in three estuaries, Asp in Guadalquivir and Glu in Tinto-Odiel. Asn has been found to be among the dominant AAs in terrestrial DOM (Berggren et al., 2010), associated to vegetation (Sieciechowicz and Ireland, 1988, Ireland and Lea, 1999) including macrophytes (Muztar et al., 1977), and preferentially consumed by bacteria in degradation experiments (Berggren et al., 2010). This could explain the increase in the mol % of Asn within estuaries as salinity decreased. In fact, in Guadalquivir and Guadiana, a negative relationship was observed between the mol % of Asn and salinity ($R^2 = 0.66$, $p < 0.01$, Fig. S1), suggesting a terrestrial origin of this AA in agreement with previous work (Berggren et al.,

2010). These results are consistent with the observation that in Guadalquivir and Guadiana, terrestrial DOM dominates the bulk DOM pool (Amaral et al., 2020). Additionally, Asn has been observed in various living crops, especially in pulse and cereals (Saio and Kimura, 1956), widely distributed in the margins of Guadalquivir (Carrasco et al., 2010) and also identified as main source of allochthonous DOM along this estuary (Amaral et al., 2020). Therefore, lateral inputs of DOM from agricultural soil could be a significant source of Asn in Guadalquivir estuary.

In contrast, the estuarine zone of Guadiana showed almost the same pattern in the relative contribution of AAs than its coastal zone (Fig. 3). This could be related to the different mixing behavior of DOM between Guadalquivir and Guadiana (Amaral et al., 2020). In Guadiana, dilution and physical mixing were the major factors explaining spatial variability as DOM from fresh and coastal waters mix along the estuary with DOM input from salt marshes near Guadiana mouth (Amaral et al., 2020). This is consistent with our observations since in Guadiana, the mol % of Asn was highest (~16 %) in the estuarine zone but increased also towards the mouth of the estuary (Fig. 2S). This may be originated from the input of organic matter from vegetation present in the Natural Park "Marismas de Castro Marim y Vila Real de Santo Antonio" located at the mouth of this estuary (www.chguadiana.es).

In the estuarine zone of Tinto- Odiel, Asn and Glu were among the predominant AAs accounting together with Ser and Gly for 51% of the total DFAA pool (Fig. 3). It should be noted that the salinity gradient in the Tinto-Odiel estuary barely exceeds two units and that this system comprises different parts (Tinto River, Odiel River, and the common marine area Padre Santo channel, Fig. 1). A major increase in the mol % of Asn (> 14%)

was observed in the fluvial zone of this estuary, probably associated with the presence of vegetation regardless of their origin (terrestrial/aquatic) (Fig. 2S). In the common marine area (Pedro Santo channel), the predominant AAs contributing 50% to the total DFFA pool are the same as those found in the coastal zones of the estuaries (Gly, Ser and Orn). In contrast, in the river transects the predominant AAs were Ser, Asn, Glu and Gly, indicating that the change observed in the relative contribution of the AA species is related to process/es occurring in the most "fluvial" zone. Glu is the precursor of Gln and it is a way of nitrogen storage, particularly in brown, red and green algae (Fattorusso and Piatelli, 1979). Glu was also among the major constituents in proteins in several macrophyte species (Muztar et al., 1977), it was also found to dominate fresh DOM in sea ice, mostly produced by algae (Amon and Fitzar, 2001) and bacteria (Gardner and Hanson, 1979), and it decreased rapidly in DOM degradation experiments (Amon and Fitzar, 2001). Our results indicate the presence of fresh DOM in the estuarine zone of Tinto-Odiel, in particular related to the river transects. Moreover, as previously mentioned, the individual concentration of Glu was significantly higher in this estuary than in the other estuaries (Fig. 2, $p < 0.05$). This could be associated with differences in the character of DOM, which in Tinto-Odiel, unlike Guadalquivir and Guadiana, is predominantly autochthonous (Amaral et al., 2020). However, differences in the AA composition within the estuary reveal also the importance of allochthonous sources of DOM composition in this estuary. The Tinto-Odiel estuary is one of the most polluted estuaries in the world due to the mining of the massive sulfide deposits in its basin and the industrial activities taking place in its margins (Davis Jr et al., 2000). Individual concentrations of Tau were also significantly higher in Tinto-Odiel than Guadalquivir and Guadiana

estuaries (Fig. 2, $p < 0.05$). In particular, Tau increased in the river transects above the Pedro Santo channel (Fig. 1).

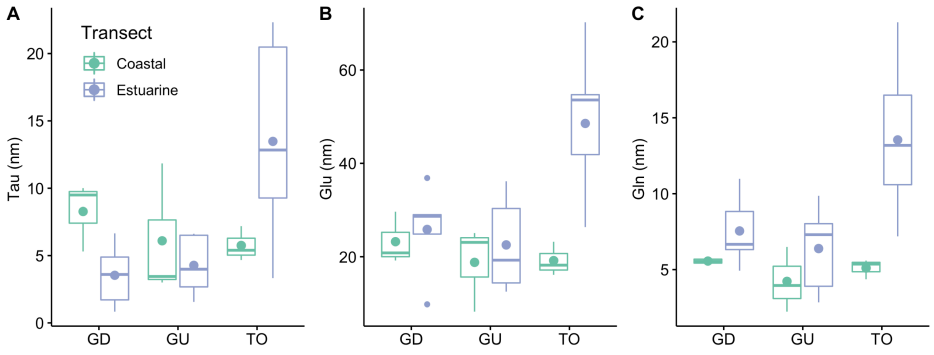

Fig. 2. Boxplot of A: taurine (Tau), B: glutamic acid (Glu) and C: glutamine (Gln) concentration in the coastal and estuarine zone of Guadalquivir (GD), Guadiana (GU) and Tinto-Odiel (TO).

Tau is a non-protein organic acid with a sulfonic group instead of the carboxyl group characteristic for amino acids and can be used as a sulfate source by bacteria (Van der Ploeg et al., 1996). The uptake of organic sulfur compounds from seawater, such as Tau, may decrease when inorganic sulfate is elevated. For example, Tinto-Odiel transports high concentrations of sulfate as a consequence of intensive mining of the massive sulfide deposits that has occurred historically in their basin, where mean concentrations of 1200 mg L^{-1} of sulfate have been observed (Olías et al., 2004). This could explain the higher concentration of Tau observed in Tinto-Odiel compared to the other estuaries. Also, Tau could be synthesized using Ser combined with sulfur-derived from sulfate by marine algae (Tevatia et al., 2015). These authors observed that sulfate supplementation increased Tau concentrations in algal experiments. Therefore, this could be also the reason for the increase in Tau concentration in the section of Tinto-Odiel rivers. Regardless of the mechanism behind the higher concentrations of Tau in Tinto-Odiel than in

the other estuaries, it is probably related to the influence of anthropogenic activities in this estuary.

The differences observed in the relative abundance of AAs between the coastal and estuarine zones might be related with changes in DOM sources and transformations during the transit along the estuaries. Our result further suggests that estuarine DOM is less diagenetically altered than coastal water DOM. Thus, as DOM is transported toward the coastal zone, alteration increases and degradation is the major factor controlling DFAA distribution in the coastal zone. Moreover, it is evident that the differences observed in DOM behavior between the three estuaries (Amaral et al., 2020) were also reflected in the AAs distribution. The DFAA composition in the Tinto-Odiel estuary indicated a more autochthonous character of DOM that could be interpreted as more labile DOM in this estuary than in the others; however, our results suggest also the presence of labile DOM from allochthonous sources, in particular in Guadalquivir. Thus, terrestrial DOM could be more labile than previously thought.

IV. 3.1.2 Amino acid based molecular indicator of diagenetic DOM alteration

The AA-C yields were similar between estuaries ($p > 0.05$) ranging from 0.06 to 1.57%. In general, higher AA- C yields are indicative of relatively fresh and bioreactive organic matter, whereas lower yields are indicative of more diagenetically altered and biorefractory material (Benner, 2002). Overall, AA-C yields appear to be most sensitive for tracking changes during the early stages of DOM degradation (Davis et al., 2009). The highest AA-C yields were observed in the estuarine zone of each estuary while the lowest were found in their coastal zone (Table 2). These results

reinforced the idea of DOM being more altered in the coastal zone than within the estuaries. Several molecular studies found that estuarine DOC is composed of both labile and recalcitrant material (Raymond and Bauer, 2000; Cauwet, 2002) where most of the labile fraction is degraded before being exported to the ocean.

Similar DI values were found among estuaries and zones ranging from -1.81 to 1.37 ($p > 0.05$, Table 2). Overall, we found higher DI values than those observed in other coastal and oceanic samples (Yamashita and Tanoue, 2003) suggesting a lower degree of DOM transformation in our estuarine systems. Noteworthy, Yamashita and Tanoue (2003) measured THAA. In our study, a clear pattern with salinity was not observed and we did not find a positive relationship between DI using DFAA concentrations or AA- C yields ($R^2 < 0.1$, $p > 0.05$) as it was observed in oceanic systems (Yamashita and Tanoue, 2003). Our observations are in agreement with Yamashita and Tanoue (2003) suggesting that the DI could be sensitive to variable sources of DOM and not suitable in systems with riverine input of terrestrial DOM, as it is the case for our estuaries. DI appears to be the most effective proxy of diagenetic alteration of DOM in intermediate stages of diagenesis on annual to decadal timescales (Davis et al., 2009). In our estuaries, water residence time is relatively high (12 and 18 days in the Guadiana and Guadalquivir estuary) (de la Paz et al., 2007; Vasconcelos et al., 2007). Our results are in agreement with the idea that DI is not appropriate to differentiate the diagenetic state of DOM in estuarine systems with several sources of DOM and relatively high water renewal rates.

Table 2. Mean ± standard deviation values and ranges (minimum-maximum) of dissolved free amino acid (DFAA) and amino acids molecular indicator in the coastal and estuarine zone of Guadalquivir, Guadiana and Tinto-Odiel estuary.

Transect	DFAA (nm)	AA-C yields	Degradation index	% β-ala	% GABA
Guadalquivir coastal	776.67 ± 480.15	0.47 ± 0.58	-0.18 ± 0.51	0.52 ± 0.13	0.17 ± 0.15
	351.23 - 776.67	0.10 - 0.58	-0.18 - 0.51	0.38-0.61	0.15 - 0.33
Guadalquivir estuarine	1052.79 ± 647.78	0.66 ± 0.52	-0.40 ± 0.86	0.92 ± 1.00	0.22 ± 0.12
	330.49 - 1772.66	0.35 - 1.57	-1.60 - 0.49	0.27-2.68	0.07 - 0.36
Guadiana coastal	671.45 ± 494.43	0.21 ± 0.18	0.21 ± 1.05	0.49 ± 0.37	0.25 ± 0.21
	170.63 - 1159.23	0.06 - 0.41	-0.69 - 1.37	0.22-0.91	0.07 - 0.48
Guadiana estuarine	585.34 ± 257.01	0.57 ± 0.31	0.44 ± 0.41	0.37 ± 0.14	0.16 ± 0.07
	230.22 - 873.92	0.14 - 0.98	0.05 - 0.92	0.16- 0.50	0.10 - 0.25
Tinto-Odiel coastal	490.46 ± 86.26	0.33 ± 0.19	0.34 ± 0.50	0.33 ± 0.10	0.16 ± 0.02
	399.43- 570.99	0.11- 0.48	-0.17- 0.83	0.23-0.42	0.14- 0.17
Tinto-Odiel estuarine	634.26 ± 326.37	0.45 ± 0.33	-0.16 ± 0.86	0.90 ± 0.74	0.38 ± 0.23
	318.48 - 1305.76	0.17 - 1.19	-1.81 - 1.12	0.23- 2.34	0.03 - 0.67

Regarding the NPAAs, the mean mol % of GABA and β-Ala was similar between estuaries and zones and accounted for < 1% of the total DFAA pool (Table 2, $p > 0.05$). The poor contribution of these NPAAs to the total DFAA pool together with the small variation observed in their distribution suggests that these AAs, such as DI, may not be appropriate to reflect changes in the degree of DOM alteration in our study system. This could also be related to the fact that NPAAs appear to be more promiment during the later stage of DOM diagenesis (e.g. > decades, Davis et al., 2009).

D-amino acids can be used as indicators of the bacterial contribution to DOM since they are commonly found in bacterial cell walls (Kaiser and Benner, 2008). However, the source of the free D-amino acids in marine environments needs to be further addressed since studies reveal that besides bacteria, many archaea and microalgae synthesize a large amount of free D-AAs during their growth (Zhang et al., 2016). In this work, we could only quantify three D-AAs: D-Ala, D- tyrosine and D-tryptophan, since the rest were below the detection limit (<1.5 nM). In fact, in most samples, D-Ala, D-Trp and D-Thr concentration were also below the detection limit, indicating a low contribution of bacterial DOM to the bulk DOM pool. This is consistent with the observations of DOM being mainly from terrestrial sources, especially in the Guadalquivir and Guadiana estuary (Amaral et al., 2020). Moreover, D-Ala was only found in the estuary zone of Tinto-Odiel, indicating the importance of bacterial activity in DOM composition in this estuary compared to the Guadalquivir and Guadiana estuary. D-Ala appears to be more widely distributed among bacterial biopolymers than other D-amino acids (e.g. Schleifer and Kandler 1972, Vanittanakom et al. 1986, Neuhaus and Baddiley 2003). Ratios of amino acid enantiomers (% D/L) correlate with DOM bioavailability (Jørgensen et

al., 1999), with low ratios indicating high DOM bioreactivity, while the relative enrichment of D-amino acid indicates DOM degradation (Amon and Fitznar, 2001). In the Tinto-Odiel estuary, D/L Ala was between 11% and 20%, indicating the presence of relatively fresh DOM (Amon and Fitznar, 2001), as it was also suggested by the composition of the predominant AAs and in previous DOM studies (Amaral et al., 2020).

Unlike their L form, D- Trp and D- Tyr are intrinsically resistant to microbial utilization and tend to accumulate in the water column as recalcitrant DOM (Jiao et al., 2014). We found D- Trp in the coastal zone of Guadiana and in the coastal and estuarine zone of Tinto- Odiel estuary, with mean D/L ratios of 45.7 % ± 1.7%, 55.8% ± 0.6 % and 54.0% ± 26.9 %, respectively, indicating the presence of bacterial reworked DOM. The most abundant D-AA was D-Tyr, which was found in the three estuaries and exhibited higher concentrations (up to 32.13 nM) than D-Ala and D-Trp (< 5.03 nM). D/L ratios of Tyr and Trp were between 34% and 65%. Overall, these findings indicate the presence of fresh but also recalcitrant DOM in the Tinto Odiel estuary, while in the Guadalquivir and Guadiana estuary the fraction of DFAA derived from microorganisms was relatively recalcitrant in nature.

IV. 3.2 Tidal cycles

Similar to the longitudinal transects, no significant differences were observed in DFAA concentration between estuaries (Table 3, $p > 0.05$). Overall, in the Guadalquivir and Guadiana estuaries, DFAA concentration showed highest concentrations during high tide and lowest at low tide.

The predominant AA species (> 10%) during the complete tidal cycle were the same as those in the coastal zone: Ser, Gly and Orn (Fig. 4).

Table 3. Salinity, dissolved free amino acid concentration (DFAA) and AA carbon yields during the tidal cycles in the three estuaries. The time of sampling is indicated.

Time (hs)	Salinity	Tide	DFAA (nM)	AA- C yields
Guadalquivir				
8	34.74	high	749.81	0.46
13	28.91	low	411.34	0.15
19	34.02	high	526.88	0.33
25	28.34	low	294.48	0.11
Guadiana				
5	30.66	low	320.06	0.18
11	35.27	high	266.15	0.20
18	30.87	low	271.66	0.15
24	35.56	high	612.48	0.48
Tinto-Odiel				
6	36.4		783.81	0.69
12	36.5		428.61	0.37
18	36.48		589.95	0.54
24	36.44		425.00	0.32

This is not surprising since sampling of the tidal cycles were performed at the mouth of each estuary. Noteworthy, the mol % of these AAs followed the typical sinusoidal shape over time reflecting the tidal cycles with highest values during high tide and lowest at low tide (Fig. 5). However, as in the estuarine zone, during low tide Asn was also among the predominant AAs in Guadalquivir and Guadiana with a mean mol % of 20% ± 3% and 16% ± 1%, respectively. These results indicated that Asn is originating from the terrestrial environment. In fact, the Asn mol % showed a marked trend with tides with higher values during low tide (Fig. 4 and Fig.

5A and 5B). This trend was also observed in Asn concentration, while, in general, the rest of AAs showed higher concentrations during high tide (Table S3A and S3B). Probably, the higher Asn mol % and concentration observed during low tides were due to a larger contribution from the rivers.

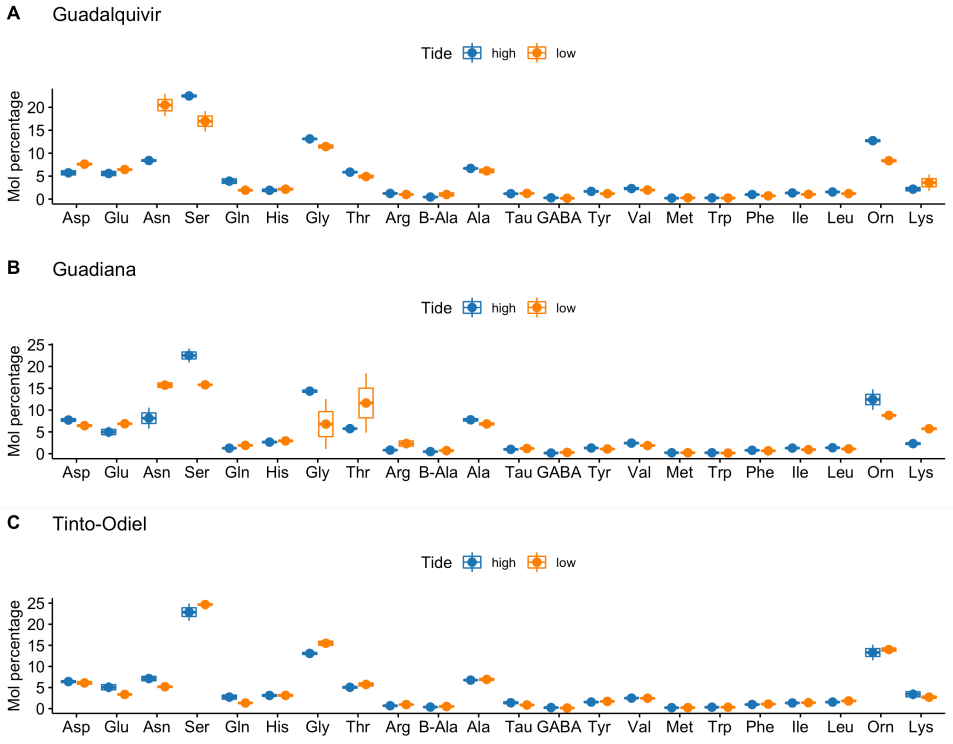

Fig. 4. Relative contribution (mol percentage) of amino acids to the total bulk of DFAA during the tidal cycles in Guadalquivir and Guadiana.

In contrast, during the tide cycle in Tinto- Odiel, salinity varied by 0.1, no clear tidal variations were observed in DFFA concentration (Table 3) and the coefficient of variation between tides was < 3% for all the AAs. However, the mol % of the predominant AAs followed also a sinusoidal shape typical of tidal cycles (Fig. 5C), suggesting that despite the smaller variability in salinity, tidal cycles also impact the DFFA composition in this estuary. Our results indicate that tidal cycles affected the concentration and composition of DFAAs, where low tide allowed a higher influence of river

discharge provoking a decrease in DFAA concentration and an enrichment in terrigenous AAs in the estuarine water. Moreover, the AA-C yields were similar than those observed in the coastal zone of Guadalquivir, Guadiana and Tinto-Odiel but lower than those observed in the estuarine zone (Table 3). Thus, input of DFAAs from allochthonous sources increased organic matter reactivity upstream.

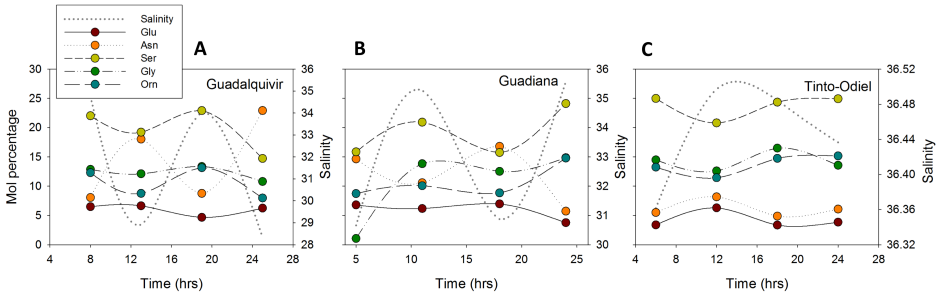

Fig. 5. Distribution of the relative contribution (mol percentage) of glutamic acid (Glu), asparagine (Asn), serine (Ser), glycine (Gly) and ornithine (Orn) in the three estuaries during the tidal study.

IV. 3.3 Relationship between amino acid composition and chromophoric and fluorescent DOM

In a previous work, DOM was chemically characterized using its optical properties along the longitudinal gradient and the tidal cycle of the three estuaries (Amaral et al., 2020). These authors analyzed chromophoric DOM (CDOM) using the absorption coefficient at 254 nm wavelength (a_{254}) and fluorescent DOM (FDOM). a_{254} is proportional to the abundance of conjugated carbon double bonds and not influenced by photodegradation (Blough and Del Vecchio, 2002). The authors found that FDOM in these estuaries is composed of four components. Component 1 (C1) and component 2 (C2) were identified as humic-like components. Component 3 (C3) and component 4 (C4) represent protein-like fluorescence resembling the AAs tryptophan and tyrosine, respectively (Amaral et al., 2020).

We used simple linear regression to test the relationship between AA composition with 1) a_{254} and 2) the fluorescent components.

A relationship between DFAA concentration with CDOM or FDOM components was not observed in the overall dataset (n = 39, p > 0.01). Yamashita et al. (2015) found that both humic and protein-like components were positively correlated with TDAA concentrations in a river-influenced area. The TDAA pool includes amino acids in free and combined form and differences in the composition of these two pools have been observed (Coffin, 1989). Thus, in CDOM, AAs are probably mainly in the combined form, which could explain the lack of relationship with the free AAs analyzed in this work. However, the mol % of individual AA species showed different trend in their relationship with CDOM, humic-like and protein-like fluorescent components (Table 4) indicating that changes in DOM degradation are reflected in CDOM and FDOM composition. The mol % of Ser, Gly and Orn, the most abundant AAs in the coastal zone of the estuaries and during high tides, showed a negative relationship with DOC concentration, CDOM and fluorescent components, mainly in Guadalquivir and Tinto-Odiel. In contrast, Asn, which was among the most abundant AA in the estuarine zone and during low tide of Guadalquivir and Guadiana, showed a positive relationship with DOM variables, which reflects the terrestrial nature of this AA as previously discussed (Berggren et al., 2010).

Table 4. Coefficient of determination R^2 of liner simple regression between the mol % of AAs and CDOM (as a_{254}), dissolved organic carbon (DOC) concentration and humic-like C1 and C2, tryptophan- like C3 and tyrosine like C4 in each estuarine (data from longitudinal and tidal cycle) and data from the three estuaries together (All). * indicated that the relationship is negative otherwise is positive. $p < 0.01$ TO: Tinto-Odiel, GD: Guadalquivir.

Mol % AA	a_{254}	DOC	C1	C2	C3	C4
			Serine*			
Guadalquivir	0.65	0.63	0.67	0.68	-	-
Tinto-Odiel	0.58	0.56	0.62	0.80	0.40	0.80
All	0.25	0.26	0.23	0.27	0.24	0.44
			Glycine*			
Guadalquivir	0.71	0.78	0.77	0.78	0.52	0.79
Guadiana	0.64	-	0.89	0.90	-	0.67
Tinto-Odiel	0.50	0.54	0.55	0.64	0.43	0.61
All	0.51	0.51	0.52	0.56	0.24	0.47
			Ornithine*			
Guadalquivir	0.47	0.49	0.53	0.53	0.18	0.57
Tinto-Odiel	0.64	0.61	0.71	0.84	0.18	0.76
All	0.34	0.33	0.32	0.36	0.18	0.21
			Asparagine			
Guadalquivir	0.92	0.21	0.95	0.95	-	0.73
Guadiana	0.35	0.28	0.45	0.48	-	0.54
Tinto-Odiel	0.72	0.64	0.74	0.77	0.43	0.80
All	0.44	0.56	0.49	0.52	-	0.27
Gln (TO)	0.53	0.60	0.65	0.78	0.42	0.74
Asp (GD)	0.73	0.37	0.83	0.84	0.70	0.66
			Tyrosine*			
Guadalquivir	0.66	0.59	0.67	0.67	-	0.72
Tinto-Odiel	0.35	0.51	0.51	0.46	-	0.51
All	0.46	-	0.47	0.47	0.33	0.20
			Phenylalanine*			
Guadalquivir	0.77	0.73	0.79	0.79	0.64	0.81
Guadiana	-	-	-	-	-	0.81
Tinto-Odiel	0.53	0.54	0.60	0.72	0.41	0.66
All	0.37	0.32	0.30	0.33	0.25	0.34
Trp*(TO)	-	0.24	-	-	0.56	

These positive trends were also found for Asp and Glu, also predominant AAs in the estuarine zone of Guadalquivir and Tinto- Odiel estuary, respectively, indicating that the composition of AAs was highly related with CDOM and FDOM inputs into these estuaries. Overall, Guadalquivir showed the strongest relationship between AAs and DOM variables followed by Tinto-Odiel and Guadiana.

Yamashita and Tanou (2003) observed a positive relationship between tyrosine-like, tryptophan-like and phenylalanine-like fluorescent components and the concentration of these AAs. Here, the mol % and concentration of Tyr and Phe showed a negative relationship with the tyrosine-like C4, while Trp was not correlated with any DOM variables in Guadalquivir and Guadiana ($p < 0.05$) but showed a negative relationship with the tryptophan-like C3 in Tinto-Odiel estuary (Table 4). The different trend in the relationship (or the lack of relationship) could be due to difference in AAs measurements, since Yamashita and Tanou (2003) measured THAA, which included free and combined AAs in proteins, and here we measured only free AAs. Also, the tyrosine-like fluorescent C4 could be a mixture of the aromatic AAs Tyr and Phe as it was observed in other work (Yamashita et al., 2015). The negative relationship observed in this work might indicate that free Tyr and Phe (and Trp in Tinto-Odiel) are incorporated into the protein material rather than being responsible for the protein-like fluorescent signal. In most cases, AAs are present in more complex, proteinaceous rather than free forms (Cowie and Hedges, 1992). Furthermore, the fluorophore associated with Tyr is a simple phenol while Trp contains an indole group and fluoresces in this region (Lackowicz, 2006). Thus, fluorescence of these fluorophores can be strongly affected by other materials as well. Mayer et al. (1999) observed that fluorescence from

terrigenous humic material could contribute to some emission intensity at the Trp and Tyr wavelengths. Additionally, Maie et al. (2007) demonstrated the influence of phenolic compounds on protein-like fluorescence signal. These authors found that a large portion of Trp peak is associated with non-proteinaceous compounds and proposed that phenols associated with tannins were the likely fluorophores contributing to Trp peak fluorescence in estuarine samples (Mai et al., 2007). Amaral et al. (2021) also found that fluorescent component that resembles the amino acid Trp could be a mixture of fluorophores of different sources. Moreover, terrestrial DOM might obscure the autochthonous relationship between tryptophan and AA concentrations (Yamashita et al., 2015). This, together with the fact that in this work we measured free AAs, could explain the lack of relationship between Trp and C3. Our result are in agreement with the observation that assignments of fluorescent peaks that imply composition of a specific compounds, such as the amino acids Tyr and Trp, complicate their interpretation as there is a number of fluorophores present in water samples with spectra overlapping in the amino acid regions (Coble et al., 2014), in particular in system with high input of terrestrial and anthropogenic DOM.

Conclusions

Our results suggest that the source of organic matter might be as important as microbial processing in determining the concentration and composition of AAs in DOM. We found changes in AAs composition between coastal and estuarine zones that suggested contrasting sources of DOM but also its degradation along the estuarine transit until reaching the coastal zone. We observed that in estuarine zone DOM is less degraded, i.e., more labile than in the coastal zone.

In contrast, the factors controlling the DFAA distribution varied among estuaries. Guadalquivir estuary showed the largest changes in the contribution of AAs to the total bulk compared to its coastal zone impacted by terrestrial and lateral inputs from surrounding watersheds and agricultural practices. Guadiana estuary showed a similar composition of AAs to their coastal zone that could be related to a conservative behavior observed in DOM distribution. Nevertheless, lateral inputs at the mouth of Guadiana from terrestrial sources were also evident in the AA composition. In the Tinto-Odiel estuary, the AA composition reflected a more autochthonous character of DOM than the other estuaries with differences also within the estuary, but it also showed the influence of allochthonous inputs mainly from anthropogenic activities. To conclude, Guadalquivir and Tinto-Odiel were characterized by the presence of more labile DOM than Guadiana estuary. Moreover, our results indicate that tidal cycles exert an influence on AA distribution where input of DFAAs from allochthonous sources increased organic matter reactivity in the interior of the estuaries.

In our systems DI and the % mol of NPAAs were not appropriate to differentiate the diagenetic state of DOM. Probably associated with the presence of several sources of DOM and the relatively high water renewal time in these estuaries. Our results further suggest that the composition of AAs was highly related with CDOM and FDOM inputs into the estuaries.

Acknowledgements

This work acknowledges the 'Severo Ochoa Centre of Excellence' accreditation (CEX2019-000928-S). Valentina Amaral was financed by the National Research and Innovation Agency of Uruguay (ANII) with a Ph.D. fellowship (POS_EXT_2015_1_122780). Cristina Romera-Castillo was

funded by the Spanish Ministry of Science and Innovation through a JIN Project with reference PID2019-109889RJ-I00. This study was financed by the Spanish CICYT (Spanish Program for Science and Technology) under contract RTI2018-100865-B-C21.

References

Abril, G., Nogueira, M., Etcheber, H., Cabeçadas, G., Lemaire, E., Brogueira, M.J., 2002. Behaviour of organic carbon in nine contrasting European estuaries. Estuar. Coast. Shelf Sci. 54, 241–262. https://doi.org/10.1006/ecss.2001.0844

Amaral, V., Romera-Castillo, C., Forja, J., 2021. Submarine mud volcanoes as a source of chromophoric dissolved organic matter to the deep waters of the Gulf of Cádiz. Sci. Rep. 11, 1–12. https://doi.org/10.1038/s41598-021-82632-3

Amaral, V., Romera-Castillo, C., García-Delgado, M., Gómez-Parra, A., Forja, J., 2020. Distribution of dissolved organic matter in estuaries of the southern Iberian Atlantic Basin: Sources, behavior and export to the coastal zone. Mar. Chem. 226, 103857. https://doi.org/10.1016/j.marchem.2020.103857

Amon, R.M.W., Fitznar, H.P., 2001. Linkages among the bioreactivity, chemical composition, and diagenetic state of marine dissolved organic matter. Limnol. Oceanogr. 46, 287–297. https://doi.org/10.4319/lo.2001.46.2.0287

Bauer, J.E., Bianchi, T.S., 2011. Dissolved Organic Carbon Cycling and Transformation, Treatise on Estuarine and Coastal Science. Elsevier Inc. https://doi.org/10.1016/B978-0-12-374711-2.00502-7

Benner, R., 2003. Molecular Indicators of the Bioavailability of Dissolved Organic Matter. Aquat. Ecosyst. 121–137.

https://doi.org/10.1016/b978-012256371-3/50006-8

Benner, R., 2002. Chemical Composition and Reactivity, Biogeochemistry of Marine Dissolved Organic Matter. Elsevier Inc. https://doi.org/10.1016/b978-012323841-2/50005-1

Benner, R., Opsahl, S., 2001. Molecular indicators of the sources and transformations of dissolved organic matter in the Mississippi river plume. Org. Geochem. 32, 597–611. https://doi.org/10.1016/S0146-6380(00)00197-2

Berggren, M., Laudon, H., Haei, M., Ström, L., Jansson, M., 2010. Efficient aquatic bacterial metabolism of dissolved low-molecular-weight compounds from terrestrial sources. ISME J. 4, 408–416. https://doi.org/10.1038/ismej.2009.120

Blough, N. V., Del Vecchio, R., 2002. Chromophoric DOM in the Coastal Environment. Biogeochem. Mar. Dissolved Org. Matter 509–546. https://doi.org/10.1016/b978-012323841-2/50012-9

Burdige, D. J., & Martens, C. S. 1988. Biogeochemical cycling in an organic-rich coastal marine basin: 10. The role of amino acids in sedimentary carbon and nitrogen cycling. *Geochimica et Cosmochimica Acta*, *52*(6), 1571-1584.

Carrasco, J.M., Piston, J.M., Berbel, J., 2010. Evolución de la productividad del agua en la Cuenca del Guadalquivir 1989-2005. Agricult. Econ. Res. 10, 59–69.

Carro, B., Borrego, J., Morales, J., 2018. Estuaries of the Huelva Coast: Odiel and Tinto Estuaries (SW Spain), in: The Spanish Coastal Systems: Dynamic Processes, Sediments and Management. p. vii. https://doi.org/10.1007/978-3-319-93169-2

Cauwet, G., Deliat, G., Krastev, A., Shtereva, G., Becquevort, S., Lancelot,

C., Momzikoff, A., Saliot, A., Cociasu, A., Popa, L., 2002. Seasonal DOC accumulation in the Black Sea: a regional explanation for a general mechanism. Mar. Chem. 79, 193–205.

Cauwet, G., 2002. DOM in the coastal zone. In: Hansell, D.A., Carlson, C.A. (Eds.),Biogeochemistry of Marine Dissolved Organic Matter. Academic Press/Elsevier Science, New York, NY, pp. 579–602.

Coble, P.G., Lead, J., Baker, A., Reynolds, D.M., Spencer, R.G.M., 2014. Aquatic Organic Matter Fluorescence.

Coffin, R.B., 1989. Bacterial uptake of dissolved free and combined amino acids in estuarine waters. Limnol. Oceanogr. 34, 531–542. https://doi.org/10.4319/lo.1989.34.3.0531

Cowie, G.L., Hedges, J.I., 1992. Sources and reactivities of amino acids in a coastal marine environment. Limnol. Oceanogr. 37, 703–724. https://doi.org/10.4319/lo.1992.37.4.0703

Cowie, G. L., Hedges, J. I. 1994. Biochemical indicators of diagenetic alteration in natural organic matter mixtures. *Nature*, *369*(6478), 304-307.

Crawford, A.C.C., Hobbie, J.E., Webb, K.L., Carolina, N., Hobbie, J.E., Webb, K.L., 1974. The Utilization of Dissolved Free Amino Acids by Estuarine Microorganisms 55, 551–563.

Dauwe, B., Middelburg, J.J., 1998. Amino acids and hexosamines as indicators of organic matter degradation state in North Sea sediments. Limnol. Oceanogr. 43, 782–798. https://doi.org/10.4319/lo.1998.43.5.0782

Dauwe, B., Middelburg, J.J., Herman, P.M.J., Heip, C.H.R., 1999. Linking diagenetic alteration of amino acids and bulk organic matter reactivity. Limnol. Oceanogr. 44, 1809–1814.

https://doi.org/10.4319/lo.1999.44.7.1809

Davis, J., Kaiser, K., Benner, R., 2009. Amino acid and amino sugar yields and compositions as indicators of dissolved organic matter diagenesis. Org. Geochem. 40, 343–352. https://doi.org/10.1016/j.orggeochem.2008.12.003

Davis Jr, R.A., Welty, A.T., Borrego, J., Morales, J.A., Pendon, J.G., Ryan, J.G., 2000. Rio Tinto estuary (Spain): 5000 years of pollution. Environ. Geol. 39 (10), 1107–1116.

de la Paz, M., Gómez-Parra, A., Forja, J., 2007. Inorganic carbon dynamic and air-water CO2 exchange in the Guadalquivir Estuary (SW Iberian Peninsula). J. Mar. Syst. 68, 265–277. https://doi.org/10.1016/j.jmarsys.2006.11.011

Gardner, W.S., Hanson, R.B., 1979. Dissolved free amino acids in interstitial waters of Georgia salt marsh soils. Estuaries 2, 113–118. https://doi.org/10.2307/1351635

Garel, E., Cai, H., 2018. Effects of Tidal-Forcing Variations on Tidal Properties Along a Narrow Convergent Estuary. Estuaries and Coasts 41, 1924–1942. https://doi.org/10.1007/s12237-018-0410-y

Garel, E., Pinto, L., Santos, A., Ferreira, Ó., 2009. Tidal and river discharge forcing upon water and sediment circulation at a rock-bound estuary (Guadiana estuary, Portugal). Estuar. Coast. Shelf Sci. 84, 269–281. https://doi.org/10.1016/j.ecss.2009.07.002

Grande, J.A., Borrego, J., Morales, J.A., 2000. A study of heavy metal pollution in the Tinto-Odiel estuary in southwestern Spain using factor analysis. Environ. Geol. 39 (10), 1095–1101.

Fattorusso, E., Piattelli, M., 2012. Amino acids from marine algae. Marine natural products: Chemical and biological perspectives, 3, 95.

Hammer, K., Kattner, G., 1986. Dissolved free amino acids in the marine environment: a carbon to nitrogen ratio shift during diatom blooms. Mar. Ecol. Prog. Ser. 31, 35–45. https://doi.org/10.3354/meps031035

Hansell, D.A., Carlson, C.A.., Repeta, D.J.. R., Schlitzer, R., 2009. Dissolved Organic Matter in the Ocean. Oceanography 22.

Hecky, R. E., Mopper, K., Kilham, P., Degens, E. T. 1973. The amino acid and sugar composition of diatom cell-walls. Marine biology, 19(4), 323-331.

Hedges, J.I., 2002. Why Dissolved Organics Matter, Biogeochemistry of Marine Dissolved Organic Matter. Elsevier Inc. https://doi.org/10.1016/b978-012323841-2/50003-8

Hedges, J.I., Keil, R.G., Benner, R., 1997. What happens to terrestrial organic matter in the ocean? Org. Geochem. 27, 195–212. https://doi.org/10.1016/S0146-6380(97)00066-1

Ireland, R. J., Lea, P. J. 1998. The Enzymes of Glutamine. Glutamate, Asparagine, and Aspartate Metabolism. In Plant amino acids (pp. 63-124). CRC Press.

Jaffé, R., Boyer, J.N., Lu, X., Maie, N., Yang, C., Scully, N.M., Mock, S., 2004. Source characterization of dissolved organic matter in a subtropical mangrove-dominated estuary by fluorescence analysis. Mar. Chem. 84, 195–210. https://doi.org/10.1016/j.marchem.2003.08.001

Jiao, N., Robinson, C., Azam, F., Thomas, H., Baltar, F., Dang, H., Hardman-Mountford, N.J., Johnson, M., Kirchman, D.L., Koch, B.P., Legendre, L., Li, C., Liu, J., Luo, T., Luo, Y.W., Mitra, A., Romanou, A., Tang, K., Wang, X., Zhang, C., Zhang, R., 2014. Mechanisms of microbial carbon sequestration in the ocean – Future research directions. Biogeosciences 11, 5285–5306. https://doi.org/10.5194/bg-

11-5285-2014

Jørgensen, N., 1982. Heterotrophic Assimilation and Occurrence of Dissolved Free Amino Acids in a Shallow Estuary. Mar. Ecol. Prog. Ser. 8, 145–159. https://doi.org/10.3354/meps008145

Jørgensen, N.O.G., Tranvik, L.J., Berg, G.M., 1999. Occurrence and bacterial cycling of dissolved nitrogen in the Gulf of Riga, the Baltic Sea. Mar. Ecol. Prog. Ser. 191, 1–18. https://doi.org/10.3354/meps191001

Kaiser, K., Benner, R., 2008. Major bacterial contribution to the ocean reservoir of detrital organic carbon and nitrogen. Limnol. Oceanogr. 53, 99–112. https://doi.org/10.4319/lo.2008.53.1.0099

Keil, R., Kirchman, D., 1991. Contribution of dissolved free amino acids and ammonium to the nitrogen requirements of heterotrophic bacterioplankton. Mar. Ecol. Prog. Ser. 73, 1–10. https://doi.org/10.3354/meps073001

Keil, R. G., Tsamakis, E., Hedges, J. I. 2000. Early diagenesis of particulate amino acids in marine systems. Perspectives in amino acid and protein geochemistry, 69-82.

Leblanc, M., Morales, J.A., Borrego, J., Elbaz-Poulichet, F., 2000. 4,500-year-old mining pollution in southwestern Spain: Long-term implications for modern mining pollution. Econ. Geol. 95, 655–661. https://doi.org/10.2113/gsecongeo.95.3.655

Lee, C., Bada, J.L., 1977. Dissolved amino acids in the equatorial Pacific, the Sargasso Sea, and Biscayne Bay. Limnol. Oceanogr. 22, 502–510. https://doi.org/10.4319/lo.1977.22.3.0502

Lee, C., Bada, J.L., 1975. Amino acids in equatorial Pacific Ocean water. Earth Planet. Sci. Lett. 26, 61–68. https://doi.org/10.1016/0012-

821X(75)90177-6

Lee, C., Wakeham, S., Arnosti, C. 2004. Particulate organic matter in the sea: the composition conundrum. AMBIO: A Journal of the Human Environment, 33(8), 565-575.

Lindroth, P., Mopper, K., 1979. High Performance Liquid Chromatographic Determination of Subpicomole Amounts of Amino Acids by Precolumn Fluorescence Derivatization with o-Phthaldialdehyde. Anal. Chem. 51, 1667–1674. https://doi.org/10.1021/ac50047a019

Mai-Thi, N.N., St-Onge, G., Tremblay, L., 2017. Contrasting fates of organic matter in locations having different organic matter inputs and bottom water O2 concentrations. Estuar. Coast. Shelf Sci. 198, 63–72. https://doi.org/10.1016/j.ecss.2017.08.044

Maie, N., Scully, N.M., Pisani, O., Jaffé, R., 2007. Composition of a protein-like fluorophore of dissolved organic matter in coastal wetland and estuarine ecosystems. Water Res. 41, 563–570. https://doi.org/10.1016/j.watres.2006.11.006

Mannino, A., Harvey, H.R., 2000. Biochemical composition of particles and dissolved organic matter along an estuarine gradient: Sources and implications for DOM reactivity. Limnol. Oceanogr. 45, 775–788. https://doi.org/10.4319/lo.2000.45.4.0775

Mayer, L.M., Schick, L.L., Loder, T.C., 1999. Dissolved protein fluorescence in two maine estuaries. Mar. Chem. 64, 171–179. https://doi.org/10.1016/S0304-4203(98)00072-3

Menanteau, L., C.line, C., Choblet, C., 2005. Les marais du Bas-Guadiana (Algarve, Andalousie): emprise, deprise et reprise humaines. Aestuaria 9, 309–331.

Morales, J.A., Garel, E., 2018. The Guadiana River Delta, The Spanish Coastal Systems: Dynamic Processes, Sediments and Management. Springer International Publishing. https://doi.org/10.1007/978-3-319-93169-2

Muztar, J., Slinger, J., Burton, H., 1977. The Chemical Composition of Aquatic Macrophytes. II Amino Acid Composition of the Protein and Non-Protein Fractions. Can. J. Plant Sci. 58, 843–849.

Neuhaus, F. C., Baddiley, J. 2003. A continuum of anionic charge: structures and functions of D-alanyl-teichoic acids in gram-positive bacteria. Microbiology and molecular biology reviews, 67(4), 686-723.

Nguyen, R. T., Harvey, H. R. 1997. Protein and amino acid cycling during phytoplankton decomposition in oxic and anoxic waters. Organic Geochemistry, 27(3-4), 115-128.

Olías, M., Nieto, J.M., Sarmiento, A.M., Cerón, J.C., Cánovas, C.R., 2004. Seasonal water quality variations in a river affected by acid mine drainage: The Odiel River (South West Spain). Sci. Total Environ. 333, 267–281. https://doi.org/10.1016/j.scitotenv.2004.05.012

Pérez, M. T., Pausz, C., & Herndl, G. J. (2003). Major shift in bacterioplankton utilization of enantiomeric amino acids between surface waters and the ocean's interior. Limnol. Oceanogr. 48(2), 755-763.

Peter, S., Shen, Y., Kaiser, K., Benner, R., Durisch-Kaiser, E., 2012. Bioavailability and diagenetic state of dissolved organic matter in riparian groundwater. J. Geophys. Res. G Biogeosciences 117, 1–10. https://doi.org/10.1029/2012JG002072

Raymond, P.A., Spencer, R.G.M., 2015. Riverine DOM. Biogeochem. Mar. Dissolved Org. Matter Second Ed. 509–533.

https://doi.org/10.1016/B978-0-12-405940-5.00011-X

Reinthaler, T., Sintes, E., Herndl, G.J., 2008. Dissolved organic matter and bacterial production and respiration in the sea-surface microlayer of the open Atlantic and the western Mediterranean Sea. Limnol. Oceanogr. 53, 122–136. https://doi.org/10.4319/lo.2008.53.1.0122

Rodríguez-Ramírez, A., Villar.as-Robles, J.J.R., P.rez-Asensio, J.N., Celestino-P.rez, S., 2019. The Guadalquivir Estuary: Spits and Marshes. In: The Spanish Coastal Systems, pp. 517–541.

Saio, K., Kimura, J., 1957. Studies on Asparagine Occurrence in Various Crops. Soil Sci. Plant Nutr. 3, 108–111. https://doi.org/10.1080/00380768.1957.10431908

Sarmento, H., Romera-Castillo, C., Lindh, M., Pinhassi, J., Sala, M.M., Gasol, J.M., Marrasé, C., Taylor, G.T., 2013. Phytoplankton species-specific release of dissolved free amino acids and their selective consumption by bacteria. Limnol. Oceanogr. 58, 1123–1135. https://doi.org/10.4319/lo.2013.58.3.1123

Schleifer, K.H., Kandler, O., 1972. Peptidoglycan types of bacterial cell walls and their taxonomic implications. Bacteriol. Rev. 36, 407–477. https://doi.org/10.1128/mmbr.36.4.407-477.1972

Sieciechowicz, K. A., Joy, K. W., Ireland, R. J. 1988. The metabolism of asparagine in plants. Phytochemistry, 27(3), 663-671.

Siezen, R. J., Mague, T. H. 1978. Amino acids in suspended particulate matter from oceanic and coastal waters of the Pacific. Marine Chemistry, 6(3), 215-231.

Taubner, R.S., Baumann, L.M.F., Bauersachs, T., Clifford, E.L., Mähnert, B., Reischl, B., Seifert, R., Peckmann, J., Rittmann, S.K.M.R., Birgel, D., 2019. Membrane lipid composition and amino acid excretion

patterns of Methanothermococcus okinawensis grown in the presence of inhibitors detected in the enceladian plume. Life 9. https://doi.org/10.3390/life9040085

Tevatia, R., Allen, J., Rudrappa, D., White, D., Clemente, T.E., Cerutti, H., Demirel, Y., Blum, P., 2015. The taurine biosynthetic pathway of microalgae. Algal Res. 9, 21–26. https://doi.org/10.1016/j.algal.2015.02.012

Van der Ploeg, J. R., Weiss, M. A., Saller, E., Nashimoto, H., Saito, N., Kertesz, M. A., Leisinger, T. 1996. Identification of sulfate starvation-regulated genes in Escherichia coli: a gene cluster involved in the utilization of taurine as a sulfur source. Journal of bacteriology, 178(18), 5438-5446.

Vanittanakom, N., Loeffler, W., Koch, U., Jung, G. 1986. Fengycin-a novel antifungal lipopeptide antibiotic produced by Bacillus subtilis F-29-3. The Journal of antibiotics, 39(7), 888-901.

Vasconcelos, R.P., Reis-Santos, P., Fonseca, V., Maia, A., Ruano, M., França, S., Vinagre, C., Costa, M.J., Cabral, H., 2007. Assessing anthropogenic pressures on estuarine fish nurseries along the Portuguese coast: A multi-metric index and conceptual approach. Sci. Total Environ. 374, 199–215. https://doi.org/10.1016/j.scitotenv.2006.12.048

Wakeham, S.G., Lee, C., Hedges, J.I., Hernes, P.J., Peterson, M.L., 1997. Molecular indicators of diagenetic status in marine organic matter. Geochim. Cosmochim. Acta 61, 5363–5369. https://doi.org/10.1016/S0016-7037(97)00312-8

Yamashita, Y., Fichot, C.G., Shen, Y., Jaffé, R., Benner, R., 2015. Linkages among fluorescent dissolved organic matter, dissolved amino acids and

lignin-derived phenols in a river-influenced ocean margin. Front. Mar. Sci. 2, 1–14. https://doi.org/10.3389/fmars.2015.00092

Yamashita, Y., Tanoue, E., 2003. Distribution and alteration of amino acids in bulk DOM along a transect from bay to oceanic waters. Mar. Chem. 82, 145–160. https://doi.org/10.1016/S0304-4203(03)00049-5

Zhang, Z.L., Zheng, Q., Jiao, N.Z., 2016. Microbial D-amino acids and marine carbon storage. Sci. China Earth Sci. 59, 17–24. https://doi.org/10.1007/s11430-015-5155-x

Supplementary material

Figures

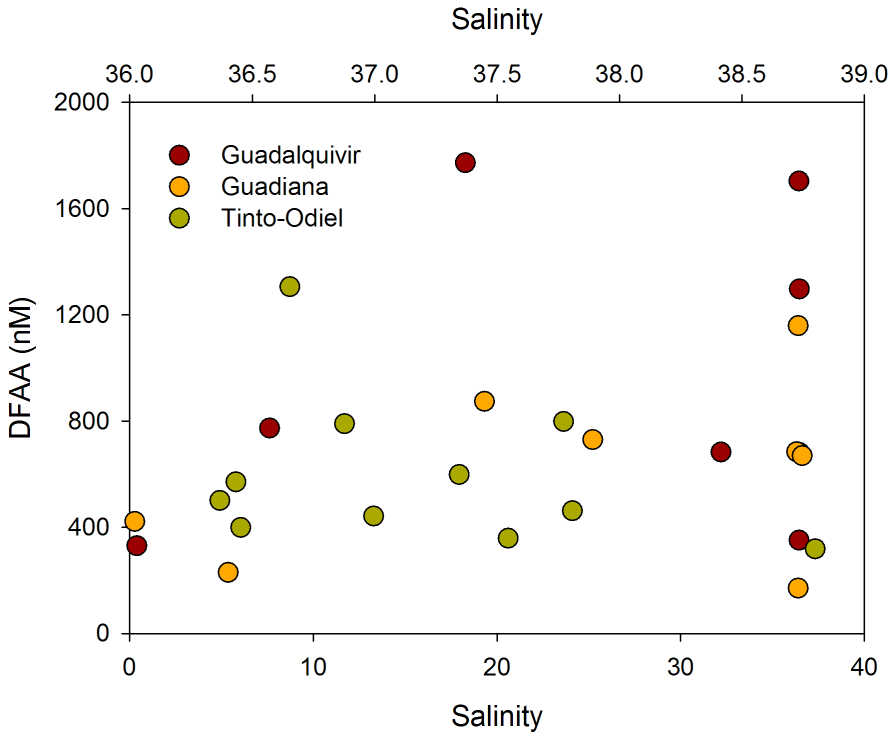

Fig. S1. Dissolved free amino acid (DFAA) concentration along the salinity gradient in Guadalquivir, Guadiana (bottom) and Tinto-Odiel (top).

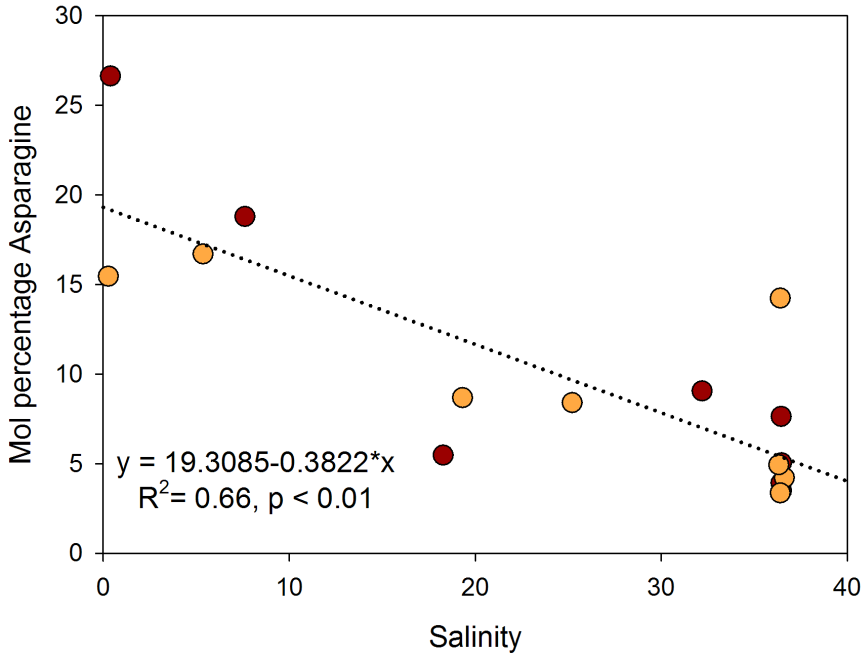

Fig. S2. Liner regression between the mol percentge of asparagine and salinity in Guadalquivir (red) and Guadiana (orange) longitudinal transects.

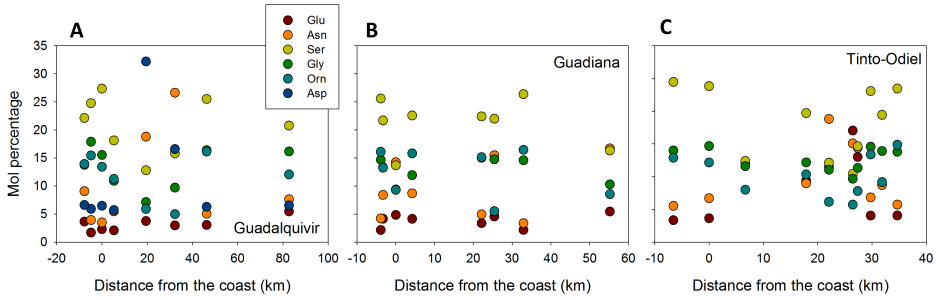

Fig. S3. Distribution of the mol percentage of glutamic acid (Glu), asparagine (Asn), serine (Ser), glycine (Gly) and ornithine (Orn) in the three estuaries during the longitudinal transects.

Tables

Table S1. AA-based indicators of DOM degradation used in this work.

Index	Description	Interpretation
AA- C yields	AA concentration normalized by DOC concentration	Increase with DOM freshness. Useful during early stage of DOM diagenesis.
Degradation index	Overall degradation status of organic matter	Decrease with DOM degradation. Useful during intermediate stage
Mol percentage of NPAAs	Relative contribution of β-ala and GABA to the total bulk of DFAA	Increase their contribution with diagenetic state. Useful during advanced stage
Ratio of AA enantiomers	Ratio between D and L concentration of each AA	Higher rates indicates more diagenetically altered material

Table S2A. Amino acid concentration (nM) during the longitudinal transect in Guadalquivir (GD), Guadiana (GU) and Tinto-Odiel estuary (TO).

Site	Zone	Asp	Glu	Asn	Ser	Gln	His	Gly	Thr	Arg	β-ala	Ala
GD1	Coast	83.80	29.65	45.25	354.86	5.54	20.72	201.42	94.64	10.08	7.86	113.00
GD24	Coast	42.77	20.83	34.34	173.84	5.31	12.85	111.55	32.73	5.33	2.59	51.57
GD25	Coast	23.02	19.19	26.80	72.96	5.83	5.03	56.77	17.67	5.00	2.04	27.06
GD2	Estuary	100.91	28.66	66.77	421.90	6.32	29.61	304.73	96.76	8.44	45.69	132.15
GD7	Estuary	45.17	24.86	61.90	151.16	6.66	22.08	94.13	36.54	6.86	1.82	47.64
GD11	Estuary	101.3	36.87	96.96	321.10	8.83	19.75	193.81	75.19	7.07	12.76	98.11
GD15	Estuary	249.0	29.01	145.29	98.98	10.98	20.44	55.15	31.60	7.38	2.56	31.20
GD19	Estuary	54.82	9.80	88.01	52.23	4.93	8.80	32.09	15.67	3.90	1.99	16.08
GU1	Coast	10.01	8.24	24.31	23.34	2.23	4.70	15.99	6.98	1.77	1.56	8.37
GU21	Coast	43.56	23.07	33.74	153.35	6.49	21.47	102.79	36.13	6.43	2.29	48.29
GU22	Coast	84.37	25.07	39.07	305.52	3.95	30.06	168.98	72.95	4.42	2.58	93.96
GU2	Estuary	48.07	14.38	28.17	171.46	2.84	18.74	98.24	39.78	3.67	3.20	51.76
GU14	Estuary	49.52	30.34	61.36	158.46	9.86	24.46	97.29	41.11	6.08	2.32	53.22
GU16	Estuary	64.75	36.16	75.89	197.28	8.02	28.88	104.3	50.31	5.74	1.44	60.58
GU24	Estuary	17.42	12.53	38.46	37.58	3.90	5.62	23.66	11.03	2.95	1.16	15.36
GU28	Estuary	30.83	19.26	65.29	92.78	7.30	12.06	62.32	28.30	3.54	1.75	32.70
TO1	Coast	35.05	18.19	33.50	119.34	5.36	18.78	73.47	29.99	3.97	1.66	38.05
TO23	Coast	26.14	16.13	27.25	92.14	4.36	16.04	58.21	23.83	3.24	1.69	26.71
TO25	Coast	35.64	23.20	32.66	133.98	5.59	21.48	78.79	31.22	3.72	1.30	38.34
TO2	Estuary	88.63	27.62	39.77	365.18	7.19	34.10	200.50	85.10	4.75	3.06	103.41

TO5	Estuary	50.69	26.36	43.69	193.30	8.76	32.62	110.52	56.92	7.11	2.16	62.96
TO6	Estuary	32.95	53.99	54.62	54.77	21.29	17.72	51.27	25.03	7.71	2.88	27.21
TO8	Estuary	43.21	56.15	53.70	117.99	11.32	21.25	72.85	31.56	5.13	2.93	41.32
TO10	Estuary	44.45	53.18	86.88	56.02	17.34	18.04	50.98	21.35	5.42	4.42	33.66
TO15	Estuary	25.05	46.65	51.59	52.49	11.2	13.26	40.62	16.68	4.39	2.14	20.7
TO17	Estuary	60.25	70.23	69.61	155.26	16.21	24.9	110.97	41.88	7.63	13.14	58.91
TO20	Estuary	18.38	54.25	48.03	33.15	15.04	5.85	30.84	13.84	3.98	7.44	22.66

Table S2B. Amino acid concentration (nM) during the longitudinal transect in Guadalquivir (GD), Guadiana (GU) and Tinto-Odiel estuary (TO).

Site	Zone	Tau	GABA	Tyr	Val	Met	Trp	Phe	Ile	Leu	Orn	Lys
GD1	Coast	5.31	0.69	21.82	37.19	3.24	4.71	13.05	21.05	21.69	174.23	27.49
GD24	Coast	10.01	0.77	10.78	17.69	1.32	1.33	6.75	9.86	11.76	109.95	7.57
GD25	Coast	9.50	1.16	5.17	8.53	0.78	0.61	2.90	4.23	4.85	42.37	9.76
GD2	Estuary	6.65	1.27	27.01	38.64	7.49	4.95	16.37	27.42	26.53	262.87	42.82
GD7	Estuary	4.89	2.43	10.88	16.23	1.66	2.28	6.46	8.93	10.39	95.14	25.34
GD11	Estuary	3.60	5.70	20.9	88.01	39.31	7.03	12.41	11.55	18.75	199.38	394.27
GD15	Estuary	1.71	1.13	6.27	11.17	1.47	1.42	3.60	5.61	6.02	45.64	7.78
GD19	Estuary	0.84	0.72	3.56	5.93	0.77	1.03	2.28	3.13	3.75	16.46	3.69
GU1	Coast	3.00	0.82	2.22	2.75	0.28	0.36	1.04	1.42	1.64	15.86	33.74
GU21	Coast	11.84	1.37	11.32	18.71	1.93	2.08	7.74	10.90	13.23	103.58	24.18
GU22	Coast	3.45	0.85	18.60	32.72	1.86	3.84	10.82	17.34	19.08	190.52	29.22
GU2	Estuary	3.99	0.64	10.66	17.98	1.19	2.11	6.56	9.70	10.78	107.88	18.10
GU14	Estuary	6.62	0.89	10.46	19.11	2.02	2.22	7.39	10.77	12.53	96.80	27.61
GU16	Estuary	6.51	0.90	14.85	21.08	1.80	3.85	8.28	11.79	12.63	138.28	20.60
GU24	Estuary	2.68	0.47	2.82	5.16	0.58	0.98	1.68	2.60	2.94	19.66	20.99
GU28	Estuary	1.56	1.07	5.65	11.32	0.86	1.33	3.77	5.99	6.50	23.27	4.74
TO1	Coast	7.18	0.87	8.46	13.02	1.05	1.78	4.83	7.15	7.79	60.93	10.53
TO23	Coast	4.67	0.62	5.57	9.44	1.02	1.13	3.38	5.04	5.78	53.45	13.61
TO25	Coast	5.4	0.83	9.85	14.18	1.23	1.5	6.25	7.81	9.26	84.89	23.88

TO2	Estuary	3.33	0.42	23.09	36.13	2.39	3.8	13.36	19.65	21.29	194.44	28.55
TO5	Estuary	4.46	1.65	15.23	21.3	1.48	3.3	8.17	11.5	11.77	101.65	14.19
TO6	Estuary	22.32	2.96	5.9	7.3	1.05	1.49	2.71	3.87	3.59	35.4	6.42
TO8	Estuary	11.85	1.99	8.53	13.75	1.41	1.44	5.19	8.6	8.11	61.86	18.4
TO10	Estuary	10.88	1.71	5.43	6.99	0.75	1.21	2.39	3.46	3.79	28.39	5.12
TO15	Estuary	13.83	1.85	5.32	6.91	0.89	0.95	2.65	3.54	3.94	27.94	5.96
TO17	Estuary	20.77	1.81	11.67	17.98	1.74	2.26	6.35	9.56	10.42	73.2	13.84
TO20	Estuary	20.38	2.13	3.68	5.59	0.95	0.85	2.02	2.74	3.14	18.21	5.32

Table S3A. Amino acid concentration (nM) during the tidal cycle.

Time (hrs)	S	Tide	Asp	Glu	Asn	Ser	Gln	His	Gly	Thr	Arg	β-ala	Ala
Guadalquivir													
8	34.74	high	36.07	48.65	60.39	165.20	36.83	10.47	96.44	46.03	10.48	4.53	50.99
13	28.91	low	32.81	27.30	74.11	79.00	7.12	7.53	49.80	22.36	4.19	1.28	28.45
19	34.02	high	34.95	24.58	46.09	120.72	15.33	12.86	70.40	29.52	5.57	1.51	34.64
25	28.34	low	21.33	18.39	67.52	43.36	6.31	7.31	31.76	12.86	2.89	4.99	15.83
Guadiana													
5	30.66	low	19.36	21.73	46.94	50.73	6.74	10.36	3.42	58.97	11.28	2.06	20.23
11	35.27	high	22.23	16.45	28.14	55.73	3.42	6.31	36.81	15.24	2.31	1.59	22.20
18	30.87	low	18.54	18.90	45.60	42.76	4.63	7.21	34.00	13.09	3.11	2.13	19.89
24	35.56	high	43.42	23.05	35.05	147.67	7.74	18.15	90.97	35.39	4.82	2.24	44.09
Tinto-Odiel													
6	36.4	-	52.76	26.48	43.13	195.78	9.74	27.39	113.48	50.56	7.03	1.51	57.73
12	36.5	-	29.42	26.92	34.99	89.19	15.81	15.26	54.00	23.38	3.88	1.64	29.09
18	36.48	-	32.13	19.75	28.71	143.63	8.43	16.43	97.27	29.57	5.89	4.78	38.14
24	36.44	-	25.27	16.32	25.85	105.95	7.49	11.39	57.66	19.71	2.01	1.49	28.56

Table S3B. Amino acid concentration (nM) during the tidal cycle.

Time (hrs)	S	Tide	Tau	GABA	Tyr	Val	Met	Trp	Phe	Ile	Leu	Orn	Lys
						Guadalquivir							
8	34.74	high	9.58	3.68	14.63	20.50	1.62	1.47	7.58	10.25	11.52	92.20	10.70
13	28.91	low	4.76	0.69	5.41	8.80	1.18	0.96	2.84	4.56	4.83	36.01	7.33
19	34.02	high	5.66	0.35	7.34	9.79	1.12	1.65	5.15	6.89	8.21	69.24	15.29
25	28.34	low	3.87	0.58	3.06	5.31	0.71	0.67	2.12	2.84	3.59	23.44	15.76
						Guadiana							
5	30.66	low	3.97	0.79	2.90	5.39	0.76	0.82	2.15	2.82	3.33	27.94	17.39
11	35.27	high	3.02	0.46	3.46	7.08	0.53	0.66	1.90	3.32	3.47	26.80	5.04
18	30.87	low	3.11	0.92	3.36	5.61	0.57	0.17	1.80	2.70	3.19	24.03	16.35
24	35.56	high	5.31	0.79	8.14	13.48	1.49	1.16	5.26	8.16	8.79	90.57	16.76
						Tinto-Odiel							
6	36.4	-	6.36	1.07	13.63	20.14	1.84	2.50	8.06	10.83	12.74	103.78	17.28
12	36.5	-	7.84	1.58	7.36	10.31	1.08	1.43	4.37	5.75	6.95	49.00	9.35
18	36.48	-	5.36	0.00	9.90	13.87	1.36	2.02	6.62	8.38	11.87	86.93	18.91
24	36.44	-	3.98	0.47	5.85	10.90	0.80	1.39	3.94	5.70	6.26	64.43	19.59

Capítulo 5

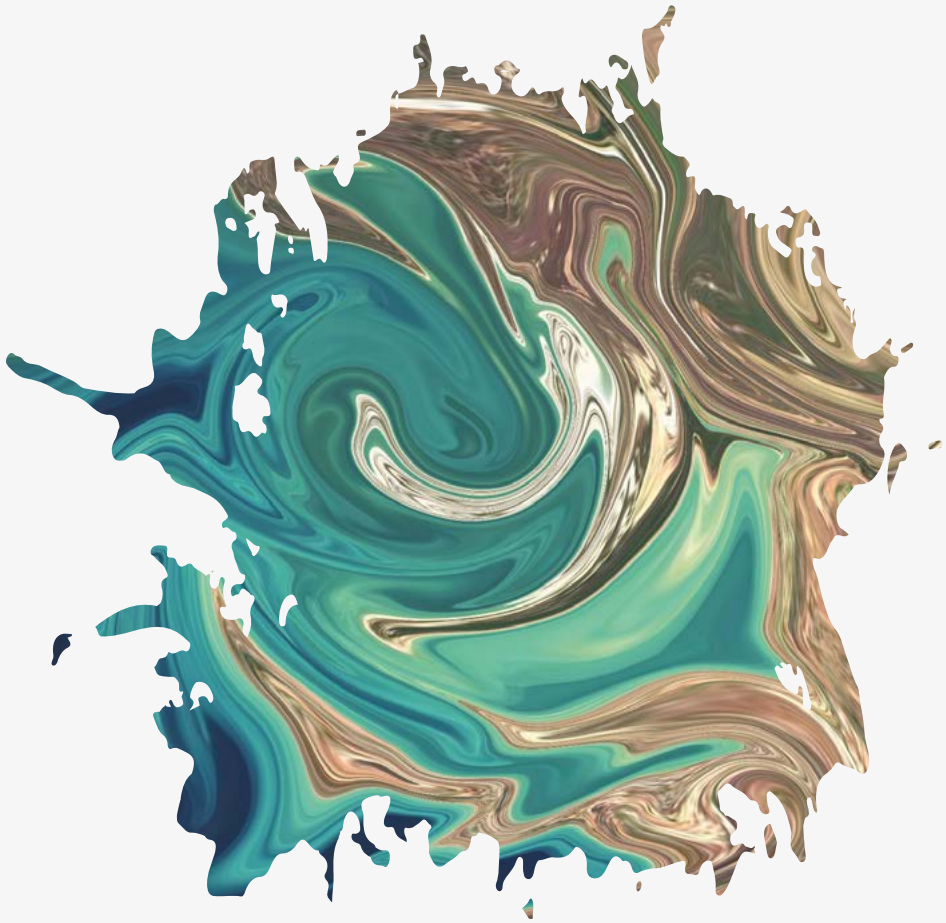

"An increased of carbon dioxide in the atmosphere would lead to global warming".
Eunice Newton Foote, 1856.

Linkages between greenhouse gases (CO_2, CH_4, and N_2O) and dissolved organic matter composition in a shallow estuary*

Amaral, V.[1,2*], Romera-Castillo, C.[3], García-Delgado, M.[1], Gómez-Parra, A.[1], Forja, J.[1]

[1]Departamento de Química-Física, INMAR, Universidad de Cádiz, Puerto Real, España.
[2]Ecología Funcional de Sistemas Acuáticos, Centro Universitario Regional Este, Universidad de la República, Rocha, Uruguay.
[3]Instituto de Ciencias del Mar-CSIC, Barcelona, España.

Publicado en *Science of the Total Environment

Graphical Abstract

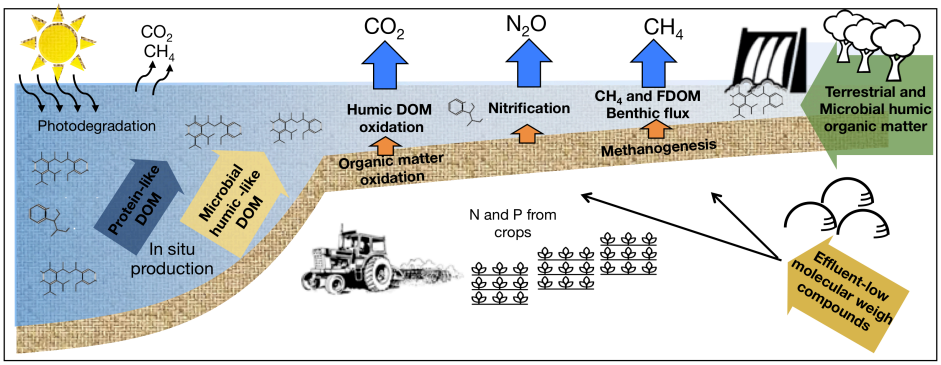

Abstract

Estuarine systems receive large amounts of organic matter that enhance the production of greenhouse gases (GHGs), such as carbon dioxide (CO_2), methane (CH_4), and nitrous oxide (N_2O). Despite considerable research on GHGs and dissolved organic matter (DOM) distribution in estuaries, little is known about the linkage between these gases and DOM composition. Here we evaluated the relationship between three GHGs (CO_2, CH_4, and N_2O) and DOM composition, determined through optical properties, in Guadalete estuary (Bay of Cadiz, Spain). The partial pressure of CO_2, and CH_4 and N_2O concentrations ranged between 332.8-6807.1 µatm, 19.9-6440.1 nM, and 6.8- 283.9 nM, respectively. Thus, the Guadalete estuary was a source of CO_2, CH_4 and N_2O to the atmosphere. We validated three PARAFAC components related to humic-like fluorescence from terrestrial, microbial and effluent sources, and one with protein-like material. Humic-like components accounted for 86% ± 6% of the total FDOM pool, indicating a predominantly allochthonous DOM origin. The three GHGs were significantly linked to DOC concentration and DOM composition, exhibiting different patterns in these linkages. Terrestrial and microbial humic-like substances with increasing aromaticity might enhance pCO_2 in

Guadalete estuary. Dissolved CH_4 concentrations showed the strongest relationship with DOM composition, indicating that humic and protein-like material are linked with their distribution. In contrast, dissolved N_2O was only related with the protein-like fraction and with humic-like material derived from anthropogenic activities (sewage and agriculture). Our results further indicate that a possible coupling between benthic fluxes of GHGs and DOM might be occurring in this shallow estuary. We conclude that it is important to account for DOM composition when studying GHGs distribution in estuarine systems to understand their roles and potential responses associated with climate change.

Keywords: carbon dioxide, methane, nitrous oxide, fluorescent DOM, estuaries

IV. 1. Introduction

Rivers and estuaries are the main links between land and ocean, connecting over 87% of the land surface area to coastal waters (Bauer and Bianchi, 2011). Estuaries receive large amounts of organic matter from rivers such as humic substances, domestic sewage and freshwater phytoplankton, which undergo major transformations within estuaries before reaching the coastal zone (Bauer and Bianchi, 2011). This provides optimal conditions for greenhouse gas (GHGs) production (Liikanen et al., 2009).

Estuaries are significant sources of all major GHGs - carbon dioxide (CO_2), methane (CH_4) and nitrous oxide (N_2O) - to the atmosphere (e.g. Bange, 2006; Borges and Abril, 2011; Cai, 2011). Auto- and heterotrophic microbial processes cycle these gases through the water column and sediments (e.g. Daniel et al., 2013; Liikanen et al., 2009). The presence of vegetation (e.g. macrophytes) also plays a relevant role in GHGs

distribution, especially in CO_2 and CH_4 concentration (Borges and Abril, 2011). The main processes controlling pCO_2 distribution are photosynthesis, aerobic and anaerobic oxidation of organic matter, lateral transport of CO_2 from marshes and tides, photochemistry, and CO_2 air-water exchange (Abril and Borges, 2005; Cai, 2011; Moran and Zepp, 1997). Traditionally, CH_4 has been considered to be mainly produced via methanogenesis during the final stage of organic matter degradation in anoxic sediments, and consumed via methanotrophy in oxic conditions (Reeburgh, 2003). However, several studies from freshwater and marine environments indicate the importance of CH_4 aerobic production via bacterial degradation of phosphonate esters in dissolved organic matter (DOM) (e.g. Karl et al., 2008; Repeta et al., 2016), photoautotrophic carbon fixation of algae and cyanobacteria (Bižić et al., 2020) and photoproduction from DOM (Li et al., 2020). On the other hand, N_2O is mainly produced as a by-product during the microbial oxidation of ammonium to nitrate (autotrophic nitrification) and as an obligate intermediate during anaerobic microbial reduction of nitrate to dissolved N_2 (heterotrophic denitrification) (Bange et al., 2010). Both processes can occur in the water column, in sediments or in the interior of suspended particles and they depend on the concentration of dissolved oxygen (DO) (Bange, 2008, 2006; Nevison et al., 2003). Additionally, benthic mineralization can be a major source of the three GHGs to the water column (e.g. Araujo et al., 2018; Meyer et al., 2008, Burgos et al., 2018).

In general, estuaries are net heterotrophic systems where respiration exceeds primary production (Gattuso et al., 1998), CH_4 far exceeds atmospheric equilibrium (Middelburg et al., 2002), and an important amount of N_2O is produced (Bange, 2006). Human activities are causing a

potential increase in GHGs emissions from estuaries. For example, agricultural land use introduces higher load of N, potentially increasing estuarine N_2O emissions to the atmosphere (Wells et al., 2018). Moreover, CH_4 emissions could also be affected by the intensity of land use, since it increases the availability of organic carbon that acts as a substrate for methanogenesis (Wells et al., 2020). The relationships found between CH_4 and CO_2 concentration with dissolved organic carbon (DOC) and DO also indicate that the processing of organic matter gives rise to the formation of these gases (Borges et al., 2019). Additionally to this terrestrial and riverine organic matter inputs, the variability of CH_4 and CO_2 emissions in estuaries can be affected by seasonal changes in groundwater discharge enriched with these gases (Rosentreter et al., 2018).

In estuaries, the supply of terrestrial DOM often dominates, however autochthonous sources and anthropogenic inputs from the watershed have also been shown to be important contributors (Bauer and Bianchi, 2011). For example, sediments may also represent an important source of DOM to the water column in shallow estuaries (Burdige and Komada, 2015; Maher and Eyre, 2010). During particulate organic matter degradation, almost 10 % accumulates as a mixture of labile and refractory DOM in sediments pore water (Burdige and Komada, 2015; Komada et al., 2013). It has been suggested that benthic fluxes of DOC to coastal and estuarine systems are similar in magnitude to riverine DOC fluxes to the ocean ($\sim 0.09 \times 10^{15}$ and $\sim 0.2–0.4 \times 10^{15}$ g C yr^{-1}, respectively) (Burdige and Komada, 2015).

The optical properties of DOM, absorbance and fluorescence, have been widely used to assess the sources and behavior of different fractions of DOM in estuaries (e.g. Coble, 2007; Yamashita et al., 2013; Coble et al.,

2014). Chromophoric DOM (CDOM) is mainly derived from the terrestrial environment but is also controlled by sediment resuspension, degradation, and production of in situ algae and vascular plants as well as anthropogenic inputs from the watershed (industrial and agricultural) (Bauer and Bianchi, 2011; Coble et al., 2014). Photodegradation is the main sink of CDOM leading to the production of CO_2, CH_4 or labile DOC that fuel microbial respiration (e.g. Moran and Zepp, 1997; Li et al., 2020). Furthermore, CDOM mineralization also releases CO_2, CH_4 and N_2O into the water column which can later be released into the atmosphere, increasing global warming (Lapierre et al., 2013; Zhou et al., 2018, 2020).Fluorescent DOM (FDOM), a fraction of CDOM, can be mainly divided into humic-like, fulvic-like and protein-like substances. The latter can be associated with aromatic amino acids such as tryptophan or tyrosine and also pigment-like compounds (Coble et al., 2014). Recent studies found that terrestrial FDOM potentially enhanced CH_4 and N_2O concentrations in lakes (Zhou et al., 2018, 2020). In estuaries, FDOM can represent ~ 70 % of the total DOM bulk (Coble, 2007), therefore, this fraction of DOM may contribute to GHGs emission from estuarine systems.

In the last decades, CDOM and GHGs distribution in estuaries have received considerable attention; however, the linkages between them remain largely unknown. Climate change is expected to influence organic matter composition in estuaries through changes into precipitation patterns, freshwater delivery, and stratification (Canuel et al., 2012). Therefore, elucidating the connections between DOM composition and greenhouse gases dynamic could provide valuable information about the role and response of estuarine systems to global change. The aim of this work was to determine DOM composition and GHGs distribution in a shallow estuary

subject to anthropogenic activities (e.g. agriculture and urbanization). To further understand the importance of DOM composition in GHGs dynamics, we tested whether CO_2, CH_4 and N_2O were significantly related to different fractions of DOM. We hypothesized that the distribution of the three gases should be significantly linked to DOM concentration and composition, and that these relationships would vary depending on the gas.

IV. 2. Methods and Material

IV. 2.1 Study site

The sampling was carried out in the estuary of the Guadalete River (max. depth 6 m, 18 km long), located in the SW of Spain (Fig. 1). Guadalete River is 157 km long and its basin covers an area of 3677 km^2. It is characterized by semidiurnal meso-tides (mean tidal range 0.98-3.20 m), and it is subjected to an elevated anthropogenic pressure (Campana et al., 2005). Extensive irrigated crops (sugar beet, cotton, sunflower, wheat and tomatoes) are found on its margins and it receives effluent discharge from farms and a sewage treatment plant from Jerez de la Frontera city (215,000 population).

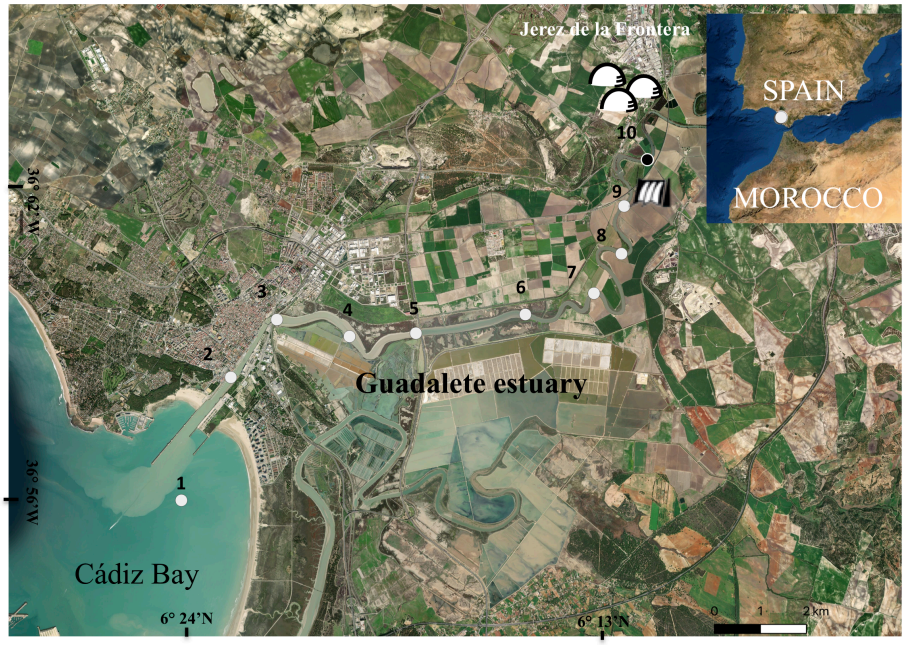

Fig. 1. Location of the sampling stations in Guadalete estuary (circles). The black dot indicates the station after the dam. The wastewater treatment plant from Jerez de la Frontera city is indicated.

Surface water samples were collected in May 2016 (spring16), November 2017 (autumn), February 2018 (winter), June 2018 (spring18) and July 2018 (summer) at ten sampling stations (n = 50). The first station was located at the estuary mouth and the last station was placed after a dam that regulates the river flow in the fluvial zone of the estuary. Sampling was performed during the falling tide and the tidal range was between 1.8 and 2.4 m. In June 2018, the sampling was performed during low tide due to weather conditions. *In situ* temperature was measured with a mercury thermometer (± 0.1 °C precision), and salinity was quantified in the laboratory using an induction salinometer Rousemount® Analytical (± 0.001 units precision). A mini CTD (YSI Castaway) was used to check the water column homogeneity. An acid-cleaned amber glass bottle (0.25 L) was used to collect nutrients (nitrate, ammonium and phosphate), alkalinity, DOC and optical properties of DOM. In May 2016, samples for chlorophyll *a*

were collected.

Samples were filtered through pre-combusted glass fiber filters (Whatman, GF/F nominal size = 0.7 µm, 450 °C, 4 h) using acid-cleaned glass filtration systems, previously rinsed with the sample. Aliquots for nutrients and DOC were frozen (-20 °C) until their analysis, while alkalinity, absorbance and fluorescence were measured immediately. Water samples for dissolved CH_4 and N_2O determinations were taken by duplicate in 250 mL airtight glass bottles, preserved with saturated mercuric chloride to inhibit microbial activity, and sealed with Apiezon® grease to prevent gas exchange. After sealing, the samples were conserved in darkness to prevent photochemical reactions, and stored at approximately 25 °C until later analysis in a controlled temperature lab (± 2 °C). Additionally, samples for quantification of DO were taken, fixed onboard and stored in darkness until their analysis.

IV. 2.2. Determination of DO, pH, alkalinity, DIC, pCO_2 and nutrients

The Winkler method was used for DO analysis (Grasshoff and Ehrhardt, 1983), by potentiometric endpoint titration (Metrohm, 906). The precision of the determinations obtained was ± 0.5 µmol kg^{-1}. We calculated the apparent oxygen utilization (AOU) using the solubility expression proposed by Weiss (1970). The DO concentration is not available for November 2017.

The pH and total alkalinity (A_T) were measured by duplicate by potentiometric titration (Metrohm 906) with a glass-combined electrode (Metrohm, 6.0253.100) previously calibrated along the whole pH scale using a TRIS buffer solution (± 0.003). The A_T measurements were validated using reference standards from A. Dickson (Scripps Institute of

Oceanography, San Diego, USA) to an accuracy of 3 µmol kg^{-1}. Dissolved inorganic carbon (DIC) and the partial pressure of CO_2 (pCO_2) were calculated from A_T and pH using the acidity constants K1 and K2 for estuarine waters proposed by Millero, (2010) with the CO2SYS program (Pierrot et al., 2006). To evaluate the effect of DOM on A_T, organic alkalinity (A_{ORG}) was calculated following Hernández-Ayón et al., (1999). Thus, we calculated corrected A_T using CO2SYS program. A_{ORG} was obtained from the subtraction of the corrected alkalinity to the A_T.

Nutrients analyses were performed in a segmented flow autoanalyzer (Skalar, San Plus) based on classic spectrophotometric methods (Grasshoff and Ehrhardt, 1983). The accuracy was ±0.10 µM for nitrate, ±0.05 mM for ammonium and ±0.02 µM for phosphate.

The concentration of chlorophyll *a* was quantified using the fluorimetric method described by Parsons et al. (1984). Chlorophyll *a* in the GF/F filters was stored at -20 °C until analysis. Chlorophyll *a* was extracted in 90% acetone, left 24 h in dark and measured in a spectrofluorometer (JASCO FP-8300), calibrated with a chlorophyll standard (Sigma- Aldrich, C6144).

IV. 2.3. Determination of DOC, CDOM and FDOM

DOC concentrations were measured using the high-temperature catalytic combustion method with a Multi N/C 3100 Analytik Jena analyzer. Potassium hydrogen phthalate was used to calibrate the system daily. Deep seawater and low carbon reference waters (Hansell CRM Program, 42–45 µM) were measured to assess instrument variability (n = 5, 43 ± 1.8 µM).

UV–visible absorption spectra were obtained scanning from 250 nm to 800 nm using a 1 cm path length quartz cuvette in a JASCO-V750

spectrometer connected to a programmable temperature control system set at 20° C. We calculated the Napierian absorption coefficients at 254 and 350 nm in m^{-1} (Green and Blough, 1994), proxies of the abundance of conjugated carbon double bonds and a quantitative indicator of CDOM, respectively (Coble, 2007). The C-specific ultraviolet absorption coefficient at 254 nm ($SUVA_{254}$), a proxy of aromaticity, was calculated by dividing the decadic absorption coefficient at 254 (in m^{-1}) by the concentration of DOC (in mg L^{-1}) (Weishaar et al., 2003).

Fluorescent measurements were performed in a spectrofluorometer (JASCO FP-8300) connected to a Peltier Thermostatted Cell Holder with stirrer accessory (EHC-813) for temperature control (20°C). A 1-cm quartz cuvette was used. Excitation and emission spectra ranged from 250 nm to 450 nm (5 nm steps) and from 300 nm to 560 nm (1 nm steps), with a bandwidth of 5 nm, and an integration time of 0.2 s. Spectra were improved by the instrument correction factors and the inner filter effect was addressed by correcting EEMs using the absorbance-based approach (Kothawala et al., 2013). Data was standardized and normalized to Raman Units (RU) based on measurements of Raman peak at 350 nm (Lawaetz and Stedmon, 2009).

We used PARAFAC modeling to characterize and identify individual fluorescent components (fluorophores) that comprise the estuary DOM using drEEMs toolbox (version 0.2.0; Murphy et al., 2013) for Matlab (R2015b). Signal from Raman and Rayleigh scattering were removed in each EEM that were then normalized by their intensities. We used non-negative constraint, split-half validation, random-initialization analyses, examination of outliers and model's residual (Stedmon and Bro, 2008) to obtain the PARAFAC model. The online repository OpenFluor database was used for the identification of the PARAFAC components (Murphy et al., 2014).

IV. 2.4. Determination of dissolved CH_4 and N_2O

Dissolved CH_4 and N_2O were determined using a gas chromatograph (Bruker® GC-450) equipped with a flame ionization detector (FID) for CH_4, operated at 300 °C, with an air flux of 300 mL min^{-1} and a hydrogen flux of 30 mL min^{-1}, and with a ^{63}Ni electron capture detector (ECD) for N_2O, operated at 350 °C. For CH_4, nitrogen was used as the carrier gas (10 mL min^{-1}). The gas was separated on a stainless-steel column (0.5 m × 1/8-in packed with 80/100 Hayesep N) and a Molecular Sieve (1.0 m ×1/8-in Porapak QS). For N_2O, a mixture of Ar/CH_4 (95%/ 5%) was used as the carrier gas (10 mL min^{-1}), and the gas was separated on two stainless-steel columns (0.5 m × 1/8-in Hayesep N, 80/100 and 2.0 m × 1/8-in Hayesep D). The detectors were calibrated daily using four standard gas mixtures certified by AbelloLinde, with CH_4 concentrations of 1952, 3078, 10064, 103829 ppbv, and N_2O concentrations of 304, 430, 474 and1766 ppbv. Standard gas mixtures were calibrated with the SCOR (Scientific Committee on Oceanic Research) standard available in Spain (Dr. Mercedes de la Paz, Instituto de Investigaciones Marinas, CSIC IIM, Vigo). We measured CH_4 and N_2O by duplicate using headspace equilibration. A quantity of 25 g (± 0.01 g) of water samples was taken using a 50 mL glass syringe (Agilent P/N 5190–1547) (Sierra et al. 2017, 2020). A volume of 25 mL with the standard gas mixture of CH_4 and N_2O concentrations similar to atmospheric values (1952 and 304 ppbv, respectively) was used to complete the volume of the syringe. To ensure mixing, the syringes were shaken for 5 minutes (VIBROMATIC Selecta) and the sample was injected manually in the chromatograph when equilibrium was reached (5 minutes).

We calculated the concentration of the gases in the water samples from the concentration measured in the headspace, using salinity of the

samples, equilibration temperature (±0.1 °C), and the expressions for solubility given by Wiesenburg and Guinasso, (1979) for CH_4, and by Weiss and Price, (1980) for N_2O.

To remove the effect of temperature and salinity on the distribution of GHGs we calculated the excess values of the three gases (ΔpCO_2, ΔCH_4, ΔN_2O) as the difference of the concentration of the dissolved gas and the expected equilibrium concentration in water. The excess of DIC (ΔDIC) was calculated as the difference between the *in situ* DIC and a theoretical DIC at atmospheric equilibrium (Abril et al., 2000).

2.5 Statistical analysis

Statistical analysis was run in R (Version 1.3.1073, RStudio). We used one-way ANOVA, and post hoc Tukey multiple comparisons of means 95% family-wise confidence level to analyzed temporal differences between samples in the dataset. We log-transformed not-normally distributed variables, and when data failed in normality or homogeneity of variance (checked with Shapiro–Wilk and Levene Test, respectively), even after simple transformations, we applied Kruskal–Wallis tests. A significance level of 0.05 was selected. We applied linear regressions analysis to explore the relationship between 1) DOM properties and inorganic constituents with salinity, 2) variables used to characterize DOM, and 3) greenhouse gases (response variable) and DOM properties (explanatory variable). A significance level of 0.01 was selected. In the third case, we added salinity and temperature as explanatory variables to remove the effect of water mass dilution. We used the variance inflation factor (VIF) to assess multi-collinearity effects between variables. VIF values > 10 are usually taken as an indication of multi-collinearity (O'Brien, 2007). We quantified the relative importance contribution of each explanatory variable to the multiple

regression models according to Grömping (2006).

IV. 3. Results

IV. 3.1. Physicochemical variations, inorganic nutrients and alkalinity distribution

The sampling period covered a wide range of environmental conditions in Guadalete estuary (Table 1). Temperature reflected the expected seasonal variations (10.8-25.8 °C) with the lowest values during autumn and winter and the highest during spring16, spring18 and summer ($p < 0.05$). Salinity ranged between 0.7 and 37.9, increasing downstream, and with no seasonal changes ($p > 0.05$). However, in spring18, salinity showed the smallest variability with values < 1 from station 5 up to 10 due to sampling at low tide. AOU varied from -22.0 to 161.5 µM, increasing upstream, and with higher values during spring18 ($p < 0.05$).

Table 1. Variation ranges and mean ± standard deviation of temperature (T, °C), salinity (S), apparent oxygen utilization (AOU, µM) and pH during each sampling. Monthly-accumulated precipitation is also shown (L m^{-2}). na: not available.

	Spring16	Autumn	Winter	Spring18	Summer
Rain	125	30	46	2	2
T	21.6 - 25.8	12.5-16.5	10.8- 12.4	21.0 - 22.1	23.4 - 24.9
	23.8 ± 1.5	14.4 ± 1.1	11.5 ± 0.5	21.6 ± 0.3	24.1 ± 0.5
S	3.7 - 37.9	1.2-37.2	1.3-36.8	0.8 - 37.2	0.8 - 37.9
	19.3 ± 12.5	14.6 ± 13.8	17.3 ± 13.7	7.5 ± 11.8	16.6 ± 16.6
AOU	-22.0 -	11.3 - 161.5	na	179.8 -	-4.4 - 104.5
	110.9	88.5 ± 48.8		231.0	55.9 ± 38.5
	56.3 ± 41.7			225.1 ± 23.7	
pH	7.54 - 7.96	7.72-8.00	7.75-7.89	7.66 - 8.02	7.26 - 7.84
	7.66 ± 0.15	7.81 ± 0.08	7.84 ± 0.05	7.77 ± 0.11	7.53 ± 0.19

Inorganic nutrients concentrations were highly variable (Fig. 2). Nitrate varied from 0.1 to 268.7 µM with higher values during spring18

compared to spring16 and summer ($p < 0.05$), while ammonium was between 1.2 and 1119.9 µM with lower values during summer compared to autumn and winter ($p < 0.05$). Phosphate was between 0.03 and 3.88 µM with the lowest values in spring18 ($p < 0.05$). In general, an increase in nutrients toward the fluvial zone was observed, although maximum values of phosphate were observed in the middle zone of the estuary (St 4 to 6). This was probably associated with lateral inputs from channels connected with crop areas.

pH ranged from 7.26 to 8.00 with the lowest values in summer. Temporal differences were not found for total alkalinity (A_T) or dissolved inorganic carbon (DIC), which varied from 2417 to 5786 µM and from 2163 to 5773 µM (Fig. 2, $p > 0.05$). On the other hand, A_{ORG} varied from 209. 5 to 540.3 µM, and showed higher values in spring18 (409 ± 75 µM) than the rest of the dates (302 ± 44 µM, $p < 0.05$). Noteworthy, during summer, the lowest values of A_{ORG} were observed (209 - 221 µM), but could only be calculated at the first three stations due to the low pH found in this sampling. The three variables, A_T, DIC and A_{ORG} decreased downstream and were negatively related with salinity (R^2 = 0.61, 0.68 and 0.63, respectively, $p < 0.01$, $n = 45$).

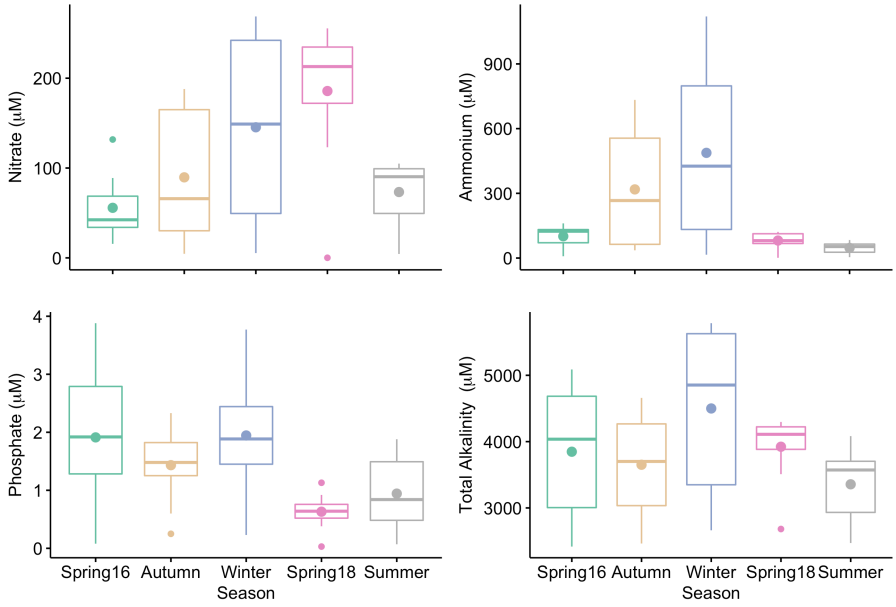

Fig. 2. Boxplot of inorganic nutrients and total alkalinity for each sampling date.

IV. 3.2. Dissolved organic matter distribution

DOC concentration varied from 117.2 to 622.0 µM with similar values between sampling dates (Table 3, $p > 0.05$). Absorption coefficients a_{254} and a_{350} varied from 2.68 to 49.60 m^{-1} and from 0.43 to 18.62 m^{-1}, respectively, and were highly related between them ($R^2 = 0.91$, $p < 0.01$, $n = 50$). Therefore, only a_{254} data will be shown here (Fig. 3). Higher values of a_{254} were observed in spring16 (Table 3, $p < 0.05$) when higher monthly-accumulated precipitation took place (Table 1). Both DOC concentration and CDOM (as a_{254} and a_{350}) decreased downstream (Fig. 3), reaching minimum values at the marine station (St 1) and showing a negative relationship with salinity ($R^2 = 0.53$, 0.47 and 0.23, respectively, $p < 0.01$, $n = 45$). $SUVA_{254}$ values ranged from 0.61 to 3.82 L mg^{-1} m^{-1}, and were higher in spring16 (2.7 ± 0.7 L mg^{-1} m^{-1}) than during the rest of the sampling period (1.9 ± 0.6 L mg^{-1} m^{-1}) ($p < 0.05$). A weak negative relationship was observed between $SUVA_{254}$ and salinity ($R^2 = 0.28$, $p < 0.01$, $n = 45$).

Four fluorescent components were identified using PARAFAC modeling and matched with previous studies using OpenFluor database (Table 2) (Murphy et al., 2014). The PARAFAC model explained 99.6% of the variables of the whole EEMs dataset. Three samples that correspond to the marine St 1 were excluded from the model due to the presence of elevated scattering. Component 1, 2 and 3 (C1, C2 and C3) were classified as humic-like and component 4 (C4) as protein-like. Humic-like components had similar values during the study period (Table 3, $p > 0.05$), accounting for 86% ± 6% of the total FDOM pool. Conversely, protein-like C4 showed seasonal variation with lower values during spring18 and summer than during autumn and winter ($p < 0.05$). A strong relationship was observed between humic-like components ($R^2 > 0.9$, $p < 0.01$, $n = 50$). Thus, for simplicity, only C1 distribution will be shown here (Fig. 3). Similar to DOC and CDOM, humic-like components increased toward the fluvial zone and were negatively related with salinity during the study period ($R^2 > 0.56$, $p < 0.01$, $n = 45$). Overall, the protein-like C4 showed a non-linear dependence with salinity ($p > 0.01$, $n = 45$), however, seasonal linear relationships showed that in spring16 and autumn, C4 was strongly related with salinity ($R^2 = 0.91$ and 0.97, respectively, $p < 0.01$, $n = 9$).

Table 2. Spectral properties (Excitation and Emission maxima) of the four components validated using PARAFAC modeling (n = 50), general assignment and possible sources according to previously identified components (OpenFluor database, TCC > 0.96). Value in parentheses is secondary maximum.

Component	Ex_{max}/Em_{max}	Description	Possible sources
C1	275/411	Microbial humic-like	Ubiquitous, allochthonous autochthonous[1-20]
C2	360/432	Humic-like	Effluents, sewage [21-22]. Low molecular weight [2]
C3	270 (385)/456	Humic/Fulvic-like	Terrestrial[23]
C4	275/370	Protein-like	Biological activity [23,24,25,26]. Wastewater[27]

[1]Amaral et al., 2020, [2]Lambert et al., 2016, [3]Chen et al. 2018,[4]Murphy et al. 2018,[5]Stedmon et al., 2007a,[6]Murphy et al., 2008,[7]Stedmon et al., 2007b,[8]Cawley et al., 2012,[9]Williams et al., 2013,[10]Yamashita et al., 2010, [11]Yamashita et al., 2013,[12]Podgorski et al., 2018,[13]Garcia et al., 2019,[14]Lapierre et al., 2013,[15]Panettieri et al., 2020,[16]Cardenas et al., 2017,[18]Goncalves-Araujo et al., 2015,[19]Harjung et al., 2018,[20]Yamashita et al., 2011,[21]Osburn et al., 2016,[22]Murphy et al., 2011,[23]Bittar et al., 2016, [24]Garcia et al., 2019b,[25]Stedmon et al., 2003,[26]Li et al., 2016,[27]Stedmon et al., 2011

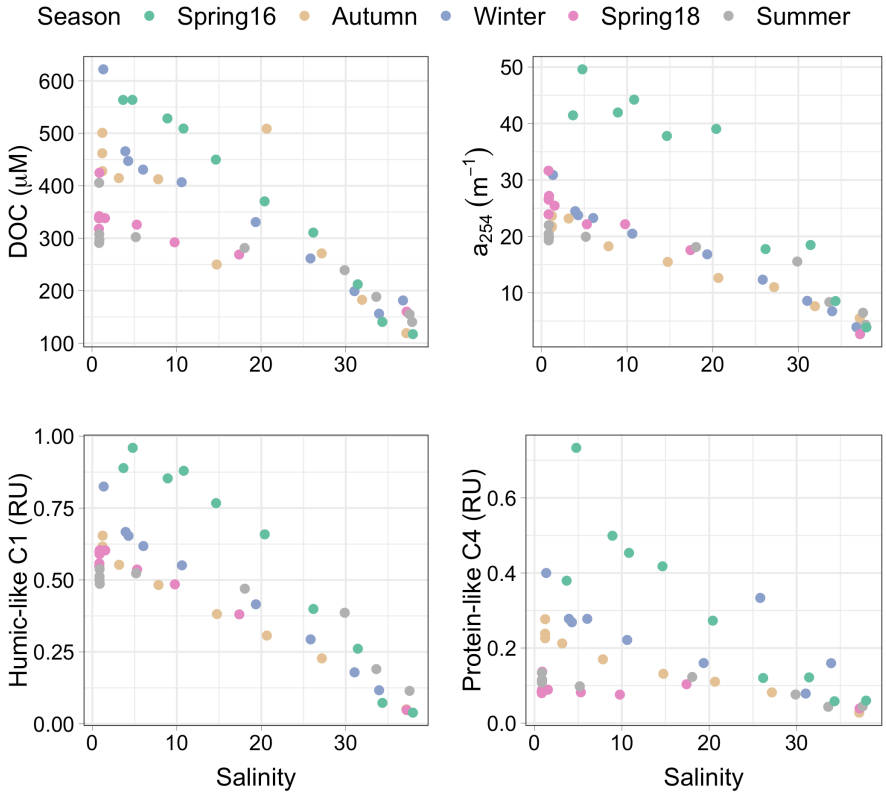

Fig. 3. Distribution of dissolved organic carbon (DOC), CDOM (as a_{254}) and fluorescent components C1 and C4 along the salinity gradient for each sampling date.

Table 3. Variation ranges and mean ± standard deviation of dissolved organic matter properties and greenhouse gases along the salinity gradient during the study period. Dissolved organic carbon (DOC), absorption coefficients at 254 and 350 nm (a_{254} and a_{350}), fluorescent components (C1 to C4, RU), partial pressure of CO_2, dissolved methane (CH_4) and nitrous oxide (N_2O) are shown.

	Spring16	Autumn	Winter	Spring18	Summer
Dissolved organic matter					
DOC (µM)	117.18 - 563.76	119.01 - 508.78	156.13 - 621.95	160.02 - 424.69	140.29 - 405.58
	376.53 ± 173.35	354.89 ± 138.25	350.11 ± 150.39	314.64 ± 67.64	260.75 ± 80.94
a_{254} (m^{-1})	3.87 - 49.60	5.52 - 23.65	3.93 - 30.88	2.68 - 31.64	4.34 - 21.98
	30.27 ± 16.43	16.08 ± 6.64	17.12 ± 8.91	22.60 ± 7.94	15.44 ± 6.53
a_{350} (m^{-1})	0.67 - 18.62	1.53 - 6.18	0.83 - 7.06	0.43 - 11.74	0.87 - 5.12
	10.59 ± 6.22	3.59 ± 1.55	3.84 ± 2.02	6.68 ± 2.84	3.16 ± 1.44
C1 (RU)	0.04 - 0.96	0.05 - 0.65	0.12 - 0.82	0.05 - 0.60	0.11 - 0.54
	0.58 ± 0.35	0.43 ± 0.20	0.48 ± 0.24	0.49 ± 0.17	0.41 ± 0.16
C2 (RU)	0.03 - 0.8	0.04 - 0.77	0.08 - 0.83	0.03 - 0.44	0.08 - 0.40
	0.44 ± 0.28	0.43 ± 0.26	0.41 ± 0.24	0.35 ± 0.12	0.29 ± 0.11
C3 (RU)	0.04 - 0.59	0.04 - 0.33	0.08 - 0.45	0.04 - 0.37	0.08 - 0.30

	0.36 ± 0.21	0.23 ± 0.10	0.28 ± 0.13	0.31 ± 0.10	0.24 ± 0.08
C4 (RU)	0.06 – 0.73	0.03 - 0.28	0.08 - 0.40	0.04 - 0.14	0.04 - 0.13
	0.31 ± 0.22	0.16 ± 0.08	0.24 ± 0.10	0.09 ± 0.03	0.09 ± 0.03
			Greenhouse gases		
pCO_2	527 - 5063	333 - 1790	538- 2112	482 - 3219	718.1 - 6807
(µatm)	2759 ± 1649	1111 ± 466	1547 ± 600	2250 ± 775	3445 ± 2092
CH_4 (nM)	19.9 - 920.7	22.5 - 3553.1	26.9 - 6440.0	20.8 - 838.8	24.0 – 1342.1
	476.1 ± 330.7	1192.7 ± 1271.6	1779.8 ± 2073.2	539.9 ± 284.8	311.3 ± 490.5
N_2O (nM)	7.8 - 147.3	8.8 - 152.7	9.9 - 283.9	8.8 - 28.1	6.8 - 167.6
	81.7 ± 51.0	92.0 ± 48.3	164.8 ± 99.2	23.5 ± 5.6	77.1 ± 53.8

IV. 3.3. Distribution of greenhouse gases (CO_2, CH_4 and N_2O)

Values of pCO_2 ranged from 333 to 6807 µatm during the study period, with the highest mean values in summer follow by spring16 and spring18 and the lowest in autumn follow by winter (Table 3). Temporal changes were only observed between summer and autumn ($p < 0.05$). The concentration of dissolved CH_4 ranged from 19.9 to 6440.0 nM with no temporal differences ($p > 0.05$). The highest value was observed at the station after the dam in winter (6440.0 nM), but when excluding this value, the maximum concentration observed in the study decreased to 3466.1 nM. The concentration of dissolved N_2O varied from 6.8 to 283.9 nM, with the lowest values during spring18 (< 28.11 nM, $p < 0.05$). The lowest values of the three gases were observed in the mouth of the estuary (St 1). Overall, an increase of pCO_2, CH_4 and N_2O was observed upstream (Fig. 4).

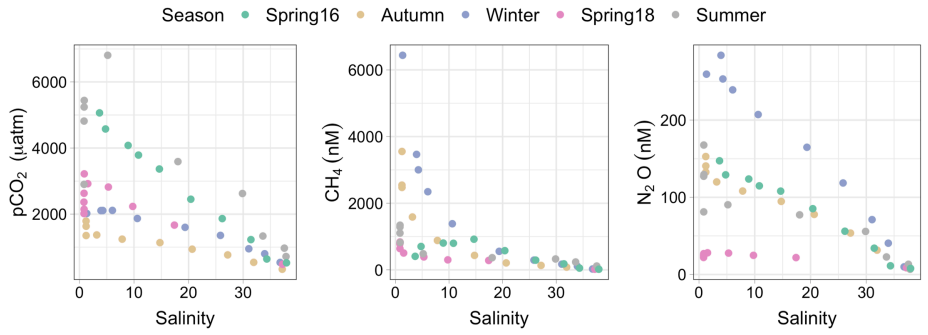

Fig. 4. Distribution of partial pressure of carbon dioxide (pCO_2), methane (CH_4) and nitrous oxide (N_2O) along the salinity gradient.

IV. 3.4. Relationship between DOM properties with GHGs and Organic alkalinity

To assess the relationship between DOM properties and the excess of the gases in the estuary, we used multiple regression models adding salinity and temperature to remove the effect of water mass dilution. Thus, we obtained the relationship between DOM variables and ΔpCO_2, ΔCH_4, ΔN_2O without the effect of dilution. We excluded the highest CDOM values from the regression models, which coincided with the highest precipitations being clearly related with terrestrial runoff (spring16, St 5 to St 10, $a_{254} > 37$ m^{-1}, $a_{350} > 13$ m^{-1}, C1 > 0.77 RU, C2 > 0.56 RU, C3 > 0.47 and C4 > 0.42 RU, n = 5). We also excluded two samples with $\Delta pCO_2 >$ 5000 µatm.

Overall, the multiple regression models explain > 84%, 71% and 58% of the variability of ΔCH_4, ΔpCO_2, and ΔN_2O, respectively, with a relative contribution of 38%-62% of DOM variables to the model (Table 4). For ΔpCO_2, we found that DOC concentrations, a_{254}, $SUVA_{254}$, and humic-like fluorescent components C1 and C3 contributed significantly to the regression models ($R^2 > 0.41$, $p < 0.01$), showing a positive trend with ΔpCO_2 (Fig. 5). For ΔCH_4, DOC concentration, a_{254}, and all the fluorescent components contributed significantly to the regression models ($R^2 > 0.38$, $p < 0.01$) also with positive trends between them (Fig. 6). Finally, for ΔN_2O, only DOC concentrations, the humic-like C2 and the protein-like C4 contributed significantly to explain its distribution ($R^2 > 0.58$, $p < 0.01$). Alike ΔpCO_2 and ΔCH_4, ΔN_2O also showed positive trends with these DOM variables (Fig. 7).

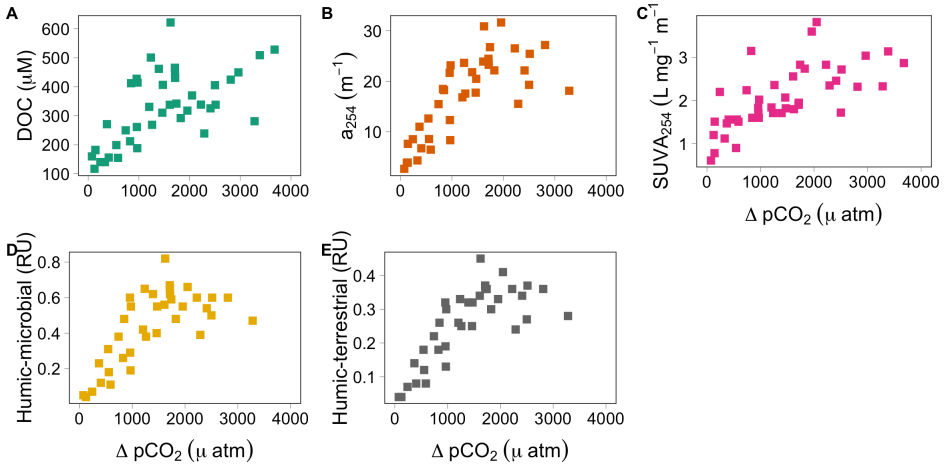

Fig. 5. Relation between the excess of the partial pressure of carbon dioxide (ΔpCO_2) and A: dissolved organic carbon (DOC), B: CDOM (as a_{254}), C: $SUVA_{254}$, D: microbial humic-like C1, and E: terrestrial humic-like C3.

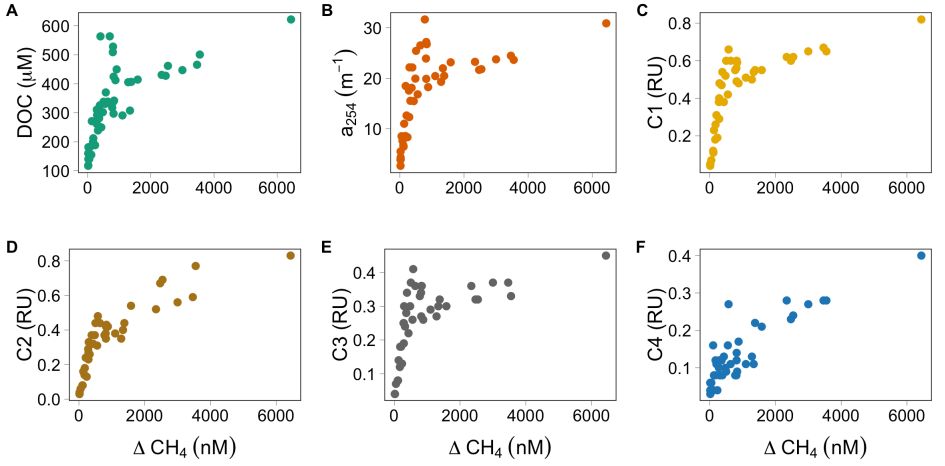

Fig. 6. Relation between the excess of dissolved methane (ΔCH_4) and A: dissolved organic carbon (DOC), B: CDOM (as a_{254}), C: the microbial humic-like C1, D: effluent humic-like C2, E: terrestrial humic-like C3, and F: protein-like C4.

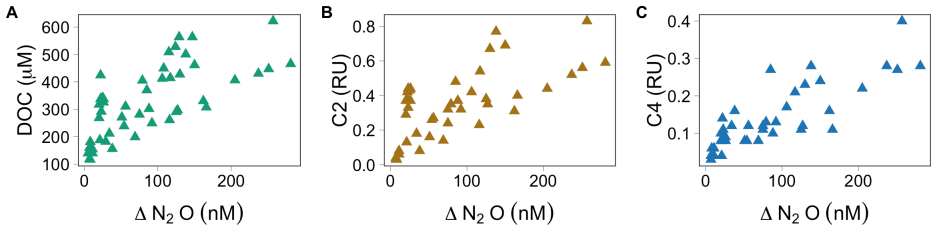

Fig. 7. Relation between the excess of nitrous oxide (ΔN_2O) and A: dissolved organic carbon (DOC), B: the effluent humic-like C2, and C: the protein-like C4, respectively.

We found positive linear relationships between A_{ORG} with CDOM (as a_{254} and a_{350}, $R^2 = 0.61$) and the humic-like components C1 and C3 ($R^2 = 0.45$ and 0.52 respectively, n = 42), while no relationship was observed with the humic-like C2 and the protein-like C4 ($p > 0.01$). Similar to ΔpCO_2, A_{ORG} was also positively related with $SUVA_{254}$ ($R^2 = 0.44$, n = 33).

IV. 4. Discussion

IV. 4.1. DOM characteristics in the estuary

The fluorescence characteristics of C1, C2 and C3 are similar to the humic fluorescence reported in earlier works (Table 2). In particular, C1 has been identified in a variety of aquatic environments from freshwater to open ocean and soils. This component has been associated with microbial humic-like material (Peak M, Coble et al., 2014) and is thought to represent both autochthonous and allochthonous DOM. On the other hand, C2 has been observed in several models applied to recycled water (wastewater, Murphy et al., 2011) and in an estuary affected by effluent discharge from treatment plants and farm wastes (Osburn et al., 2016). Therefore, C2 may be associated with discharges from the treatment plant located in Jerez de la Frontera city and farm wastes. Finally, C3 was the least common fluorescent component with only one match in the OpenFluor database (Bittar et al., 2016). This component has been described as a possible mixture of humic

and fulvic-like components of terrestrial origin (Stedmon et al., 2003), related to freshwater discharge in a tidal saltmarsh estuary (Bittar et al., 2016).

The characterization of the humic-like components showed potentially different sources (Table 2), but the similar pattern observed between them suggests that the processes that control their distribution may be coupled, as it was observed in other estuary (Yamashita et al., 2013). Thus, during the rainy season, the DOM pool is expected to contain a higher proportion of humic-like material derived from riverine discharge than during the dry season (Del Castillo et al., 1999). However, no temporal changes were observed in the distribution of the three humic-like components or DOC concentration ($p > 0.05$), suggesting that other processes than terrestrial runoff are controlling the distribution of DOM in this estuary.

Component 4 (C4) was identified as a protein-like component that could be a combination of Coble's peak N and T (Table 2). Peak N has been associated with phytoplankton derived labile material and Peak T has fluorescence properties similar to the amino acid tryptophan, which has also been associated with freshly produced DOM (Coble et al., 2014). However, C4 showed the lowest values in spring and summer (Table 3) when the highest concentration of chlorophyll was observed (Burgos et al., 2015). On the other hand, this component could be also the result of microbial activity from domestic sewage and farm wastes (Stedmon et al., 2011), which are enriched with tryptophan signal (Coble et al., 2014; Osburn et al., 2016). Thus, in this work, C4 could be also related with the direct discharge from the sewage treatment plant of Jerez de la Frontera and the farm channels located on its margins. Unlike the humic-like components, C4 showed

temporal changes associated with the precipitation regime, with the highest values matching the highest precipitations (Table 1, spring16 and winter), and the consequent larger discharge of organic matter from the sewage plants during the dry months (spring18 and summer). Probably, *in situ* microbial production of C4 may be occurring downstream, while upstream, the sewage plant is likely the main source of tryptophan-like signal. This could explain the relatively constant contribution of C4 to the total FDOM pool from St 5 (12% ± 4%) until St 10, near the sewage plant (13% ± 3%) (Fig.1). The highest contribution of C4 was observed in the marine St 1 (23% ± 8%). An autochthonous character of the protein-like components in combination with allochthonous sources has been observed in other estuarine systems (Yamashita et al., 2013).

DOC concentrations were highly related with FDOM components, mainly with the humic-like fraction (C1+C2+C3, $R^2 = 0.91$, $p < 0.01$, $n = 46$), showing almost identical patterns (Fig. 3), and to a lesser extent, with the protein-like C4 ($R^2 = 0.61$, $p < 0.01$, $n = 46$). From the relationship of the total fluorescence of the DOM and DOC concentration for all the samples, we obtain a y-intercept of 95.6 µM, which is the DOM colourless fraction. Since the mean DOC concentration during the study period was 327.7 µM, we estimated that a 71 % of the DOC pool in the Guadalete estuary is composed of fluorescent material. Even though in this estuary DOM has mainly an allochthonous character, the mean $SUVA_{254}$ values were intermediate and similar to those found in rivers during low freshwater discharges (2.8 L mg^{-1} m^{-1}, Kellerman et al., 2018). Our results indicate that the processes that control DOC and CDOM distribution in the estuary are coupled. They also showed that although DOM is mainly allochthonous and has mainly a humic-nature, there is another major source contributing to its

characteristics together with terrestrial runoff.

Several studies have shown that DOM contributions to A_T can be significant, especially in riverine and coastal waters (e.g. Kuliński et al., 2014). Here, we found A_{ORG} values higher than those observed in seawater, but similar to those observed in rivers (Kuliński et al., 2014). On average, A_{ORG} accounted for the 8.5% ± 1.8% of A_T, similar to the contribution found in rivers (Kulinski et al., 2014). A_{ORG} increased with increasing humic-like material from microbial or terrestrial sources, as well as with increasing aromaticity. This result is in agreement with several works that found that A_{ORG} is mainly formed by humic substances derived from terrestrial sources and/or benthic flux (Cai et al., 1998; Lukawska-Matuszewska et al., 2018). This shows that the production of A_{ORG} should be taken into account when quantifying CO_2 in shallow estuaries dominated by humic-like material.

IV. 4.2. Greenhouse gases distribution in Guadalete estuary

Several physical and biogeochemical processes can be involved in the spatial and temporal distribution of pCO_2, CH_4 and N_2O concentrations, such as riverine discharge, estuarine mixing, tidal pumping, benthic flux, and emission to the atmosphere, as well as microbial production and consumption of these gases within the estuary (Bange, 2006; Barnes and Upstill-Goddard, 2011; Borges and Abril, 2011).

Guadalete estuary acts as a source of CO_2, CH_4 and N_2O to the atmosphere, as it has been previously observed (Burgos et al., 2017, 2015). Values of CH_4 and N_2O concentrations were in the range of those previously found in the estuary (Burgos et al., 2015), but above those found in other estuaries (e.g. Middelburg et al., 2002, Rosentreter et al., 2018, Wells et al., 2018). In contrast, pCO_2 showed higher values than those previously found by Burgos et al. (2017) but similar to other estuaries (Abril and Borges,

2005). The increase of pCO_2 and CH_4 concentration observed upstream has been described in other estuaries and related to aerobic and anaerobic oxidation of terrestrial organic matter (Chen et al., 2008; Lin et al., 2016). On the other hand, N_2O production has been associated with nitrification process enhanced by the input of nutrients from wastewater upstream (Lin et al., 2016). This increase in the three gases upstream was also observed in other estuaries of the Gulf of Cádiz affected by anthropogenic pressure, but in general, with higher freshwater discharges than Guadalete estuary (Guadalquivir and Guadiana estuaries, Sierra et al., 2020). However, the mean concentrations of the three gases were higher in Guadalete estuary than in Guadalquivir and Guadiana estuaries, especially for CH_4 and N_2O. Thus, other processes together with freshwater inputs from riverine and lateral discharge may be playing a central role in GHGs distribution in this shallow estuary. Previous works in sediment pore waters of Guadalete estuary found that they acts as a source of CO_2, CH_4 and N_2O to the water column (Burgos et al., 2018). Moreover, the authors suggested that the amount of organic matter that reaches the sediments may play a larger role in CH_4 concentration than the effect of temperature (Burgos et al., 2018). This could explain the lack of seasonality found in both DOM and GHGs distribution in this human impacted estuary.

On the other hand, pCO_2 distribution showed maximum values during summer in the inner zone of Guadalete estuary (from St 6 to 9, 6807.1 to 4816.0 µatm), probably associated with the intensification of microbial activity with temperature (Cai, 2011). In contrast, values close to atmospheric equilibrium were observed in the marine zone (St 1, 332.8-537.7 µatm) coinciding with AOU negative values, likely as a result of photosynthetic activity. Coastal systems may be heterotrophic due to

terrestrial organic material inputs (Smith and Hollibaugh, 1993), or autotrophic if more organic matter is produced than remineralized (Gattuso et al., 1998). Autotrophic estuaries usually have a large coverage of macrophytes (e.g. seagrasses) or phytoplankton community (Maher and Eyre, 2012). A positive relation between ΔDIC and pCO_2 normalized to a temperature of 20 °C (pCO2@20 °C) with AOU, as well as a negative relationship between pH normalized to a constant temperature of 20 °C (pH@20 °C) and AOU are indicative of CO_2 net production (Borges and Abril, 2011). These trends between ΔDIC, pCO_2 @ 20 and pH @ 20 with AOU were found in Guadalete estuary (Fig. 8) indicating that this estuary is heterotrophic, supported by external inputs of organic matter (Borges and Abril, 2011). The theoretical lines of those relationships were drawn assuming atmospheric CO_2 equilibrium at AOU = 0. Overall, most of ΔDIC and pCO_2@20 °C data points were above the theoretical line (Fig. 8A and B), while most of the pH@20 °C data points were below the theoretical line (Fig. 8C). This could be due to allochthonous inputs of CO_2 either from freshwater discharge or from lateral inputs as well as the contribution of anoxic organic carbon degradation from sediments (e.g. Borges and Abril, 2011; Burgos et al., 2017). Furthermore, the high diffusive benthic fluxes of DIC observed in Guadalete (Burgos et al., 2018) suggest that benthic production can play an important role in pCO_2 distribution, mainly in the inner zone of the estuary.

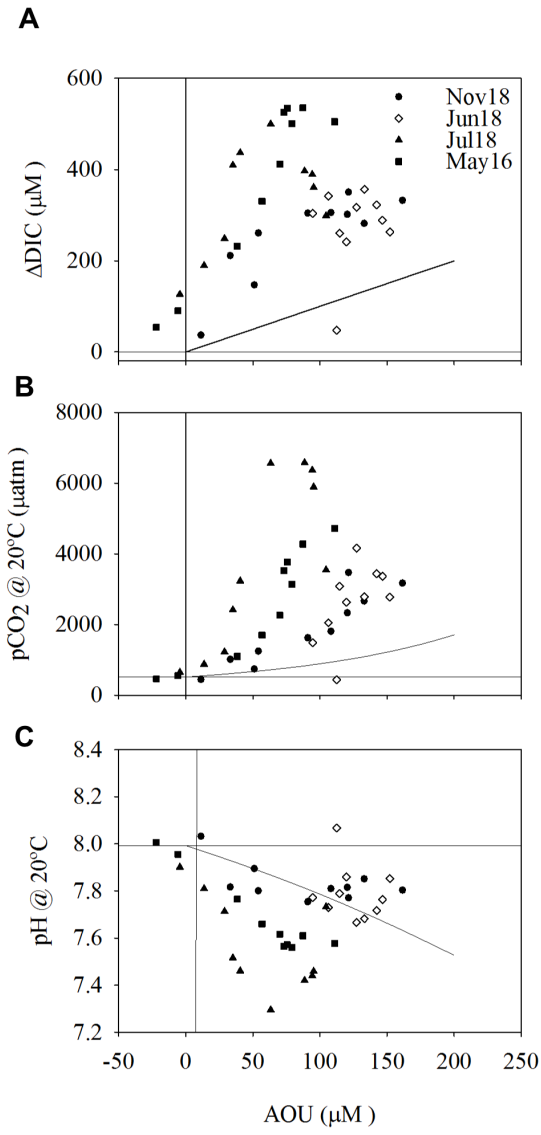

Fig. 8. Excess of dissolved inorganic carbon (A: ΔDIC), B: pCO_2 and C: pH normalized to 20°C versus apparent oxygen utilization (AOU) during the study period. The solid lines represent the theoretical evolution of the variables due to aerobic oxidation of organic matter.

Autotrophic nitrification (oxidation of NH_4 to NO_3) and heterotrophic denitrification (reduction of NO_3 to N_2) dominate N_2O formation in estuaries, indicating that dissolved N concentration should be positively related to N_2O. The positive linear relationships found here between ΔN_2O with AOU and NO_3 (R^2 = 0.78 and 0.83, $p < 0.01$, n = 40), indicates a N_2O production by autotrophic nitrification in the water column (Bange, 2006). However, the slope from the linear relationship between ΔN_2O and AOU suggests that 0.98 nmol of N_2O was produced per μmol of O_2 consumed. This ratio is one order of magnitude higher than those observed in other aquatic environments (Nevison et al., 2003), suggesting that other processes along with nitrification are contributing to the N_2O concentration found in Guadalete estuary. Moreover, benthic mineralization

can be a major source of N_2O to the water column in this estuary (Burgos et al., 2017). Denitrification in sediments is related to the supply of NO_3, organic matter, and oxygen depletion (Canfield, 1993). In Guadalete estuary, the oxygen penetration depth in sediments is less than 2 cm (Burgos et al., 2018) with an organic matter content of 3.2% in the marine zone and 8.4%-8.7 % in the middle and inner zone (Campana et al., 2005). That makes an ideal environment for denitrification to occur. Thus, in Guadalete estuary N_2O distribution was influenced by heterotrophic denitrification occurring in sediments, but also by autotrophic nitrification, in agreement with previous works (Burgos et al. 2015, 2017, 2018).

IV. 4.3. Linkage between DOM composition and greenhouse gases

Overall, DOM and GHGs distribution were partly controlled by the dilution effect during estuarine mixing. However, the weak R^2 values < 0.56 indicated that there are other processes rather than the dilution affecting their distribution. Hence, the coupling observed in this work between DOM properties and the distribution of the three greenhouse gases might be due to other factors rather than estuarine mixing. Two possible explanations are i) the influence of DOM characteristics in GHGs distribution observed in this work when removing the dilution effect (Table 4), and ii) benthic coupling between DOM and GHGs from the sediments to the water column.

The excess of the three gases were positively related with DOC concentrations (Table 4, Fig. 5A, 6A and 7A), indicating that their variations are linked to organic matter mineralization. Several works have indicated the importance of organic matter quantity in the GHGs distribution (e.g., Harley et al., 2015; Borges et al., 2018; Sierra et al., 2020). In this work, we found that the quality of DOM also affects GHGs

distribution in Guadalete estuary. The positive relationship observed between DOM variables and ΔpCO_2, ΔCH_4, and ΔN_2O varied depending on the gas (Table 4). This further indicates that DOM characteristics might influence the distribution of each of the three gases.

Overall, humic-like material from both terrestrial and microbial sources appears to be linked to pCO_2 concentration in Guadalete estuary (Fig. 5D and 5E). Rivers drain freshwater with elevated both organic and inorganic carbon, however according to Borges et al. (2006) CO_2 supply from rivers may be minor compared to its emission from estuaries. Moreover, we found the maximum ΔpCO_2 values before the dam (e.g. St 6 in summer 6476 µatm), indicating that most of the ΔpCO_2 is produced within the estuary. Our results indicate that microbial and terrestrial humic-like material fuel respiration in Guadalete estuary. In addition, the terrestrial C3 was described as a mixture of fulvic and humic-like compounds (Table 3). Fulvic acid in aquatic environments generally derives from plant litter and soils, and contains a significant content of aromatic carbon from lignin degradation (25%-30% of total carbon) (Malcolm, 1990). In this regards, ΔpCO_2 was positively related with the aromaticity index $SUVA_{254}$ (Table 4, Fig. 5C), suggesting that the contribution of condensed aromatic compounds from terrestrial source may increase pCO_2 values. Moreover, Sjögersten et al., (2016) found a strong relationship between CO_2 emissions and aromatic content in permafrost peatlands, and suggested that this chemical characteristic gives DOM the potential for rapid degradation under optimal conditions. It is also plausible that photochemical degradation of humic-like material contribute to CO_2 production (Miller and Zepp, 1995). The breakdown of high-molecular weight humic compounds by solar sunlight can produce CO_2 directly, and also indirectly by the rapid bacterial

utilization of labile photoproducts (e.g. Miller and Zepp, 1995, Moran and Zepp, 1997). Another possibility could be DOM photodegradation occurring in superficial sediments during low tide, between 30% and 40% of these are emerged, hence exposed to solar sunlight. However, humic-like C1 and C3 did not follow a pattern related with solar radiation (e.g. seasonal changes), indicating that the input of these components exceeded their photodegradation in Guadalete estuary. Despite photochemical mineralization of microbial and terrestrial humic-like DOM could be another source of CO_2, this source may be minor as it has been observed in other estuaries (Clark et al., 2004). We can conclude that decomposition of humic-like material derived from both terrestrial and microbial mineralization of DOM might be responsible for most of the ΔpCO_2 values in Guadalete estuary.

On the other hand, humic and protein-like FDOM may have an impact on ΔCH_4 production in this estuary (Table 4). However, the humic-like fraction of FDOM explained a larger proportion of the ΔCH_4 variability than the protein-like fraction. The accumulation of chromophoric terrestrial material may enhance CH_4 production in estuaries, as it has been observed in lakes (Zhou et al., 2018). These authors found that terrestrial CDOM input rather than protein material enhances dissolved CH_4 concentration in a eutrophic lake. Moreover, Araujo et al., (2018) found that a higher content of terrestrially derived organic matter contribute to high rates of methanogenesis in estuarine sediments and fluxes into the water column. On the other hand, aromatic amino acid, in particular tryptophan, enhanced CH_4 formation (Veluswamy et al., 2017). This could explain the positive relationship between CH_4 and C4. Several studies have indicated production of CH_4 in oxic surface waters from different marine and

freshwater ecosystems, such as lakes, reservoirs and oceans (Repeta et al., 2016; Bižić et al., 2020; León-Palmero et al., 2020). For example, the aerobic production of CH_4 as a by-product of methylphosphonate decomposition (MnP) in phosphate stressed waters (Karl et al., 2008). This has been observed in oceans and lakes (e.g. Repeta et al., 2016; Yao et al., 2016) under phosphate limitation, but no information was found for estuarine systems. According to Yao et al., (2016), CH_4 production by this process decreased in freshwater cultures with increasing PO_4 concentration, until complete inhibition at PO_4 > 30 µM. Although Guadalete estuary is not limited by P (0.03 < PO_4 < 3.88 µM), we calculated the ratio of DIN to total phosphorous (TP), which is a useful proxy of P limitation in aquatic environments (Axler et al., 1994) to determine its relationship with ΔCH_4 concentration. We found a positive relationship between this ratio and ΔCH_4 (R^2 = 0.26, p < 0.01, n = 50, PO_4 < 3.88 µM) that improves with decreasing PO_4 concentrations (R^2 = 0.62, p < 0.01, n = 22, PO_4 < 1.00 µM). This trend suggests that degradation of MnP from DOM could be contributing to CH_4 production in Guadalete estuary. However, further investigation is needed in aquatic environments not limited by P since there is evidences that some bacteria produce CH_4 when MnP is provided, whether or not it is the only P source (Yao et al., 2016).

Similar to CO_2, CH_4 production from photodegradation of CDOM was observed in a wide range of aquatic ecosystems across the land ocean continuum (Zhang and Xie, 2015; Li et al. 2020) with production rates increasing from ocean to land associated with and increase in CDOM (Li et al., 2020). This abiotic process is related to oxic CH_4 production through the breakdown of CDOM by solar irradiation that could release organic compounds that serve as precursors for non-microbial CH_4 production

(Keppler et al., 2009). Photoproduction of CH_4 could be also occurring in Guadalete estuary since humic-like substances dominate it and it presents CDOM amounts up to 18.6 m^{-1}. Another possible aerobic source is the *in situ* production of CH_4 by processes associated to the phytoplankton community (e.g. Bižić et al., 2020; León-Palmero et al., 2020). Unfortunately, data from chlorophyll *a* were only available for spring16, with chlorophyll *a* values between 0.7 and 12.2 µg L^{-1}, increasing upstream. A positive linear relationship was observed between CH_4 and chlorophyll *a* at $S > 20$ ($R^2 = 0.98$, $p < 0.01$, $n = 4$). Thus, CH_4 production in Guadalete estuary may be related to the marine phytoplankton community. This could explain the positive relationship with the protein-like C4. However, further investigation of oxic production of CH_4 in shallow estuaries is needed since, in general, benthic fluxes rather than oxic processes can explain the CH_4 concentrations found in estuaries (e.g. Borges and Abril, 2011, Araujo et al., 2018). Probably, in well-mixed shallow estuaries, such as Guadalete, sediment fluxes, riverine and lateral inputs may be more important in CH_4 emission than aerobic production in the water column.

Among the greenhouse gases, ΔN_2O was strongly related with the proteinaceus material (C4), showing a positive trend (Fig. 7B). This fraction contains N-enriched molecules of low aromaticity, and represents the most biolabile fraction of FDOM (Stubbins et al., 2014). There is evidence that the concentration of low molecular weight organic compounds controls the rate of denitrification (Baker and Vervier, 2004). Additionally, the fraction of DOM coming from effluents related to elevated discharge of nitrogen compounds (C2, wastewaters and farm discharges) and molecules with low aromaticity and molecular weight (Lambert et al., 2016) was also related with ΔN_2O (Table 4, Fig. 7C). Our results are in agreement with previous

works suggesting that N_2O is largely influenced by anthropogenic activities with high-DIN loading (Lin et al., 2016, Wells et al., 2018). We found that tryptophan-like compounds may enhance N_2O production rather than the humic-like fraction from microbial or terrestrial sources. Therefore, the increase in domestic loads (sewage) and the use of nitrogen-based fertilizers may favor N_2O production in estuaries.

Benthic fluxes are a major source of GHGs in Guadalete estuary, with higher values in the inner part of the estuarine than in the marine zone (Burgos et al., 2018). This benthic production variability could explain the higher concentrations of these gases found in the inner part of the estuary. On the other hand, heterotrophic microbial provide the major pathway for the transformation of particulate organic carbon to DOC, and ultimately to CO_2. For example, CH_4 production in coastal sediments is associated with bacterial remineralization of organic matter. It is more intense in shallow and productive environments where it is likely to be the dominant decomposition reaction of particulate organic matter to DOM (Martens and Klump, 1984). In this regard, sediment-water DOC fluxes can contribute up to 80% of the total estuarine DOC pool (Warnken and Santschi, 2004). Also, higher amounts of DOC, CDOM, and humic-like material have been observed in estuarine pore water samples than in surface water samples (Yang et al., 2014). In general, the fluorescence signal observed in the sediments is the same as those observed in the water column (Komada et al., 2002). Based on DOC concentrations found in porewater samples in the inner zone of Guadalete estuary (Burgos et al., 2018), we calculated DOC diffusive benthic flux of 1.0 and 7.2 mmol m^{-2} d^{-1}. These values are, in general, higher than those reported for other estuaries (0.1 to 3 mmol m^{-2} d^{-1}, Burdige and Komada, 2015). The humic-like fraction deposited in the sediments may be

metabolized and recycled back to the water column. We hypothesized that methanogenesis occurring in sediments could be releasing CH_4 and DOM with fluorescent signal to the water column, mainly in the humic-like fraction. Consequently, in shallow estuaries, FDOM release from sediments could be coupled with CH_4 benthic flux, and it could be as important to DOM distribution as terrestrial runoff.

IV. 5. Conclusions

Using the optical properties of DOM, we found that pCO_2, CH_4, and N_2O distribution in Guadalete estuary are related to the characteristic of the organic matter. Our results further suggest that the three GHGs will respond differently to changes in DOM composition. Estuaries worldwide are subjected to increasingly environmental perturbations, such as anthropogenic nutrient loading, land use change, hydrologic modifications as well as extreme climate events that influence freshwater discharges (e.g. droughts, floods) (Canuel et al., 2012, Wetz and Yoskowitz, 2013). These changes will affect organic matter composition in estuaries, hence impacting GHGs distribution. Therefore, it is important to account for DOM composition when studying GHGs distribution. Overall, pCO_2 in Guadalete estuary appears to be linked to humic-like material from both terrestrial and microbial sources, especially the aromatic content of DOM. On the other hand, CH_4 concentration appears to be highly related with both fractions of DOM, humic and protein-like material. In contrast, dissolved N_2O seems mainly related only with the protein-like fraction of DOM, associated with low molecular weight and high N-content compounds derived from anthropogenic activities (sewage and agriculture). Moreover, benthic coupling between DOM and GHGs distribution may be another plausible explanation for the positive relationships found here. A possible coupling

between benthic flux of CH_4 and DOM might be occurring in Guadalete estuary, especially in the inner zone. Thus, methanogenesis in sediments could be shaping the composition of DOM in the water column. We can conclude that in shallow estuaries, benthic flux of DOM and GHGs may be coupled.

Acknowledgements

We thank Ana Sierra for her assistance with GHGs measurements and Ana Isabel González for her participation in field and lab work. Valentina Amaral was financed by the National Research and Innovation Agency of Uruguay (ANII) with a Ph.D. fellowship (POS_EXT_2015_1_122780). Cristina Romera-Castillo was funded by the Spanish Ministry of Science and Innovation through a JIN Project with reference PID2019-109889RJ-I00. This study was financed by the Spanish CICYT (Spanish Program for Science and Technology) under contract RTI2018-100865-B-C21. Gastón Pereyra performed the final language revision. We thank James Sippo for his help with language. This manuscript was improved by comments from three anonymous reviewers.

References

Abril, G., Borges, A.V., 2005. Carbon Dioxide and Methane Emissions from Estuaries 187–207. https://doi.org/10.1007/978-3-540-26643-3_8

Abril, G., Etcheber, H., Borges, A. V., Frankignoulle, M., 2000. Excess atmospheric carbon dioxide transported by rivers into the Scheldt estuary. Comptes Rendus l'Academie Sci. - Ser. IIa Sci. la Terre des Planetes 330, 761–768. https://doi.org/10.1016/S1251-8050(00)00231-7

Abril, G., Iversen, N., 2002. Methane dynamics in a shallow non-tidal estuary (Randers Fjord, Denmark). Mar. Ecol. Prog. Ser. 230, 171–181. https://doi.org/10.3354/meps230171

Amaral, V., Romera-Castillo, C., García-Delgado, M., Gómez-Parra, A., Forja, J., 2020. Distribution of dissolved organic matter in estuaries of the southern Iberian Atlantic Basin: Sources, behavior and export to the coastal zone. Mar. Chem. 226, 103857. https://doi.org/10.1016/j.marchem.2020.103857

Araujo, J., Pratihary, A., Naik, R., Naik, H., Naqvi, S.W.A., 2018. Benthic fluxes of methane along the salinity gradient of a tropical monsoonal estuary: Implications for

CH4 supersaturation and emission. Mar. Chem. 202, 73–85. https://doi.org/10.1016/j.marchem.2018.03.008

Axler, R.P., Rose, C.R., Tikkanen, C.A., 1994. Phytoplankton nutrient deficiency as related to atmospheric nitrogen deposition in northern Minnesota acid-sensitive lakes. Can. J. Fish. Aquat. Sci. 51, 1281–1296. https://doi.org/10.1139/f94-128

Baker, M.A., Vervier, P., 2004. Hydrological variability, organic matter supply and denitrification in the Garonne River ecosystem. Freshw. Biol. 49, 181–190. https://doi.org/10.1046/j.1365-2426.2003.01175.x

Bange, H.W., 2008. Gaseous Nitrogen Compounds (NO, N2O, N2, NH3) in the Ocean, Nitrogen in the Marine Environment. https://doi.org/10.1016/B978-0-12-372522-6.00002-5

Bange, H.W., 2006. Nitrous oxide and methane in European coastal waters. Estuar. Coast. Shelf Sci. 70, 361–374. https://doi.org/10.1016/j.ecss.2006.05.042

Barnes, J., Upstill-Goddard, R.C., 2011. N2O seasonal distributions and air-sea exchange in UK estuaries: Implications for the tropospheric N2O source from European coastal waters. J. Geophys. Res. Biogeosciences 116. https://doi.org/10.1029/2009JG001156

Bauer, J.E., Bianchi, T.S., 2011. Dissolved Organic Carbon Cycling and Transformation, Treatise on Estuarine and Coastal Science. Elsevier Inc. https://doi.org/10.1016/B978-0-12-374711-2.00502-7

Bittar, T.B., Berger, S.A., Birsa, L.M., Walters, T.L., Thompson, M.E., Spencer, R.G.M., Mann, E.L., Stubbins, A., Frischer, M.E., Brandes, J.A., 2016. Seasonal dynamics of dissolved, particulate and microbial components of a tidal saltmarsh-dominated estuary under contrasting levels of freshwater discharge. Estuar. Coast. Shelf Sci. 182, 72–85. https://doi.org/10.1016/j.ecss.2016.08.046

Bižić, M., Klintzsch, T., Ionescu, D., Hindiyeh, M.Y., Günthel, M., Muro-Pastor, A.M., Eckert, W., Urich, T., Keppler, F., Grossart, H.P., 2020. Aquatic and terrestrial cyanobacteria produce methane. Sci. Adv. 6, 1–10. https://doi.org/10.1126/sciadv.aax5343

Borges, A. V., Abril, G., 2011. Carbon Dioxide and Methane Dynamics in Estuaries, Treatise on Estuarine and Coastal Science. https://doi.org/10.1016/B978-0-12-374711-2.00504-0

Borges, A. V., Darchambeau, F., Lambert, T., Bouillon, S., Morana, C., Brouyère, S., Hakoun, V., Jurado, A., Tseng, H.C., Descy, J.P., Roland, F.A.E., 2018. Effects of agricultural land use on fluvial carbon dioxide, methane and nitrous oxide concentrations in a large European river, the Meuse (Belgium). Sci. Total Environ. 610–611, 342–355. https://doi.org/10.1016/j.scitotenv.2017.08.047

Borges, A. V., Darchambeau, F., Lambert, T., Morana, C., Allen, G., Tambwe, E., Sembaito, A.T., Mambo, T., Wabakhangazi, J.N., Descy, J.-P., Teodoru, C.R., Bouillon, S., 2019. Variations of dissolved greenhouse gases (CO2, CH4, N2O) in the Congo River network overwhelmingly driven by fluvial-wetland connectivity. Biogeosciences 16, 3801–3834. https://doi.org/10.18907/jjsre.10.2_212_3.

Burdige, D.J., Berelson, W.M., Coale, K.H., McManus, J., Johnson, K.S., 1999. Fluxes of dissolved organic carbon from California continental margin sediments. Geochim. Cosmochim. Acta 63, 1507–1515. https://doi.org/10.1016/S0016-7037(99)00066-6

Burdige, D.J., Komada, T., 2015. Sediment Pore Waters, Biogeochemistry of Marine Dissolved Organic Matter: Second Edition. Elsevier Inc. https://doi.org/10.1016/B978-0-12-405940-5.00012-1

Burgos, M., Ortega, T., Bohórquez, J., Corzo, A., Rabouille, C., Forja, J.M., 2018. Seasonal variation of early diagenesis and greenhouse gas production in coastal sediments of

Cadiz Bay: Influence of anthropogenic activities. Estuar. Coast. Shelf Sci. 200, 99–115. https://doi.org/10.1016/j.ecss.2017.10.016

Burgos, M., Ortega, T., Forja, J.M., 2017. Temporal and spatial variation of N2O production from estuarine and marine shallow systems of Cadiz Bay (SW, Spain). Sci. Total Environ. 607–608, 141–151. https://doi.org/10.1016/j.scitotenv.2017.07.021

Burgos, M., Sierra, A., Ortega, T., Forja, J.M., 2015. Anthropogenic effects on greenhouse gas (CH4 and N2O) emissions in the Guadalete River Estuary (SW Spain). Sci. Total Environ. 503–504, 179–189. https://doi.org/10.1016/j.scitotenv.2014.06.038

Cai, W.J., 2011. Estuarine and coastal ocean carbon paradox: CO 2 sinks or sites of terrestrial carbon incineration? Ann. Rev. Mar. Sci. 3, 123–145. https://doi.org/10.1146/annurev-marine-120709-142723

Cai, W.J., Wang, Y., Hodson, R.E., 1998. Acid-base properties of dissolved organic matter in the estuarine waters of Georgia, USA. Geochim. Cosmochim. Acta 62, 473–483. https://doi.org/10.1016/S0016-7037(97)00363-3

Cai, W.J., Zhao, P., Wang, Y., 2000. pH and pCO2 microelectrode measurements and the diffusive behavior of carbon dioxide species in coastal marine sediments. Mar. Chem. 70, 133–148. https://doi.org/10.1016/S0304-4203(00)00017-7

Campana, O., Rodríguez, A., Blasco, J., 2005. Biodisponibilidad de metales pesados en el Estuario del Río Guadalete (SO Península Ibérica). Ciencias Mar. 31, 135–147. https://doi.org/10.7773/cm.v31i12.100

Canfield, D.E., 1993. Organic Matter Oxidation in Marine Sediments. Interact. C, N, P S Biogeochem. Cycles Glob. Chang. I, 333–363. https://doi.org/10.1007/978-3-642-76064-8_14

Canuel, E.A., Cammer, S.S., McIntosh, H.A., Pondell, C.R., 2012. Climate change impacts on the organic carbon cycle at the land-ocean interface. Annu. Rev. Earth Planet. Sci. 40, 685–711. https://doi.org/10.1146/annurev-earth-042711-105511

Cárdenas, C., Gerea, M., Garcia, P.E., Pérez, G.L., Diéguez, M.C., Rapacioli, R., Reissig, M., Queimaliños, C., 2017. Interplay between climate and hydrogeomorphic features and their effect on the seasonal variation of dissolved organic matter in shallow temperate lakes of the Southern Andes (Patagonia, Argentina): a field study based on optical properties. Ecohydrology 10. https://doi.org/10.1002/eco.1872

Carini, S., Weston, N., Hopkinson, C., Tucker, J., Giblin, A., Vallino, J., 1996. Gas exchange rates in the Parker River Estuary, Massachusetts. Biol. Bull. 191, 333–334. https://doi.org/10.1086/bblv191n2p333

Cawley, K.M., Ding, Y., Fourqurean, J.W., Jaffé, R., 2012. Characterising the sources and fate of dissolved organic matter in Shark Bay , Australia : A preliminary study using a preliminary study using optical properties and stable carbon isotopes 63, 1098–1107. https://doi.org/10.1071/mf12028

Chen, C.T.A., Zhai, W., Dai, M., 2008. Riverine input and air-sea CO2 exchanges near the Changjiang (Yangtze River) Estuary: Status quo and implication on possible future changes in metabolic status. Cont. Shelf Res. 28, 1476–1482. https://doi.org/10.1016/j.csr.2007.10.013

Chen, M., Jung, J., Lee, Y.K., Hur, J., 2018. Surface accumulation of low molecular weight dissolved organic matter in surface waters and horizontal off-shelf spreading of nutrients and humic-like fluorescence in the Chukchi Sea of the Arctic Ocean. Sci. Total Environ. 639, 624–632. https://doi.org/10.1016/j.scitotenv.2018.05.205

Clark, C.D., Hiscock, W.T., Millero, F.J., Hitchcock, G., Brand, L., Miller, W.L., Ziolkowski, L., Chen, R.F., Zika, R.G., 2004. CDOM distribution and CO 2 production on the Southwest Florida Shelf. Mar. Chem. 89, 145–167.

https://doi.org/10.1016/j.marchem.2004.02.011
Coble, P.G., 2007. Marine Optical Biogeochemistry: The Chemistry of Ocean Color. Chem. Rev. 107, 402–418. https://doi.org/10.1021/cr050350+
Coble, P.G., Lead, J., Baker, A., Reynolds, D.M., Spencer, R.G.M., 2014. Aquatic Organic Matter Fluorescence.
Daniel, I., DeGrandpre, M., Farías, L., 2013. Greenhouse gas emissions from the Tubul-Raqui estuary (central Chile 36°S). Estuar. Coast. Shelf Sci. 134, 31–44. https://doi.org/10.1016/j.ecss.2013.09.019
Del Castillo, C.E., Coble, P.G., Morell, J.M., López, J.M., Corredor, J.E., 1999. Analysis of the optical properties of the Orinoco River plume by absorption and fluorescence spectroscopy. Mar. Chem. 66, 35–51. https://doi.org/10.1016/S0304-4203(99)00023-7
Donis, D., Flury, S., Stöckli, A., Spangenberg, J.E., Vachon, D., McGinnis, D.F., 2017. Full-scale evaluation of methane production under oxic conditions in a mesotrophic lake. Nat. Commun. 8. https://doi.org/10.1038/s41467-017-01648-4
García, P.E., Queimaliños, C., Diéguez, M.C., 2019. Natural levels and photo-production rates of hydrogen peroxide (H2O2) in Andean Patagonian aquatic systems: Influence of the dissolved organic matter pool. Chemosphere 217, 550–557. https://doi.org/10.1016/j.chemosphere.2018.10.179
Gattuso, J.., Frankignoulle, M., Wollast, R., 1998. Carbon and carbonate metabolism in coastal aquatic ecosystems. Annu. Rev. Ecol. Syst. 29, 405–434.
Gonçalves-Araujo, R., Stedmon, C.A., Heim, B., Dubinenkov, I., Kraberg, A., Moiseev, D., Bracher, A., 2015. From fresh to marine waters: Characterization and fate of dissolved organic matter in the Lena River Delta Region, Siberia. Front. Mar. Sci. 2, 1–13. https://doi.org/10.3389/fmars.2015.00108
Green, S.A., Blough, N. V, 1994. Optical absorption and fluorescence of chromophoric properties dissolved organic matter in natural waters. Limnology 39, 1903–1916.
Grömping, U., 2006. Relative importance for linear regression in R: The package relaimpo. J. Stat. Softw. 17, 1–27. https://doi.org/10.18637/jss.v017.i01
Harley, J.F., Carvalho, L., Dudley, B., Heal, K. V., Rees, R.M., Skiba, U., 2015. Spatial and seasonal fluxes of the greenhouse gases N2O, CO2 and CH4 in a UK macrotidal estuary. Estuar. Coast. Shelf Sci. 153, 62–73. https://doi.org/10.1016/j.ecss.2014.12.004
Harjung, A., Sabater, F., Butturini, A., 2018. Hydrological connectivity drives dissolved organic matter processing in an intermittent stream. Limnologica 68, 71–81. https://doi.org/10.1016/j.limno.2017.02.007
Hernández-Ayón, J.M., Belli, S.L., Zirino, A., 1999. pH, alkalinity and total CO2 in coastal seawater by potentiometric titration with a difference derivative readout. Anal. Chim. Acta 394, 101–108. https://doi.org/10.1016/S0003-2670(99)00207-X
Jiang, L.Q., Cai, W.J., Wang, Y., 2008. A comparative study of carbon dioxide degassing in river- and marine-dominated estuaries. Limnol. Oceanogr. 53, 2603–2615. https://doi.org/10.4319/lo.2008.53.6.2603
Karl, D.M., Beversdorf, L., Björkman, K.M., Church, M.J., Martinez, A., Delong, E.F., 2008. Aerobic production of methane in the sea. Nat. Geosci. 1, 473–478. https://doi.org/10.1038/ngeo234
Kellerman, A.M., Guillemette, F., Podgorski, D.C., Aiken, G.R., Butler, K.D., Spencer, R.G.M., 2018. Unifying Concepts Linking Dissolved Organic Matter Composition to Persistence in Aquatic Ecosystems. Environ. Sci. Technol. 52, 2538–2548. https://doi.org/10.1021/acs.est.7b05513

Keppler, F., Boros, M., Frankenberg, C., Lelieveld, J., McLeod, A., Pirttilä, A.M., Röckmann, T., Schnitzler, J.P., 2009. Methane formation in aerobic environments. Environ. Chem. 6, 459–465. https://doi.org/10.1071/EN09137

Komada, T., Burdige, D.J., Crispo, S.M., Druffel, E.R.M., Griffin, S., Johnson, L., Le, D., 2013. Dissolved organic carbon dynamics in anaerobic sediments of the Santa Monica Basin. Geochim. Cosmochim. Acta 110, 253–273. https://doi.org/10.1016/j.gca.2013.02.017

Komada, T., Schofield, O.M.E., Reimers, C.E., 2002. Fluorescence characteristics of organic matter released from coastal sediments during resuspension. Mar. Chem. 79, 81–97. https://doi.org/10.1016/S0304-4203(02)00056-7

Kothawala, D.N., Murphy, K.R., Stedmon, C.A., Weyhenmeyer, G.A., Tranvik, L.J., 2013. Inner filter correction of dissolved organic matter fluorescence. Limnol. Oceanogr. Methods 11, 616–630. https://doi.org/10.4319/lom.2013.11.616

Kuliński, K., Schneider, B., Hammer, K., Machulik, U., Schulz-Bull, D., 2014. The influence of dissolved organic matter on the acid-base system of the Baltic Sea. J. Mar. Syst. 132, 106–115. https://doi.org/10.1016/j.jmarsys.2014.01.011

Lambert, T., Bouillon, S., Darchambeau, F., Massicotte, P., Borges, A. V., 2016. Shift in the chemical composition of dissolved organic matter in the Congo River network. Biogeosciences 13, 5405–5420. https://doi.org/10.5194/bg-13-5405-2016

Lapierre, J.F., Guillemette, F., Berggren, M., Del Giorgio, P.A., 2013. Increases in terrestrially derived carbon stimulate organic carbon processing and CO 2 emissions in boreal aquatic ecosystems. Nat. Commun. 4. https://doi.org/10.1038/ncomms3972

Lawaetz, A.J., Stedmon, C.A., 2009. Fluorescence intensity calibration using the Raman scatter peak of water. Appl. Spectrosc. 63, 936–940. https://doi.org/10.1366/000370209788964548

León-Palmero, E., Contreras-Ruiz, A., Sierra, A., Morales-Baquero, R., Reche, I., Reche, I., 2020. Dissolved CH4 coupled to photosynthetic picoeukaryotes in oxic waters and to cumulative chlorophyll ia/i in anoxic waters of reservoirs. Biogeosciences 17, 3223–3245. https://doi.org/10.5194/bg-17-3223-2020

Li, P., Lee, Sang Hee, Lee, Soo Hyung, Lee, J.B., Lee, Y.K., Shin, H.S., Hur, J., 2016. Seasonal and storm-driven changes in chemical composition of dissolved organic matter: a case study of a reservoir and its forested tributaries. Environ. Sci. Pollut. Res. 23, 24834–24845. https://doi.org/10.1007/s11356-016-7720-z

Li, Y., Fichot, C.G., Geng, L., Scarratt, M.G., Xie, H., 2020. The Contribution of Methane Photoproduction to the Oceanic Methane Paradox. Geophys. Res. Lett. 47, 0–2. https://doi.org/10.1029/2020GL088362

Liikanen, A., Silvennoinen, H., Karvo, A., Rantakokko, P., Martikainen, P.J., 2009. Methane and nitrous oxide fluxes in two coastal wetlands in the northeastern Gulf of Bothnia, Baltic Sea. Boreal Environ. Res. 14, 351–368.

Lin, H., Dai, M., Kao, S.J., Wang, L., Roberts, E., Yang, J.Y.T., Huang, T., He, B., 2016. Spatiotemporal variability of nitrous oxide in a large eutrophic estuarine system: The Pearl River Estuary, China. Mar. Chem. 182, 14–24. https://doi.org/10.1016/j.marchem.2016.03.005

Lukawska-Matuszewska, K., Grzybowski, W., Szewczun, A., Tarasiewicz, P., 2018. Constituents of organic alkalinity in pore water of marine sediments. Mar. Chem. 200, 22–32. https://doi.org/10.1016/j.marchem.2018.01.012

Maher, D.T., Eyre, B.D., 2012. Carbon budgets for three autotrophic Australian estuaries: Implications for global estimates of the coastal air-water CO 2 flux. Global

Biogeochem. Cycles 26. https://doi.org/10.1029/2011GB004075

Maher, D.T., Eyre, B.D., 2010. Benthic fluxes of dissolved organic carbon in three temperate Australian estuaries: Implications for global estimates of benthic DOC fluxes. J. Geophys. Res. Biogeosciences 115. https://doi.org/10.1029/2010JG001433

Martens, C.S., Val Klump, J., 1984. Biogeochemical cycling in an organic-rich coastal marine basin 4. An organic carbon budget for sediments dominated by sulfate reduction and methanogenesis. Geochim. Cosmochim. Acta 48, 1987–2004. https://doi.org/10.1016/0016-7037(84)90380-6

Meyer, R.L., Allen, D.E., Schmidt, S., 2008. Nitrification and denitrification as sources of sediment nitrous oxide production: A microsensor approach. Mar. Chem. 110, 68–76. https://doi.org/10.1016/j.marchem.2008.02.004

Middelburg, J.J., Nieuwenhuize, J., Iversen, N., Høgh, N., De, H., Middelburg, J.J., Nieuwenhuize, J., Iversen, N., Hogh, N., Wilde, H.D.E., Helder, W.I.M., 2002. Methane Distribution in European Tidal Estuaries. Biogeochemistry 59, 95–119.

Miller, W.L., Zepp, R.G., 1995. Photochemical production of dissolved inorganic carbon from terrestrial organic matter: Significance to the oceanic organic carbon cycle. Geophys. Res. Lett. 22, 417–420. https://doi.org/10.1029/94GL03344

Millero, F.J., 2010. Carbonate constants for estuarine waters.pdf. Mar. Freshw. Res. 61, 139–142.

Moran, M.A., Zepp, R.G., 1997. Role of photoreactions in the formation of biologically labile compounds from dissolved organic matter. Limnol. Oceanogr. 42, 1307–1316. https://doi.org/10.4319/lo.1997.42.6.1307

Murphy, K.R., Stedmon, C.A., Waite, T.D., Ruiz, G.M., 2008. Distinguishing between terrestrial and autochthonous organic matter sources in marine environments using fluorescence spectroscopy. Mar. Chem. 108, 40–58. https://doi.org/10.1016/j.marchem.2007.10.003

Murphy, K.R., Hambly, A., Singh, S., Henderson, R.K., Baker, A., Stuetz, R., Khan, S.J., 2011. Organic matter fluorescence in municipal water recycling schemes: Toward a unified PARAFAC model. Environ. Sci. Technol. 45, 2909–2916. https://doi.org/10.1021/es103015e

Murphy, K.R., Stedmon, C.A., Graeber, D., Bro, R., 2013. Fluorescence spectroscopy and multi-way techniques. PARAFAC. Anal. Methods 5, 6557–6566. https://doi.org/10.1039/c3ay41160e

Murphy, K.R., Stedmon, C.A., Wenig, P., Bro, R., 2014. OpenFluor- An online spectral library of auto-fluorescence by organic compounds in the environment. Anal. Methods 6, 658–661. https://doi.org/10.1039/c3ay41935e

Murphy, K.R., Timko, S.A., Gonsior, M., Powers, L.C., Wünsch, U.J., Stedmon, C.A., 2018. Photochemistry Illuminates Ubiquitous Organic Matter Fluorescence Spectra. Environ. Sci. Technol. 52, 11243–11250. https://doi.org/10.1021/acs.est.8b02648

Nevison, C., Butler, J.H., Elkins, J.W., 2003. Global distribution of N2O and the ΔN2O-AOU yield in the subsurface ocean. Global Biogeochem. Cycles 17, 1–18. https://doi.org/10.1029/2003gb002068

O'Brien, R.M., 2007. A caution regarding rules of thumb for variance inflation factors. Qual. Quant. 41, 673–690. https://doi.org/10.1007/s11135-006-9018-6

Osburn, C.L., Handsel, L.T., Peierls, B.L., Paerl, H.W., 2016. Predicting Sources of Dissolved Organic Nitrogen to an Estuary from an Agro-Urban Coastal Watershed. Environ. Sci. Technol. 50, 8473–8484. https://doi.org/10.1021/acs.est.6b00053

Panettieri, M., Guigue, J., Chemidlin Prevost-Bouré, N., Thévenot, M., Lévêque, J., Le Guillou, C., Maron, P.A., Santoni, A.L., Ranjard, L., Mounier, S., Menasseri, S.,

Viaud, V., Mathieu, O., 2020. Grassland-cropland rotation cycles in crop-livestock farming systems regulate priming effect potential in soils through modulation of microbial communities, composition of soil organic matter and abiotic soil properties. Agric. Ecosyst. Environ. 299, 106973. https://doi.org/10.1016/j.agee.2020.106973

Podgorski, D.C., Zito, P., McGuire, J.T., Martinovic-Weigelt, D., Cozzarelli, I.M., Bekins, B.A., Spencer, R.G.M., 2018. Examining Natural Attenuation and Acute Toxicity of Petroleum-Derived Dissolved Organic Matter with Optical Spectroscopy. Environ. Sci. Technol. 52, 6157–6166. https://doi.org/10.1021/acs.est.8b00016

R Core Team. R: A language and environment for statistical computing. R Foundation for Statistical Computing, Vienna, Austria. https ://www.R-proje ct.org/. (2020).

Reeburgh, W.S., 2003. Global methane biogeochemistry. Treatise on Geochemistry 4, 65-89.

Repeta, D.J., Ferrón, S., Sosa, O.A., Johnson, C.G., Repeta, L.D., Acker, M., Delong, E.F., Karl, D.M., 2016. Marine methane paradox explained by bacterial degradation of dissolved organic matter. Nat. Geosci. 9, 884–887. https://doi.org/10.1038/ngeo2837

Rosentreter, J.A., Maher, D.T., Erler, D. V., Murray, R., Eyre, B.D., 2018. Factors controlling seasonal CO2 and CH4 emissions in three tropical mangrove-dominated estuaries in Australia. Estuar. Coast. Shelf Sci. 215, 69–82. https://doi.org/10.1016/j.ecss.2018.10.003

Sierra, A., Jiménez-López, D., Ortega, T., Fernández-Puga, M.C., Delgado-Huertas, A., Forja, J., 2020. Methane dynamics in the coastal – Continental shelf transition zone of the Gulf of Cadiz. Estuar. Coast. Shelf Sci. 236. https://doi.org/10.1016/j.ecss.2020.106653

Sjögersten, S., Caul, S., Daniell, T.J., Jurd, A.P.S., O'Sullivan, O.S., Stapleton, C.S., Titman, J.J., 2016. Organic matter chemistry controls greenhouse gas emissions from permafrost peatlands. Soil Biol. Biochem. 98, 42–53. https://doi.org/10.1016/j.soilbio.2016.03.016

Smith, S. V., Hollibaugh, J.T., 1993. Coastal metabolism and the oceanic organic carbon balance. Rev. Geophys. 31, 75–89.

Stedmon, C.A., Tranvik, L., Slätis, T., Martinsen, W., Markager, S., Kronberg, L., 2007. Photochemical production of ammonium and transformation of dissolved organic matter in the Baltic Sea. Mar. Chem. 104, 227–240. https://doi.org/10.1016/j.marchem.2006.11.005

Stedmon, C., Bro, R., 2008. Characterizing dissolved organic matter fluorescence with parallel factor analysis: a tutorial. Limnol. Oceanogr. Methods 6, 572–579. https://doi.org/doi:10.4319/lom.2008.6.572b

Stedmon, C.A., Markager, S., Bro, R., 2003. Tracing dissolved organic matter in aquatic environments using a new approach to fluorescence spectroscopy. Mar. Chem. 82, 239–254. https://doi.org/10.1016/S0304-4203(03)00072-0

Stedmon, C.A., Seredyńska-Sobecka, B.B., Boe-Hansen, R., Le Tallec, N., Waul, C.K., Arvin, E., Stedmon, C.A., Seredyńska-Sobecka, B.B., Waul, C.K., Boe-Hansen, R., Le Tallec, N., 2011. A potential approach for monitoring drinking water quality from groundwater systems using organic matter fluorescence as an early warning for contamination events. Water Res. 45, 6030–6038. https://doi.org/10.1016/j.watres.2011.08.066

Stubbins, A., Lapierre, J.F., Berggren, M., Prairie, Y.T., Dittmar, T., Del Giorgio, P.A., 2014. What's in an EEM? Molecular signatures associated with dissolved organic fluorescence in boreal Canada. Environ. Sci. Technol. 48, 10598–10606.

https://doi.org/10.1021/es502086e

Veluswamy, H.P., Lee, P.Y., Premasinghe, K., Linga, P., 2017. Effect of Biofriendly Amino Acids on the Kinetics of Methane Hydrate Formation and Dissociation. Ind. Eng. Chem. Res. 56, 6145–6154. https://doi.org/10.1021/acs.iecr.7b00427

Wanninkhof, R., 2014. Relationship between wind speed and gas exchange over the ocean revisited. Limnol. Oceanogr. Methods 12, 351–362. https://doi.org/10.4319/lom.2014.12.351

Warnken, K.W., Santschi, P.H., 2004. Biogeochemical behavior of organic carbon in the Trinity River downstream of a large reservoir lake in Texas, USA. Sci. Total Environ. 329, 131–144. https://doi.org/10.1016/j.scitotenv.2004.02.017

Weishaar, J., Aiken, G., Bergamaschi, B., Fram, M., Fujii, R., Mopper, K., 2003. Evaluation of specific ultra-violet absorbance as an indicator of the chemical content of dissolved organic carbon. Environ. Chem. 41, 843–845. https://doi.org/10.1021/es030360x

Weiss, R.F., 1970. The solubility of nitrogen, oxygen and argon in water and seawater. Deep. Res. Oceanogr. Abstr. 17, 721–735. https://doi.org/10.1016/0011-7471(70)90037-9

Weiss, R.F., Price, B.A., 1980. Nitrous Oxide Solubility in water and seawater. Mar. Chem. 8, 347–356.

Wells, N.S., Chen, J.J., Maher, D.T., Huang, P., Erler, D. V., Hipsey, M., Eyre, B.D., 2020. Changing sediment and surface water processes increase CH4 emissions from human-impacted estuaries. Geochim. Cosmochim. Acta 280, 130–147. https://doi.org/10.1016/j.gca.2020.04.020

Wells, N.S., Maher, D.T., Erler, D. V., Hipsey, M., Rosentreter, J.A., Eyre, B.D., 2018. Estuaries as Sources and Sinks of N2O Across a Land Use Gradient in Subtropical Australia. Global Biogeochem. Cycles 32, 877–894. https://doi.org/10.1029/2017GB005826

Wetz, M.S., Yoskowitz, D.W., 2013. An "extreme" future for estuaries? Effects of extreme climatic events on estuarine water quality and ecology. Mar. Pollut. Bull. 69, 7–18. https://doi.org/10.1016/j.marpolbul.2013.01.020

Wiesenburg, D.A., Guinasso, N.L., 1979. Equilibrium Solubilities of Methane, Carbon Monoxide, and Hydrogen in Water and Sea Water. J. Chem. Eng. Data 24, 356–360.

Williams, C.J., Frost, P.C., Xenopoulos, M.A., 2013. Beyond best management practices: Pelagic biogeochemical dynamics in urban stormwater ponds. Ecol. Appl. 23, 1384–1395. https://doi.org/10.1890/12-0825.1

Yamashita, Y., Kloeppel, B.D., Knoepp, J., Zausen, G.L., Jaffé, R., 2011. Effects of Watershed History on Dissolved Organic Matter Characteristics in Headwater Streams. Ecosystems 14, 1110–1122. https://doi.org/10.1007/s10021-011-9469-z

Yamashita, Y., Scinto, L.J., Maie, N., Jaffé, R., 2010. Dissolved Organic Matter Characteristics Across a Subtropical Wetland's Landscape: Application of Optical Properties in the Assessment of Environmental Dynamics. Ecosystems 13, 1006–1019. https://doi.org/10.1007/s10021-010-9370-1

Yamashita, Y., Boyer, J.N., Jaffé, R., 2013. Evaluating the distribution of terrestrial dissolved organic matter in a complex coastal ecosystem using fluorescence spectroscopy. Cont. Shelf Res. 66, 136–144. https://doi.org/10.1016/j.csr.2013.06.010

Yamashita, Y., Panton, A., Mahaffey, C., Jaffé, R., 2011. Assessing the spatial and temporal variability of dissolved organic matter in Liverpool Bay using excitation-emission

matrix fluorescence and parallel factor analysis. Ocean Dyn. 61, 569–579. https://doi.org/10.1007/s10236-010-0365-4

Yang, L., Choi, J.H., Hur, J., 2014. Benthic flux of dissolved organic matter from lake sediment at different redox conditions and the possible effects of biogeochemical processes. Water Res. 61, 97–107. https://doi.org/10.1016/j.watres.2014.05.009

Yao, M., Henny, C., Maresca, J.A., 2016. Freshwater bacteria release methane as a by-product of phosphorus acquisition. Appl. Environ. Microbiol. 82, 6994–7003. https://doi.org/10.1128/AEM.02399-16

Zhang, G.L., Zhang, J., Liu, S.M., Ren, J.L., Zhao, Y.C., 2010. Nitrous oxide in the Changjiang (Yangtze River) Estuary and its adjacent marine area: Riverine input, sediment release and atmospheric fluxes. Biogeosciences 7, 3505–3516. https://doi.org/10.5194/bg-7-3505-2010

Zhang, Y., Xie, H., 2015. Photomineralization and photomethanification of dissolved organic matter in Saguenay River surface water. Biogeosciences 12, 6823–6836. https://doi.org/10.5194/bg-12-6823-2015

Zhou, Y., Xiao, Q., Yao, X., Zhang, Y., Zhang, M., Shi, K., Lee, X., Podgorski, D.C., Qin, B., Spencer, R.G.M., Jeppesen, E., 2018. Accumulation of Terrestrial Dissolved Organic Matter Potentially Enhances Dissolved Methane Levels in Eutrophic Lake Taihu, China. Environ. Sci. Technol. 52, 10297–10306. https://doi.org/10.1021/acs.est.8b02163

Zhou, Y., Xiao, Q., Zhou, L., Jang, K.S., Zhang, Y., Zhang, M., Lee, X., Qin, B., Brookes, J.D., Davidson, T.A., Jeppesen, E., 2020. Are nitrous oxide emissions indirectly fueled by input of terrestrial dissolved organic nitrogen in a large eutrophic Lake Taihu, China? Sci. Total Environ. 722, 1–13. https://doi.org/10.1016/j.scitotenv.2020.138005

Parte V

Síntesis y conclusiones finales

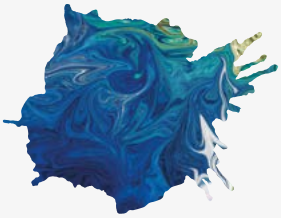

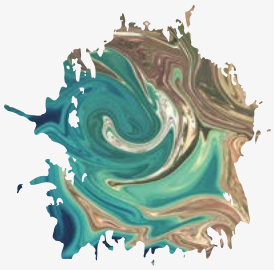

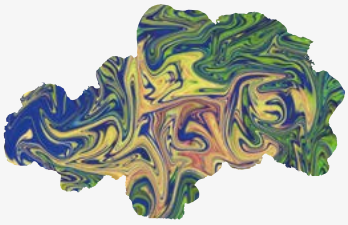

V. SINTESIS Y CONCLUSIONES FINALES

En esta sección se ha realizado una síntesis de los resultados obtenidos en la presente tesis doctoral en las dos zonas de estudio: la plataforma continental del golfo de Cádiz, incluyendo los estuarios que desembocan en las costas suratlánticas (Guadalquivir, Guadiana y Tinto – Odiel), y el estuario del Guadalete, que desemboca en la bahía de Cádiz (Fig. 5.1). El golfo de Cádiz es la única conexión entre el mar Mediterráneo y el océano Atlántico a través del estrecho de Gibraltar, por tanto, tiene un rol clave en la circulación de masas de agua del Atlántico Norte.

La distribución de la DOM en la plataforma del golfo de Cádiz está determinada principalmente por la actividad biológica, los procesos de mezcla de las masas de agua y la presencia de afloramientos costeros, la variabilidad estacional y los aportes continentales. La FDOM está compuesta por una variedad de fluoróforos que van desde componentes del tipo húmico terrestre, microbiano, material terrestre fotodegradado hasta compuesto del tipo proteico mezclados con hidrocarburos policíclicos aromáticos. Los patrones de circulación de las diferentes masas de agua no son suficientes para explicar la distribución de la DOM, excepto por los principales fluoróforos del tipo húmico. Por otro lado, los procesos biogeoquímicos a escala local determinan la distribución del DOC, CDOM y los fluoróforos del tipo proteína. Los valores más bajos de DOC y de los fluoróforos proteicos coinciden con el periodo de bajas temperaturas y mezcla de la columna de agua (primavera e invierno). Por otro lado, la distribución de los fluoróforos húmicos del tipo terrestre y microbiano tiene una menor variabilidad estacional que los compuestos derivados de material fotodegradado y los del tipo proteína. Estos últimos representan más del

60% del *pool* total de FDOM en verano (Fig. 5.1), posiblemente asociado al aumento en la actividad biológica con la temperatura.

En la zona mesopelágica de la plataforma del golfo de Cádiz (200 y 1000 m de profundidad) existen diferencias espaciales en la distribución de la DOM relacionada con la presencia de afloramientos costeros en la zona del Guadiana y Trafalgar. En estas zonas hay una producción de DOC en paralelo con el envejecimiento de las masas de agua debido a la oxidación microbiana posiblemente de POC a DOC. Por el contrario, en el resto de la plataforma predomina la mineralización de DOC a CO_2. En cuanto a la FDOM, en las aguas profundas del GoC existe una producción de compuestos húmicos y consumo de material proteico.

Los volcanes de fango submarinos constituyen una fuente de DOM a las aguas profundas de la plataforma continental del golfo de Cádiz. Existe una producción neta de DOC, CDOM y FDOM en los sedimentos superficiales que generan flujos bentónicos de DOM hacia la columna de agua desde los volcanes de fango Anastasya, San Petersburg y Pipoca. En base a el área promedio de los tres volcanes (3.6 ± 0.8 km^2) se estima un flujo de DOC hacia las aguas profundas del golfo de Cádiz de 4.74×10^3 g C d^{-1} (Fig. 5. 1).

Sin embargo, el origen de la DOM varía entre los volcanes y estaría relacionado con el grado de actividad volcánica en que se encuentra cada uno de ellos. Es decir, con la intensidad de la extrusión de los fluidos volcánicos que provienen de los sedimentos profundos y con las características de las comunidades microbianas que allí habitan. Anastasya es el volcán más activo de los tres y se caracteriza por la presencia de organismos que viven en condiciones extremófilas (Palomino et al., 2016). Este volcán presenta los

mayores valores de flujos bentónicos de la fracción ópticamente activa de la DOM, en particular, de los compuestos del tipo húmico microbiano y proteicos del tipo tirosina. Los flujos bentónicos de estos compuestos están relacionados con los fluidos volcánicos provenientes de los sedimentos profundos y con la actividad de las bacterias sulfatorreductoras en los sedimentos. Por otro lado, Pipoca es el volcán menos activo por lo que la producción neta observada de DOM posiblemente esté más bien influenciada por procesos abióticos como condensación, fragmentación o disolución de material particulado a disuelto (Coble et al., 2014; Liu y Lee, 2007), lo que estaría indicando la diversidad en el origen de un mismo componente fluorescente.

La DOM proveniente de los ríos entra a los océanos principalmente a través de los estuarios y representa una fracción significativa en el ciclo global del carbono (Bauer y Bianchi, 2011). El golfo de Cádiz recibe el aporte de agua dulce de tres estuarios principales: Guadalquivir, Guadiana y Tinto-Odiel. La DOM proveniente de los estuarios del Guadalquivir y Guadiana es principalmente de origen alóctono donde predominan los compuestos fluorescentes húmicos que representan un ~ 70% del *pool* total de la FDOM. Estos estuarios reciben aportes laterales debido a la presencia de humedales (marismas) y actividad antropogénica (agricultura). Por ejemplo, en el estuario del Guadalquivir la DOM tiene un comportamiento no conservativo principalmente debido a la presencia de plantaciones de regadío en la zona media del estuario, mientras que en el Guadiana la DOM tiene un comportamiento conservativo ya que la entrada de DOM terrestre se da en la desembocadura donde se encuentra una gran extensión de marismas. Por otro lado, en el estuario del río Tinto-Odiel predomina la DOM de origen autóctono, con un mayor contenido de compuestos fluorescentes de tipo

proteico, asociado a las bajas descargas de agua dulce y una mayor influencia marina, así como a la contaminación antropogénica (actividad minera e industrial). El estuario Tinto-Odiel es uno de los estuarios más contaminados del mundo debido a la extracción de sulfuros en su cuenca y a las actividades industriales que ocurren en sus márgenes. Asimismo, la distribución y características de la DOM en estos estuarios están fuertemente influenciadas por los ciclos de mareas, principalmente en el Guadalquivir y Guadiana. Durante marea baja la contribución de los compuestos de tipo húmico al *pool* total de FDOM alcanza un 80% debido a una mayor influencia del aporte desde los ríos. Por otro lado, durante la marea alta la contribución de los compuestos de origen proteicos aumenta casi al doble, ya que están asociados a la producción de DOM en la zona marina. En ese sentido, en Tinto-Odiel la contribución de los compuestos del tipo húmico y proteicos fueron similares durante todo el ciclo mareal (47% ± 1.7% y 53% ± 5.2%, respectivamente) debido a la mayor influencia marina de este estuario. A pesar de que este estudio se realizó durante la estación seca (caudal Guadalquivir: 164 m^3 s^{-1}), los tres estuarios actúan como fuente de DOM a la zona costera del golfo de Cádiz. Se estima un flujo de 0.14, 0.41 y 1.08 × 10^8 g C d^{-1} desde los estuarios Guadiana, Tinto-Odiel y Guadalquivir, respectivamente, hacia la costa (Fig. 5.1). Sin embargo, su influencia se observa solo en los primeros kilómetros de costa (< 16 km). Alrededor del 70% de la FDOM exportada por estos estuarios es de tipo húmica y proviene en su mayoría del Guadalquivir, mientras que a lo largo del año en la plataforma continental predominan los compuestos de origen proteico. Los resultados obtenidos mediante el análisis de Py-GC-MS para caracterizar la DOM coincidieron con los encontrados empleando las propiedades ópticas de la DOM. Las fracciones de DOM provenientes de

plantas vasculares (lignina, fenoles, hidrocarburos aromáticos) fueron más abundante en el Guadalquivir, seguido del Guadiana y Tinto-Odiel, mientras que los compuestos derivados de la producción *in situ* y contaminantes antropogénicos fueron más abundantes en Tinto- Odiel (compuestos de metileno). Por tanto, la Py-GC-MS es una técnica útil y complementaria a la espectroscopía de fluorescencia que mejora la caracterización de la DOM en sistemas estuarinos.

Asimismo los resultados obtenidos mediante análisis de aminoácidos para caracterizar la DOM estuvieron en concordancia con los observados empleando sus características ópticas y moleculares. La composición de los DFAA varía entre la zona costera y el interior de los estuarios del Guadalquivir, Guadiana y Tinto-Odiel, indicando diferencias en las fuentes de DOM así como su degradación a lo largo del gradiente de salinidad. Dentro de los estuarios la DOM estaría menos degradada que en la zona costera. Además, los factores que controlan la distribución de los DFAA varía también entre estuarios. En el Guadalquivir es evidente la importancia de los aportes terrestres así como las prácticas agrícolas que ocurren en sus márgenes en la distribución de los aminoácidos, mientras que en el Guadiana las entradas terrestres estarían más asociada a la presencia de marismas en su desembocadura. En el estuario Tinto-Odiel, la composición de DFAA refleja un carácter más autóctono de la DOM y la importancia de los aportes alóctonos proveniente principalmente de las actividades industriales que ocurren en su cuenca. Por otro lado, los ciclos de marea ejercen una influencia en la distribución de los DFAA, donde la entrada de estos desde fuentes alóctonas aumenta la reactividad de la DOM en el interior de los estuarios. Por último, la composición de los DFAA estaría fuertemente relacionada con las características de la CDOM y FDOM.

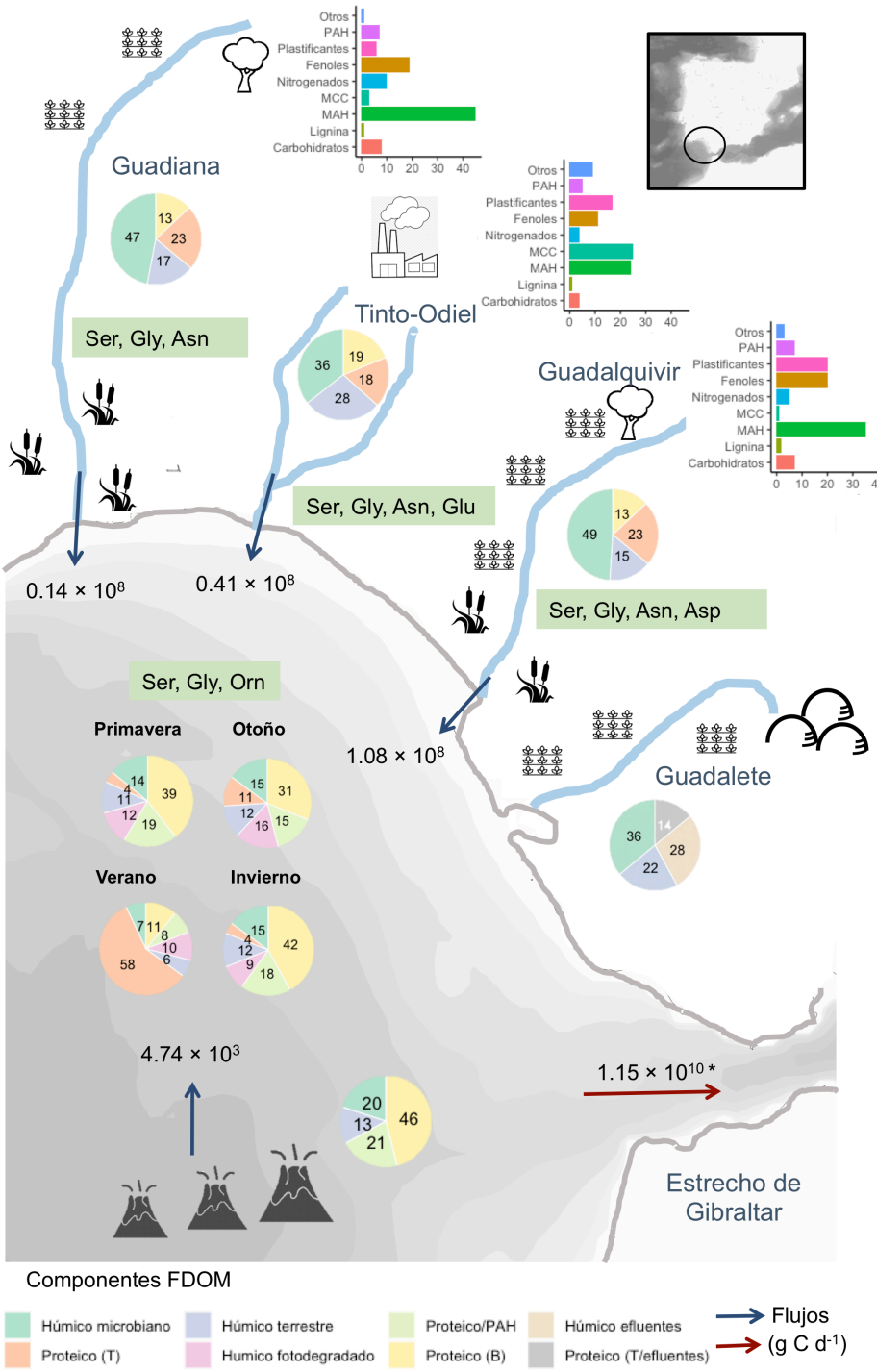
Otros
PAH
Plastificantes
Fenoles
Nitrogenados
MCC
MAH
Lignina
Carbohidratos
0 10 20 30 40
Guadiana
47
13
23
17
Ser, Gly, Asn
Tinto-Odiel
36
19
18
28
Guadalquivir
49
13
23
15
Ser, Gly, Asn, Glu
Ser, Gly, Asn, Asp
0.14 × 10⁸
0.41 × 10⁸
1.08 × 10⁸
Ser, Gly, Orn
Primavera
Otoño
Verano
Invierno
Guadalete
36
14
28
22
4.74 × 10³
20
13
46
21
1.15 × 10¹⁰ *
Estrecho de Gibraltar
Componentes FDOM
Húmico microbiano
Proteico (T)
Húmico terrestre
Humico fotodegradado
Proteico/PAH
Proteico (B)
Húmico efluentes
Proteico (T/efluentes)
Flujos
(g C d⁻¹)

Fig. 5.1. Biogeoquímica de la materia orgánica disuelta en el Golfo de Cádiz. Las flechas azules indican los aportes de carbono orgánico disuelto (en g C d^{-1}) desde los principales estuarios: Guadalquivir, Guadiana, Tinto-Odiel. La flecha roja representa el intercambio de flujo neto a través del estrecho de Gibraltar (g C d^{-1}) tomado de Álvarez-Salgado et al., 2020. Los gráficos de torta indican el % relativo de los componentes fluorescentes encontrados en el Golfo de Cádiz. Los gráficos de barra indican las proporciones relativas (%) de los productos analizados mediante pirólisis de cromatografía de gases y espectroscopia de masas en los estuarios Guadalquivir, Guadiana y Tinto-Odiel (MAH y PAH = hidrocarburos aromáticos monocíclicos y policíclicos, MCC = compuestos de cadena de metileno). Además se indican los aminoácidos libres disueltos predominantes (> 10%) en la zona costera del Golfo de Cádiz y en el interior de cada estuario (Ser: serina, Gly: glicina, Orn: ornitina, Asn: asparagina, Asp: ácido aspártico, Glu: ácido glutámico).

La degradación de la DOM da lugar a la producción de gases de efecto invernadero, como el CO_2, el CH_4 y N_2O, que juntos contribuyen en un 80% al aumento de la temperatura atmosférica media mundial (IPCC, 2013). El CO_2 es el principal producto de la descomposición de la materia orgánica y se produce en todos los procesos (aerobios y anaerobios), el CH_4 se produce por la metanogénesis y el N_2O por la nitrificación y la desnitrificación (Abril y Borges, 2005; Bange, 2008; Reeburgh, 2003). Existe evidencia a nivel global de un aumento en las perturbaciones ambientales a las cuales están sujetos los estuarios, como por ejemplo, aumento en la carga de nutrientes debido a las actividades antropogénicas, cambios en el uso de la tierra, modificaciones hidrológicas así como aumento en la frecuencia de fenómenos climáticos extremos que influyen en las descargas de agua dulce (sequías/inundaciones) (Canuel et al., 2012; Wetz y Yoskowitz, 2013). Por tanto, estos cambios afectan a la composición de la DOM y, por ende, a las emisiones de gases invernadero a la atmósfera. En esta Tesis doctoral se estudiaron las relaciones entre distintas fracciones de la DOM (húmica, proteica) proveniente de diversas fuentes (terrestre, producción microbiana *in situ* o efluentes) con la distribución de los gases invernadero CO_2, CH_4 y N_2O en un estuario somero del golfo de Cádiz, el estuario del río Guadalete. La distribución de estos gases en el estuario del río Guadalete está

fuertemente relacionada con las características de la DOM. A este respecto, la distribución del CO_2 estaría relacionada con compuestos de tipo húmico de origen terrestre y microbiano, donde un aumento en la aromaticidad de la DOM potenciaría la concentración de este gas. Posiblemente, debido a una rápida degradación microbiana así como fotoquímica de los compuestos del tipo húmico que contribuyen a la producción de CO_2 (Miller y Zepp, 1995; Sjögersten et al., 2016). Por el contario, la concentración de N_2O parece estar sólo relacionada con la fracción proteica de la DOM, asociada a compuestos de bajo peso molecular y alto contenido de nitrógeno derivado de efluentes de aguas tratadas y de la actividad agrícola que ocurre en los márgenes de este estuario. Por último, la concentración del CH_4 estaría relacionada con ambas fracciones de la DOM, húmica y proteica, y se potenciaría tanto con un aumento de compuestos origen terrestre, producción *in situ* o actividades antropogénicas. Asimismo, podría estar ocurriendo un acoplamiento entre el flujo bentónico de CH_4 y DOM en el estuario del río Guadalete dada su escasa profundidad (z_{max} = 6 m), especialmente en la zona interna del estuario. Por tanto, la metanogénesis que ocurre en los sedimentos estaría influenciando la composición de la DOM presente en la columna de agua. Las interrelaciones que pudieran existir entre la composición de la DOM y la distribución de gases invernadero son importantes para explicar el comportamiento de los estuarios bajo escenarios de cambio global.

Los componentes fluorescentes identificados en la plataforma continental del golfo de Cádiz fueron encontrados tanto en los estuarios que allí desembocan como en los volcanes de fango submarinos ubicados entre los 500 y 1000 m, con excepción del fluoróforo asociado a material fotodegradado (C4, Tabla 5.1). Este componente podría tratarse de material

húmico terrestre procedente de los estuarios y que se encuentra afectado por la fuerte radiación y mayores tiempos de residencia en la zona costa-océano del golfo de Cádiz. Por otro lado, en el estuario del río Guadalete se identificaron dos componentes fluorescentes que no se observaron en el resto del golfo de Cádiz (C2 y C4). Ambos componentes estaban relacionados con la presencia de efluentes provenientes de la agricultura y de una planta de tratamiento de aguas residuales localizada aguas arriba del estuario. El estuario del río Guadalete desemboca en la bahía de Cádiz con un caudal muy bajo, lo que podría explicar la presencia de estos dos componentes únicamente en este estuario, indicando así la importancia de las condiciones locales en la composición de la DOM.

Tabla 5.1. Correspondencia de cada componente fluorescente identificado en cada set de datos de los distintos sistemas del golfo de Cádiz estudiados en esta Tesis empleando la base de datos OpenFluor (TCC > 0.95). Se indica el máximo de excitación y emisión.

Plataforma continental	Guadalquivir, Guadiana, Tinto-Odiel	Volcanes de fango	Guadalete
C1 270 (320)/411	C1 270 (320)/419	C2 320/405	C1 275/411
C2 300/359	C3 300/358	-	-
C3 275 (370)/446	C2 275 (370)/454	C1 270 (365)/454	C3270 (385)/456
C4 250/430	-	-	-
C5 280/317 (378)	-	C3 280/375	-
C6 275/303	C4 275/311	C4 275/303	-

Las conclusiones específicas han sido detalladas al final de cada uno de los capítulos de este trabajo de Tesis. En este apartado se presentan a modo de síntesis las conclusiones más relevantes de toda la Tesis doctoral.

1- En la zona de plataforma del golfo de Cádiz existe una fuerte variabilidad temporal y espacial en la distribución de la DOM asociada a las características ambientales, hidrográficas y biogeoquímicas a nivel local. La distribución de la DOM de origen húmico está influenciada por factores físicos (circulación masas de agua) mientras que la concentración de DOC y DOM de origen proteico está determinada por factores biogeoquímicos (actividad biológica). Al aumentar la resolución espacial se observaron comportamientos opuestos en la eliminación/acumulación de DOC en la zona mesopelágica (200- 1000 m de profundidad) asociados a la presencia de afloramientos costeros. En general, nuestros resultados destacan la importancia de las características hidrográficas y biogeoquímicas locales en la dinámica de la DOM en sistemas costeros complejos, influenciados por descargas fluviales, afloramientos costeros y corrientes superficiales regidas por la estacionalidad.

2- Los sedimentos de los volcanes de fango submarinos actúan como una fuente de DOC, CDOM y FDOM a las masas de agua profundas del golfo de Cádiz a través de los fluidos (*cold seeps*) y la actividad de las bacterias sulfatorreductoras. Los flujos bentónicos promedio estimados de DOC y CDOM fueron de 0.11 ± 0.04 mmol m^{-2} d^{-1} y 2.86 m^{-1} L m^{-2} d^{-1}, respectivamente, relativamente más altos que en otros sedimentos marinos. Los compuestos del tipo

proteína representan > 60% del total de la FDOM fluorescente y su producción está estrechamente relacionada con la actividad volcánica.

3- Los estuarios del Guadalquivir, Guadiana y Tinto- Odiel son una fuente de DOM a la zona costera, en particular el estuario del río Guadalquivir. Las características químicas y moleculares de la DOM exportada desde los estuarios a la zona costera depende de las condiciones locales, como las características de la cuenca y la reactividad biogeoquímica de la DOM dentro de cada estuario.

4- El origen de la DOM y el procesamiento microbiano determinan la distribución de los DFAA en los estuarios y zona costera del golfo de Cádiz. Según estos análisis, la DOM se encuentra más degradada en la zona costera de los estuarios que dentro de los mismos. Además los factores que controlan la distribución dentro de los estuarios varia entre ellos, asociados principalmente al uso de suelos en sus cuencas y márgenes. Estos resultados son consistente con los análisis ópticos y mediante Py-GC-MS de la DOM.

5- La DOM proveniente de distintas fuentes (terrestre, microbiana, antropogénica) influye de forma específica en la concentración de los gases de efecto invernadero, CO_2, CH_4 y N_2O, en el estuario del Guadalete. Variaciones en la composición de la DOM debido a cambios en el uso de la tierra o del régimen de precipitaciones, podrían tener un impacto en los flujos de estos gases a la atmósfera. Por tanto, es importante considerar la composición de la DOM en los estudios de la distribución de estos gases en sistemas estuarinos con objeto de comprender su rol y las posibles respuestas asociadas a escenarios de cambio climático.

Referencias

Abril, G., Borges, A.V., 2005. Carbon Dioxide and Methane Emissions from Estuaries 187–207. https://doi.org/10.1007/978-3-540-26643-3_8

Álvarez-Salgado, X. A., Otero, J., Flecha, S., & Huertas, I. E. (2020). Seasonality of dissolved organic carbon exchange across the Strait of Gibraltar. *Geophysical Research Letters*, *47*(18), e2020GL089601.

Bange, H.W., 2008. Gaseous Nitrogen Compounds (NO, N2O, N2, NH3) in the Ocean, Nitrogen in the Marine Environment. Elsevier Inc. https://doi.org/10.1016/B978-0-12-372522-6.00002-5

Bauer, J.E., Bianchi, T.S., 2011. Dissolved Organic Carbon Cycling and Transformation, Treatise on Estuarine and Coastal Science. Elsevier Inc. https://doi.org/10.1016/B978-0-12-374711-2.00502-7

Canuel, E.A., Cammer, S.S., McIntosh, H.A., Pondell, C.R., 2012. Climate change impacts on the organic carbon cycle at the land-ocean interface. Annu. Rev. Earth Planet. Sci. 40, 685–711. https://doi.org/10.1146/annurev-earth-042711-105511

Coble, P.G., Lead, J., Baker, A., Reynolds, D.M., Spencer, R.G.M., 2014. Aquatic Organic Matter Fluorescence.

IPCC [Intergovernmental Panel of Climate Change], 2013. (Stocker, T.F., Qin, D., Plattner, G.K., Tignor, M., Allen, S.K., Boschung, J., Nauels, A., Xia, Y., Bex, V., Midgley, P.M., Eds.) Climate Change 2013: The Physical Science Basis. Contribution of Working Group I to the Fifth Assessment Report of the IPCC. Cambridge University Press, Cambridge, United Kingdom and New York, NY, USA, 1535p.

Liu, Z., Lee, C., 2007. The role of organic matter in the sorption capacity of marine sediments. Mar. Chem. 105, 240–257. https://doi.org/10.1016/j.marchem.2007.02.006

Miller, W.L., Zepp, R.G., 1995. Photochemical production of dissolved inorganic carbon from terrestrial organic matter: Significance to the oceanic organic carbon cycle. Geophys. Res. Lett. 22, 417–420. https://doi.org/10.1029/94GL03344

Palomino, D., López-González, N., Vázquez, J.T., Fernández-Salas, L.M., Rueda, J.L., Sánchez-Leal, R., Díaz-del-Río, V., 2016. Multidisciplinary study of mud volcanoes and diapirs and their relationship to seepages and bottom currents in the Gulf of Cádiz continental slope (northeastern sector). Mar. Geol. 378, 196–212. https://doi.org/10.1016/j.margeo.2015.10.001

Reeburgh, W.S., 2003. Global methane biogeochemistry. Treatise on Geochemistry 4, 65-89.

Sjögersten, S., Caul, S., Daniell, T.J., Jurd, A.P.S., O'Sullivan, O.S., Stapleton, C.S., Titman, J.J., 2016. Organic matter chemistry controls greenhouse gas emissions from permafrost peatlands. Soil Biol. Biochem. 98, 42–53. https://doi.org/10.1016/j.soilbio.2016.03.016

Wetz, M.S., Yoskowitz, D.W., 2013. An "extreme" future for estuaries? Effects of extreme climatic events on estuarine water quality and ecology. Mar. Pollut. Bull. 69, 7–18. https://doi.org/10.1016/j.marpolbul.2013.01.020

"It is clear, therefore, that the information content of organic molecules, which also carry imbedded stable isotopic signatures and radiochemical clocks, is unsurpassed by any other seawater component. The 1012 diverse organic molecules dissolved in every milliliter of seawater are the only constituents whose stored information approaches the richness needed to understand where that water has been and what has happened within it over time…"

John Hedges, *Biogeochemistry of DOM* (2002)

UCA Universidad de Cádiz

cei·mar campus de excelencia internacional del mar

IN·MAR Instituto universitario de investigación marina

Institut de Ciències del Mar

UNIVERSIDAD DE LA REPÚBLICA URUGUAY

ANII AGENCIA NACIONAL DE INVESTIGACIÓN E INNOVACIÓN

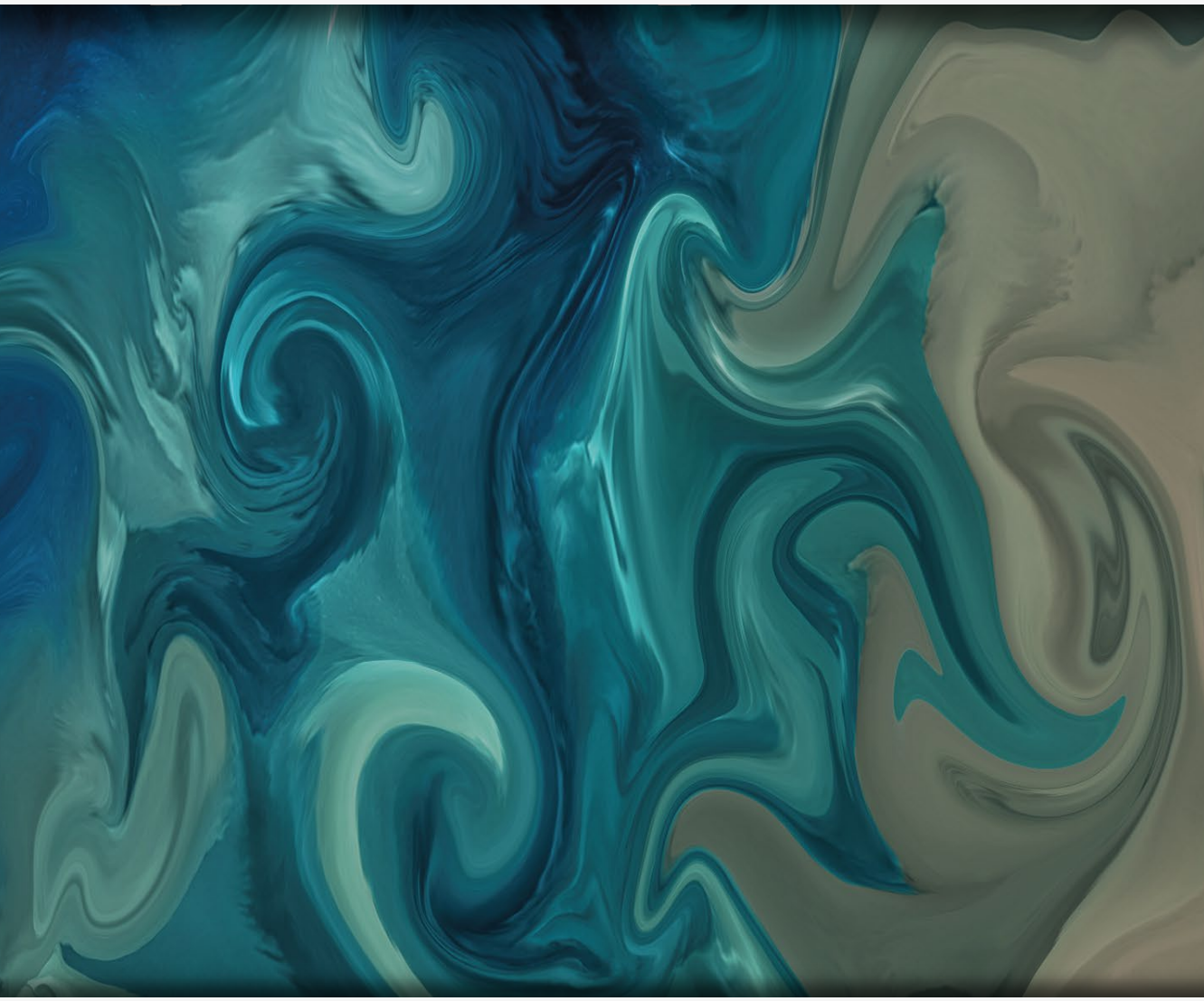

Doctoral Thesis
2021